State and Parameter Estimation of Vehicle-Trailer Systems

by

Amin Habibnejad Korayem

A thesis
presented to the University of Waterloo
in fulfillment of the
thesis requirement for the degree of
Doctor of Philosophy
in
Mechanical and Mechatronics Engineering

Waterloo, Ontario, Canada, 2021

© Amin Habibnejad Korayem 2021

Examining Committee Membership

The following served on the Examining Committee for this thesis. The decision of the Examining Committee is by majority vote.

External Examiner:	Name: Homayoun Najjaran Title: Professor, Mechanical and Manufacturing Engineering University of British Columbia
Supervisor(s):	Name: Amir Khajepour Title: Professor, Mechanical and Mechatronics Engineering Name: Baris Fidan Title: Professor, Mechanical and Mechatronics Engineering
Internal Member:	Name: William Melek Title: Professor, Mechanical and Mechatronics Engineering
Internal Member:	Name: Ehsan Hashemi Title: Research Assistant Professor, Mechanical and Mechatronics Engineering
Internal-External Member:	Name: Christopher Nielsen Title: Associate Professor, Electrical and Computer Engineering

Author's Declaration

I hereby declare that I am the sole author of this thesis. This is a true copy of the thesis, including any required final revisions, as accepted by my examiners.

I understand that my thesis may be made electronically available to the public.

Abstract

Vehicle-trailer systems have different unstable modes that should be considered in their stability control, including trailer snaking, jack-knifing, and roll-over. In general, vehicle control systems require vehicle parameters and states, including geometric parameters, mass, tire forces, and side slip angles which some are not constant or can be measured economically. In a vehicle-trailer system, the trailer states and parameters such as articulation angle, trailer geometric parameters, trailer mass, trailer tire forces, and yaw rate need to be measured or identified/estimated, in addition to the unknown vehicle states/parameters. The trailer states and parameters can be measured by sensors such as Inertial Measurement Unit (IMU), wheel torque sensors, and force measurement units. However, most of these sensors are not commercially viable to be used in a vehicle or trailer due to significant extra costs.

Estimation algorithms are the other tools to identify the parameters and states of the system without imposing extra costs. Accurate state and parameter estimators are needed for the development and implementation of a stability control system for a vehicle-trailer system. The main purpose of this research is to design real-time state and parameter estimation algorithms for vehicle-trailer systems.

Correspondingly, a comprehensive overview of different model-based and non-model-based techniques/algorithms used for estimating vehicle-trailer states and parameters are provided. The vehicle-trailer system equations of motion are then presented and based on the presented vehicle-trailer model, the possibility of the trailer states and parameters estimation are investigated for different possible vehicle-trailer on-board sensor settings.

Two different methods are proposed to estimate trailer mass for arbitrary vehicle-trailer configurations: model-based and Machine Learning (ML). The stability of the model-based estimation algorithm is analyzed, establishing the convergence of the estimation error to zero. In the proposed ML-based approach, a deep neural network is designed to estimate trailer mass. The inputs of the ML-based method are selected based on the vehicle-trailer model and are normalized by the vehicle mass, tire sizes, and geometry so that retraining of the network is not needed for different towing vehicles. The simulation and experimental results demonstrate that the trailer mass can be estimated with with acceptable computational costs.

In this thesis, ultrasonic sensors along with kinematics and dynamics equations of a towing vehicle are used to develop three approaches for hitch angle estimation. The first

approach is based on direct calculation of hitch angle using certain a priori geometric information and distance measurements of four Ultra sonic sensors. As the second and third approaches, kinematic and dynamic models of the vehicle-trailer system are used to develop least-square and Kalman filter based recursive hitch angle estimations. A more reliable hitch angle estimation scheme is then proposed as the integration of the algorithms developed following each of the three approaches via a switching data fusion logic. It is shown that the proposed integrated hitch angle estimation scheme can be used for any ball type trailer with a flat or symmetric V-nose frontal face without any priori information on the trailer parameters.

Additionally, a new approach in estimating the lateral tire forces and hitch-forces of a vehicle-trailer system is introduced. It is shown that the proposed hitch-force estimation is independent of trailer mass and geometry. The designed lateral tire forces and hitch-force estimation algorithms can be used for any ball type trailer without any priori information on the trailer parameters. A vehicle-trailer model is proposed to design an observer for the estimation of the hitch-forces and lateral tire forces. Simulations studies in CarSim along with experimental tests are used to validate the presented method to confirm the accuracy of the developed observer.

Moreover, using the vehicle-trailer lateral dynamics along with the LuGre tire model, an estimation system for the lateral velocity of a vehicle-trailer is proposed. It is shown that the proposed estimation is robust to the road conditions. An affine quadratic stability approach is used to analyze the stability of the proposed estimation. The test results confirm the accuracy of the developed estimation and convergence of the vehicle-trailer lateral velocity estimation to the actual value.

Model-based and ML-based estimators are developed for estimating road angles for arbitrary vehicle-trailer configurations. The estimators are shown to be independent from road friction conditions. The model-based method employs unknown input observers on the vehicle-trailer roll and pitch dynamic models. In the proposed ML-based estimator, a recurrent neural network with Long-short-term-memory gates is designed to estimate the road angles. The inputs to the ML-based method are normalized by the vehicle wheel-base, mass, and CG height to make it applicable to any towing vehicle with the need of retraining. The simulation and experimental results justify the convergence of the road angle estimation error.

Acknowledgements

This dissertation would not have been possible without the guidance and the help of several individuals who in one way or another contributed and extended their valuable assistance in the preparation and completion of this study. First and foremost, I would like to express my deepest and sincerest gratitude to my PhD supervisors, Prof. Amir Khajepour and Prof. Baris Fidan, because of their great support, encouragement, and guidance for my research and education during my PhD program at the University of Waterloo. I am sure that I could not have been here without their help, support, and guidance. I have learned a lot from my supervisors, and I'm sure the gained technical skills and meticulous planning skills will assist me in the future throughout my career.

I would like to further thank Dr. Homayoun Najjaran for accepting to hold the external examiner position for my PhD defence examination. I am also thankful to my committee members Dr. William Melek, Dr. Ehsan Hashemi and Dr. Christopher Nielsen for agreeing to be in my PhD committee.

I would like to acknowledge the Natural Sciences and Engineering Research Council of Canada (NSERC), Ontario Research Fund (ORF), and General Motors for their financial support. Special thanks to Dr. Bakhtiar Litkouhi, Dr. Alireza Kasaizadeh, and Dr. Annie Zhao at the GM Research and Development Center in Warren, MI, USA and Dr. Hojjat Izadi, Dr. Joseph Moore, and Dr. Mansoor Alghooneh at Gm Canadian Technical Center for their technical support and valuable comments in improving my research.

I would like to thank the technicians in the MVS laboratory, Jeff Graansma, Aaron Sherratt, and Adrian Neill for helping me in the road experiments.

I am also thankful to my dear friend, Reza Hajiloo, for his endless friendship. I have had a great time at Waterloo because of some amazing people who have been a valuable source of assistance, affection, and friendship. I highly appreciate my friends including Mehdi Abroshan, Ehsan Mohammadbagher, Hamed Jamshidifar, Neel P Bhatt, Shamim Mashrouteh, Hassan Askari, Ruihe Zhang, Yukun Lu, Chen Tang, and Mobin Khamooshi at the University of Waterloo.

Last but not least, I would like to thank my parents, Moharam Habibnejad Korayem and Fariba Azari Korayem, and my brother, Alireza Habibnejad Korayem, for all the support you have shown me through this journey and endless love.

Dedication

Dedicated to my beloved parents.

Table of Contents

List of Tables

List of Figures

Nomenclature

α_i	Slip angle at each axle
δ	Steering angle
δ_l	Lower bound of the steering angle
δ_u	Upper bound of the steering angle
δ_{k-j}	Kronecker delta function
δ_{th}	Steering angle threshold
$\dot{\omega}$	Wheel rotational acceleration
$\hat{\phi}$	Calculated hitch angle by the ultra-sonic sensors
κ	Average lumped model
λ	Slip ratio
$\mathbf{I}_\omega$	Wheel yaw momentum of inertia
$\mathbf{T}_t$	Total effective torques at each corner
Φ_k	Regression signal
Z_k	Output signal
μ	Road friction coefficient
μ_j	Normalised friction force

μ_R	Rolling resistance
μ_c	Normalised Coulomb friction coefficient
μ_s	Normalised static friction coefficient
ω	Wheel angular velocity
ψ_t	Trailer roll angle
ψ_v	Vehicle roll angle
ρ	Air density
σ_0	Tire rubber stiffness
τ	Engine torque
θ	Hitch angle
θ_t	Trailer pitch angle
θ_v	Vehicle pitch angle
θ_{th}	Hitch angle threshold
A	Projected cross-sectional area of the vehicle
a_1	Vehicle CG distance to front axle
a_2	Trailer CG distance to front axle
a_{x1}	Vehicle longitudinal acceleration
a_{x2}	Trailer longitudinal acceleration
a_{y1}	Vehicle lateral acceleration
a_{y2}	Trailer lateral acceleration
a_{z1}	Vehicle vertical acceleration
a_{z2}	Trailer vertical acceleration

b_1	Vehicle CG distance to rear axle
b_2	Trailer CG distance to rear axle
C_0	Total resistance force coefficient
C_1	Total resistance force coefficient
c_d	Drag coefficient
C_ψ	Roll damping
C_θ	Pitch damping
C_{yf}	Vehicle tire cornering stiffness at front axle
C_{yr}	Vehicle tire cornering stiffness at rear axle
d_i	Ultra-sonic sensor measurement
d_t	Trailer axle distance
e	Vehicle rear axle distance to hitch-point
F_R	Resistance force
f_t	Forget gate vector
$F_{xf,i}$	Vehicle longitudinal tire force at front axle
$F_{xr,i}$	Vehicle longitudinal tire force at rear axle
$F_{xt,i}$	Trailer longitudinal tire force
F_{xT}	Longitudinal hitch force
$F_{yf,i}$	Vehicle lateral tire forces at front axle
$F_{yr,i}$	Vehicle lateral tire forces at rear axle
$F_{yt,i}$	Trailer lateral tire force
F_{yT}	Lateral hitch force

g_t	State update vector
h_{pc}	Distances between the pitch axes and the center of gravity
h_{rc}	Distances between the roll axes and the center of gravity
i_t	Input gate vector
I_x	Roll moments of inertia
I_y	Pitch moments of inertia
I_{z1}	Vehicle moment of inertia
I_{z2}	Trailer moment of inertia
K_ψ	Roll stiffness
K_θ	Pitch stiffness
l_1	Vehicle wheel-base
l_2	Trailer wheel-base
m_1	Vehicle mass
m_2	Trailer mass
o_t	Output gate vector
P	Air spring pressure
r_1	Trailer yaw rate
r_2	Trailer yaw rate
r_p	Road profile
R_{eff}	Effective tire radius
S	Suspension deflection
T_s	Sensor sampling rate

Tw_1	Vehicle front axle length
Tw_2	Vehicle rear axle length
Tw_3	Trailer width
u	Vehicle longitudinal velocity
V	Lyapunov candidate function
v_1	Vehicle lateral velocity
v_2	Trailer lateral velocity
v_k	Measurement noises
V_s	Stribeck velocity
v_{rx}	Longitudinal relative velocity
v_{ry}	Lateral relative velocity
w_k	Process noises
w_{fx}	Longitudinal uncertainties
w_{fy}	Lateral uncertainties
Z_{ij}	Vehicle/trailer corner normal displacements
α	Trailer front face angle
β	State threshold designed parameter
σ_0	Rubber stiffness in both longitudinal and lateral directions
σ_1	Rubber damping in both longitudinal and lateral directions
σ_2	Relative viscous damping in both longitudinal and lateral directions
$\tilde{\omega}_t$	Wheel speed estimation error

Chapter 1

Introduction

Vehicle-trailers, or tractor-trailers, are mainly used to carry goods or groups of people that cannot be transported by vehicles with only one rigid body as the turning radius of articulated vehicles including vehicle-trailers are quite small. Such articulated vehicles have different unstable modes that should be considered in their stability control. Generally, a vehicle control system depends on the vehicle responses and parameters that are sometimes unknown. Therefore, accurate estimators are needed for the unmeasurable parameters and states of the vehicle.

1.1 Motivation

Vehicle-trailers are important parts of the global transportation system, however, they are perilous vehicles both for themselves and other road users because of their multiple modes of instability. With respect to single unit vehicles, vehicle-trailer systems have different unstable modes, including trailer snaking, jack-knifing, and roll-over. Jack-knifing is mainly attributed to tire/ground friction force saturation that may occur during hard braking processes or in curved-path negotiations. If a vehicle towing a trailer skids, the trailer can push the towing vehicle from behind until it spins the vehicle around and collapses. Similar to jack-knifing, trailer snaking, also called trailer sway, is an unstable yaw motion mode of the trailer. Trailer snaking motion usually occurs when side forces cause the trailer to move side to side behind the towing unit. Trailer roll-over happens if high lateral

forces are applied to the vehicle during a sharp turning maneuver at higher speeds. These unstable modes exists for both commercial and recreational trailers, however, there are some differences between the two. For instance, in commercial vehicle-trailer systems, the trailer weight to vehicle weight ratio is much higher than the trailer weight to vehicle weight ratio in recreational vehicle-trailer systems.

Based on the Transport Canada Collision Database, 1,898 motor fatalities and 11,5956 personal injuries were reported [1]. Engineers have tried to decrease the percentage of accidents by developing active safety systems for vehicles. These include Anti-lock Braking System (ABS), Traction Control System (TCS), Electronic Stability Control (ESC) and Active Steering Control (ASC), etc. It is well known that unstable modes of vehicle semi-trailers cause many highway accidents and casualties. For heavy vehicles, similar to passenger cars, active safety systems require accurate estimation of the states and parameters of both the vehicle and trailer, which cannot be measured directly. By taking the stability control of the trailer into account, trailer states/parameters such as articulated angle, trailer geometries, trailer mass, and trailer hitch forces, need to be estimated. The overall diagram representation of control and estimation blocks for vehicle-trailer systems is illustrated in Fig. 1.1. Fig. 1.1 shows how vehicle state estimation is essential from different aspects.

The trailer states and parameters can be measured by sensors such as inertial measurement unit, wheel torque sensors, and force measurement units. However, to measure more parameters and states more sensors are required that results in higher costs. Estimation algorithms can be used to offset the extra costs of the sensors while achieving a higher safety in vehicle-trailers. Choosing a good combination of sensors, meaning the sufficient number of sensors that make the system observable, is imperative to accurately estimate the states/parameters.

Trailer states/parameters are divided into three groups - constant parameters such as geometrical parameters, semi-constant parameters such as mass and CG location, and time varying such as hitch angle forces. The trailer geometric parameters, including the axle location, trailer width, trailer length, and trailer height, are the constant parameters of the trailer. Trailer longitudinal/lateral velocities, hitch point forces, trailer yaw rate, trailer tire forces, and articulated angle are the examples of time varying states/parameters that need to be estimated.

The parameters relating to the trailer mass are semi-constant parameters since the

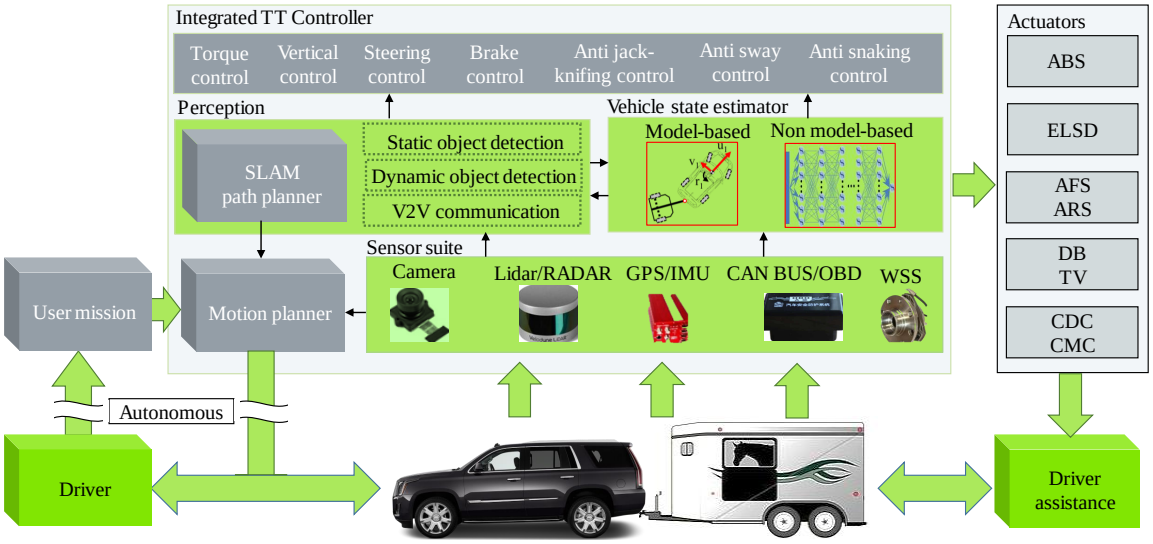

Figure 1.1: The overall block diagram representation of control and estimation blocks for vehicle-trailer systems.

trailer mass is constant during operation, however, it may change as loads receive/deliver. The parameters related to the load, are the trailer sprung mass, trailer momentum of inertia and trailer Center of Gravity (CG) location.

The main purpose of this PhD research is to design a real-time state and parameter estimation algorithms for vehicle-trailer systems. The estimated parameters/states can be used in vehicle-trailer's control and safety systems. There is much research that has been done for estimating the vehicle (generally vehicle without trailer) states/parameters, however, when a trailer is attached, the system dynamic changes and the existing vehicle estimation algorithms are no longer be valid and require adjustment or fully be redeveloped.

Two major approaches have been adopted in the literature to tackle trailer state estimation problems. One is the modified kinematic-based approach, which uses stochastic estimators or nonlinear observers. This method does not need tire model information, however, sensor noise and bias need to be estimated or calculated precisely to obtain accurate outcomes.

The other state estimation practice is model-based and utilizes Inertial Measurement

Unit (IMU) data (longitudinal and lateral acceleration in addition to yaw rate measurements) and corrects the estimation with tire forces using stochastic observers such as the Kalman filter and sliding mode observer. Although this approach seems promising, it requires accurate tire parameters and accurate information about the road surface, including the road friction coefficient which may not be available or hard to measure.

1.2 Objectives

One of the main objectives of this research is to develop real-time estimation algorithms for the states and parameters of vehicle-trailer systems. The main states/parameters that have been considered in this thesis include:

- Hitch forces and angle
- Trailer mass, moment of inertia, and CG location
- Trailer tire forces
- Trailer yaw rate and slip angle
- Trailer axle location

The states/parameters listed above are the ones essential for proper stability control of a vehicle-trailer system. In order to estimate the trailer states and parameters, different estimation methods including model-based and non-model-based are used and applied. The second objective of this work is to make/develop real-time state/parameter estimators robust to surface friction changes. This is especially important as the road condition detection is hard and not reliable in practice.

1.3 Thesis Outline

The work done in the literature on vehicle-trailer states and parameters estimation are presented in Chapter 2. Chapter 2 provides a comprehensive overview of different model-based and non-model-based techniques/algorithms used for estimating vehicle-trailer system states and parameters. The main features, limitations, and assumptions for each

estimation method are discussed. Summary tables for vehicle-trailer estimation techniques are provided.

In Chapter 3, the vehicle-trailer equations of motion are presented. Based on the presented vehicle-trailer model, the possibility of the trailer states and parameters estimation are investigated for different possible vehicle-trailer on-board sensor settings.

In the fourth chapter, two different approaches are proposed to estimate trailer mass for arbitrary vehicle-trailer configurations; model-based and Machine Learning (ML). In Section 4.2, the proposed model-based trailer mass estimation is described and the convergence of the trailer mass estimate is analyzed. In Section 4.3, an overall structure of the proposed ML approach is described and a DNN trailer mass estimator is designed using different number of neurons at different layers. A sensitivity analysis with respect to all available measurements from the vehicle-trailer system, which are used as the DNN inputs, is also presented in Section 4.3, along with a discussion of selection of the inputs of the DNN based on this sensitivity analysis. In Section 4.4, training and testing the designed DNN with a set of real-time vehicle-trailer system data is explained. The trailer mass estimation results with the model-based and ML approaches are presented and compared in Section 4.5 with discussion.

In Chapter 5, ultra-sonic sensors along with kinematics and dynamics equations of a towing vehicle are used to develop three approaches for hitch angle estimation. The first approach is based on direct calculation of hitch angle using a priori geometric information and distance measurements of four ultra-sonic sensors. An angle estimate is generated for each of the six possible sensor-pair combinations, and these six estimates are passed through a voting algorithm to produce a single estimate. In Section 5.2, the methodology of the hitch angle estimation and algorithms to estimate the hitch angle are described. In Section 5.3, the hitch angle estimation by using ultra-sonic sensors measurements as well as the trailer front face angle estimation are introduced. As the second and third methods, kinematic and dynamic models of the vehicle-trailer system are used to develop least-squares and Kalman filter based recursive hitch angle estimations. The kinematic equation for hitch angle is presented in Section 5.4. Moreover, the trailer axle location estimation is developed in Section 5.4. The estimated trailer mass is used in the designed hitch angle estimation algorithm based on the vehicle-trailer dynamic method and finally, results with discussions are provided in Section 5.5.

In Chapter 6, a new approach in estimating the lateral tire forces and hitch-forces

of a vehicle-trailer system is introduced. In Section 6.2, a vehicle-trailer system model is presented in the state space form. In Section 6.3, algorithms to estimate the hitch-forces are developed and discussed, and the state constraints are presented. The designed lateral tire forces and hitch-force estimations algorithm can be used for any ball type trailer without any priori information on the trailer parameters. The estimator stability analysis and estimation error convergence rate are investigated in Section 6.4. Finally, simulation and experimental results are provided in Section 6.5 with discussions. The results confirm the accuracy of the developed observer.

Using a 3-degree-of-freedom lateral dynamic vehicle-trailer system model with the Lu-Gre tire model, a constrained unscented transformation based scheme for estimating the lateral velocity of a vehicle-trailer is proposed in Chapter 7. In Section 7.2, the vehicle-trailer system model is presented in the state space form. An observer is designed for the lateral velocity estimation in Section 7.2 with stability analysis. It is shown that the proposed lateral velocity estimation scheme is robust to the road condition. An affine quadratic stability approach is used to analyze the stability of the proposed estimation scheme. Finally, the proposed lateral velocity estimator is validated by simulation and experimental studies with discussions in Section 7.3.

Chapter 8 proposes two different approaches for estimating the road angles for arbitrary vehicle-trailer configurations independent from the road friction conditions: Model-based and machine learning. The model-based method employs unknown input observers on the vehicle-trailer roll and pitch dynamic models. In Section 8.2, the vehicle-trailer pitch/roll dynamic is analyzed, and the proposed model-based road angle estimation using unknown input observer approach is described. In Section 8.3, an overall structure of the proposed non-model-based approach is described and a machine learning based road angle estimator is designed using recurrent neural network with long-short-term-memory gates. A sensitivity analysis with respect to all available measurements from the vehicle-trailer system to find the inputs to the network is also presented in Section 8.3. In Section 8.4, training and testing the designed LSTM-RNN with a set of real-time vehicle-trailer system data is explained. The road angle estimation results using the model-based and machine learning are presented and compared in Section 8.5.

Finally, conclusions are made in Chapter 9 with suggestions for future works.

Chapter 2

Background and Literature

2.1 Introduction

This chapter provides a comprehensive overview of different model-based and non-model-based techniques/algorithms used for estimating vehicle-trailer states and parameters. The main features, limitations, and assumptions for each estimation method are discussed. This chapter is organized as follows: In Section 2.2, the literature on estimating hitch angle, lateral velocity, coupling forces, tire forces, roll and slip angles, trailer mass, and geometrical parameters are reviewed. Moreover, the details of non-model-based estimation techniques for vehicle-trailer system state estimation is reviewed in Section 2.2. Conclusions are provided in Section 2.3.

2.2 Literature Review on Vehicle-Trailer State and Parameter Estimation Techniques

Compared to single unit vehicles, vehicle-trailers are more susceptible to instability. Hence, any improvement in their stability control would significantly improve transportation safety.

To decrease the number and fatality of accidents, various safety systems have been developed [2, 3, 4, 5, 6]. These systems help the driver maintain vehicle stability in critical driving situations. In general, vehicle control systems depend on vehicle parameters and

state variables, which are sometimes unknown and/or cannot be directly measured. Such unknown parameters and states need to be estimated on-line using estimation algorithms using available sensor measurements. In current practice, vehicle control systems are usually deactivated when a trailer is connected due to the changes in the vehicle dynamics model and unknown trailer parameters. In most cases, it is possible to measure some of the unknown parameters and states in a vehicle-trailer system, however, cost, compatibility, and communication limitation between the trailer and towing vehicle constrain implementation of such direct measurements. Estimation algorithms are then required to estimate the parameters and states without imposing extra costs and complexities.

Although state and parameter estimations are used extensively in single unit vehicles, the lack of scholarly work in vehicle-trailer state and parameter estimation is noticeable. This is plausible due to various types of trailers that can be attached to a vehicle. There are in general three approaches in the literature to estimate the vehicle-trailer states and parameters as summarized in Fig. 2.1:

1. *Model-based estimation methods*: Vehicle-trailer models including kinematic, single track, roll/pitch/yaw, quarter vehicle-trailer, and higher-order models are used in these model-based techniques to estimate and predict the states and parameters of vehicle-trailer systems. These approaches can provide accurate results in both static and dynamic responses.

2. *Data driven estimation methods*: The states and parameters of the vehicle-trailer system are estimated using measured sensory data by applying different data training and data fusion techniques.

3. *Data-fusions methods based on vision/radar based methods*: Vision and radar data about the surrounding objects and the vehicle/trailer motion are used to estimate the vehicle-trailer states and parameters. Data fusion techniques are utilized to estimate the vehicle-trailer system states/parameters more accurately by different combinations of the above two approaches.

Typically the vehicle-trailer system states and parameters are either assumed to be known [7, 8, 9, 10] or estimated based on the vehicle-trailer's dynamic responses [11, 12, 13]. Given that the vehicle-trailer states and parameters need to be available for vehicle-trailer control and active safety systems, the real-time estimation of the vehicle-trailer

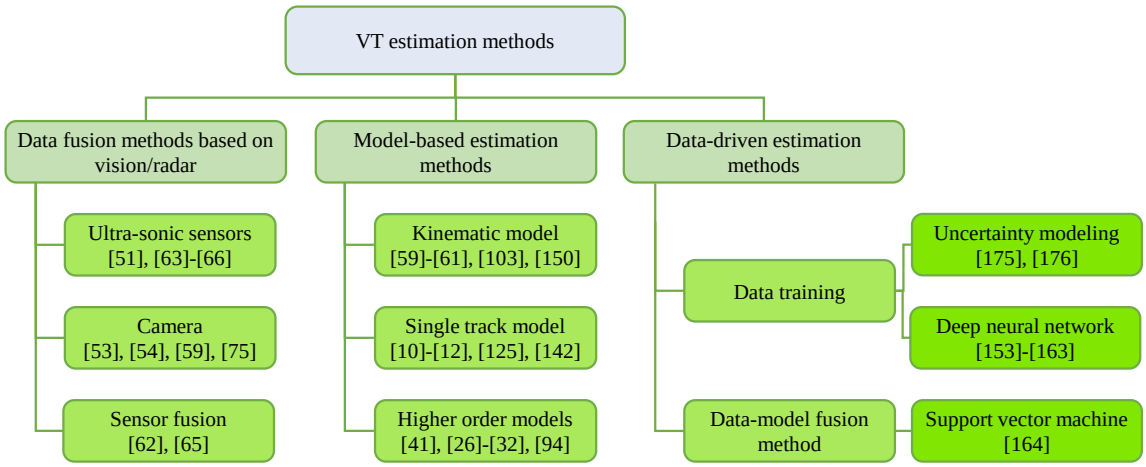

Figure 2.1: Classification of the vehicle-trailer estimation methods.

states/parameters are crucial for improving the performance of vehicle-trailer control and active safety systems.

In many research works, a specific form of the vehicle-trailer kinematic/dynamic model is considered to estimate the vehicle-trailer states and parameters [14, 15, 16]. However, it is very difficult and challenging to estimate vehicle-trailer system states and parameters simultaneously such as center of gravity location, sprung mass, and, most importantly, tire's cornering stiffness due to the correlation with each other [17, 18, 19].

This section reviews the literature on vehicle-trailer state and parameter estimation for the hitch angle, lateral velocity, coupling forces, tire forces, roll and slip angles, trailer mass, and geometrical parameters.

2.2.1 Hitch Angle Estimation

Hitch angle estimation is needed in vehicle-trailer motion control mainly to prevent trailer snaking and jack-knifing. In [20], the hitch angle estimation is based on the vehicle-trailer equations of motion, where the linear tire model has been used for deriving these equations of motion. Another hitch angle estimation is proposed in [21] based on the vehicle-trailer kinematic model. By considering the nonlinear kinematic model under the effect of varying slip angles, estimation of the hitch angle of load-haul-dump trucks has

been studied in [22, 23]. By taking the Ackermann steering geometry into account, the hitch angle can be represented as a function of the vehicle's steering angle and velocity. Use of this function together with the vehicle steering angle and velocity measurements for hitch angle estimation is studied in [24, 25, 26, 27]. By considering the vehicle-trailer kinematic and dynamic models, hitch angle estimation has been investigated in many other research works to develop reliable methods for vehicle-trailer state and parameter estimation [28, 29, 30, 31, 32, 33, 34].

There also exist works on estimation of the hitch angle based on vision through the vehicle rear camera. By detecting the angle between the trailer front face and the vehicle by a fixed camera at the rear end of the vehicle, the hitch angle has been estimated in [35, 36, 37]. The hitch angle can also be measured directly by potentiometer or encoder sensors connected to the hitch point [38]. This approach however, requires sensor connection at the hitch point, which may not be practical for recreational vehicle-trailer systems.

The hitch angle can also be found by ultra-sonic sensor measurements. In [39], ultra-sonic sensors were utilized to measure the hitch angle to develop a car parking assistant system for a vehicle-trailer system. To do so, the ultra-sonic sensors that are located in the rear bumper of the vehicle, measure the distance between the vehicle rear bumper to the trailer front face. Thus, different equations can be written to calculate the hitch angle θ based on multiple sensor combinations. For instance, using the ultra-sonic sensor's data, θ can be calculated from [39, 40, 41, 42, 34]:

$$\theta = \alpha - \arcsin \frac{d_1 - d_2}{c_2}, \tag{2.1}$$

where, α is the trailer front face angle. These sensors are sensitive to temperature changes and sever whether conditions and become unreliable when the trailer front face changes from one trailer to another. To correct the determined hitch angle by the ultra-sonic sensors, the vehicle-trailer kinematic model was considered [40, 41].

In the hitch angle equation (2.1), α is the only required trailer parameter. Therefore, if the trailer front face angle estimation is available, the hitch angle kinematic relation (2.1) works for any unknown trailer. Further discussion on trailer parameter estimation feasibility is provided in Chapter 3.

2.2.2 Vehicle-Trailer Velocity Estimation

Vehicle velocity in both lateral and longitudinal directions play an important role in stability control systems. To measure the longitudinal/lateral velocities, Global-Positioning-Systems (GPSs) can be used, however, they suffer from poor accuracy, signal availability, refreshing frequency, and their lack of reception in some geographical areas for the most commonly used GPSs in vehicles. Variety of approaches have been proposed for lateral velocity estimation in the literature. A vehicle state estimator was presented in [43] by combining data of magnetometer, GPS, and IMU and utilizing a stochastic filter integrated with a Kalman Filter (KF) to cancel the effect of disturbances in the magnetometer. The kinematic model equations were used to estimate the vehicle longitudinal and lateral velocities using KF based estimation algorithms in [44, 45], and non-linear observers in [46]. These methods do not employ a tire model, however, sensor noise should be considered in detail for reliable estimation. In addition, to mitigate noise effects and address the low excitation scenarios, some kinematic-based methodologies have been utilized in the estimation algorithms.

Estimation of the vehicle-trailer lateral velocity is essential for the vehicle stability control module to enable combined vehicle-trailer active safety systems. Correspondingly, a lateral velocity estimator based on the data received from a low-cost inertial measurement unit was proposed in [47]. Based on the more detailed nonlinear lateral dynamics model of the vehicle-trailer system [48, 49], an Extended KF (EKF) approach was used to estimate the vehicle-trailer lateral velocity in [50].

The vehicle-trailer velocity can also be estimated using vision based method. In [51], a model-based state observer was proposed to estimate the lateral velocity using a forward-looking monocular camera. Utilizing a monocular camera may lead to the increase of computational effort as well as addition of the uncertainty term due to the camera calibrations[52, 53]. Moreover, the assumptions of invariant road surface with static features are invalidated if the road surface is soft and disturbed by the passing vehicle or if the surface is reflective as in the case of standing water or snow. Such road conditions need to be taken into account in off-highway applications

Although lateral velocity estimation is investigated extensively in single unit vehicles, there is a large lack of scholarly work in vehicle-trailer lateral velocity estimations. Based on the literature, the current lateral velocity estimators are almost all for single vehicle units that cannot be used for vehicle-trailer combinations. Therefore, designing and developing

optimal real-time vehicle-trailer lateral velocity estimator is one of the open topics in this area.

2.2.3 Vehicle-Trailer Coupling and Tire Force Estimation

Lack of the knowledge of the system's parameters is the major issue when an accurate model is needed for vehicle stability and traction control systems. However, model-free control techniques could be another solution when the system parameters are unknown [54, 55, 56, 57]. In a vehicle-trailer arrangement, the vehicle states and parameters are usually assumed to be known, measured, or estimated based on the vehicle's dynamics and its responses [58, 59, 60]. A KF state estimator was designed in [61] to estimate the tire cornering stiffness, sideslip, and roll angles of a vehicle-semitrailer system simultaneously. In [61], a five degree-of-freedom single-track model was considered, and the tire model was assumed to be linear which may not be a valid assumption in harsh maneuvers. The vehicle's longitudinal and lateral tire forces have been estimated by applying an EKF on a vehicle bicycle model in [62], where the vehicle system dynamics were derived by the use of a shaping filter.

The lateral and normal forces at the hitch-point, also called fifth wheel in commercial vehicles, were measured by a multi-axis force sensor unit, and the measured hitch-forces were used for the roll stability advisor system. A sliding mode observer was used to estimate the effect of the trailer (forces) on the vehicle. The longitudinal and lateral hitch-forces were estimated by applying a sliding mode observer and using the measured vehicle and trailer accelerations in [63, 64, 65]. The roll stability of a commercial vehicle-trailer system was investigated by utilizing hitch-force measurements in [66]. However, the approach in [66] is subject to the extraneous hardware and wiring complexity, which is not desirable for the automotive industry.

The effect of hitch loading on a vehicle was investigated and the designed hitch load estimator algorithm was validated experimentally in [67]. To estimate the hitch-forces, the vehicle tire forces are needed. Tire force estimation is used extensively in single unit vehicles; however, literature on vehicle-trailer tire force estimations especially with unknown trailer configurations is very scarce.

Tire forces are important terms in the vehicle equations of motion. To be able to model the vehicle behaviour accurately, an accurate tire model should be considered. The tire

behaviour has been modeled in numerous studies and used for vehicle and vehicle-trailer state estimation or stability analysis [68, 69, 70]. One of the most well-known tire models is the Pacejka model, where the tire behaviour is modeled by a group of curved lines that are generated from experimental tests to represent the relationship between the road friction coefficients, slip ratio, slip angle, and tire forces [71]. Another widely used tire model is the LuGre tire model, which uses relative velocities in longitudinal and lateral directions to model the tire behaviour in pure-slip conditions [72] and combined-slip modes [73].

Sliding mode observer design is a common technique used for estimating the states and parameters of vehicle and vehicle-trailer systems. In [74, 75, 12, 76], sliding mode observers were designed to estimate forces in the vehicle-trailer system. A similar estimation method was applied to a mining truck in [77]. The vehicle's longitudinal and lateral tire forces have been estimated by applying an EKF on a vehicle bicycle model [78], where a trained neural network model was used to estimate the tire cornering stiffness.

Tire forces can also be measured indirectly by strain-gauge based mechanisms in the wheel hub, as presented in [79]. However, it is expensive to implement this approach on production vehicles. Shear stress measurement systems using strain gauges mounted on the axle bar can be used to provide more accurate measurements, however, utilization of strain gauges for force measurements in vehicle systems bears installation and calibration issues [80].

Table 2.1: Vehicle-trailer force, geometry parameters, and velocity estimation.

Estimated state/parameter	Case study	Measurements used	Model used	Estimations methodology	Assumptions	References
Tire cornering stiffness, roll angle, CG height, sideslip angle, trailer momentum of inertia	Agricultural vehicle with trailer	ϕ_1, ϕ_2, u r_1, r_2, δ	Single-track model	KF, DEKF	u is a slow changing state, articulated angle and steering angle are small	[61, 81]
Normal tire forces long/lat velocity	Agricultural heavy vehicle	δ, r_1	Single-track model	UKF	Pacejka tire model, road grade/bank angle are known	[82]
vehicle lateral velocity and yaw rate	Articulated heavy vehicle	θ, $\dot{\theta}$, δ	Four-wheel vehicle model	EKF	Pitch and heave motion are ignored	[83]
Vehicle/trailer yaw rate, tire forces	Heavy duty vehicle	a_{x1}, a_{y1}, a_{x2}, a_{y2}	Kinematic model	SMO	The axle is rigid and superbly symmetrical	[84]
Hitch forces	Commercial vehicle	a_{x1}, a_{y1} δ, a_{y2}	VT single-track model	SMO	Rigid axle, same roll center and CG	[64, 67]
VT tire forces	Heavy articulated vehicle	S	Vertical VT model	SMO	States and inputs are bounded	[75]
Lateral velocity	Long articulated vehicle	r_1, r_2	VT lateral dynamics	EKF	Process and measurement noise with Gaussian distribution	[50]
Lateral tire force	Vehicle and semi-trailer	$a_{x,1}$, τ, ω	Lagrange's equation, Newtonian mechanics	SOSMO, NSMO	Constant longitudinal speed	[12, 74] [76]
Cornering stiffness, fifth wheel and roll stiffness	Vehicle and semi-trailer	ϕ, $\dot{\phi}$, δ	5-DOF Vehicle semitrailer model	GA, MGA	Constant roll, fifth-wheel and sideslip stiffness	[85]

Table 2.1 summarises the papers cited in this work based on their approaches, measurement signals, and critical assumptions they had considered for estimating the vehicle-trailer forces and lateral velocities.

2.2.4 Vehicle-Trailer Roll and Sideslip Angle Estimation

Unavailability of some of the system states and parameters is a major problem when an accurate model is needed for stability control systems. This problem also exists in the case of vehicle with trailer especially for roll dynamics since the vehicle and trailer suspension parameters are required. An unknown input observer was used in [86, 87] to estimate the roll angle for the vehicle and semi-trailer vehicle which has a right impact on the vehicle-trailer ride comfort and stability [88, 89, 90]. By considering the roll dynamics of heavy articulated vehicles, roll angle estimation via Luenberger observer was studied in [91]. In [91], an intelligent fault monitoring system was also proposed to increase the accuracy of the roll angle estimation for a prototype heavy vehicle active suspension system. In [61], roll and sideslip angles were estimated for vehicle semi-trailer systems using a KF state estimator, assuming a linear tire model.

The sideslip angle, which is one of the most crucial states for stability of the vehicles, was estimated for the vehicle-trailer system by considering a five degrees-of-freedom (DoF) yaw–roll vehicle linear model in [92, 61]. In [93], an observer was designed to accurately estimate the roll and sideslip angles for both the vehicle and the trailer on high friction surfaces while tire capacity was well below the limits of tire adhesion. However, performance of this observer is reported to be influenced by approaching the limits of adhesion [93]. The trailer's tires could reach the limits of adhesion and become saturated if either the tire road friction coefficient drops or they are saturated longitudinally by heavy braking. Simulation results for a state observer to estimate the lateral and longitudinal velocities (from which the sideslip angle can be obtained) of vehicle-trailers on roads with an unknown slope angle values were presented in [82]. However, this state estimator requires an accurate vehicle tire model as well as good knowledge of the friction coefficient value between the tire and the road. In [94], an algorithm was developed to estimate the vehicle sideslip angle and yaw rate by considering the steering wheel angle excitation. This algorithm relies on lateral acceleration and wheel angular velocity sensors. The results show that the algorithm is able to estimate the sideslip angle with sufficient accuracy on various surfaces with different handling manoeuvres. Three extended Kalman filter state estimators were designed

simultaneously to estimate the trailer sideslip angle in [95], where the effects of body roll on the sensing of lateral acceleration have been investigated as well.

2.2.5 Vehicle-Trailer Mass and Parameter Estimation

In vehicle-trailer systems, snaking and jack-knifing are the two distinct yaw instability modes, which are defined based on the saturated axle. Trailer snaking motion usually occurs when side forces cause the trailer to move side to side behind the towing unit and generally happens on slippery road surfaces. On the other hand, jack-knifing is mainly attributed to tire/ground friction force saturation that may occurs during hard braking or in curved-path negotiations. If a vehicle towing a trailer skids, the trailer can push the towing vehicle from behind until it spins the vehicle around and collapse [96, 97, 98, 99, 100, 101]. One of the most important parameter that relates to the mentioned vehicle-trailer instability modes is the trailer Center of Gravity (CG) location that relates to the payload condition. The CG location defines the instability type; meaning that jack-knifing is more willing to occur when the CG location is close to the hitch point. However, the trailer will sway if the CG location stand far from the hitch point and close to the end of the trailer [97, 68, 102, 103, 104].

Generally, a trailer is used for carrying goods and products, and special trailers can be designed for carrying heavy payloads. The trailer's payload is dependent on its usage and measuring the payload can improve the stability investigation of the vehicle-trailer system. However, measuring the payload directly is costly and as a result, payload estimation is highly sought. The trailer mass can vary depending on the goods and loads the trailer carries [105]. Given that the trailer mass cannot be measured directly using low cost sensors, it is necessary to estimate it via the integration and processing of data acquired from the sensors installed on conventional vehicle-trailer systems.

Techniques for weighing trucks in motion have been intensively studied recently [106, 107]. In [108], the vehicle weight was estimated by utilizing the vehicle velocity and driving torque, and designing a sliding mode term along with a low-pass filter to ensure the convergence of the estimation error to zero. The article [109] presented a method to identify the commercial vehicles payload based on the vehicle longitudinal acceleration and measured trailer's air spring.

Model-based and machine learning approaches were proposed to estimate trailer mass

for arbitrary vehicle-trailer configurations [110]. In [110], the stability of the model-based estimation algorithm was analyzed, and a generic machine learning based approach was designed to estimate the trailer mass with unknown trailer parameters. A Recursive Least Square (RLS) method was proposed in [111] to estimate both the vehicle mass and road angle. The proposed method in this work for both vehicle mass and road angle estimation were validated experimentally. The dynamics of the sprung and unsprung mass were investigated to design a full vehicle state estimator in [112]. Similarly, the trailer mass and yaw inertia were estimated by using an RLS based algorithm to maintain the stability of the vehicle-trailer system in [113].

Table 2.2: Vehicle-trailer lateral load transfer and trailer mass estimation.

Estimated state/parameter	Case study	Measurements used	Model used	Estimations methodology	Assumptions	References
Payload, CG location	Commercial vehicle	a_{y1}, P	Single-track model	RLS	μ is constant, tire deflection and pitch motion are neglected	[109]
Lateral load transfer	Articulated heavy freight vehicle	a_{x1}, a_{y1}, a_{z1}	Kinematic model	EKF	Unsprung mass is neglected	[114, 115]
Trailer load transfer ratio	Heavy articulated vehicle	z_i, r_1, u, a_{y1}	VT roll dynamics model	FBA	Constant roll center and pressure center	[116, 117]
Trailer mass, CG location, trailer yaw/roll rate	Commercial vehicle	a_{x1}, a_{y1} r_1, P	-	RLS, DKF	Trailer mass and geometry are known	[118]
Trailer mass and inertia	Long articulated vehicle	$F_{y,i}$, u, v_1	VT Lateral dynamics	RLS	No roll, pitch and bounce motion	[113]
Trailer mass	Vehicle and semi-trailer	$a_{x,1}$, τ, ω	Longitudinal dynamic model	-	There is no process and measurement noise	[12]

Note: VT: Vehicle-trailer, DKF: Dual Kalman filter, RLS: Recursive least squares, FBA: Filter based approach, EKF: Extended Kalman filter.

Table 2.2, summarises the papers cited in this work based on their approaches, measurement signals, and critical assumptions they had considered for estimating the vehicle-trailer lateral load transfer and trailer mass.

2.2.6 Non-Model-Based Vehicle-Trailer State Estimation

Data-driven based methods are largely considered effective tools for system modelling, as they are suitable to model complex systems using their ability to identify relationships from input–output data pairs. Particularly, the relationships from input–output vehicle-trailer data pairs can be used for vehicle-trailer system state and parameter estimation as shown in Fig. 2.2. Training neural networks using collected data to estimate vehicle parameters and states are widely studied in the literature [119, 120, 121, 122, 123, 124, 125, 126].

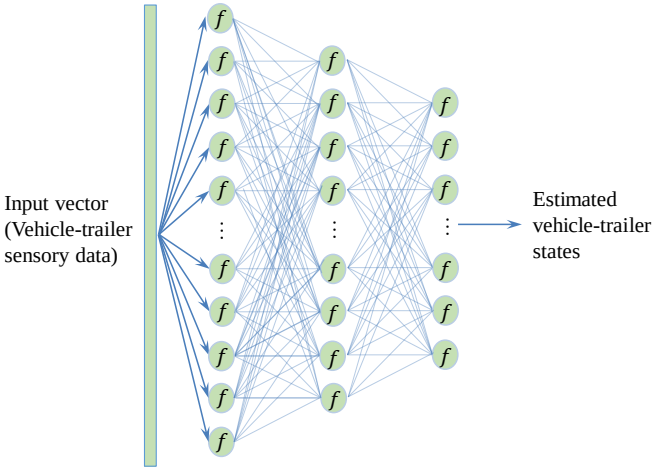

Figure 2.2: Deep neural network model for vehicle-trailer state estimation.

Among the studies following this approach, sparse autoencoder and softmax regression were used in [127], to form a Deep Neural Network (DNN) structure to classify the road excitation for semi-active suspension systems. Correspondingly, a hybrid-learning based classification method was proposed in [128] to classify the braking intensity to three levels by developing a supervised random forest model. A recurrent neural state estimator was designed to estimate the vehicle roll angle in [129]. The inputs of the designed estimator were selected based on the vehicle dynamic model. The proposed estimator contains long

short-term memory cells and predicts the roll angle based on the lateral acceleration, steering wheel angle, and outputs of the control system. Similarly, the vehicle roll angle was estimated using a neural network method in [130]. The performance of the trained neural network in [130] for estimating the vehicle roll angle indicates that the neural network results are comparable with model-based estimation techniques and in some cases the neural network approach performs better than the model-based estimation.

A general regression neural network was proposed to estimate the vehicle sideslip angle in [131, 132]. The results of this works indicate that the neural network is able to reach an excellent estimation quality while generalizing over the different tires, surfaces, and driving situations. In [133], a machine learning approach was proposed to estimate the engine torque which is very important in the automotive industry. In this work, an engine torque model was used to investigate the importance of the inputs to the designed neural network.

Moreover, the trailer mass information can be used for estimating other vehicle-trailer system parameters as well. For instance, since conventional vehicles usually come with independent suspensions, the normal tire load transfer can be determined from the static load on the sprung mass [134, 135]. Correspondingly, a neural network approach was developed and tested to improve the accuracy of multiple sensor weight in motion systems in [136] by considering the suspension displacements. In this work, due to the difficulty to inverse the model that describes the dynamical vehicle pavement interaction, the neural network method was utilized to estimate the static truck weight. The simulation and experimental results for the designed DNN in [136] demonstrate an accurate estimation on the truck weight. However, the algorithm was tested and validated for one vehicle and there is no confirmation for the designed neural network to be generic among the vehicle types. In [137], a DNN approach was proposed to estimate the vehicle-trailer system states/parameters. In this work, the proposed DNN gives decent angle estimation, with the network trained on LIDAR data being superior. However, the model-based approaches were shown to be more accurate and more robust [137].

Table 2.3: Vehicle-trailer hitch, roll, sideslip, and yaw angle estimation studies.

Estimated state/parameter	Case study	Measurements used	Model used	Estimations methodology	Assumptions	References
Tire cornering stiffness for both vehicle and trailer	Agricultural vehicle with trailer	δ, θ, τ	Single-track model	KF	Low speed conditions, trailer parameters assume to be known	[138]
Sideslip angle	Articulated heavy vehicle	ϕ_1, a_{y1}, a_{y2} r_1, r_2, δ	VT roll dynamic model	LAEKF, LAUKF, FUKF	C and μ are known, articulated angle and steering angle are small	[95, 93]
Sideslip angle, yaw angle	Articulated vehicle	ω, δ, X,Y	Four-wheel vehicle model	MHE, NMHE	Known trailer parameters, constant low longitudinal speed	[139, 140]
Vehicle velocity, articulated angle	Load Haul dump vehicle	a_{x1},δ	Kinematic model	EKF, PF, MHE, GA	Disturbances are normally distributed	[141]
Articulated angle	Heavy goods vehicle	T_{sh}	Kinematic model	Vision based UKF	Flat trailer front face, trailer length is known	[35, 36, 37]
Articulated angle	Articulated vehicle	d_t	Kinematic model	KF, EKF	Flat surface, with no slipping	[42, 34, 41, 39, 40]
Articulated angle	Articulated vehicle	C_{am}	-	Vision based	Known hitch point location	[29, 28, 36] [142, 143]
Articulated angle	Commercial vehicle	r_1, v_1 δ	VT single-track model	LO	Low speed, wide trailer front face, roll motion is ignored	[20, 27, 25, 24, 26]
Roll angle	Vehicle semi trailer vehicle	r_1, u, v_1	VT dynamic model	UIO, SOSMO	Pitch and bounce dynamics are neglected	[87, 86] [144]
Roll angle with fault detection	Heavy articulated vehicle	δ, r_1, u, v_1	VT roll dynamic model	LO	Hydraulic flow is incompressible	[91]
Roll angle	Heavy articulated vehicle	r_1, a_{y1}	VT roll dynamics model	HMM	Possible number of observation	[145]
Articulated angle	Articulated vehicle	C_{am}	-	MLE, OLS, PCA	The point cloud is assumed to be bivariate Gaussian distributed	[33]
Vehicle and trailer heading angle	Articulated vehicle	δ, r_1, r_2	Nonlinear kinematic model	AUKF	There is no side angle, Gaussian noise	[146]
Sideslip angle	Articulated vehicle	δ, u, v_1	Lateral dynamics	LO	CG located at the middle VT track width	[147, 148]

2.3 Conclusions and Discussions

In this chapter, an overview of state and parameter estimation for vehicle-trailer systems, and the main approaches for vehicle-trailer states/parameters estimations were reviewed. Although the estimation techniques have been widely applied in this areas, they still encounter many limitations such as limited coverage, model simplification, and severe assumptions that may not be valid all the time. For the existed estimators in the literature, the discussed algorithms were summarized in tables, and their critical assumptions were highlighted. Table 2.3, summarizes the papers cited in this work based on their approaches, measurement signals, and critical assumptions they had considered for estimating the vehicle-trailer system states and parameters.

In addition, as Machine Learning (ML) techniques used for vehicle-trailer state and parameter estimation were also reviewed. It was discussed that collecting consistent data is the biggest challenge of such methods.

Based on the related works in the literature, non-model-based techniques require large amount of data with an acceptable level of consistency, while model-based techniques require significant excitation levels to achieve an accurate estimation of the vehicle-trailer state and parameter estimation. As some of the existing estimators in the literature have been validated by simulation studies, additional investigations are needed to prove the efficacy of the proposed methods with experimental studies.

Based on the literature, the hybrid approaches that are designed based on the system kinematic/dynamics relations and non-model-based approaches for vehicle-trailer state and parameter estimations, have better performance. Hybrid approaches are built upon understandings of the nature of the system, and the network needs to be constructed in a way that captures the physical principles without significantly increasing the network complexity and thus causes much slower training. Therefore, conventional ML approaches still remains a competitive candidate for vehicle-trailer system state estimation because of two reasons: first, it is usually simpler and easy to build and train; second, they do not require much a priori knowledge of the nature of the system [149].

Chapter 3

Vehicle-Trailer Modeling

3.1 Introduction

In this chapter first, the motion dynamics of the vehicle-trailer system is modeled and then, the trailer parameter estimation feasibility is investigated based on the trailer on-board sensor configurations. A full trailer states and parameters estimation scheme is also presented in this chapter for different possible vehicle-trailer on-board sensor settings. The remainder of this chapter is organized as follows: In Section 3.2, the main vehicle-trailer kinematic and dynamic models are presented, and the incorporation of the LuGre tire model is explained in Section 3.3. The trailer parameter estimation feasibility is investigated in Section 3.4 based on the trailer on-board sensor settings, and the minimum sensory requirements for full vehicle-trailer estimation is reviewed by considering the vehicle-trailer kinematic and dynamic models in the literature. Conclusions and discussions are provided in Section 3.5.

3.2 Vehicle-Trailer Modeling

A 3-DoF model is considered to represent the motion dynamics of the vehicle-trailer system of interest. Fig. 3.1 illustrates a schematic representation of the vehicle-trailer system configuration. In Fig. 3.1, m_1, m_2, I_{z1} and I_{z2} are the masses and yaw moments of the vehicle and trailer, respectively. The yaw rates of the vehicle and trailer are denoted by

r_1 and r_2. Longitudinal and lateral velocities at the vehicle Centers of Gravity (CG) are denoted by u and v_1, respectively. $F_{xf,i}$, $F_{xr,i}$, $F_{xt,i}$, $F_{yf,i}$, $F_{yr,i}$, and, $F_{yt,i}$ with $i \in (R, L)$ in which R and L refer to the Right and Left side of the vehicle, are the longitudinal/lateral tire forces at front and rear axles of the vehicle, and trailer's axle, respectively. F_{xT} and F_{yT} represent the coupling forces, also known as hitch forces, in longitudinal and lateral directions of the trailer, respectively according to Fig. 3.1.

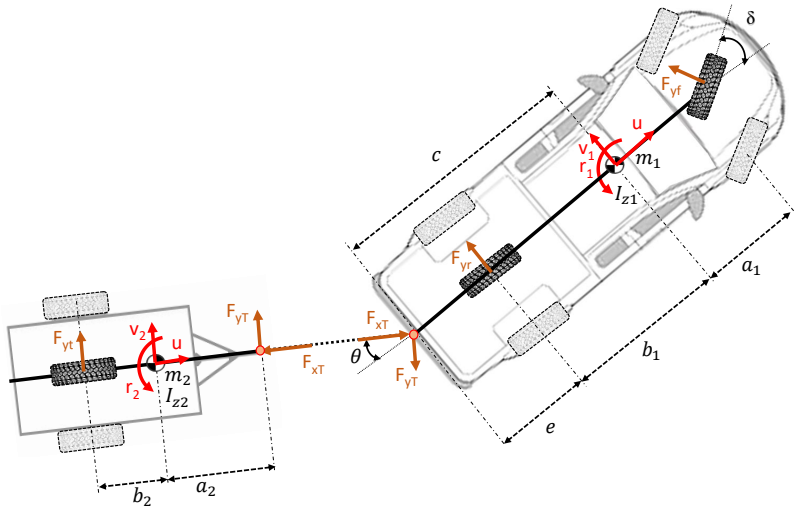

Figure 3.1: Free body diagram of a vehicle-trailer system.

Since they have less influence on the yaw stability, the pitch and body-roll of the vehicle-trailer are neglected [96, 150]. To derive a linear vehicle-trailer model, the following assumptions have been made: (1) the forward speed u remains constant; (2) the vehicle steering angle δ and articulation angle θ are small; and (3) all products of variables are ignored. The equations of motion for the vehicle-trailer system are as follows [96, 151]:

$$m_1(\dot{v}_1 + ur_1) = F_{yf} + F_{yr} - F_{yT}, \tag{3.1}$$

$$I_{z1}\dot{r}_1 = a_1F_{yf} - b_1F_{yr} + cF_{yT}, \tag{3.2}$$

$$m_2(\dot{v}_2 + ur_2) = F_{yt} + F_{yT}, \tag{3.3}$$

$$I_{z2}\dot{r}_2 = -b_2F_{yt} + a_2F_{yT}. \tag{3.4}$$

The linear hitch coupling equations are given by [68]

$$v_2 = -a_2 r_2 - u\theta + v_1 - c r_1, \tag{3.5}$$

$$r_2 = \dot{\theta} + r_1. \tag{3.6}$$

Eliminating coupling forces, the equations (3.1) to (3.6) yield to

$$-m_2 a_2 \ddot{\theta} + (m_1 + m_2)\dot{v}_1 - m_2(a_2 + c)\dot{r}_1 = -u(m_1 + m_2)r_1 + F_{yf} + F_{yr} + F_{yt}, \tag{3.7}$$

$$c m_2 a_2 \ddot{\theta} - c m_2 \dot{v}_1 + (I_{z1} + c^2 m_2 + c m_2 a_2)\dot{r}_1 = c m_2 u r_1 + a_1 F_{yf} - b_1 F_{yr} - c F_{yt}, \tag{3.8}$$

$$(I_{z2} + a_2^2 m_2)\ddot{\theta} - a_2 m_2 \dot{v}_1 + (I_{z2} + a_2^2 m_2 + c m_2 a_2)\dot{r}_1 = m_2 a_2 u r_1 - l_2 F_{yt}, \tag{3.9}$$

where l_2 is the trailer wheel-base. The lateral tire forces at front and rear axles of the vehicle, and trailer's axle are determined using a linear tire model. The linear tire model is considered to address the lateral forces at each axle $F_{iy} = c_i \alpha_i, i \in [f, r, t]$ where α_i is representing the slip angle at each axle as follows [68]:

$$\alpha_f = \delta - \frac{v_1 + a_1 r_1}{u}, \tag{3.10a}$$

$$\alpha_r = -\frac{v_1 - b_1 r_1}{u}, \tag{3.10b}$$

$$\alpha_t = \frac{l_2\dot{\theta} + u\theta + (l_2 + c)r_1 - v_1}{u}. \tag{3.10c}$$

By substituting the lateral tire forces and the side slip angles defined in (3.10), the linear lateral vehicle dynamic model is represented by

$$\mathbf{M}\dot{\mathbf{x}} = \mathbf{D}\mathbf{x} + \mathbf{C}\delta, \tag{3.11a}$$

$$\mathbf{x} = \begin{bmatrix} v_1 & r_1 & \dot{\theta} & \theta \end{bmatrix}^T, \tag{3.11b}$$

$$\mathbf{M} = \begin{bmatrix} m_1 + m_2 & -m_2(a_2 + c) & -m_2 a_2 & 0 \\ -cm_2 & M_{22} & cm_2 a_2 & 0 \\ -a_2 m_2 & M_{32} & I_{z2} + a_2^2 m_2 & 0 \\ 0 & 0 & 0 & 1 \end{bmatrix}, \tag{3.11c}$$

$$\mathbf{D} = -\frac{1}{u} \begin{bmatrix} D_{11} & D_{12} & -c_t l_2 & -c_t u \\ D_{21} & D_{22} & c l_2 c_t & c c_t u \\ -l_2 c_t & D_{32} & l_2^2 c_t & l_2 c_t u \\ 0 & 0 & -u & 0 \end{bmatrix}, \tag{3.11d}$$

$$\mathbf{C} = \begin{bmatrix} c_f & a_1 c_f & 0 & 0 \end{bmatrix}^T, \tag{3.11e}$$

where $M_{22} = I_{z1} + c^2 m_2 + c m_2 a_2$, $M_{32} = I_{z2} + a_2^2 m_2 + c m_2 a_2$, $D_{11} = c_f + c_r + c_t$, $D_{12} = a_1 c_f - b_1 c_r - (l_2 + c) c_t + (m_1 + m_2) u^2$, $D_{21} = a_1 c_f - b_2 c_r - c c_t$, $D_{22} = a_1^2 c_f + b_1^2 c_r + c(l_2 + c) c_t - c m_2 u^2$, $D_{32} = l_2(l_2 + c) c_t - m_2 a_2 u^2$. The model (3.11) can also be presented in the conventional state space form as

$$\dot{\mathbf{x}} = \mathbf{A}\mathbf{x} + \mathbf{B}\delta, \tag{3.12}$$

where $\mathbf{A} = \mathbf{M}^{-1}\mathbf{D}$ and $\mathbf{B} = \mathbf{M}^{-1}\mathbf{C}$. To study the static stability of the vehicle-trailer system, the equilibrium condition ($\dot{\mathbf{x}} = 0$) is considered. Thus, by considering Routh's stability criterion under the constant longitudinal velocity assumption, the stability of the system leads to the following condition for the understeer coefficient [68]

$$l_1 + K_{us} u^2 > 0, \tag{3.13a}$$

$$K_{us} = \frac{m_1(c_r b_1 - c_f a_1) - m_2 b_2 (c_f(a_1 + c) + c_r e)}{c_f c_r l_1}, \tag{3.13b}$$

where l_1 is the vehicle wheel-base. The stability condition defined by the understeer coefficient is used for finding the critical velocity and also comparing the linear and non-linear lateral dynamic presented. As mentioned, the linear lateral dynamic presented in (3.12) is derived based on the linear tire model. In the linear tire model, it is assumed that the tire forces has a linear relationship with the slip angle which may not be a realistic assumption for the situation where the slip angle is large. Therefore, to address this issue, a non-linear vehicle-trailer lateral dynamic is described in the next section.

3.3 Incorporation of the LuGre Tire Model

In this section, the vehicle-trailer lateral dynamics is incorporated with the LuGre tire model to better represent the non-linear behaviour of the system due to tire interactions.

3.3.1 LuGre Tire Model

Tire forces are the key features for driving the vehicle equation of motion. To be able to model the vehicle behaviour accurately, an accurate tire model should be considered. The tire behaviour has been modeled in numerous studies and used for vehicle state estimation or stability analysis [152, 69, 153, 154, 70]. The tire behaviour is modeled by a group of curved lines that find the relationship between the tire-road friction, normal tire load, slip ratio, slip angle, and tire forces. These curved lines are generated from the experimental test, and the most well-known tire model is Pacejka model [71]. Compared to other conventional models, the LuGre tire model uses relative velocities in both longitudinal and lateral directions ($v_{rx} = R_e\omega - u$ and $v_{ry} = u\alpha$, where R_e and ω represent the tire effective radius and angular velocity, respectively) rather than slip ratio $\lambda = v_{rx}/max[R_e\omega, u]$ and slip angle α to model the tire behaviour.

As mentioned, the longitudinal and lateral relative velocities are obtained by $v_{rx} = R_e\omega - u$ and $v_{ry} = u\alpha$. v_{rx}, v_{ry}, α, u, R_e, and ω are all defined in the tire coordinate system at each corner (e.g. for front tire in single-track model, they lead to $v_{rx,f}$, $v_{ry,f}$, α_f, $u_f = u$, $R_{e,f}$, and ω_f). The average lumped model friction state (deflection) of the bristle/patch element located at the point ζ is denoted by $\mathbf{z} = [\mathcal{Z}_x(\zeta, t), \mathcal{Z}_y(\zeta, t)]^T \in \mathbf{R}^2$, with longitudinal component, $\mathcal{Z}_x(\zeta, t)$ and lateral component, $\mathcal{Z}_y(\zeta, t)$. The tire internal lateral state $\mathcal{Z}_y(\zeta, t)$ has the following dynamics under the pure-slip assumption [72]:

$$\dot{\mathcal{Z}}_y(\zeta, t) = v_{ry} - \left(\frac{\sigma_0|v_{ry}|}{\Theta g(v_{ry})} + \kappa R_e|\omega|\right)\mathcal{Z}_y(\zeta, t), \tag{3.14a}$$

$$g(v_{ry}) = \mu_c + (\mu_s - \mu_c)e^{-|\frac{v_{ry}}{V_s}|^{\bar{\tau}}}, \tag{3.14b}$$

where μ_c and μ_s are the normalised Coulomb and static friction, respectively. σ_0, Θ, and κ represent the tire rubber stiffness, road friction condition, and average lumped model, respectively. σ_0 and Θ are the tire specifications that are obtainable by experimental tests

[155]. The average lumped model, κ, is suggested to be set by $\kappa = 7/6L$, where L is the tire patch length [72]. For the distributed LuGre tire model, the tire parameter $\bar{\tau}$, is 0.5. The transient between the two friction states is addressed by the Stribeck velocity, V_s.

The tire internal lateral state, $\mathcal{Z}_y$, is obtained under the pure-slip assumption. Given that the tire model with the mentioned assumptions cannot address the decreasing lateral tire capacities caused by the tire slippage, a modified LuGre tire model known as combined-slip LuGre tire model was proposed in [73]. In the proposed model, the internal state $\mathcal{Z}_j, j \in [x, y]$ for both longitudinal and lateral directions with the combined-slip condition is described as [73]

$$\dot{\mathcal{Z}}_j = v_{rj} - C_0 \mathcal{Z}_j - \kappa R_e |\omega| \mathcal{Z}_j, \tag{3.15a}$$

$$C_0 = \frac{\| \mathbf{M}_c^2 \mathbf{v}_r \| \sigma_{0j}}{g(\mathbf{v}_r) \mu_{cj}^2}, \tag{3.15b}$$

$$g(\mathbf{v}_r) = \frac{\| \mathbf{M}_c^2 \mathbf{v}_r \|}{\| \mathbf{M}_c \mathbf{v}_r \|} + \left(\frac{\| \mathbf{M}_s^2 \mathbf{v}_r \|}{\| \mathbf{M}_s \mathbf{v}_r \|} - \frac{\| \mathbf{M}_c^2 \mathbf{v}_r \|}{\| \mathbf{M}_c \mathbf{v}_r \|} \right) e^{-\sqrt{|\frac{\| \mathbf{v}_r \|}{V_s}|}}, \tag{3.15c}$$

$$\mathbf{M}_s = \begin{bmatrix} \mu_{sx} & 0 \\ 0 & \mu_{sy} \end{bmatrix}, \mathbf{M}_c = \begin{bmatrix} \mu_{cx} & 0 \\ 0 & \mu_{cy} \end{bmatrix}, \tag{3.15d}$$

$$\mathbf{v}_r = [v_{rx}, v_{ry}]^T. \tag{3.15e}$$

The transient function $g(\mathbf{v}_r)$, represents the relation between the Coulomb and static friction in the combined-slip tire model. The longitudinal relative velocity in the traction and brake cases are defined by $v_{rx} = \lambda R_e \omega$ and $v_{rx} = \lambda u$, respectively. By considering the internal lateral tire states, the normalised friction force, $\mu_j = F_j / F_z$ where $F_j, j \in [x, y]$ and F_z represent the longitudinal, lateral, and normal tire forces, respectively, with the average lumped LuGre model yields to

$$\boldsymbol{\mu} = \boldsymbol{\sigma_0} \mathbf{z} + \boldsymbol{\sigma}_1 \dot{\mathbf{z}} + \boldsymbol{\sigma}_2 \mathbf{v}_r, \tag{3.16a}$$

$$\boldsymbol{\sigma}_j = \begin{bmatrix} \sigma_{jx} & 0 \\ 0 & \sigma_{jy} \end{bmatrix}, j \in [0, 1, 2], \tag{3.16b}$$

where $\boldsymbol{\mu} \in \mathbf{R}^2$ describes the normalised friction force in both longitudinal and lateral directions. $\boldsymbol{\sigma}_0$, $\boldsymbol{\sigma}_1$, and $\boldsymbol{\sigma}_2$ represent the rubber stiffness, rubber damping, and relative viscous damping, in both longitudinal and lateral directions, respectively. As shown in (3.16a), the calculated tire forces obtained by the average lumped LuGre model-based on the distributed normal force over the patch line. The LuGre tire models in (3.14a) and (3.15a) are used to develop the vehicle-trailer lateral dynamics as described in the next subsection.

3.3.2 Lateral Dynamics with Pure-Slip LuGre Tire Model

In this subsection, the vehicle-trailer lateral dynamics described in (3.12) is incorporated with the LuGre tire model for pure-slip cases.

Steady-state dynamics

By considering $\dot{\mathcal{Z}}_y(\zeta, t) = 0$ at steady-state, the steady-state LuGre model is obtained as follows:

$$\mu_{yi} = \left(\frac{\rho_i}{u|\alpha_i| + \gamma_i \rho_i} + \sigma_{2y,i} \right) u\alpha_i, \tag{3.17a}$$

$$\rho_i = \Theta g(v_{ry,i}), \tag{3.17b}$$

$$\gamma_i = \kappa_i R_{e,i} \omega_i / \sigma_{0y,i}, \tag{3.17c}$$

where $i \in [f, r, t]$, and the slip angle at each axle is presented by α_i which is described in (3.10). To analyse the effect of slip angle, the normalised lateral tire force (3.17a) expressed as follows for the cases where $|\alpha_i| \ll \gamma_i \rho_i / u$:

$$\mu_{yi} = \Theta \left(\frac{1}{\gamma_i} + \sigma_{2y,i} \right) u\alpha_i, \tag{3.18}$$

where $\Theta \in (0, 1]$ is a constant coefficient that represents the effect of road condition which benefits in presenting the tire model close to the real tire behaviour [156, 157]. The linear tire model was compared with normalised lateral forces of the pure-slip LuGre model in [156]. For the steady-state behaviour, the vehicle-trailer lateral dynamics with normalised lateral forces of the pure-slip LuGre model leads to

$$-m_2 a_2 \ddot{\theta} + (m_1 + m_2)\dot{v}_1 - m_2(a_2 + c)\dot{r}_1 = -u(m_1 + m_2)r_1 + \mu_{yf} F_{zf} + \mu_{yr} F_{zr} + \mu_{yt} F_{zt}, \tag{3.19}$$

$$cm_2 a_2 \ddot{\theta} - cm_2 \dot{v}_1 + (I_{z1} + c^2 m_2 + cm_2 a_2)\dot{r}_1 = cm_2 u r_1 + a_1 \mu_{yf} F_{zf} - b_1 \mu_{yr} F_{zr} - c\mu_{yt} F_{zt}, \tag{3.20}$$

$$(I_{z2} + a_2^2 m_2)\ddot{\theta} - a_2 m_2 \dot{v}_1 + (I_{z2} + a_2^2 m_2 + cm_2 a_2)\dot{r}_1 = m_2 a_2 u r_1 - l_2 \mu_{yt} F_{zt}, \tag{3.21}$$

where $F_{zf} = (m_1 g b_1 - m_2 g a_2 e/l_2)/l_1$, $F_{zr} = (m_1 g a_1 + m_2 g a_2 (l_1 + e)/l_2)/l_1$, and $F_{zt} = a_2 g m_2 / l_2$. The normal axle forces are measured using acceleration measurement and load transfer [158, 159]. The normalised lateral force (3.17a) can be re-written in the following form by considering the non-linear part:

$$\mu_{yi} = k_i u \alpha_i - \frac{1}{\gamma_i \left(1 + \frac{\gamma_i \rho_i}{u|\alpha_i|}\right)} u \alpha_i = \Lambda_i \alpha_i, \tag{3.22}$$

where $\alpha_i, i \in [f, r, t]$ is the slip angle as defined in (3.10). The term $\kappa_i u \alpha_i$ is represented the linear part of (3.18). The second term in (3.22) illustrates the non-linear behaviour of the lateral tire forces which happens when the slip angle is large. By considering the static normal force distribution at each axle and replacing (3.22) in equations (3.19) to (3.21), the vehicle-trailer lateral dynamics are represented in the state space form

$$\dot{\mathbf{x}} = \mathbf{A}(t)\mathbf{x} + \mathbf{B}(t)\delta + \mathbf{H}(t), \tag{3.23}$$

$$\begin{aligned} \mathbf{A}(t) &= \mathbf{M}^{-1}\mathbf{D}_n(t), \\ \mathbf{B}(t) &= \mathbf{M}^{-1}\mathbf{C}_n(t), \end{aligned} \tag{3.24a}$$

$$\mathbf{D}_n = -\begin{bmatrix} D_{n,11} & D_{n,12} & -k_t F_{zt} l_2 & -k_t F_{zt} u \\ D_{n,21} & D_{n,22} & c l_2 k_t F_{zt} & c k_t F_{zt} u \\ -l_2 k_t F_{zt} & D_{n,32} & l_2^2 k_t F_{zt} & l_2 k_t F_{zt} u \\ 0 & 0 & -1 & 0 \end{bmatrix}, \tag{3.24b}$$

$$\mathbf{C}_n = \begin{bmatrix} k_f F_{zf} u & a_1 k_f F_{zf} u & 0 & 0 \end{bmatrix}^T, \tag{3.24c}$$

$$\begin{aligned} D_{n,11} = k_f F_{zf} + k_r F_{zr} + k_t F_{zt}, D_{n,12} = a_1 k_f F_{zf} - b_1 \\ k_r F_{zr} - (l_2 + c) k_t F_{zt} + (m_1 + m_2) u, D_{n,21} = a_1 k_f F_{zf} \\ -b_2 k_r F_{zr} - c k_t F_{zt}, D_{n,32} = l_2 (l_2 + c) k_t F_{zt} - m_2 a_2 u, \\ D_{n,22} = a_1^2 k_f F_{zf} + b_1^2 k_r F_{zr} + c(l_2 + c) k_t F_{zt} - c m_2 u, \end{aligned} \tag{3.24d}$$

where $\mathbf{M}$ is defined in (3.11c). In (3.23), the $\mathbf{H}(t)$ term represents the non-linear behaviour of the system in pure-slip condition, and is calculated as shown in (3.25), where

$$\mathbf{H}(t) = \frac{1}{\mathrm{W}} \begin{bmatrix} \sum_i \phi_i \left(I_{z1} I_{z2} + I_{z1} a_2^2 m_2 + I_{z2} m_2 c^2 + \mathcal{D}_i \right) \alpha_i - \phi_t m_2 I_{z2} c^2 \alpha_t \\ \sum_i \phi_i \left(\mathcal{E}_i (a_2^2 m_1 m_2 + \mathcal{F}_i) \right) \alpha_i \\ \sum_i \phi_i \left(-\mathcal{E}_i \left(m_1 m_2 a_2 (a_2 + c) + I_{z2} (m_1 + m_2) \right) + m_2 (I_{z1} a_2 - l_2 c) \right) \alpha_i - \phi_t \mathcal{K} \alpha_t \\ 0 \end{bmatrix} \tag{3.25}$$

$$\mathrm{W} = I_{z1} m_1 m_2 a_2^2 + I_{z2} m_1 m_2 c^2 + I_{z1} I_{z2} m_1 + I_{z1} I_{z2} m_2, \tag{3.26a}$$

$$\mathcal{D}_f = I_{z2} a_1 c m_2, \mathcal{D}_r = -I_{z2} b_1 c m_1, \mathcal{D}_t = -I_{z1} a_2 l_2 m_2, \tag{3.26b}$$

$$\begin{aligned} \mathcal{F}_f = 2 m_1 I_{z2} a_1 + I_{z2} c m_2, \mathcal{F}_r = I_{z2} c m_2 - 2 m_1 I_{z2} b_1, \\ \mathcal{F}_t = c a_2 l_2 m_1 m_2 - m_1 I_{z2} c, \end{aligned} \tag{3.26c}$$

$$\mathcal{K} = l_2 (m_1 m_2 c^2 + a_2 m_1 m_2 c + I_{z1} m_1 + I_{z1} m_2), \tag{3.26d}$$

$$\mathcal{E}_f = a_1, \mathcal{E}_r = -b_1, \mathcal{E}_t = -c, \phi_i = \frac{-1}{\gamma_i \left(1 + \frac{\gamma_i \rho_i}{u |\alpha_i|} \right)} u F_{zi}. \tag{3.26e}$$

$\mathbf{H}(t)$ can be used to find the magnitude of the non-linear behaviour of the system in pure-slip condition comparing with linear model.

Remark 3.1: The norm of the non-linear term $\mathbf{H}(t)$ is a bounded function of the vehicle front/rear and trailer slip angles [160].

The non-linear term $\mathbf{H}(t)$ can also be expressed in terms of state vector. To do so, for the large slip angle ($|\alpha_i| \gg \gamma_i \rho_i / u$), the normalised lateral forces shown in (3.17a) are written as $\mu_{yi} = \rho_i sgn(\alpha_i) + \sigma_{2y,i} u \alpha_i$, leading to

$$\mathbf{H}(t) = \mathcal{A}(t)\mathbf{x} + \mathcal{B}(t)\delta, \tag{3.27}$$

$$\mathcal{A} = \mathbf{A} + \mathbf{Q}_A, \tag{3.28a}$$

$$\mathcal{B} = \mathbf{B} - \mathbf{Q}_B, \tag{3.28b}$$

$$\mathbf{Q}_A = -\frac{1}{u}\begin{bmatrix} m_1 & m_1 a_1 & -l_2 & -u \\ cm_1 & m_1 + m_2 & cl_2 & cu \\ -l_2 & l_2(l_2 + c) & l_2^2 & l_2 u \\ 0 & 0 & -u & 0 \end{bmatrix}, \tag{3.28c}$$

$$\mathbf{Q}_B = \begin{bmatrix} b_1 & a_1 & cl_1 & a_2 a_1 \end{bmatrix}^T. \tag{3.28d}$$

By substituting (3.27) into (3.23), the vehicle-trailer lateral dynamics for large slip angles ($|\alpha_i| \gg \gamma_i \rho_i / u$) can be written as

$$\dot{\mathbf{x}} = \underbrace{(\mathbf{A} + \mathcal{A})}_{\bar{\mathbf{A}}}\mathbf{x} + \underbrace{(\mathbf{B} + \mathcal{B})}_{\bar{\mathbf{B}}}\delta. \tag{3.29}$$

Remark 3.2: The term $\mathbf{H}(t)$ is a matched function of the lateral dynamic model for the large slip angles and can be incorporated with the system model[161, 162].

Transient dynamics

The average lumped LuGre tire model (3.14a) can be rewritten as

$$\begin{aligned}\dot{\mathcal{Z}}_{yi}(t) &= -\left(\frac{\sigma_0|v_{ry}|}{\Theta g(v_{ry})}+\kappa R_e|\omega|\right)\mathcal{Z}_y(\zeta,t)+v_{ry} = -\left(\sigma_0\gamma_i(t)+\frac{\sigma_0 u|\alpha_i(t)|}{\rho_i(t)}\right)\mathcal{Z}_y(\zeta,t)+v_{ry}\\ &= -\underbrace{\frac{\sigma_{0i}u}{\rho_i(t)}\left(\frac{\gamma_i(t)\rho_i(t)}{u}+|\alpha_i(t)|\right)}_{\mathcal{P}_\mathbf{i}(\mathbf{t})}\mathcal{Z}_{yi}(t)+v_{ry,i}(t),\end{aligned} \tag{3.30}$$

where $\rho_i(t)$ and $\gamma_i(t)$ are defined in (3.17b) and (3.17c), respectively. To analyse the transient mode of the average lumped LuGre tire model, the solution of (3.14a) is derived as follows:

$$\mathcal{Z}_{yi}(t) = \mathcal{Z}_{yi}(0)e^{-t\mathcal{P}_i(t)}+\int_0^t e^{-\mathcal{P}_i(\tau)(t-\tau)}v_{ry,i}(\tau)d\tau. \tag{3.31}$$

For small slip angles ($|\alpha_i(t)| \ll \gamma_i(t)\rho_i(t)/u$), the linear part leads to $\mathcal{P}_i(t) = \sigma_{0i}\gamma_i(t) = \kappa_i R_{e,i}\omega_i(t)$. Thus, the solution of (3.14a) becomes $\mathcal{Z}_{yi}(t) = \int_0^t e^{-\kappa_i R_{e,i}\omega_i(\tau)(t-\tau)}v_{ry,i}(\tau)d\tau$ assuming zero initial condition, which is a simpler version of (3.31). By considering $\omega_i(t) \in [\omega_l, \omega_u]$ where ω_u and ω_l are the wheel angular speeds' upper and lower bounds, the $\int_0^t e^{-\kappa_i R_{e,i}\omega_i(\tau)(t-\tau)}v_{ry,i}(\tau)d\tau$ is an increasing function of t which leads the internal tire state to

$$\frac{u\alpha_i(t)(1-e^{-\kappa_i R_{e,i}\omega_u t})}{\kappa_i R_{e,i}\omega_u} < \mathcal{Z}_{yi}(t) < \frac{u\alpha_i(t)(1-e^{-\kappa_i R_{e,i}\omega_l t})}{\kappa_i R_{e,i}\omega_l}. \tag{3.32}$$

Thus, the normalised lateral force $\mu_{yi}(t), i \in [f, r, t]$ for the linear cases can be written as

$$\mu_{yi}(t) = \Theta[\frac{1}{\gamma_i(t)}+e^{-\kappa_i R_{e,i}\omega_i(t)t}\left(\sigma_{1i}-\frac{1}{\gamma_i(t)}\right)+\sigma_{2i}]u\alpha_i(t). \tag{3.33}$$

By substituting (3.33) in equations (3.19) to (3.21), the lateral dynamic model is obtained as

$$\dot{\mathbf{x}}(t) = \bar{\bar{\mathbf{A}}}(t)x(t)+\bar{\bar{\mathbf{B}}}\delta(t)+\bar{\mathbf{H}}(t), \tag{3.34}$$

where $\bar{\bar{\mathbf{A}}}(t)$ has the same elements as $\mathbf{A}(t)$ in (3.23) has but $k_i(t) \in [f, r, t]$ is replaced by

$$\bar{k}_i(t) = \Theta \left[\frac{1}{\gamma_i(t)} + e^{-\kappa_i R_{e,i} \omega_i(t) t} \left(\sigma_{1i} - \frac{1}{\gamma_i(t)} \right) + \sigma_{2i} \right]. \tag{3.35}$$

The non-linear part $\bar{\mathbf{H}}(t)$ is the same as $\mathbf{H}(t)$ shown in (3.25) but $\phi_i(t)$ is to be replaced by $\bar{\phi}_i(t) = \phi_i(t) + \Phi_i(t)$ where

$$\begin{aligned} \Phi_i(t) = -e^{-\sigma_{0i}\gamma_i(t)t/\rho_i(t)} \Theta \left(\sigma_{1i} - \frac{1}{\gamma_i(t)} \right) + \\ e^{-\sigma_{0i}\gamma_i(t)t} \left(\sigma_{1i} - \frac{\rho_i(t)}{u|\alpha_i(t)| + \gamma_i(t)\rho_i(t)} \right) e^{-\sigma_{0i} u |\alpha_i(t)| t/\rho_i(t)}. \end{aligned} \tag{3.36}$$

$\Phi_i(t)$ in (3.36) exponentially converges to zero. Therefore, a reasonable estimation accuracy will be obtained by considering the steady-state lateral dynamic model (3.29).

3.4 Full Vehicle-Trailer State Estimation Scheme

In this section first, the trailer parameter estimation feasibility is investigated based on the trailer on-board sensor settings, then a full trailer state and parameter estimation scheme is presented.

3.4.1 Parameter Estimation Feasibility

Since several states/parameters of the trailer need to be estimated for control and stability analysis purposes, different set of sensors can be considered. Therefore, it would be better to first check the trailer state and parameter estimation feasibility with respect to different sets of sensors, which can be used in the system. Fig. 3.2 illustrates the feasibility of states/parameters estimation by considering different set of sensors in which the check and cross marks mean the state and parameter with the set of sensors shown in the first left column can be estimated or not. Given that the kinematic relationships are valid in low speed operations, the estimation process is divided into two regions, low speed conditions in which the kinematic relationships are valid, and high speed conditions in which some assumptions such as small hitch angle or small steering angle, are valid. The assumptions for the low speed condition are as follows:

- The vehicle-trailer is driven by low speed, $u < 35$km/h,
- Hitch angle is measured by ultra-sonic sensors,
- Kinematic relation for hitch angle is valid,

and the assumptions for the high speed condition are as follows:

- The vehicle-trailer is driven by high speed, $u > 35$km/h,
- Vehicle and trailer both have same longitudinal acceleration, $a_{x1} \approx a_{x2}$,
- The hitch angle and steering angle are small.

To reach high speeds, the vehicle-trailer must first pass a low speed region. Therefore, any constant/geometrical trailer parameter that estimates in the low speed condition can be considered as a known trailer parameter with some level of uncertainty in the high speed operation. In other words, the idea behind the motion categorization is to estimate the trailer parameters as much as possible in the low speed operation as long as the mentioned assumptions are valid, and then use them with some level of uncertainty in the high speed operation as known parameters.

Based on the estimation and control purposes, the states/parameters can be categorized into three groups based on their priority. By considering the effect of trailer on the towing vehicle, the hitch forces, CG location, and hitch angle are the most important info among the trailer states/parameters. For instance, the CG location plays an important role in trailer instability modes especially for trailer snaking as the poles of the system are related to the CG location value. Therefore, hitch forces, hitch angle, and CG location are considered as primary states/parameters and highlighted in dark green.

Due to the fact that control goals are not unique, other parameters and states may add to the primary states/parameters but generally, the rest of states/parameters are considered as secondary states/parameters and highlighted in light green except trailer tire's forces. As shown in the literature, the trailer tire forces rarely need to be estimated. Therefore, trailer tire's forces in both longitudinal and lateral directions are considered as the tertiary states/parameters and highlighted in yellow.

	Set of sensors		States/Parameters											
			F_{xT}	F_{yT}	a_2	Θ	F_{xt}	F_{yt}	r_2	α_t	m_2	I_{z2}	l_2	v_2
1	• Vehicle IMU • Wheel speed/torque	Low Speed	✓	✓	✗	✗	✗	✗	✗	✗	✗	✗	✗	✗
		High Speed	✓	✓	✗	✗	✗	✗	✗	✗	✗	✗	✗	✗
2	• Vehicle IMU • Wheel speed/torque • Hitch Angle [Ultrasonic] • Tractor GPS	Low Speed	✓	✓	✓	✓	✓	✓	✓	✓	✓	✓	✓	✓
		High Speed	✓	✓	✓	✓	✓	✓	✓	✓	✓	✓	✓	✓
3	• Vehicle IMU • Tractor GPS • Trailer IMU	Low Speed	✗	✗	✗	✓	✗	✗	✓	✗	✗	✗	✗	✗
		High Speed	✗	✗	✗	✓	✗	✗	✓	✗	✗	✗	✗	✗
4	• Vehicle IMU • Wheel speed/torque • Trailer IMU	Low Speed	✓	✓	✓	✓	✓	✓	✓	✓	✓	✓	✓	✓
		High Speed	✓	✓	✓	✓	✓	✓	✓	✓	✓	✓	✓	✓
5	• Vehicle IMU • Tractor GPS • CAN bus (Trailer axle length)	Low Speed	✗	✗	✗	✓	✗	✗	✓	✓	✗	✗	✓	✗
		High Speed	✗	✗	✗	✗	✗	✗	✗	✓	✗	✗	✓	✗
6	• Vehicle/Trailer IMU • Wheel speed/torque • Tractor GPS	Low Speed	✓	✓	✓	✓	✓	✓	✓	✓	✓	✓	✓	✓
		High Speed	✓	✓	✓	✓	✓	✓	✓	✓	✓	✓	✓	✓

- ❖ F_{xT}: Longitudinal hitch force.
- ❖ F_{yT}: Lateral hitch force.
- ❖ a_2: Trailer's CG location (the length from hitch point to trailer center of gravity).
- ❖ Θ: Hitch angle.
- ❖ F_{xt}: Long trailer tire force.
- ❖ F_{yt}: Lateral trailer tire force.
- ❖ r_2: Trailer's yaw rate.
- ❖ α_t: Trailer slip angle.
- ❖ m_2: Trailer's mass.
- ❖ I_{z2}: Trailer momentum of inertia.
- ❖ l_2: Trailer's axel location (the length from hitch point to trailer axel).
- ❖ v_2: Trailer lateral velocity.

( ) Primary states/parameters ( )Secondary states/parameters ( )Tertiary states/parameters

Figure 3.2: The feasibility of trailer's state and parameter estimation.

For each cases based on the system model and measurement signals, the system state and parameter estimations can be addressed. For instance, the estimation scheme for the second case in the Fig. 3.2 where the towing vehicle has IMU, ultra-sonic, and wheel speed/torque sensors is fully explained in the next sub section.

3.4.2 Unknown Trailer State and Parameter Estimation Scheme

For the second case in Fig. 3.2, the vehicle, not trailer, is equipped with an IMU, wheel speed/torque sensor, and ultra-sonic sensors. In this subsection, the general form of the vehicle-trailer equations of motion are introduced to investigate estimation of unknown trailer parameters/states for the second case of the sensor configuration as shown in Fig. 3.2.

For a typical vehicle-trailer system configuration, as illustrated in Fig. 3.1, based on the linear hitch coupling equations, the hitch angle rate $\dot{\theta}$, is the difference between the vehicle and trailer yaw rates (3.6). Thus, by assuming no lateral slip for the trailer, the well-known hitch angle kinematic equation is obtained as [163, 164, 24, 25, 26, 27]:

$$\dot{\theta} = \frac{u \sin\theta}{l_2} - \frac{u \tan\delta}{a_1 + b_1}\left(1 + \frac{e\cos\theta}{l_2}\right), \tag{3.37}$$

where l_2 is the trailer wheel-base. In the hitch angle kinematic equation (3.37), l_2 is the only trailer parameters. Therefore, if the measured/estimated value of the trailer wheel-base is available, the equation (3.37) can be used for any unknown trailer.

As mentioned, the hitch angle is the key variable to investigate the trailer estimation feasibility, which can be calculated based on the hitch coupling equations (3.6). The hitch angle can also be estimated based on the ultra-sonic sensors that are mounted on the rear bumper of the vehicle as shown in (2.1). The estimated hitch angle from the ultra-sonic sensors, $\hat{\theta}$, is then used to identify the trailer wheel-base, also know as trailer axle location. Hence, (3.37) can be written in a discrete Static Parametric Model (SPM) to identify the trailer axle location as:

$$\left(\frac{\hat{\theta}_k - \hat{\theta}_{k-1}}{T_s} + \frac{u_k \tan\delta}{a_1 + b_1}\right) l_2 = u_k \sin\hat{\theta}_k + \frac{u_k e \cos\hat{\theta}_k \tan\delta}{a_1 + b_1}, \tag{3.38}$$

where T_s is the sensor sampling rate. Given that the both regression and output signals in (3.38) are a function of vehicle states, (3.38) can be used to estimate the trailer axle location.

Typically, the vehicle-trailer longitudinal motion equation is considered to estimate the trailer mass. By following the Newtonian law for the forward motion of the vehicle-trailer system, the longitudinal motion equation is obtained as follows:

$$F_{x,fL} + F_{x,fR} + F_{x,rL} + F_{x,rR} - (m_1 + m_2)a_{x1} - F_R = 0, \tag{3.39}$$

where

$$F_R = \mu_R m_1 g + \frac{1}{2}\rho c_d A u^2 = C_0 + C_1 u^2, \tag{3.40}$$

represents the resistance force, c_d is the drag coefficient, μ_R is rolling resistance, ρ is air density, and A is representing the projected cross-sectional area of the vehicle. As introduced by (3.40), the resistance force is a quadratic function of the longitudinal velocity

with two coefficients C_0 and C_1. The longitudinal tire forces can be estimated by considering the wheel dynamics [165]. Therefore, by substituting (3.39) in (3.40) the trailer mass equation is obtained as follows:

$$m_2 = \frac{\mathbf{R}_t \left(\mathbf{T}_t - \mathbf{I}\dot{\boldsymbol{\omega}}_{t,m}\right)}{a_{x1}} - m_1 - \frac{C_0 + C_1 u^2}{a_{x1}} + W_m, \tag{3.41a}$$

$$\mathbf{R}_t = \begin{bmatrix} R_{eff,fL}^{-1} & R_{eff,fR}^{-1} & R_{eff,rL}^{-1} & R_{eff,rR}^{-1} \end{bmatrix}^T, \tag{3.41b}$$

$$\mathbf{T}_t = \begin{bmatrix} T_{fL} & T_{fR} & T_{rL} & T_{rR} \end{bmatrix}^T, \tag{3.41c}$$

$$\dot{\boldsymbol{\omega}}_{t,m} = \begin{bmatrix} \dot{\omega}_{fL} & \dot{\omega}_{fR} & \dot{\omega}_{rL} & \dot{\omega}_{rR} \end{bmatrix}^T, \tag{3.41d}$$

$$\mathbf{I} = \begin{bmatrix} I_{\omega,fL} & 0 & 0 & 0 \\ 0 & I_{\omega,fR} & 0 & 0 \\ 0 & 0 & I_{\omega,rL} & 0 \\ 0 & 0 & 0 & I_{\omega,rR} \end{bmatrix}, \tag{3.41e}$$

where $\boldsymbol{\omega}_{t,m}$ represents the wheel angular velocity at each corner that measured by the wheel speed sensor and to calculate the derivative of this signal Newton's difference quotient technique is used, and the generated signals passed by a low-pass filter. W_m represents the longitudinal uncertainty due to the acceleration measurement, inaccurate resistance force, geometry, and forces. W_m is mostly contributed to the sensor measurement including: longitudinal acceleration, longitudinal velocity, and wheel speed sensor measurement. Estimation algorithms should be considered to cancel the effect of the uncertainty term W_m. More discussion on the estimation algorithm to cancel the effect of uncertainty term is provided in the next chapter.

It has been shown that by following the Newtonian law for the forward motion of the vehicle-trailer system, the trailer mass is obtainable by (3.41a). Therefore, the trailer mass, axle location and, hitch angle are theoretically obtainable by considering the kinematic relations of the vehicle-trailer systems. To investigate other trailer states/parameters listed in Fig. 3.2 estimation feasibility, the 3-degree-of-freedom vehicle-trailer dynamic model is considered as presented in (3.23).

In Fig. 3.1, F_{xT} and F_{yT} represent the coupling forces, also known as hitch forces, in longitudinal and lateral directions, respectively. From the vehicle-trailer lateral dynamics (3.11a), a direct relation for hitch forces and lateral vehicle velocity is obtained as:

$$\mathbf{E}\begin{bmatrix} v_1 \\ F_{xT} \\ F_{yT} \end{bmatrix} = \mathbf{F}, \tag{3.42a}$$

$$\mathbf{E} = \begin{bmatrix} -\frac{C_f}{u}\sin\delta & 1 & 0 \\ -\frac{C_f}{u}\cos\delta - \frac{C_r}{u} & 0 & -1 \\ -\frac{C_r b_1}{u} - \frac{C_f}{u}\cos\delta a_1 & 0 & e+b_1 \end{bmatrix}, \tag{3.42b}$$

$$\mathbf{F} = \begin{bmatrix} F_1 & F_2 & F_3 \end{bmatrix}^T, \tag{3.42c}$$

where $F_1 = m_1 a_{x1} - F_{xf}\cos\delta - F_{xr} + \sin\delta(\frac{C_f}{u}a_1 r_1 - C_f\delta)$, $F_2 = m_1 a_{y1} - F_{xf}\sin\delta + \cos\delta(\frac{C_f}{u}a_1 r_1 - C_f\delta) - \frac{C_r}{u}b_1 r_1$, $F_3 = I_{z1}\dot{r}_1 - F_{xf}\sin\delta a_1 + \cos\delta a_1 C_f(\frac{a_1 r_1}{u} - \delta) + \frac{C_r}{u}b_1^2 r_1$. Therefore, by following the lateral dynamics, a direct relation for hitch forces and lateral vehicle velocity can be obtained as shown in (3.42a).

The trailer CG location and yaw momentum of inertia are correlated based on the vehicle-trailer lateral dynamics. Given the vehicle-trailer lateral dynamics in relations (3.7) to (3.9), the coupled relations for trailer CG location and yaw momentum of inertia can be represented by the following relation:

$$\begin{bmatrix} r_2 & F_{xT}\sin\theta - F_{yT}\cos\theta + C_t b_2\frac{r_1-\dot{\theta}}{u} \\ 0 & -m_2 r_2 - C_t\frac{r_1-\dot{\theta}}{u} \end{bmatrix}\begin{bmatrix} I_{z2} \\ a_2 \end{bmatrix} = \begin{bmatrix} C_t b_2\frac{l_2\dot{\theta}+u\theta+(l_2+c)r_1-v_1}{u} \\ F_{yT}\cos\theta - F_{xT}\sin\theta - m_2(a_{y1} - (e+b_1)r_1) - F_{yt} \end{bmatrix}, \tag{3.43}$$

where $F_{yt} = -C_t(l_2\dot{\theta} + u\theta + (l_2+c)r_1 - v_1)/u$, and C_t represent the trailer lateral tire force and cornering stiffness, respectively. Based on the presented equation for vehicle-trailer systems, the trailer parameters listed in Fig. 3.1 can be estimated for both low and high speed operations. The estimation scheme for unknown trailer parameters/states based on the second case sensor configuration is shown in Fig. 3.3.

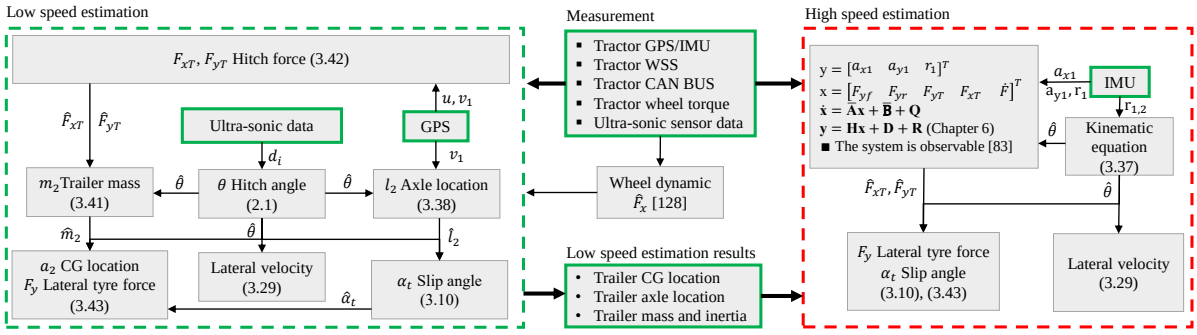

Figure 3.3: Trailer state and parameter estimation feasibility for the second sensor configuration at low and high speeds.

As mentioned, the presented model and measurements are contributed with uncertainties. For instance, W_m in (3.41a) represents the longitudinal uncertainty due to the acceleration measurement, inaccurate resistance force, geometry, and forces which is mostly contributed to the sensor measurement. To cancel the effect of process and measurement noise, optimal filters and estimation algorithms can be applied. The KF approach has been demonstrated to be the strongest method for estimating parameters and multi-sensory data fusion problems with a low computational cost [166, 167]. For the vehicle-trailer system state/parameter identification and estimation issues, two modified KF methods are generally utilized including the UKF and the EKF methods. The EKF method is to prepare almost maximum-likelihood prediction of parameters and states of a discretized linear/nonlinear equations of the motion of the system [168]. The EKF is not an optimal estimator due to its linear counterpart, however, it is optimal if the state transition model and measurement equipment are both linear. Furthermore, EKF has several limitations, however, the literature indicates that it has succeeded in precise estimation for nonlinear model of the vehicle-trailer [169, 170]. In the EKF, the state distribution is assembled based on a Gaussian random variable, which is spread through the linearized model of the system. The UKF is an extension of the Unscented Transformation (UT) which is a method for estimating a random variable [171]. The UKF method estimates the states of the system by espousing a deterministic sampling algorithm which is known as sigma points that could correctly calculate the realistic covariance and mean of the Gaussian random variable with the reasonable level of accuracy [172, 173]. Moreover, the UKF method has less computational cost by terminating the Jacobian matrices, which is the

advantage of UKF by comparison with EKF [174]. Therefore, for estimating the states of the system with uncertain variables, the UKF method is applicable. Given that the observeability is a sufficient condition for implementation of optimal filters (e.g. KF) or estimation algorithms, the estimation error of the UKF is investigated in [175].

3.5 Conclusions and Discussions

In this chapter, an overview of the vehicle-trailer model using linear and nonlinear tire models was introduced. It has been shown that adding a non-linear tire model modifies the fidelity of the model and increases the model accuracy. By considering the LuGre tire model in vehicle-trailer modeling, the system modeling became non-linear. In this particular case, there was a possibility to separate the linear and nonlinear parts, considering the nominal motion dynamics (corresponding to the non-slip case without significant nonlinearity) as the linear part and representing the difference between the high-fidelity nonlinear system model and the linear nominal system model by an additive nonlinearity. The $H(t)$ term in (3.25) represented this additive nonlinearity in the system in pure-slip condition while the other terms are representing the nominal linear behaviour of the system.

A full possible solution for estimating the states and parameters of an unknown trailer was also investigated and the state and parameter estimation feasibility was discussed based on the different on-board sensor settings. The main benefits of state estimations is not only improving the performance of vehicle-trailer control systems, but also enabling autonomous vehicle-trailers.

The proposed approach for the feasibility of the trailer parameter/state estimations have two algorithms for low and high speed conditions. In low speed conditions ($v_x < 35$ km/h), the kinematic relationship between the trailer and vehicle as well as linear tire model are considered to estimate the trailer parameters/states. Then, as the speed of vehicle-trailer increases, the low speed assumptions are no longer valid and instead the high speed assumptions are considered. The estimator algorithms for high speeds are dependent on the low speed estimator outputs (the trailer constant parameters).

Chapter 4

Trailer Mass Estimation

4.1 Introduction

For heavy duty vehicles as well as passenger cars, active safety systems require accurate estimation of the states and parameters of both the vehicle and the trailer, which cannot be measured directly. Trailer mass is an important one of these parameters. An over-loaded trailer could easily place the vehicle-trailer system in unstable conditions. Trailer mass is also important from the driver viewpoints, noting that commercial vehicle drivers are held responsible for traffic safety on the roads and before departure they are required to keep the trailer's payload within the legal range. While the payload value can typically be found from the load description, there are instances where it is not available. Given that the trailer mass can vary depending on the goods and loads the trailer carries, and the trailer mass cannot be measured directly using low cost sensors, it is necessary to estimate it via the integration and processing of data acquired from the sensors installed on conventional vehicle-trailer systems.

The existed vehicle mass estimators in the literature are for vehicle unit itself and when a trailer connects to the towing vehicle, the vehicle mass estimators may not work as the dynamic of the system changes. Therefore, the trailer mass estimation needs to be investigated individually for vehicle-trailer configuration.

For both system model-based and Machine Learning (ML) based approaches, three main challenges exist in the vehicle/trailer mass estimation: (a) reliable identification of

unknown trailer parameters and road friction conditions; (b) modularity of the designed estimators being applicable to different vehicle-trailer configurations; (c) limitations of the available sensors and available measurements. Aiming to develop an estimation approach which tackles all these challenges, the main contribution of this chapter is the design of two novel trailer mass estimators that are modularly applicable to different trailer types and road friction coefficients, one following a system theoretic approach based on vehicle-trailer dynamic model and one based on Deep Neural Networks (DNNs), where the vehicle-trailer dynamics are used to define appropriate inputs for the DNN to be able to make the design modular. Moreover, the performance of the proposed two designs are verified via simulations and experiments compared with existing methods in the literature. The analysis and test results indicate that the proposed designs are accurate and modular with acceptable computational costs, which empower the methods to be implemented on real time. This chapter is organized as follows: In Section 4.2, the proposed dynamic system model-based trailer mass estimation approach is described and the convergence of the trailer mass estimate is analyzed. In Section 4.3, an overall structure of the proposed ML approach is described and a DNN trailer mass estimator is designed using different number of neurons at different layers. A sensitivity analysis with respect to all available measurements from the vehicle-trailer system, which are used as the DNN inputs, is also presented in Section 4.3, along with a discussion of selection of the inputs of the DNN based on this sensitivity analysis. In Section 4.4, training and testing the designed DNN with a set of real-time vehicle-trailer system data is explained. The trailer mass estimation results with the model-based and ML approaches are presented and compared in Section 4.5 with discussion.

4.2 Model-Based Trailer Mass Estimation

The estimated trailer mass can be used for estimating other vehicle/trailer parameters. For instance, since regular vehicles usually come with independent suspensions, the normal tire load transfer can be determined by analysing the static load on the sprung mass [134]. To do so, a dynamic system model-based observer designed for trailer mass estimation is presented in this section.

For the design, a three degree of freedom vehicle-trailer model is considered to investigate the vehicle-trailer states/parameters that are related mathematically to the trailer

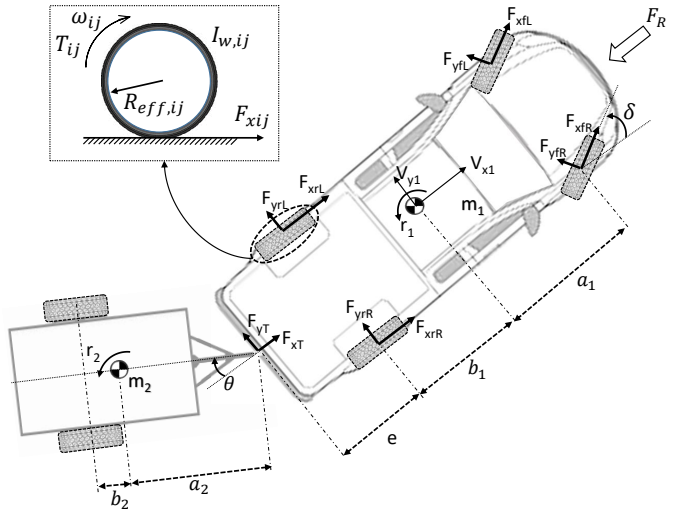

Figure 4.1: A schematic view of a vehicle-trailer system.

mass. A model is considered to derive the dynamic equations of the vehicle-trailer system. Fig. 4.1 shows a schematic representation of a vehicle-trailer system.

In Fig. 4.1, m_1, m_2, r_1, and r_2 are the masses and yaw rates of the vehicle and trailer, respectively. Longitudinal and lateral velocities at the vehicle centers of gravity are denoted by V_x and V_y, respectively. F_{xfi}, F_{xri}, F_{yfi}, and F_{yri}, with $i \in (R, L)$, where R and L refer to the Right and Left side of the vehicle, are the longitudinal and lateral tire forces at front and rear axles of the vehicle, respectively. F_{xT} and F_{yT} represent the coupling forces, also known as hitch forces, in longitudinal and lateral directions, respectively. The equations of motion for the vehicle-trailer system are as follows:

$$\begin{aligned} m_1 a_{x1}(t) = {} & F_{x,rL}(t) + F_{x,rR}(t) + F_{x,fL}(t)\cos\delta(t) + F_{xT}(t) \\ & + F_{x,fR}(t)\cos\delta(t) - F_{y,fL}(t)\sin\delta(t) + F_{y,fR}(t)\sin\delta(t), \end{aligned} \tag{4.1}$$

$$\begin{aligned} m_1 a_{y1}(t) = {} & F_{y,fL}(t)\cos\delta(t) + F_{y,fR}(t)\cos\delta(t) + F_{y,rL}(t) \\ & + F_{y,rR}(t) + F_{yT}(t) + (F_{x,fL}(t) + F_{x,fR}(t))\sin\delta(t), \end{aligned} \tag{4.2}$$

$$m_2 a_{x2}(t) = F_{x,tR}(t) + F_{x,tL}(t) - F_{xT}(t)\cos\theta(t) + F_{yT}(t)\sin\theta(t), \tag{4.3}$$

$$m_2 a_{y2}(t) = F_{y,tR}(t) + F_{y,tL}(t) - F_{yT}(t)\cos\theta(t) - F_{xT}(t)\sin\theta(t), \tag{4.4}$$

where θ represents the hitch angle. Longitudinal and lateral velocities at the vehicle and trailer centers of gravity are denoted by a_{x1}, a_{y1}, a_{x2} and a_{y2}, respectively. In equations (4.1) to (4.4), it is assumed that the longitudinal and lateral accelerations, yaw rate, and steering angle are measurable and the vehicle geometric parameters such as CG location and vehicle length are known. Moreover, the longitudinal tire forces are calculated based on the wheel dynamic as follows [165]:

$$F_{x,ij}(t) = \frac{1}{R_{eff,ij}} \left(T_{ij}(t) - I_{\omega,ij}\dot{\omega}_{ij}(t) \right), \tag{4.5}$$

where $i \in (f, r)$ (front and rear axle), $j \in (L, R)$ (left and right tire). Also, $R_{eff,ij}$ is the wheel effective radius, T_{ij} represents the effective torque on the wheel, $F_{x,ij}$ is the longitudinal tire force, $\dot{\omega}_{ij}$ is the wheel acceleration, $I_{\omega,ij}$ is the wheel momentum of inertia. The goal is to develop a trailer mass estimator utilizing conventional sensor measurements including: wheel speed, vehicle accelerations, and wheel torque. The proposed model-based trailer mass estimation algorithm works based on the torque and wheel speed of the vehicle's tire at each corner as well as the vehicle's longitudinal acceleration as shown in Fig. 4.1. By having the total torque for the vehicle provided by engine and the percentage of torque distribution, the wheel torque at each corner can be calculated. The vehicle longitudinal acceleration is measured by an Inertia Measurement Unit (IMU). Ignoring the torsion stiffness of the axles and the viscous damping of the bearing, the longitudinal tire forces are related to the wheel speed and applied torque as shown in (4.5). The longitudinal dynamic is considered for the trailer mass estimation. If the vehicle-trailer system has lateral movement, the engine's torque is used for both longitudinal and lateral movements. Given that the engine's torque that is used for the lateral movement is not distinguishable from the engine's torque that is used for the longitudinal movement, for the trailer mass estimation, it is assumed that the vehicle-trailer system moves forward ($V_x > 0$) with the small steering angle ($|\delta| < \delta_{th}$, where δ_{th} is the steering angle threshold). By considering these assumptions, the measured engine's torque can be used directly in the longitudinal dynamic for trailer mass estimation. These assumptions have been made to avoid the lateral movement of the vehicle-trailer system. Therefore, the trailer mass estimation algorithm runs once the above-mentioned assumptions are satisfied.

By following the Newtonian law for the forward motion of the vehicle-trailer system, the longitudinal motion equation is obtained as follows:

$$F_{x,fL} + F_{x,fR} + F_{x,rL} + F_{x,rR} - (m_1 + m_2)a_{x1} - F_R = 0, \tag{4.6}$$

where [151]

$$F_R = \mu_R m_1 g + \frac{1}{2}\rho c_d A V_x^2 = C_0 + C_1 V_x^2, \tag{4.7}$$

represents the resistance force, c_d is the drag coefficient, μ_R is rolling resistance, ρ is air density, and A is representing the projected cross-sectional area of the vehicle. As introduced by (4.7), the resistance force is a quadratic function of the longitudinal velocity with two coefficients C_0 and C_1. By inserting (4.5) in (4.6) the trailer mass equation is obtained as follows:

$$m_2 = \frac{\mathbf{R}_t \left(\mathbf{T}_t - \mathbf{I}\dot{\boldsymbol{\omega}}_{t,m}\right)}{a_{x1}} - m_1 - \frac{F_R}{a_{x1}} + W_m, \tag{4.8}$$

where $\mathbf{R}_t$, $\mathbf{T}_t$, $\boldsymbol{\omega}_{t,m}$, and $\mathbf{I}$ present the wheel radius, torque, rotational speed, and momentum of inertia, which are illustrated in (3.41b), (3.41c), (3.41d), and (3.41e), respectively. Moreover, W_m represents the longitudinal uncertainty due to the acceleration measurement, inaccurate resistance force, geometry, and forces. W_m is mostly contributed to the sensor measurement including: longitudinal acceleration, longitudinal velocity, and wheel speed sensor measurement. $\boldsymbol{\omega}_{t,m}$ represents the wheel rotational speed at each corner that measured by the wheel speed sensor. As the model uncertainty is contributed to the sensor measurements, it is zero mean.

Next we propose use of a Proportional-Integral-Derivative (PID) observer designed approach, which has been used in the literature for estimating the velocity and traction forces [176, 155, 165, 177], to establish the following trailer mass estimation law:

$$\hat{m}_2 = \frac{\mathbf{R}_t \left(\mathbf{T}_t - \mathbf{I}\dot{\boldsymbol{\omega}}_{t,m}\right)}{a_{x1}} - m_1 - \frac{F_R}{a_{x1}} - \boldsymbol{\sigma}_1 \tilde{\boldsymbol{\omega}}_t + \sigma_2 \int \tilde{m}_2^m dt, \tag{4.9}$$

where $\boldsymbol{\sigma}_1^T \in \mathbf{R}^4$ and σ_2 are design parameters, and $\tilde{\boldsymbol{\omega}}_t = \boldsymbol{\omega}_{t,m} - \hat{\boldsymbol{\omega}}_t$ is the estimation error for wheel speed. The trailer mass estimation error denotes by $\tilde{m}_2^m = m_2^m - \hat{m}_2$ where $m_2^m = \mathbf{R}_t \left(\mathbf{T}_t - \mathbf{I}\dot{\boldsymbol{\omega}}_{t,m}\right)/a_{x1} - m_1 - F_R/a_{x1}$ is the measured trailer mass value ignoring the sensor noise and disturbance effects, that are represented by the model uncertainty term, W_m, and the previous time step value is used for the other term ($\hat{m}_2$) in this relation to make the algorithm implementable. If W_m is zero mean, the integral of the trailer mass measurement in (4.9) over time will eliminate the effect of uncertainty leading to

$\int \tilde{m}_2^m dt \approx \int \tilde{m}_2 dt$. The discrete-time recursive implementation of (4.9) is described in Algorithm 1.

The estimated wheel speed rate at each corner is described as:

$$\dot{\hat{\boldsymbol{\omega}}}_t = \mathbf{I}^{-1}[\mathbf{T}_t - \mathbf{R}_t^T a_{x1}\hat{m}_2 - \mathbf{R}_t^T a_{x1} m_1 + \mathbf{R}_t^T a_x \boldsymbol{\sigma}_3 \int \tilde{\boldsymbol{\omega}}_t dt + \mathbf{R}_t^T a_{x1}\sigma_2 \int \tilde{m}_2 dt], \tag{4.10}$$

where $\boldsymbol{\sigma}_3^T \in \mathbf{R}^4$ is also a design parameter. Given the fact that $\int w_t(\tau)d\tau = \int w_{t,m}(\tau)d\tau$ based on the zero mean measurement noise assumption, the estimated wheel speed $\hat{\boldsymbol{\omega}}_t$ is used as an auxiliary term for trailer mass estimation.

Theorem 4.1. The error dynamics for the trailer mass estimation (4.9) based on the wheel dynamic with time-varying parameter $\boldsymbol{\omega}_t$ is exponentially stable.

Proof: Subtracting the trailer mass (4.8) from the estimated trailer mass (4.9) yield to the trailer mass estimation error $\tilde{m}_2 = \boldsymbol{\sigma}_1 \tilde{\boldsymbol{\omega}}_t - \sigma_2 \int \tilde{m}_2 dt + W_m$. The time derivative of the error dynamic leads to:

$$\dot{\tilde{m}}_2 = -\sigma_2 \tilde{m}_2 + \boldsymbol{\sigma}_1 \dot{\tilde{\boldsymbol{\omega}}}_t + \dot{W}_m. \tag{4.11}$$

Substituting (4.10) from the wheel speed rate $\dot{\boldsymbol{\omega}}_{t,m} = \mathbf{I}^{-1}[\mathbf{T}_t - \mathbf{R}_t^T(a_{x1}m_2 - a_{x1}m_1 + a_{x1}W_m)]$ yields to:

$$\mathbf{I}\dot{\tilde{\boldsymbol{\omega}}}_t = -\mathbf{R}_t^T a_{x1}\tilde{m}_2 + \mathbf{R}_t^T a_{x1} W_m - \mathbf{R}_t^T a_{x1}\boldsymbol{\sigma}_3 \int \tilde{\boldsymbol{\omega}}_t dt - \mathbf{R}_t^T a_{x1}\sigma_2 \int \tilde{m}_2 dt. \tag{4.12}$$

By taking the time derivative from (4.12), and replacing the error dynamic of the trailer mass estimation showed in (4.11), yield to:

$$\begin{aligned}\ddot{\tilde{\boldsymbol{\omega}}}_t = -\mathbf{I}^{-1}\mathbf{R}_t^T a_{x1}\left(-\sigma_2\tilde{m}_2 + \boldsymbol{\sigma}_1\dot{\tilde{\boldsymbol{\omega}}}_t + \dot{W}_m\right) + \mathbf{I}^{-1}\mathbf{R}_t^T a_{x1}\dot{W}_m - \mathbf{I}^{-1}\mathbf{R}_t^T a_{x1}\boldsymbol{\sigma}_3\tilde{\boldsymbol{\omega}}_t \\ -\mathbf{I}^{-1}\mathbf{R}_t^T a_{x1}\sigma_2\tilde{m}_2,\end{aligned} \tag{4.13}$$

which can be written in the following state space form:

$$\begin{bmatrix}\dot{\tilde{\boldsymbol{\omega}}}_t \\ \ddot{\tilde{\boldsymbol{\omega}}}_t\end{bmatrix} = \underbrace{\begin{bmatrix}\mathbf{0}_{4\times4} & \mathbf{1}_{4\times4} \\ -\mathbf{I}^{-1}\mathbf{R}_t^T a_{x1}\boldsymbol{\sigma}_3 & -\mathbf{I}^{-1}\mathbf{R}_t^T a_{x1}\boldsymbol{\sigma}_1\end{bmatrix}}_{\mathbf{M}} \begin{bmatrix}\tilde{\boldsymbol{\omega}}_t \\ \dot{\tilde{\boldsymbol{\omega}}}_t\end{bmatrix}, \tag{4.14}$$

where $\mathbf{M}$ is Hurwitz. Therefore, the error dynamic (4.14) is exponentially stable provided by $\boldsymbol{\sigma}_1, \boldsymbol{\sigma}_3 > 0$. Thus, $\tilde{\boldsymbol{\omega}}_t \to 0$ and $\dot{\tilde{\boldsymbol{\omega}}}_t \to 0$. ■

Therefore, the estimation error dynamic illustrated in (4.11) asymptotically turns to

$$\dot{\tilde{m}}_2 = -\sigma_2 \tilde{m}_2 + \dot{W}_m, \tag{4.15}$$

which is an exponentially stable dynamic for $\forall \sigma_2 > 0$. And has attenuation for uncertainties with the gain $\frac{1}{\sigma_2}$. To implement the algorithm on real-time testing, the discretized form of the trailer mass error dynamic is used. The proposed dynamic system model-based trailer mass estimation algorithm is summarized in Algorithm 1.

Algorithm 1 Trailer mass estimation algorithm

Trailer Mass Estimation

Initialization:

T_s= Sampling rate, $\mathbf{R}_t$= Effective radius, $\mathbf{I}$= Wheel momentum of inertia, $C_{0,1}$= Resistance force coefficients, $\boldsymbol{\sigma}_{1,2,3}$= Observer gains, m_1= Vehicle mass, δ_{th}= Steering angle threshold.

Main Loop:

$\boldsymbol{\omega}_{t,m}$,$\dot{\boldsymbol{\omega}}_{t,m}$= Measured by wheel speed sensors, input,

a_{x1}= Measured by IMU, input,

V_x, δ= Measured by CAN bus, input.

If isempty $(\hat{\boldsymbol{\omega}}_t, \dot{\hat{\boldsymbol{\omega}}}_t, \hat{m}_2)$

$\hat{\boldsymbol{\omega}}_t = \dot{\hat{\boldsymbol{\omega}}}_t = \mathbf{0}$,

$\hat{m}_2$ = Initial guess.

If $V_x > 0, |\delta| < \delta_{th}$

$\tilde{\boldsymbol{\omega}}_t = \boldsymbol{\omega}_{t,m} - \hat{\boldsymbol{\omega}}_t$,

$\dot{\tilde{\boldsymbol{\omega}}}_t = \dot{\boldsymbol{\omega}}_{t,m} - \dot{\hat{\boldsymbol{\omega}}}_t$,

$$\mathbf{M} = \begin{bmatrix} \mathbf{0}_{4\times4} & \mathbf{1}_{4\times4} \\ -\mathbf{I}^{-1}\mathbf{R}_t^T a_{x1}\boldsymbol{\sigma}_3 & -\mathbf{I}^{-1}\mathbf{R}_t^T a_{x1}\boldsymbol{\sigma}_1 \end{bmatrix},$$

$\mathbf{M}_d = e^{\mathbf{M}T_s}$,

$$\begin{bmatrix} \tilde{\boldsymbol{\omega}}_t \\ \dot{\tilde{\boldsymbol{\omega}}}_t \end{bmatrix} = \mathbf{M}_d \begin{bmatrix} \tilde{\boldsymbol{\omega}}_t \\ \dot{\tilde{\boldsymbol{\omega}}}_t \end{bmatrix},$$

Estimate the trailer mass:

$m_2^m = \mathbf{R}_t\left(\mathbf{T}_t - \mathbf{I}\dot{\omega}_{t,m}\right)/a_{x1} - m_1 - (C_0 + C_1 V_x^2)/a_{x1}$,

$\hat{m}_2 = \left(\mathbf{R}_t\left(\mathbf{T}_t - \mathbf{I}\dot{\boldsymbol{\omega}}_{t,m}\right)\right)/a_{x1} - m_1 - (C_0 + C_1 V_x^2)/a_{x1} - \boldsymbol{\sigma}_1\tilde{\boldsymbol{\omega}}_t + \sigma_2(m_2^m - \hat{m}_2)T_s$, output.

Update variables:

$\hat{\boldsymbol{\omega}}_t = \boldsymbol{\omega}_{t,m} - \tilde{\boldsymbol{\omega}}_t$,

$\dot{\hat{\boldsymbol{\omega}}}_t = \dot{\boldsymbol{\omega}}_{t,m} - \dot{\tilde{\boldsymbol{\omega}}}_t$,

else:

$\hat{m}_2 = \hat{m}_2$, output.

4.3 Machine Learning Based Approach

Machine learning based approach is another method to estimate the trailer mass using collected data. Among the studies following this approach, a dual level reinforcement estimator was proposed in [178] to estimate the mining haul trucks' total mass. A neural network approach was designed and tested to improve the accuracy of multiple sensor weight in motion system [136]. In this work, due to the difficulty to inverse the model that describes the dynamics between the vehicle and pavement interaction, the neural network method was used to estimate the static truck weight. A DNN was considered in this work to estimate the static truck weight and the results demonstrate an accurate estimation on the truck weight [136]. However, the algorithm indication that is not generic and needs to be trained for other vehicle types.

In design of a DNN based trailer mass estimator, the inputs of the DNN estimator need to be selected properly. Proper sensors are required to measure these inputs and feed them into the DNN. Sensors that are available on a test vehicle include: IMU, Wheel Speed Sensor (WSS), CAN bus information, ultra-sonic sensor measurements, and engine torque measurement. The vehicle longitudinal/lateral accelerations and yaw rate are measured by the vehicle's IMU. The wheel speed, wheel torque, and steering angle are measured from the regular ABS wheel speed sensors, electric actuators, and CAN bus. The hitch angle is measurable by the ultra-sound sensors that are mounted on the rear bumper of the vehicle [39].

4.3.1 Deep Neural Networks Input Sensitivity Analysis

A sensitivity analysis over all of the measurable inputs is provided to check the importance of the measurable vehicle states and parameters with respect to the trailer mass. In other words, to realize how much effective each measurement data is with respect to the trailer mass, the sensitivity analysis has been investigated. The Gradient Boosting Regression Tree (GBRT) is used to evaluate the input importance. GBRT begins by training a decision tree in which each observation is assigned an equal weight. By evaluating the first tree, the weights of those observations that are difficult to classify and lower are increased. By evaluating the weights for neurons the importance of the inputs with respect to the output which is the trailer mass is generated. The importance of the inputs with respect to the trailer mass is shown in Fig. 4.2.

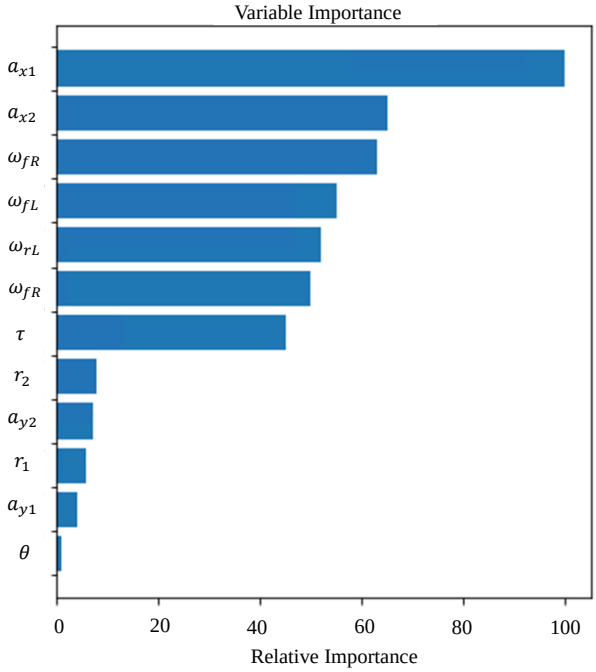

Figure 4.2: The input feature importance of the all available measurements for trailer mass estimation.

As can be seen in Fig. 4.2, the hitch angle, lateral acceleration, and yaw rate for both vehicle and trailer are less important and have less effect on the network for estimating the trailer mass than the other available inputs. Therefore, there is no need to consider all of the available inputs for the network since their effectiveness are not the same. The vehicle-trailer equation of motion is considered to pick the right inputs for estimating trailer mass. As can be seen in (4.8), if the inputs of the DNN set based on (4.8), the trained DNN is able to estimate the presented function and provide the trailer mass estimation. In order to drive (4.8), it is assumed that the vehicle-trailer system moves forward with small steering angle ($|\delta| < \delta_{th}$, where δ_{th} is the steering angle threshold). Therefore, data with large steering angles are removed from the training data-set. Moreover, it is obvious that if the trailer has lateral slip, the hitch angle will not be small. The trailer lateral slip causes the lateral tire forces which means the vehicle traction forces will take care of both longitudinal and lateral movements of the trailer. Therefore, it is assumed that the hitch angle is also small ($|\theta| < \theta_{th}$, where θ_{th} is the hitch angle threshold) to be able to

consider the longitudinal equation of motion only. The data with large hitch angle values are removed from the training data-set.

As can be seen in (4.6), the measurable inputs for the DNN are including: the longitudinal acceleration, wheel speed, engine torque, and resistance force. Based on (4.7), the resistance force is a quadratic function of longitudinal velocity. Therefore, the input vector of the DNN is considered as follows:

$$\mathbf{A_t} = \begin{bmatrix} a_{x1} & a_{x2} & \mathbf{R}_t^T diag(\boldsymbol{\omega}_t) & \mathbf{T}_t^T & C_0 + C_1 V_x^2 \end{bmatrix}^T, \tag{4.16}$$

where C_0 and C_1 are the total resistance force coefficients, described in (4.7), that are related to the vehicle specification. As the vehicle-trailer is assumed to move forward with small steering angle, the longitudinal acceleration of the vehicle is almost the same as the longitudinal acceleration of the trailer. Thus, the final input vector for training and testing the DNN is considered as follows:

$$\mathbf{A_t} = \begin{bmatrix} a_{x1} & \mathbf{R}_t^T diag(\boldsymbol{\omega}_t) & \mathbf{T}_t^T & C_0 + C_1 V_x^2 \end{bmatrix}^T. \tag{4.17}$$

The sensitivity analysis result for the selected inputs shown in (4.17) is illustrated in Fig. 4.3. As Fig. 4.3 illustrates, longitudinal acceleration, wheel speeds, and engine torque are the most important factor for trailer mass estimation while the resistance force model has less influence on the trailer mass estimation. Given that the longitudinal acceleration, wheel speeds, and engine torque are the most important factor, four back steps of them are considered as extra inputs to the network.

4.3.2 Deep Neural Networks Structure

To estimate trailer mass, a 15 hidden layers (systematic experimentation is used to discover what works best for the specific tractor-trailer data-set) neural network with different neurons at each layer, decreasing from layer to layer, is considered. Each neuron's output is the input of the neurons in the next layer. The schematic view of the considered neural network is shown in Fig. 4.4. For training the DNN, an activation function for each neuron should be considered. As the inputs can take both positive and negative value, a Leaky rectified linear unit function is considered for the neuron activation function. The considered activation function is described as follows [179]:

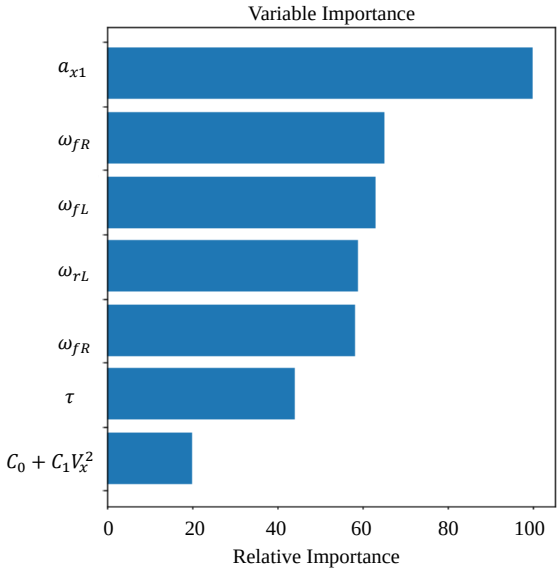

Figure 4.3: The input feature importance of the selected measurements for trailer mass estimation.

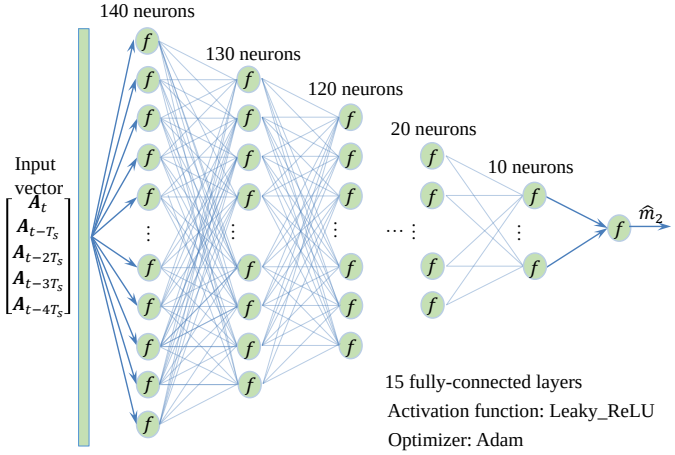

Figure 4.4: The neural network structure.

$$f(x) = \begin{cases} x, & x > 0 \\ ax, & Otherwise \end{cases}, 0 < a \ll 1, \tag{4.18}$$

where the Leaky rectified linear function has a small slope for negative values. By setting the inputs, activation function, number of layers/neurons, and output for the training set, the training process starts to obtain weights and biases of the neurons. To deal with over-fitting issue, L2 regularization, where it drops all features with no significant impact, has been used.

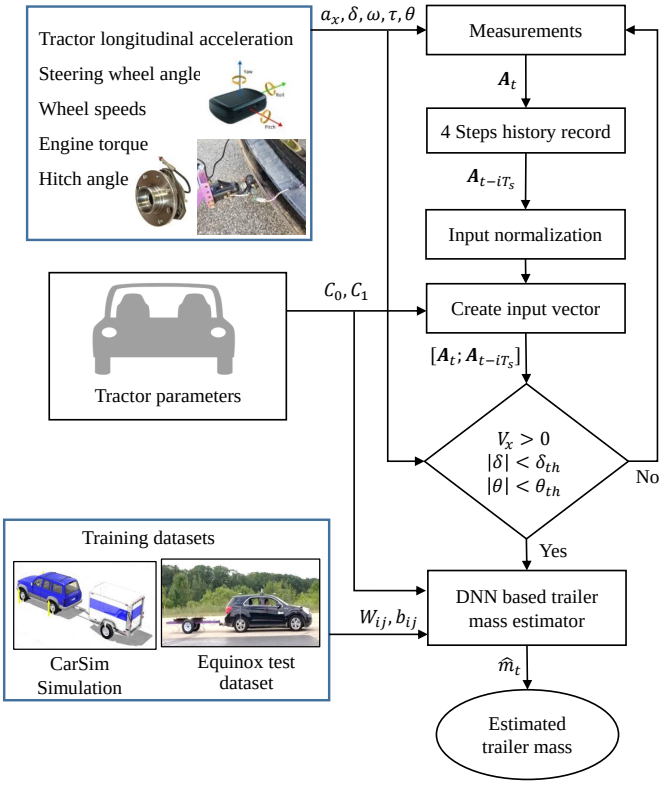

Figure 4.5: Overall trailer mass estimation procedure.

By utilizing the generated weights and biases, the estimated trailer mass is calculated as follows:

$$\hat{m}_2 = f(\mathbf{b}_{15,1} + \mathbf{w}_{15,1} \sum_{h=1}^{H_{14}} \mathbf{L}_{14,h}) - m_1,$$
$$\mathbf{L}_{i,j} = f(\mathbf{b}_{i,j} + \mathbf{w}_{i,j} \sum_{j=1}^{H_i} \mathbf{L}_{i-1,j}), \tag{4.19}$$

where $i \in [1, 2, ..., 14]$, and $\mathbf{H}_{1\times 14} = [140, 130, ..., 20, 10]$. First layer's input vector is defined as $\mathbf{L}_{\mathbf{0},(\mathbf{1},\mathbf{2},...,\mathbf{140})} = [\mathbf{A}_t; \mathbf{A}_{t-T_s}; \mathbf{A}_{t-2T_s}; \mathbf{A}_{t-3T_s}; \mathbf{A}_{t-4T_s}]$, where T_s represents the sampling rate. The overall algorithm for DNN based trailer mass estimation is shown in Fig. 4.5.

As Fig. 4.5. illustrates, vehicle states including: vehicle longitudinal acceleration, steering wheel angle, wheel speeds, engine torque, and hitch angle measure with the sensors at each time step. Then four previous time steps of the current time step of the measurement signals record as a memory signal. By utilizing the towing vehicle parameters including: the vehicle mass, tire sizes, and geometry, the DNN input vector produces. Then the mentioned assumptions check to ensure that the vehicle-trailer is moving forward and straight and if the assumptions are violated, the algorithm will wait till the conditions satisfy. As the vehicle steering wheel angle, hitch angle, and velocity turn into the acceptable range, the generated weights and biases utilize to estimate trailer mass.

4.4 Data-set

To train and test the network both experimental and simulation test results are considered. A high-fidelity CarSim model is used to collect the data for almost 50 maneuvers for two different vehicles with different trailer attached to them. For instance, 10 Single Lane Change (SLC) maneuvers are considered in CarSim including 5 tests with E-class SUV and 5 tests with a pick-up truck. Moreover, at each test, the trailer payload and geometry, CG location, and track width, have been changed to collect sufficient data.

For the experimental collected data, an electric Chevrolet Equinox AWD with an attached trailer, which is shown in Fig. 4.6, has been used as a vehicle-trailer system. The specifications of the vehicle and trailer are listed in Table 4.1. The vehicle-trailer system is capable of collecting the required data for training/testing the designed DNN and dynamic system model-based estimators by having the required sensors including: IMU, Global-Positioning-System (GPS), wheel speed sensor, torque measurement sensor, and potentiometer sensor. The longitudinal/lateral accelerations and yaw rate of the vehicle and trailer are measured with a 6-axis IMU (and GPS) system RT2000. The wheel speed and wheel torques which can be measured using the regular ABS wheel speed sensors, and electric actuators, respectively.

Measured signals are communicated using a CAN-bus. Real-time acquisition and processing of sensory information and the developed trailer mass estimation algorithm is re-

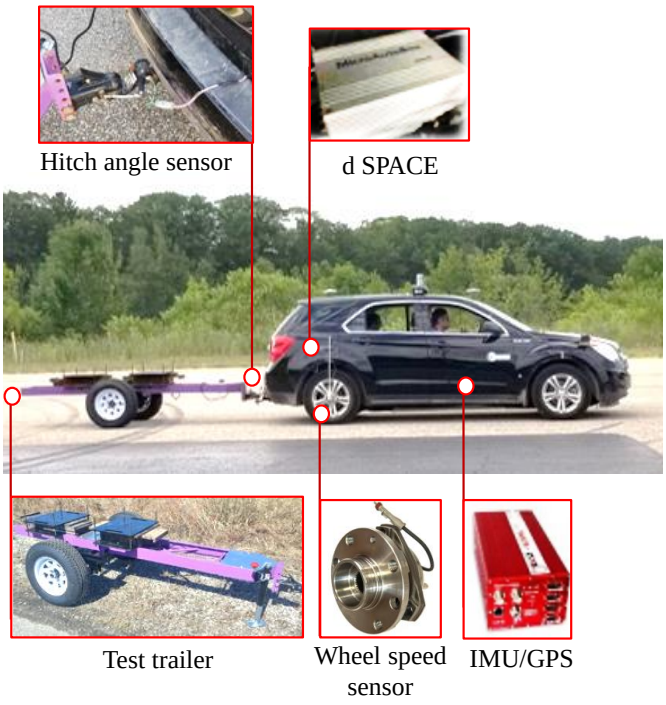

Figure 4.6: AWD test vehicle with trailer

alized using the dSPACE MicroAutobox. The dSPACE compiles measurements for MATLAB/Simulink, and the trailer mass estimation algorithm run in MATLAB/Simulink by utilizing the provided measurements. The sampling frequency for the experiment is fixed to 200 [Hz].

To train and test the network, the DNN inputs should be normalized to have a same magnitude. To do so, each input of the network is normalized by its maximum value over the entire training data-set to make sure that all the inputs are scaled from -1 to 1. Moreover, the DNN input vector must feed to the network by the same sampling rate. Therefore, experimental signals are pre-processed (resampled, filtered and segmented). The total number of tests for both experimental and simulation tests are listed in Table 4.2.

As can be seen in Table 4.2, several different maneuvers have been used to train/test the network including: Single Lane Change (SLC), Double Lane Change (DLC), sine shape steer, random steer, Step Steer (SS), and full turn maneuvers. 75% of the collected data

Table 4.1: Vehicle-trailer parameters for trailer mass estimation.

Parameters	Values		
	E-class SUV	Pick-up truck	Equinox
m_1, Vehicle's Mass (kg)	1807	2249	2270
I_{z1}, Vehicle's moment of Inertia around z axes (kg.m2)	2687	5757	4605
a_1, Vehicle's CG to front axle (m)	1.18	1.4	1.42
b_1, Vehicle's CG to rear axle (m)	1.77	3.07	1.44
e, Vehicle's rear axle to hitch-point (m)	1.17	1.2	1.14
Tw_1, Front axle length (m)	1.57	1.7	1.62
R_{eff}, Effective tire radius (m)	0.39	0.38	0.34
m_2, Trailer's Mass (kg)	1400	815	665
a_2, Trailer's CG to hitch-point (m)	2	1.5	1
b_2, Trailer's CG to axle (m)	1	2.5	0.8
Tw_3, Trailer width (m)	1.8	1.8	1.35

are used to train the network (training data-set) while 25% of them are used to test the network (testing data-set). The simulation and experimental results of the trailer mass estimator are illustrated in next section.

4.5 Simulation and Experiment Tests

In this section, the presented trailer mass estimation algorithms are validated by both simulation and experimental studies. Moreover, the performance of the designed observer and DNN based algorithms are compared in this section.

Table 4.2: Test scenarios for trailer mass estimation

Equinox test		CarSim simulation	
Scenarios	Amount	Scenarios	Amount
SLC	5	SLC	10
DLC	8	DLC	10
Sine	2	Sine	10
Random	5	Random	5
SS	7	SS	5
Full turn	4	Full turn	2

4.5.1 Designed Observer Results

The dynamic system model-based trailer mass estimator performance is examined by utilizing a CarSim model with the parameters listed in Table 4.1. The simulation runs for different trailer masses to evaluate the trailer mass estimation. In this simulation, the vehicle-trailer starts moving straight with the initial speed of 20 km/h and keep accelerating for 12 seconds. The steering angle and longitudinal/lateral accelerations of the vehicle are shown in Fig. 4.7. This simulation is conducted for two conditions of loaded and unloaded trailer. The trailer is unloaded in test-1 and has 850 kg payload in test-2. The simulation result is shown in Fig. 4.7.

As Fig. 4.7 illustrates, the estimated trailer mass value has almost 11% errors out of the actual trailer mass for both loaded and unloaded trailer test. As seen in Fig. 4.7, from t=6s to t=9.4s, the steering wheel angle and the hitch angle are larger than $\delta_{th} = \theta_{th} = 0.1rad$, which means the assumption is not valid. Therefore, the last output at t=6s is kept for the estimated trailer mass value (dashed lines from t=6s to t=9.4s). Moreover, as the stability of the method is guaranteed mathematically, the results justify the convergence of the trailer mass estimation error as well. To be able to make the estimator more accurate and realistic, more test data with different setting including different road conditions, different tire types, and different vehicle parameters should be considered.

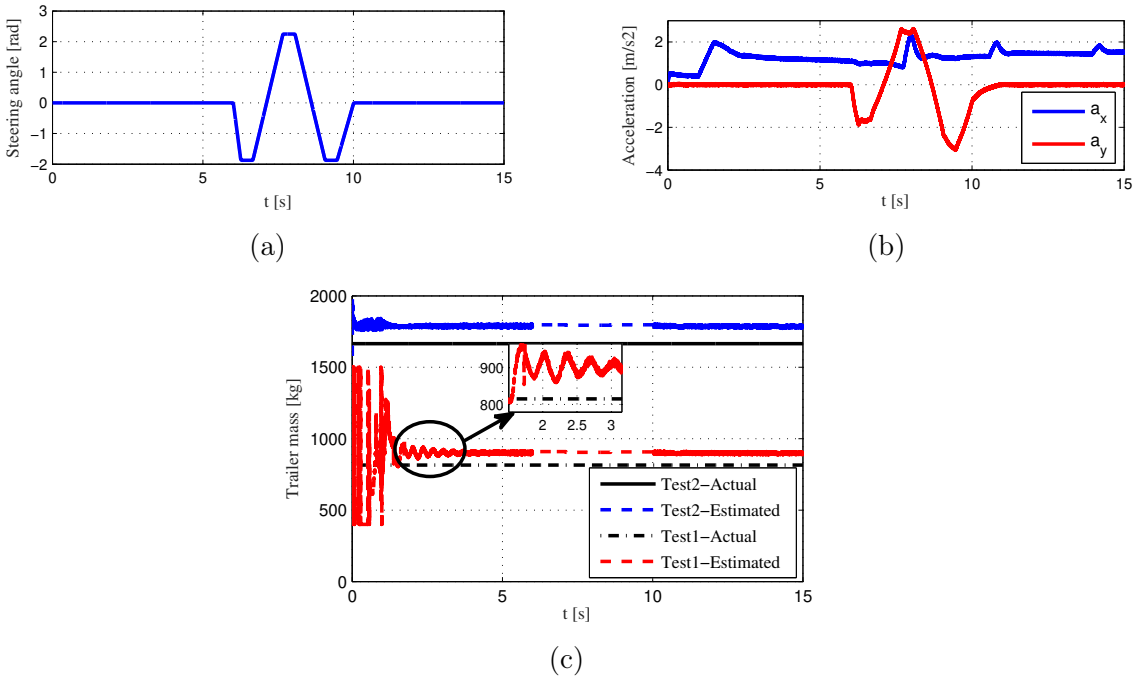

Figure 4.7: The trailer mass estimation based on the designed observer for a double lane change maneuver: a) Steering wheel angle b) Vehicle longitudinal/lateral accelerations c) Trailer mass estimation.

4.5.2 Deep Neural Network Estimation Results

An adaptive learning rate optimization algorithm called Adam optimizer is considered for training the network as shown in Fig. 4.4. By training the DNN with a maximum iteration of 1000 and batch size of 256, the weights and biases of the neurons are calculated. The calculated weights and biases are used to estimate trailer mass over the testing data-set (unseen data). The results for the trailer mass estimation is illustrated in Fig. 4.8.

As Fig. 4.8 illustrates, the Root Mean Square (RMS) of the trailer mass estimation error is 69.57 kg, which is almost 10 percent errors out of the actual trailer mass (690 kg). Moreover, as discussed in the previous section, to be able to estimate trailer mass, it is assumed the steering angle is small. Therefore, as can be seen in Fig. 4.8 part (e), the algorithm stops estimating the trailer mass for 1 second (from second 8 to 9) due to the large steering angle and keeps the previous result until the steering angle value becomes

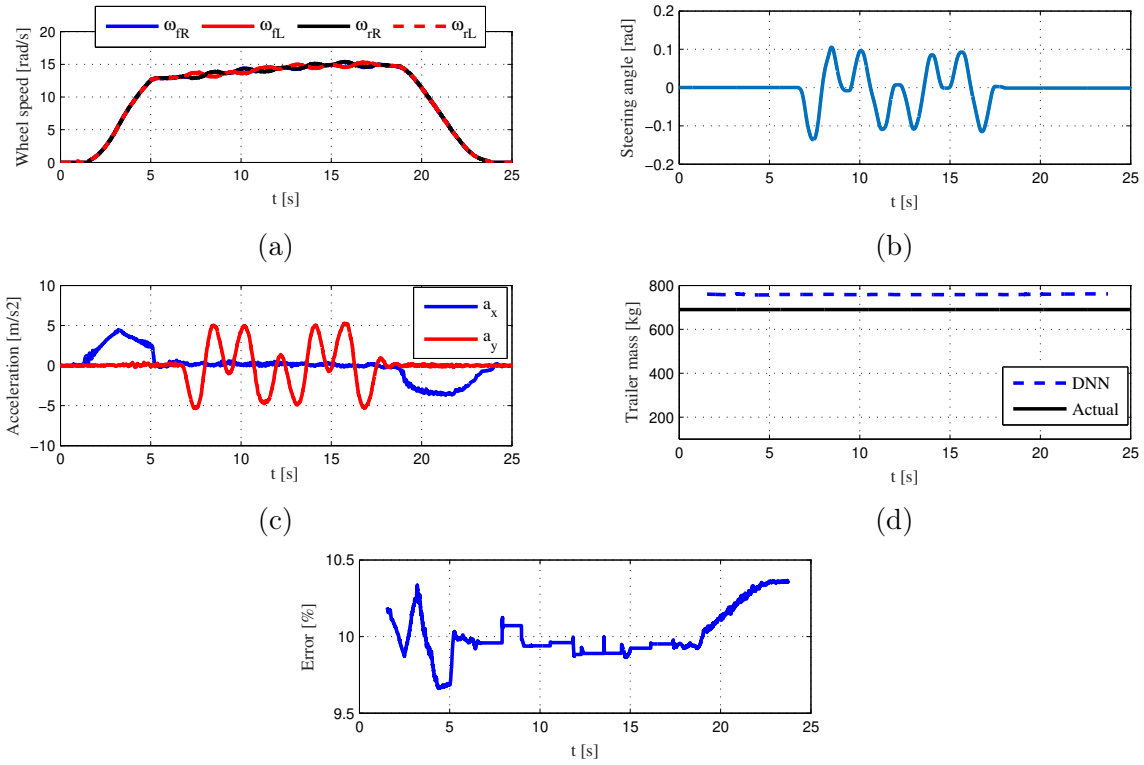

Figure 4.8: The trailer mass estimation based on the designed neural network for double lane change maneuvers (unseen experimental test data): a) Vehicle wheel speeds b) Steering wheel angle c) Vehicle longitudinal/lateral accelerations d) Trailer mass estimation e) Estimation error.

small again.

The algorithm is also tested for a random steer maneuver and the results are shown in Fig. 4.9. As can be seen in the results, the RMS of the trailer mass estimation error is 70.17 kg, which is 10.17 percent errors out of the actual trailer mass.

To investigate the performance of the designed DNN based trailer mass estimator, a double lane change maneuver is considered and the results are shown in Fig. 4.10. As can be seen in the results, the RMS of the trailer mass estimation error is 69.27 kg, which is 10.04 percent errors out of the actual trailer mass. It can be seen from the DNN results that

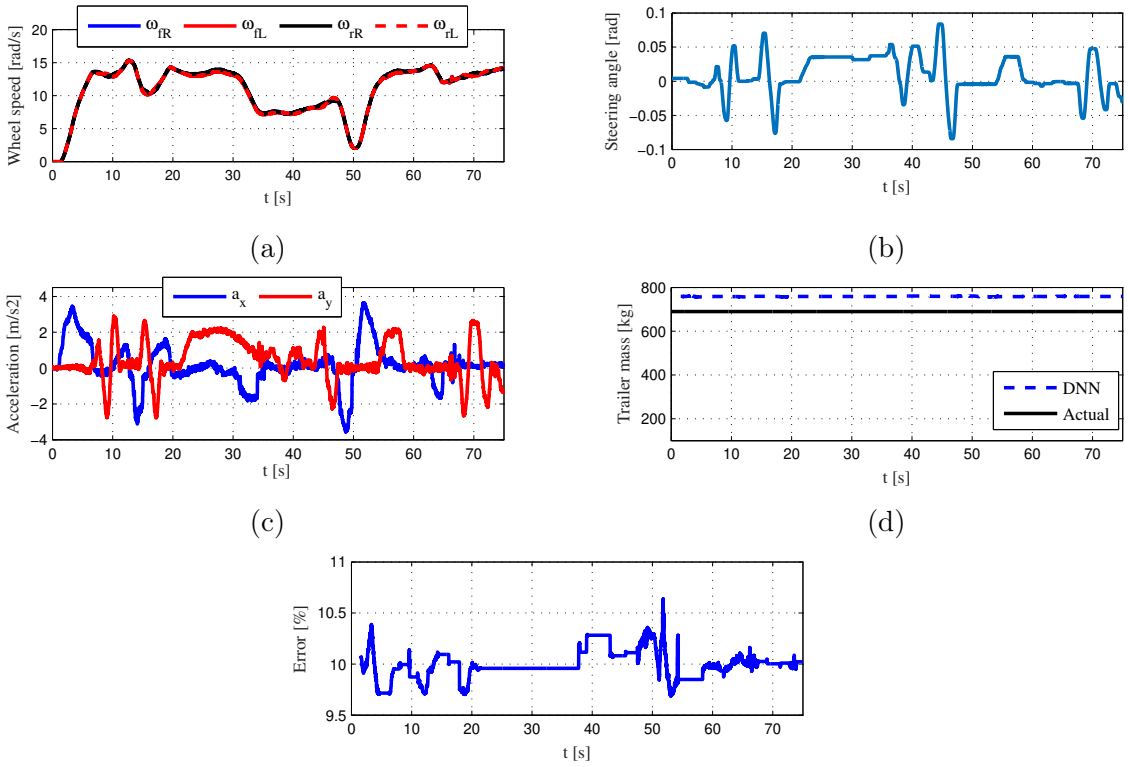

Figure 4.9: The trailer mass estimation based on the designed neural network for random steer maneuver (unseen experimental test data): a) Vehicle wheel speeds b) Steering wheel angle c) Vehicle longitudinal/lateral accelerations d) Trailer mass estimation e) Estimation error.

the error is in bias and is moving around 10% of the actual value. To solve the bias issue there are four alternatives including: adding neuron layers, adding more training samples, dropout, and decreasing regularization parameter. The proposed network is designed based on these four alternatives, and the bias error of almost 10% was the best performance of the network that we have achieved by testing the different network structures. The comparison between the designed dynamic system model-based approach and DNN approach for trailer mass estimation is investigated in the discussion section.

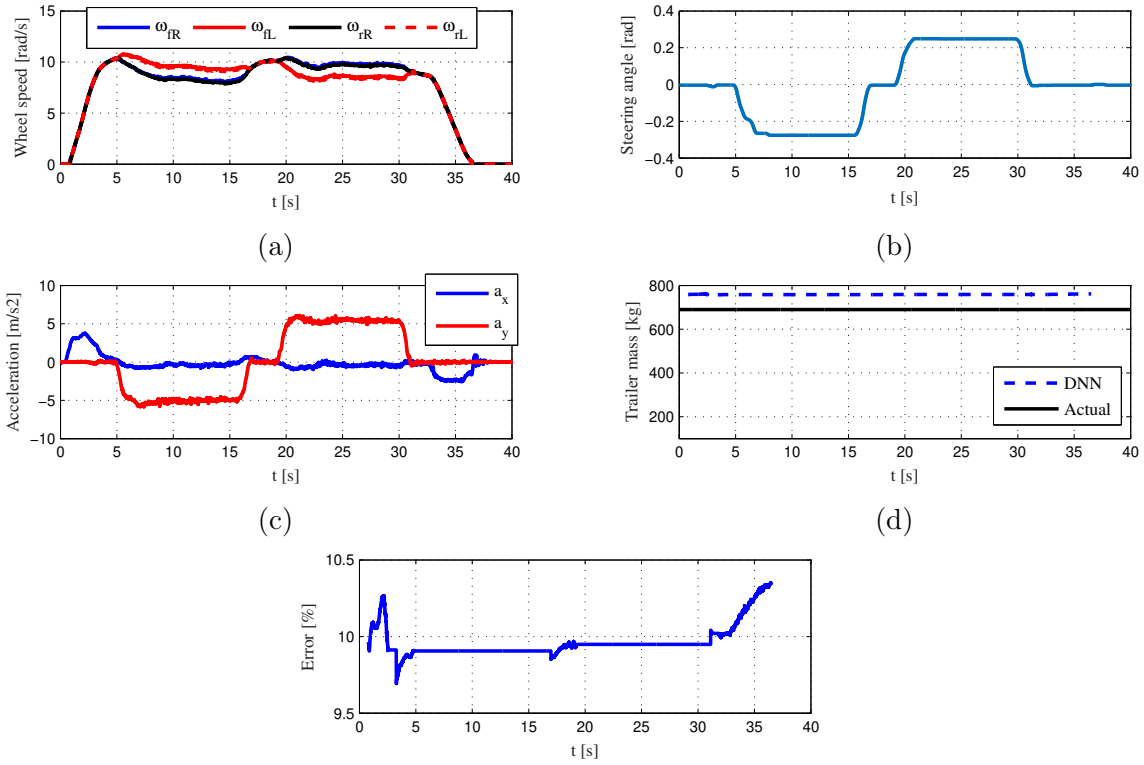

Figure 4.10: The trailer mass estimation based on the designed neural network for step steer maneuvers (unseen experimental test data): a) Vehicle wheel speeds b) Steering wheel angle c) Vehicle longitudinal/lateral accelerations d) Trailer mass estimation e) Estimation error.

4.5.3 Discussions

The estimated trailer mass results illustrate that both dynamic system model-based and DNN approaches are capable of estimating trailer mass; however, their performances differ. Due to the fact that the DNN inputs are designed based on the vehicle-trailer equation of motion, the designed network is a function estimator between the measured inputs to the output. The network is trained based on the data that contains low speed operation of the vehicle-trailer to be able to estimate trailer mass at the beginning of the motion. As has been mentioned, it is assumed that the steering angle is small. Therefore, if the

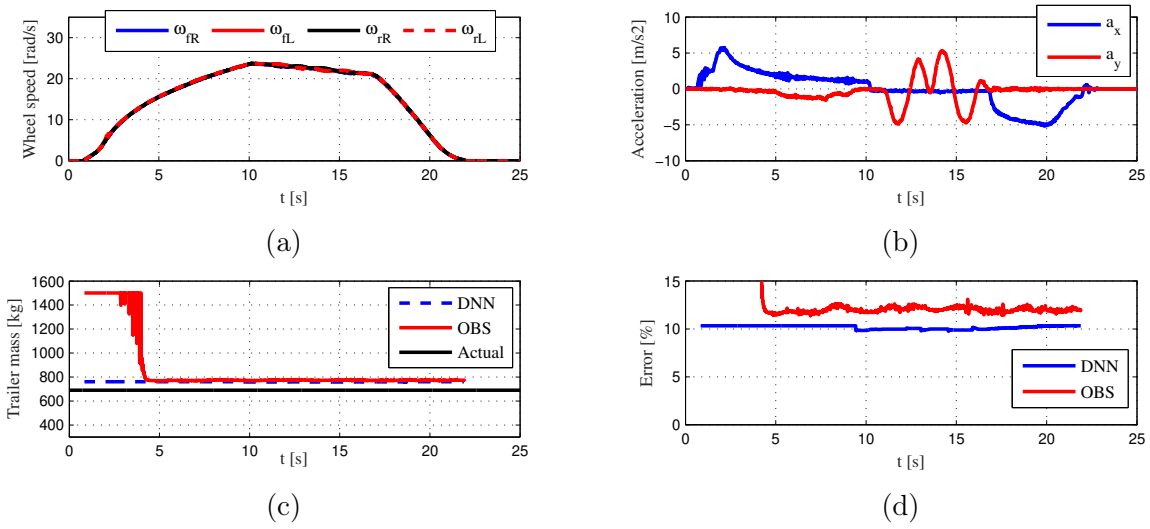

Figure 4.11: The trailer mass estimation based on both the designed neural network and observer for an acceleration and brake maneuver (unseen experimental test data): a) Vehicle wheel speeds b) Vehicle longitudinal/lateral accelerations c) Estimated trailer mass d) Estimation error.

driver applies large steering angle the data will not feed to the trained DNN. Similarly, for harsh maneuvers when the steering angle is larger than the specified threshold, the dynamic system model-based approach stop working. Moreover, it is assumed that the vehicle-trailer is operating in a flat road. Therefore, the data will feed to the network as soon as these assumptions become valid.

To compare the performance of the dynamic system model-based and DNN approaches for estimating the trailer mass, an experimental test, involving a double lane change maneuver, has been considered. The experimental test runs for 25 seconds. The wheel speeds and longitudinal/lateral accelerations of the vehicle are shown in Fig. 4.11.

The estimation errors for both DNN and dynamic system model-based approaches are shown in Fig. 4.11. As can be seen in Fig. 4.11, the error convergence rate with DNN method is much higher than that for the dynamic system model-based approach. Frankly, there is no settling time for the DNN method since its output is calculated by multiplying the weights by the inputs. Moreover, the estimation performance for the dynamic system model-based estimator is almost the same with the DNN approach. The dynamic system

model-based approach estimation error increases for harsh maneuvers since the linearity assumptions are violated. However, if the training data-set is rich enough and contains adequate data for hash maneuvers, the estimation error for the DNN based estimator will not increase as the network is trained for harsh maneuvers as well.

To compare the method with other existing machine-learning architectures, a Recurrent Neural Network (RNN) is considered. To do so, a fifteen hidden layers with different neurons at each layers (same as the proposed DNN, Fig. 4.4) is trained and tested for estimating the trailer mass by considering the same input vector as presented in (4.17). The NRMS [180] of the error for trailer mass estimation is shown in Table 4.3 for the designed dynamic system model-based observer (OBS) and ML approaches (DNN and RNN).

As Table 4.3 illustrates, the maximum error percentage with respect to different longitudinal velocities is less than 10.11%. The RNN and DNN approaches have almost the same error percentage. Moreover, the percentage error for both the RNN and DNN approaches are almost the same as the reinforcement learning approaches in [136, 178]. However, the algorithms in [136, 178] were tested and validated for one vehicle and there is no confirmation for the designed neural network to be generic and transferable to other vehicles without training. Given that the DNN is much easier to implement and has less computational cost by comparing with RNN architecture, the proposed DNN method is recommended for estimating the trailer mass. In average, the RNN takes two and half hours to train while the DNN takes two hours to train with an Intel Core i7 machine, a Nvidia GeForce 670 GPU, and 32 GB of RAM.

Table 4.3: NRMS of the errors for the dynamic system model-based and the DNN trailer mass estimators.

Estimation	@ u=25	@ u=35	@ u=45	@ u=55
Technique	km/h [%]	km/h [%]	km/h [%]	km/h [%]
OBS	9.51	9.34	10.49	10.11
DNN	8.53	8.67	8.5	8.41
RNN	8.93	8.99	9.1	8.91

The trailer mass estimation results shows that the DNN algorithm is generic, and if the vehicle specifications change, the algorithm can still estimate the trailer mass since the vehicle parameters, including the vehicle mass, tire sizes, and geometry, are considered in the input vector. Therefore, the algorithm can estimate the trailer mass properly. Although both the dynamic system model-based and DNN approaches are capable of estimating trailer mass accurately, the DNN method's estimation error might decrease if the network were trained with a more-comprehensive data-set that contains more vehicle-trailer configuration information. In this research, three different types of vehicle have been considered in the data-set used to train and test the network. Aiming to increase the accuracy of the proposed method, training with a more-comprehensive data-set with different types of vehicles and trailers is considered as a potential future work of this research.

4.6 Conclusions

In this chapter, two approaches have been introduced to estimate trailer mass: dynamic system model-based and machine learning approaches. The stability of the dynamic system model-based estimation algorithm was guaranteed mathematically, and the test results indicated the convergence of the trailer mass estimation error. The test results for the dynamic system model-based trailer mass estimator reported almost 12% errors. The ML-based approach has high potential for trailer mass estimation and is applicable for vehicle-trailers with different configurations since its inputs were designed based on the vehicle-trailer dynamic model. The maximum error percentage for the DNN based trailer mass estimator is 10%, almost the same with the model-based estimator error. As the inputs of the DNN contain the vehicle parameter, including the vehicle mass, tire sizes, and geometry, the designed DNN can be used for any towing vehicle with different specifications. In other words, the trained DNN is generic, and so there is no need to re-train the network for a new towing vehicle. In this chapter, three different types of vehicle were reflected in the data-set used to train and test the network. The simulation results demonstrate that the trailer mass estimation error is not affected as the towing vehicle specifications change. To improve the trailer mass estimation results, more experiment results for training/testing the method are needed.

Chapter 5

Hitch Angle Estimation

5.1 Introduction

Hitch angle or articulated angle is the angle between the vehicle and trailer at the hitch point. In this chapter, the estimation of the hitch angle is investigated to develop a reliable estimation method for any unknown trailer connected to a towing vehicle with a ball-joint coupling. The trailer axle location and trailer mass are identified/estimated first to make the hitch angle estimation algorithm independent from the trailer type. To do so, the following assumptions are made:

1. The vehicle geometric parameters such as CG location and vehicle length are known or can be estimated.
2. In the vehicle-trailer system model, the pitch and bouncing motions, longitudinal/lateral load transfers, and aerodynamic forces are ignored.
3. The road is assumed flat, no road angles.

These assumptions have been considered to simplify the estimation model. In this chapter, three approaches have been proposed to calculate/estimate the hitch angle, (A) using ultra-sonic sensors, (B) using kinematic approaches and (C) using dynamic equations. Ultimately, to estimate the hitch angle more accurately, the data fusion technique is considered to combine the estimated hitch angle value generated by the approaches.

Based on the designed algorithm for estimating the hitch angle, the estimated trailer axle location, trailer front face angle, and trailer mass are used in the hitch angle estimation algorithm to make the algorithm generic for any ball type trailer. It is shown that the proposed integrated hitch angle estimation can be used for any unknown ball type trailers without any prior information on the trailer parameters since the required parameters of the trailer are estimated. The remaining of this chapter is as follows: In Section 5.2, the methodology of the hitch angle estimation and algorithms to estimate the hitch angle are described. In Section 5.3, the hitch angle estimation by using ultra-sonic sensors measurements as well as the trailer front face angle estimation are introduced. The kinematic equation for hitch angle is presented in Section 5.4. Moreover, the trailer axle location estimation is developed in Section 5.4. The estimated trailer mass is used in the designed hitch angle estimation algorithm based on the vehicle-trailer dynamic method and finally, results with discussions are provided in Section 5.5.

5.2 Hitch Angle Estimation Using Ultra-sonic Sensors

It is assumed that the trailer has flat or symmetric V-nose frontal face. A general symmetric V-nose surface can be defined to present the trailer frontal face, as schematically shown in Fig. 5.1. Also, this shape can represent the trailer with flat frontal face when the trailer front face angle, denoted by α in Fig.5.1, is zero. The trailer front face angle has impact on the hitch angle, shown by ϕ in Fig. 5.1, calculation by ultra-sonic sensors data. Also, to make the hitch angle estimation algorithm generic for any ball type trailer, the trailer front face angle needs to be identified first.

To identify the trailer frontal face angle α, trigonometric relations in Fig. 5.1 can be used. In Fig. 5.1, S_1 to S_4 denote the locations of the ultra-sonic sensors on the vehicle rear bumper. a and b are the distances between the sensors. L_1 and L_2 denote the distances of the hitch-point to the vehicle rear bumper and trailer front face, respectively. d_1 to d_4 represent the distance values that ultra-sonic sensors 1 to 4 measures, respectively as indicated in Fig. 5.1.

Different equations can be written to calculate the value of α based on multiple sensor combinations. For instance, using the data from sensors 1 and 2, α can be calculated as shown in (2.1).

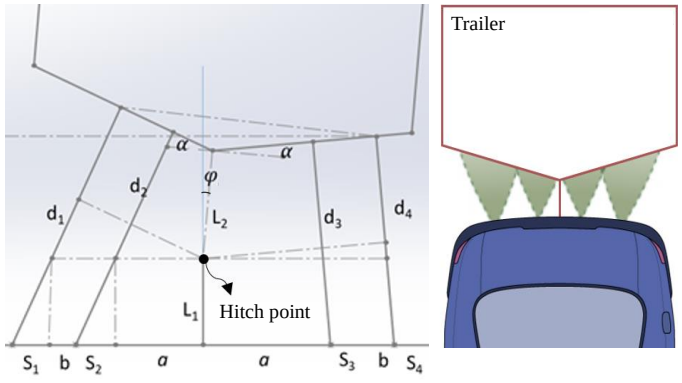

(a) (b)

Figure 5.1: a) Ultra-sonic sensors location, b) Schematic view of the ultra-sonic sensors on the vehicle rear bumper.

To identify the trailer frontal shape, the following two conditions are defined. As the first step of the estimation process, these conditions should be satisfied:

1. For a specific period (n sampling time), the steering angle is almost zero:

$$|\delta|_n < \delta_T, \tag{5.1}$$

where, δ is the steering angle value and δ_T is a defined threshold close to zero.

2. For the same specific period (n sampling time), there is almost no changes in the value of the sensor data:

$$|(\nabla d_i)|_n < \varepsilon, \tag{5.2}$$

where, $\nabla d_i,\ i \in \{1, 2, 3, 4\}$, are the changes in the sensors' data over n sampling periods and ε is a threshold defined based on the cleanness of the sensor signals. As long as these conditions are satisfied, it is guaranteed that the trailer is in line with respect to the vehicle. Having these conditions satisfied and $\varphi \cong 0$, the front face angle is determined by:

$$\alpha = \arcsin \frac{d_1 - d_2}{b}. \tag{5.3}$$

Therefore, for symmetric V-nose shape, at least two sensors should work properly and provide valid data to determine angle α. Having the trailer front face angle (α), the hitch

angle estimates using the geometry of the vehicle-trailer. The following equations can be written according to Fig. 5.1. Each equation is written to find the value of L_2 based on each sensor data (d_1 to d_4):

$$L_2 = \frac{1}{\cos\alpha}\left[d_1 - \frac{L_1}{\cos\left(\widehat{\varphi}+\alpha\right)} - (a+b-L_1 tan\left(\widehat{\varphi}+\alpha\right))\sin(\widehat{\varphi}+\alpha)\right], \tag{5.4}$$

$$L_2 = \frac{1}{\cos\alpha}\left[d_2 - \frac{L_1}{\cos\left(\widehat{\varphi}+\alpha\right)} - (a-L_1 tan\left(\widehat{\varphi}+\alpha\right))\sin(\widehat{\varphi}+\alpha)\right], \tag{5.5}$$

$$L_2 = \frac{1}{\cos\alpha}\left[d_3 - \frac{L_1}{\cos\left(\widehat{\varphi}+\alpha\right)} + (a+L_1 tan\left(\widehat{\varphi}-\alpha\right))\sin(\widehat{\varphi}-\alpha)\right], \tag{5.6}$$

$$L_2 = \frac{1}{\cos\alpha}\left[d_4 - \frac{L_1}{\cos\left(\widehat{\varphi}+\alpha\right)} + (a+b+L_1 tan\left(\widehat{\varphi}-\alpha\right))\sin(\widehat{\varphi}-\alpha)\right], \tag{5.7}$$

where, $\hat{\phi}$ is the estimated hitch angle. By equalizing each pair of equations (5.4) to (5.7), one equation will be generated that estimates the hitch angle for different sensor combination. Therefore, totally six equations will be generated for six different sensor combinations among which two of them are explicit formula and the rest are implicit which are solved by the Newton-Raphson method in this research. Therefore, the hitch angle estimation block can be shown as seen in Fig. 5.2 where, $\hat{\phi};\ i,j \in \{1,2,3,4\}$ is the estimated hitch angle by utilizing ultra-sonic sensors number i and j. In hitch angle estimation block with ultra-sonic sensors data, the sensor data and trailer frontal shape are the inputs to the estimation block and the outputs are the six different estimated hitch angle from different sensor combinations. These values can be compared in a voting block to identify a more accurate hitch angle and detect any faulty sensors by some additional logics. The considered voting block in this research is designed based on the cleanness and reliability of the sensor signals.

5.3 Hitch Angle Estimation Using Kinematic Equations

The hitch angle can also be estimated based on the vehicle-trailer center of rotation by taking the Ackermann steering geometry into account.

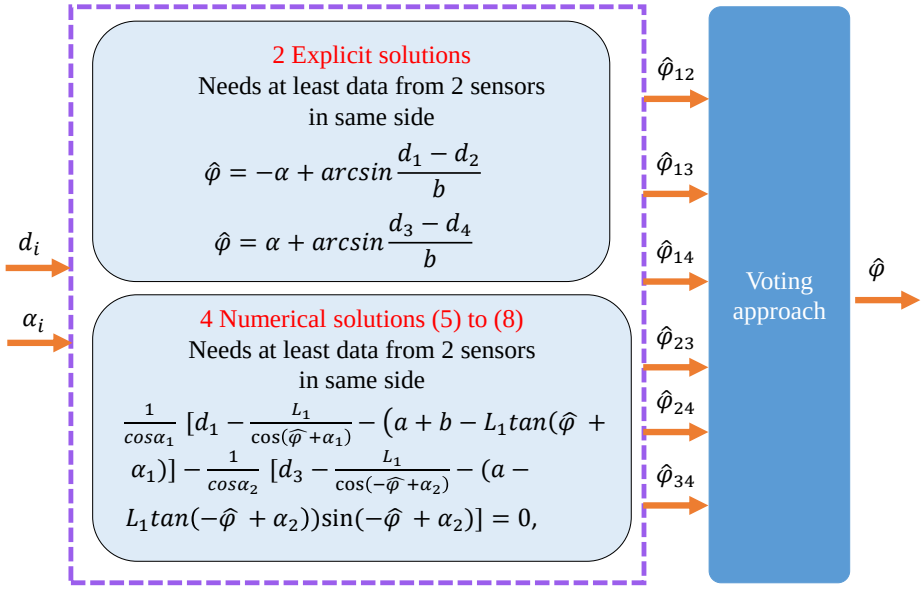

Figure 5.2: Hitch angle estimation block with ultra-sonic sensors data.

5.3.1 Kinematic Model

The kinematic equation can be obtained by analysing the center of rotation as shown in Fig. 5.3. The vehicle-trailer center of rotation is related to the steering angle. The kinematic equation of the vehicle-trailer is a function of the vehicle steering angle and longitudinal velocity. Given the longitudinal and lateral kinematics of the vehicle-trailer system, the trailer velocity in both longitudinal and lateral directions are obtained based on the vehicle velocity as:

$$\begin{aligned} V_{x2} &= V_{x1}\cos\theta_{km} + (V_{x1} - (b_1 + e)\omega_1)\sin\theta_{km}, \\ V_{y2} &= V_{x1}\sin\theta_{km} - (V_{y1} - (b_1 + e)\omega_1)\cos\theta_{km}. \end{aligned} \tag{5.8}$$

The hitch angle, shown by θ_{km}, is calculated by the difference between the vehicle and trailer yaw angle as follows:

$$\theta_{km} = \beta - \alpha. \tag{5.9}$$

By taking the derivative of (5.9), the hitch angle rate yields to:

$$\dot{\theta}_{km} = \omega_2 - \omega_1. \tag{5.10}$$

Thus, by assuming no lateral slip for the trailer, the hitch angle rate is calculated as [163]:

$$\dot{\theta}_{km} = \frac{V_{x1} \sin \theta_{km}}{L_2} - \frac{V_{x1} \tan \delta}{a_1 + b_1} \left(1 + \frac{e \cos \theta_{km}}{L_2}\right), \tag{5.11}$$

where δ is the steering angle and V_{x1} is the vehicle longitudinal velocity. L_1, b_1, and e are the constant geometrical values of the vehicle and L_2 is the trailer wheel base, also known as trailer axle location.

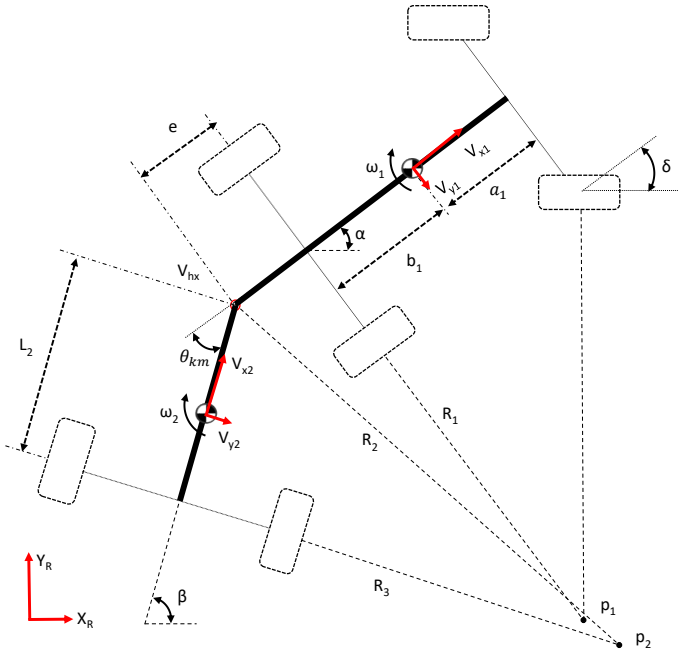

Figure 5.3: Vehicle-trailer center of rotations.

As can be seen in (5.11), the trailer axle location is the only parameter required to be given/known from the trailer in the kinematic equation of the hitch angle. Therefore, to make the hitch angle estimation algorithm generic for any ball type trailer, the trailer axle location is estimated.

5.3.2 Trailer Axle Location Estimation

Trailer axle location which is denoted by L_2 in Fig. 5.3, needs to be identified because when an unknown trailer is connected to a towing vehicle, L_2 is needed for the kinematic hitch angle equation as shown in (5.11). The trailer axle location is estimated by using a gradient algorithm. The location of trailer axle is a constant trailer parameter. By utilizing the calculated hitch angle from ultra-sonic sensors data, the axle location is estimated. In this section, a parametric model of the trailer axle location is presented. To estimate the trailer axle location, the discrete gradient algorithm with parameter projection is applied. By discretizing (5.11), hitch angle kinematic equation yields to:

$$\hat{\theta}_{km,k} = \left(\frac{V_{1x,k} \sin \hat{\theta}_{km,k}}{L_2} - \frac{V_{1x,k} \tan \delta}{a_1 + b_1} (1 + \frac{e \cos \hat{\theta}_{km,k}}{L_2}) \right) T_s + \hat{\theta}_{km,k-1}. \tag{5.12}$$

The estimated hitch angle from the ultra-sonic sensors, $\hat{\phi}$, is used to identify the trailer axle location. Hence, $\hat{\theta}_{km,k}$ is replaced by $\hat{\varphi}_k$ in (5.12). Then (5.12) is written in a Static Parametric Model (SPM) to identify the trailer axle location as:

$$\left(\frac{\hat{\varphi}_k - \hat{\varphi}_{k-1}}{T_s} + \frac{V_{x1,k} \tan \delta}{a_1 + b_1} \right) L_2 = V_k \sin \hat{\varphi}_k + \frac{V_{x1,k} e \cos \hat{\varphi}_k \tan \delta}{a_1 + b_1}. \tag{5.13}$$

The right hand side of (5.13) is the output signal and the regression signal, ϕ_k, is defined as follows:

$$\underbrace{\left(\frac{\hat{\varphi}_k - \hat{\varphi}_{k-1}}{T_s} + \frac{V_{x1,k} \tan \delta}{a_1 + b_1} \right)}_{\phi_k} \underbrace{L_2}_{\zeta} = \underbrace{\left(V_{x1,k} \sin \hat{\varphi}_k + \frac{V_{x1,k} e \cos \hat{\varphi}_k \tan \delta}{a_1 + b_1} \right)}_{z_k}. \tag{5.14}$$

Since the measurement from the sensors are in the discrete domain, the discrete gradient approach is used for estimating the trailer axle location. The axle location is bounded as the axle location of most of the available trailers in the market is from 1 to 6 meters. Therefore, a priori knowledge about the axle location is considered as $1 < L_2 < 6$. The estimation error is defined as the difference between the actual and estimated axle location value. By considering the SPM model for the trailer axle location which is shown in (5.14), the estimation error yields to:

$$\varepsilon_k = z_k - \hat{z}_k = \frac{z_k - \zeta_{k-1}\phi_k}{m_{s,k}^2}, \tag{5.15}$$

where $m_{s,k}^2 = 1 + \alpha\phi_k^T\phi_k$ is the normalization factor. The discrete gradient algorithm with parameter projection is considered to estimate the trailer axle location as:

$$\hat{z}_k = \zeta_k\hat{\phi}_k, \tag{5.16}$$

$$\zeta_0 \leq \zeta^* \leq \zeta_{\max}\ ,\ \bar{\zeta}_k = \zeta_{k-1} + \alpha\varepsilon_k\phi_k, \tag{5.17}$$

$$\zeta_k = \zeta_0 + \left(\bar{\zeta}_k - \zeta_0\right)\min\left(1, \frac{\zeta_{\max}}{\left|\bar{\zeta}_k - \zeta_0\right|}\right). \tag{5.18}$$

The estimated trailer axle location, $\hat{\phi}_k$, is then used in the hitch angle estimation algorithm.

5.3.3 Hitch Angle Estimation Using Kinematic Equation

To estimate the hitch angle, the Extended Kalman Filter (EKF) is applied to the nonlinear kinematic equation of hitch angle (5.11). The estimated trailer axle location is used in the kinematic hitch angle equation to make the hitch angle estimation independent from the trailer parameters. The discretized kinematic equation (5.12) is considered as the system model in the following form:

$$\begin{gathered} x_k = f_{k-1}\left(x_{k-1}, u_{k-1}, w_{k-1}\right) = \theta_{km,k-1} + w_{k-1} \\ + \left(\frac{V_{1x,k}\sin\theta_{km,k-1}}{\hat{L}_2} - \frac{V_{1x,k}\tan\delta}{a_1+b_1}\left(1 + \frac{e\cos\theta_{km,k-1}}{\hat{L}_2}\right)\right)T_s, \\ y_k = h_k\left(x_k, v_k\right) = \varphi_k + v_k, \end{gathered} \tag{5.19}$$

where the hitch angle is calculated based on the ultra-sonic sensors data. In addition, $w_k \sim (0, Q_k)$ and $v_k \sim (0, R_k)$ are the process and measurement noises with zero means and the covariance of Q_k and R_k, respectively. w_k and v_k are white and uncorrelated noises ($E(w_k, w_j^T) = Q_k\delta_{k-j}$, $E(v_k, v_j^T) = R_k\delta_{k-j}$, and $E(v_k, w_j^T) = 0$), where δ_{k-j} is the

Kronecker delta function of $k-j$. By following the EKF approach, the linearized model over the prediction value is determined as

$$\begin{cases} F_{k-1} = \left.\frac{\partial f_{k-1}}{\partial x}\right|_{\hat{x}_{k-1}} = \frac{V_k T_s \cos\hat{\theta}^+_{km,k-1}}{\hat{L}_2} + \frac{eV_{1x,k}\tan\delta\sin\hat{\theta}^+_{km,k-1}}{a_1+b_1} + 1, \\ L_{k-1} = \left.\frac{\partial f_{k-1}}{\partial w}\right|_{\hat{x}_{k-1}} = 1. \end{cases} \tag{5.20}$$

Thus, the update EKF gain is calculated as:

$$\begin{cases} k_k = p_k^- H_k^T \left(H_k p_k^- H_k^T + M_k R_k M_k^T\right)^{-1}, \\ \hat{x}_k^+ = \hat{x}_k^- + k_k \left(y_k - h_k\left(\hat{x}_k^-, 0\right)\right), \\ p_k^+ = \left(I - k_k H_k\right) p_k^-. \end{cases} \tag{5.21}$$

Eventually, the hitch angle is estimated by applying an EKF on the kinematic equation shown in (5.19). The hitch angle kinematic equation in (5.19) is valid under the assumption of no lateral slip for the trailer. This assumption is most likely valid for the low speed operation. For the cases where the trailer has lateral slip, which occur often at high speed operation, the dynamic equations of the vehicle-trailer system are considered to estimate the hitch angle which is proposed in the next section.

5.4 Hitch Angle Estimation Using Dynamic Equations

The dynamic equations of the vehicle-trailer system are utilized to estimate the hitch angle. To do so, by considering the vehicle-trailer system as a single unit, the dynamic of the trailer is derived with respect to the vehicle motion, which is introduced in this section.

5.4.1 Vehicle-Trailer Dynamic Model

By considering the equations of motion of the vehicle-trailer system, the hitch angle is written in the state space form. A 3-DoF model is considered to derive the dynamic equations of the vehicle-trailer system. Fig. 3.1 illustrates a schematic representation of a vehicle-trailer system. The equations of motion for the vehicle-trailer system is written as:

$$m_1 a_{x1} = F_{x,rR} + F_{x,rL} + \left(F_{x,fR} + F_{x,fL}\right)\cos\delta + F_{xT} - \left(F_{y,fR} + F_{y,fL}\right)\sin\delta, \tag{5.22}$$

$$m_1 a_{y1} = (F_{y,fR} + F_{y,fL})\cos\delta + F_{y,rR} + F_{y,rL} + F_{yT} + (F_{x,fR} + F_{x,fL})\sin\delta, \tag{5.23}$$

$$m_2 a_{x2} = F_{x,tR} + F_{x,tL} - F_{xT}\cos\theta_D + F_{yT}\sin\theta_D, \tag{5.24}$$

$$m_2 a_{y2} = F_{y,tR} + F_{y,tL} - F_{yT}\cos\theta_D + F_{xT}\sin\theta_D, \tag{5.25}$$

where θ_D denotes the hitch angle value that is estimated by the dynamic approaches. In equations (5.22) to (5.25), the longitudinal and lateral accelerations, yaw rate, and steering angle are measurable. Moreover, the vehicle geometric parameters such as CG location and vehicle length are known. The kinematic relationships of the vehicle-trailer systems are obtained as:

$$a_{x1} = \dot{V}_{x1} - \omega_1 V_{y1}, \tag{5.26}$$

$$a_{y1} = \dot{V}_{y1} + \omega_1 V_{x1}, \tag{5.27}$$

$$\omega_2 = \dot{\theta}_D + \omega_1, \tag{5.28}$$

$$V_{y2} = (V_{y1} - (b_1 + e)\omega_1)\cos\theta_D + V_{x1}\sin\theta_D - a_2\omega_2. \tag{5.29}$$

The tire forces are determined using a bi-linear tire model. To simplify the model, axle forces, F_{yf} and F_{yr}, are replaced by the lateral tire forces ($F_{yf} = F_{y,fR} + F_{y,fL}$ and $F_{yr} = F_{y,rR} + F_{y,rL}$). The linear relationships between the tire forces and slip angles are presented in the following:

$$F_{yf} = \begin{cases} C_{yf}\alpha_f, & |\alpha_f| < \alpha_{max} \\ C_{yf}\alpha_{max}, & Otherwise \end{cases}, F_{yr} = \begin{cases} C_{yr}\alpha_r, & |\alpha_r| < \alpha_{max} \\ C_{yr}\alpha_{max}, & Otherwise \end{cases}, \tag{5.30}$$

where α_{max} is 4 deg. C_{yf} and C_{yr} are the front and rear tire cornering stiffness of the vehicle, respectively. $\alpha_f = \delta - (v_1 + a_1 r_1)/(u)$ and $\alpha_r = -(v_1 - b_1 r_1)/(u)$ are the front and rear tire side slip angles that are calculated in (3.10). Moreover, the longitudinal tire forces are calculated based on the wheel dynamic as shown in (4.5) [165]. In the vehicle-trailer system model, the pitch and bouncing motions, longitudinal/lateral load transfer,

and aerodynamic forces are ignored. By combining (5.22) with the lateral tire model, the dynamic hitch angle equations of a vehicle-trailer system can be written as:

$$\begin{aligned}&((m_1+m_2)a_{y1}-F_{xf}\sin\delta-C_{yf}\alpha_f\cos\delta-C_{yr}\alpha_r)\tan\theta_D\\&=(m_1+m_2)\,a_{x1}-F_{xf}\cos\delta+C_{yf}\alpha_f\sin\delta-F_{xr},\end{aligned}\tag{5.31}$$

where $F_{xf}=F_{x,fL}+F_{x,fR}$ and $F_{xr}=F_{x,rL}+F_{x,rR}$ are the front and rear axle longitudinal tire forces, respectively. As can be seen in (5.31), the trailer mass is required for the estimation of the hitch angle. To make the dynamic based hitch angle estimation algorithm independent from the trailer type and trailer mass, the estimated trailer mass is considered which is described in Chapter 4.

5.4.2 Hitch Angle Estimation Using Dynamic Equations

The hitch angle can also be estimated by considering the equations of motion of the vehicle-trailer system. To do so, the hitch angle dynamic equation, shown in (5.31), is considered. The recursive least square method can be applied to the dynamic hitch angle equation to estimate the hitch angle. Based on this equation, the regression and the output signal are defined as follows:

$$\chi_k=\tan\theta_{D,k},\tag{5.32}$$

$$\Phi_k=(\mathrm{m_1}+\widehat{\mathrm{m}}_2)\,\mathrm{a_{y1,k}}-\mathrm{F_{xf,k}}\sin\delta_\mathrm{k}-\mathrm{C_{yf}}\alpha_{\mathrm{f,k}}\cos\delta_\mathrm{k}-\mathrm{C_{yr}}\alpha_{\mathrm{r,k}},\tag{5.33}$$

$$\mathrm{Z_k}=(\mathrm{m_1}+\widehat{\mathrm{m}}_2)\,\mathrm{a_{x1,k}}-\mathrm{F_{xf,k}}\cos\delta_\mathrm{k}+\mathrm{C_{yf}}\alpha_{\mathrm{f,k}}\sin\delta_\mathrm{k}-\mathrm{F_{xr,k}},\tag{5.34}$$

where, Φ_k is the regression and $\mathrm{Z_k}$ is the output signal. The recursive least-square algorithm is written as follows:

$$\widehat{\chi}_{k+1}=\widehat{\chi}_k+K_{K+1}(\mathrm{Z_{k+1}}-\Phi_{k+1}\widehat{\chi}_k),\tag{5.35}$$

$$K_{k+1}=\frac{P_k\Phi_{k+1}}{\lambda+\Phi_{k+1}P_k\Phi_{k+1}},\tag{5.36}$$

$$P_{k+1}=(1-K_{k+1}\Phi_{k+1})p_k/\lambda.\tag{5.37}$$

The recursive least-square algorithm with forgetting factor, λ, guarantees that $X_k \to X_k^*$ as $t \to \infty$, if Φ_k is persistently exciting. The X_k^* is the tan of the actual hitch angle value. To calculate the Φ_k and Z_k, the vehicle longitudinal velocity, yaw rate and lateral acceleration are measured by the vehicle IMU.

As mentioned, the hitch angle equation (5.11) is valid under the assumption of no lateral slip for the trailer. Moreover, the calculated hitch angle based on the ultra-sonic sensors is noisy and is not accurate in severe weather conditions. Therefore, in order to estimate the hitch angle more accurately, the data fusion technique is considered as follows:

$$\widehat{\theta}_f = \begin{cases} \widehat{\theta}_{Km} & if \quad v_x < v_{th} \\ \widehat{\theta}_D & if \quad v_x > v_{th} \;\&\; |\delta| > \delta_{th} \\ \widehat{\varphi} & Otherwise \end{cases}, \tag{5.38}$$

where v_{th} and δ_{th} are the designed thresholds for the longitudinal velocity and steering angle that above it the trailer slip angle might be large. Based on several tests and simulation results, the v_{th} and δ_{th} are chosen to be 30 km/h and 4 deg, respectively. The overall hitch angle estimation scheme is illustrated in Fig. 5.4.

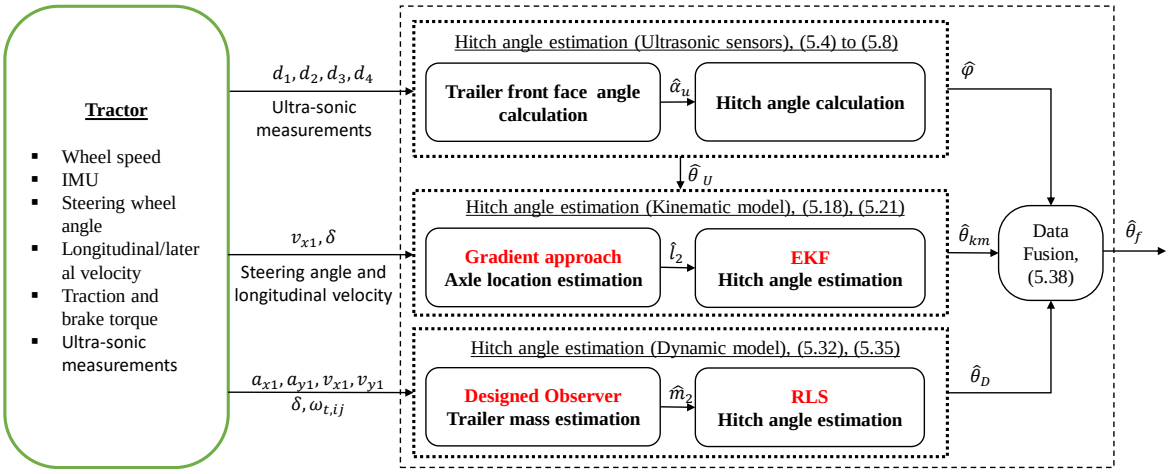

Figure 5.4: Overall hitch angle estimation scheme.

5.5 Simulation and Experimental Tests

In this section the presented hitch angle estimation is validated by both simulation and experimental studies.

5.5.1 Simulation Results

A CarSim model with the parameters listed in Table 5.1 is used to evaluate the proposed estimation algorithm. The simulation is run for different steering angles as well as different velocities to evaluate the hitch angle estimation. The trailer axle location is also estimated, simultaneously with the hitch angle. Therefore, both parameter and state estimations are evaluated with the CarSim model.

Table 5.1: Vehicle-trailer parameters for hitch angle estimation

Parameters	Description	Value
m_1	Vehicle's mass (kg)	2260
I_{z1}	Vehicle's yaw moment of inertia (kg.m2)	4160
a_1	Vehicle's CG to front axle (m)	1.21
b_1	Vehicle's CG to rear axle (m)	1.74
e	Vehicle's rear axle to hitch-point (m)	1.27
Tw_1	Front axle length (m)	1.62
Tw_2	Rear axle length (m)	1.57
R_{eff}	Effective tire radius (m)	0.34
m_2	Trailer's mass (kg)	665
a_2	Trailer's CG to hitch-point (m)	2
b_2	Trailer's CG to axle (m)	1
Tw_3	Trailer width (m)	1.8

The first simulation investigates the proposed trailer mass estimation performance,

with the vehicle-trailer going straight at an initial speed of 20 km/h, and accelerating. This simulation is conducted for two conditions: a loaded and an unloaded trailer. The trailer is unloaded in test-1, and has 220 kg payload in the test-2. The simulation result is shown in Fig. 5.5.

As can be seen in Fig. 5.5, the trailer mass is estimated by the designed observer introduced in Chapter 4. The trailer mass estimation steady state error is 7%. Given that the trailer mass is a constant parameter of the trailer, it needs to be estimated per operation. Since the trailer mass estimation convergence is guaranteed (*Theorem 4.1*), the estimated trailer mass can be used for the hitch angle estimation.

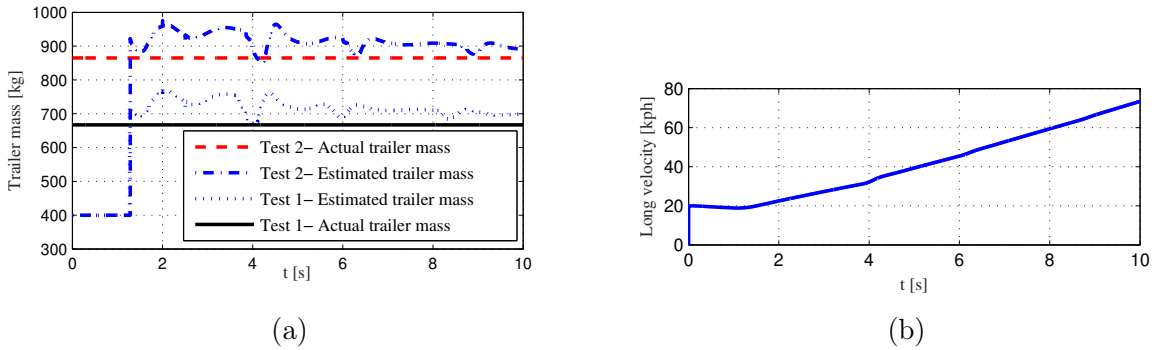

(a) (b)

Figure 5.5: a) Trailer mass estimation, b) Vehicle-trailer longitudinal velocity.

To investigate the hitch angle estimation methods developed above, a Double Lane Change (DLC) maneuver is applied (Fig. 5.6a). Since the ultra-sonic sensors' data are not available in the simulation, the hitch angle that would be calculated by ultra-sonic sensor data is instead generated by adding white noise to the actual value of the hitch angle provided by the CarSim model.

Since the sensors may fail to detect the trailer front face, the data generated between 5.5 and 7 seconds are removed. Moreover, two jumps in the data are added to the actual value of the hitch angle at 1 and 14 seconds to cover the sensors' false detections. Fig. 5.6b shows the generated hitch angle by ultra-sonic sensor data. The estimated hitch angle based on kinematic equation (5.21), is shown in Fig. 5.6c. This equation accurately estimates the hitch angle while the assumption of no lateral slip for the trailer is valid. As can be seen in the results, as speed increases, the assumption is no longer valid. Therefore, the kinematic method for estimating hitch angle is not appropriate for high-speed operations. Moreover,

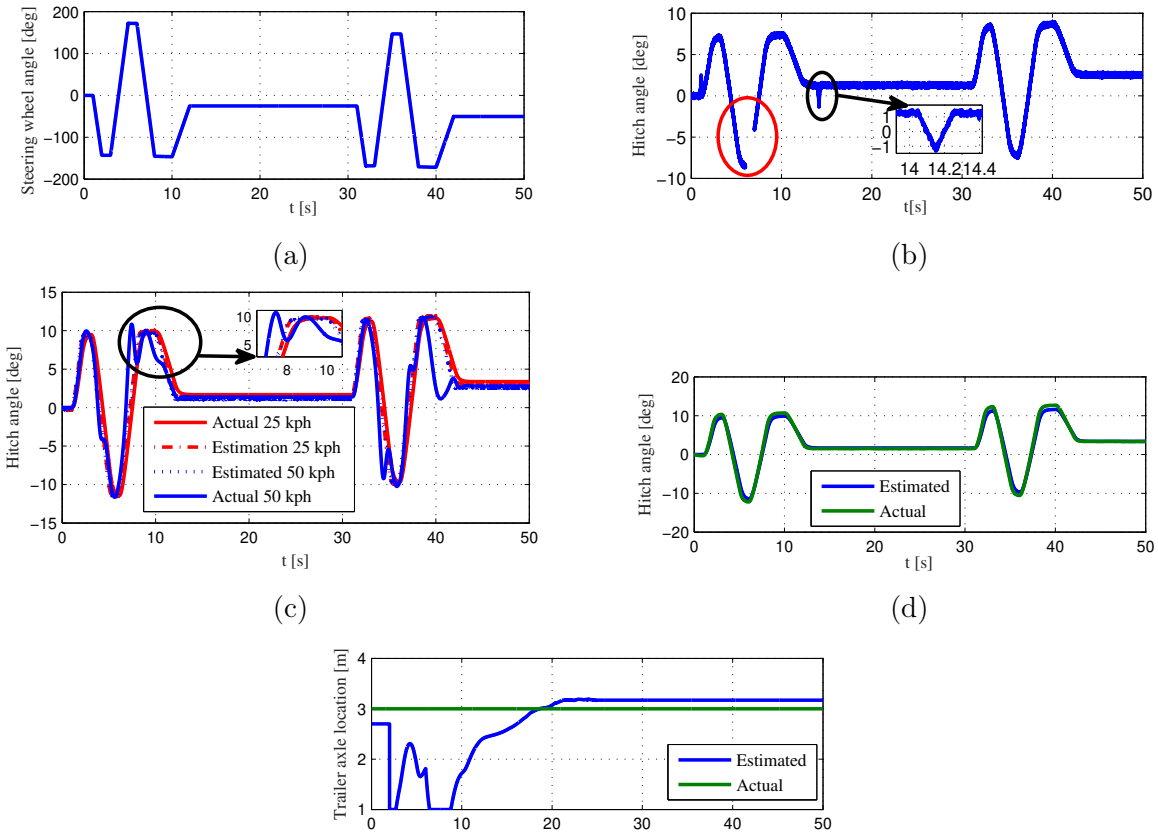

Figure 5.6: a) Steering wheel angle, b) Generated hitch angle by ultra-sonic sensors, c) Estimated hitch angle based on the kinematic model, d) Estimated hitch angle based on the vehicle-trailer model, e) Estimated trailer axle location.

given that the estimated trailer axle location is used in the kinematic equation to estimate the hitch angle, the estimated value becomes more accurate when the estimated trailer axle location converges to its actual value as shown in Fig. 5.6e. The estimated hitch angle with respect to the vehicle-trailer dynamic model is shown in Fig. 5.6d. The estimated hitch angle based on the dynamic model of the vehicle-trailer (5.35) accurately follows the actual hitch angle.

To estimate the hitch angle more accurately, the data fusion technique shown in Fig. 5.4

is applied. Results are shown in Fig. 5.7.

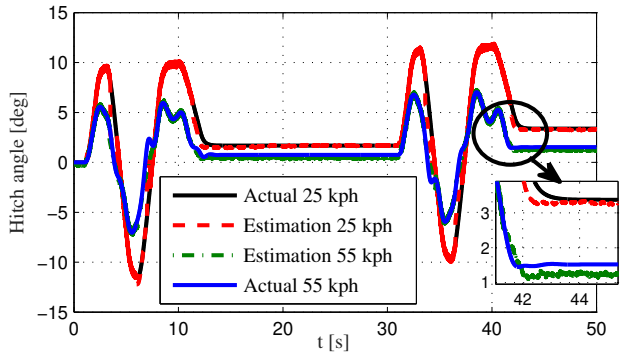

Figure 5.7: Estimated hitch angle based on the proposed algorithm by applying a double lane change maneuver.

As Fig. 5.7 illustrates, the designed hitch angle estimation algorithm, follows the actual hitch angle in both low and high-speed operations. Based on the data fusion technique described in (5.38), the estimated hitch angle is provided by ultra-sonic sensors, kinematic or dynamic approaches based on the vehicle-trailer operation conditions.

To further evaluate the algorithm, a step steer maneuver, shown in Fig. 5.8a, is considered. As mentioned in Section 5.4, to estimate the hitch angle, first the axle location is estimated (Fig. 5.8b). The estimated axle location has the steady state error of 11%. To utilize the estimated axle location in the hitch angle estimation algorithm, the axle location estimator stops working when the axle location estimation error rate converges to a small value. Therefore, a small steady state error remains for the estimated axle location.

As can be seen in the Fig. 5.8, the hitch angle estimation algorithm accurately estimates the hitch angle with the maximum error of 16% for both high and low speed operations. Prior estimation of the trailer front face angle, mass, and axle location, makes the hitch angle estimation algorithm independent of trailer geometry. In other words, no matter what the connected trailer geometry is, the hitch angle estimation algorithm works properly and estimates the hitch angle with acceptable accuracy. When an unknown ball type trailer connects to the towing vehicle, first information require about the trailer is estimated for use in the hitch angle estimation algorithm.

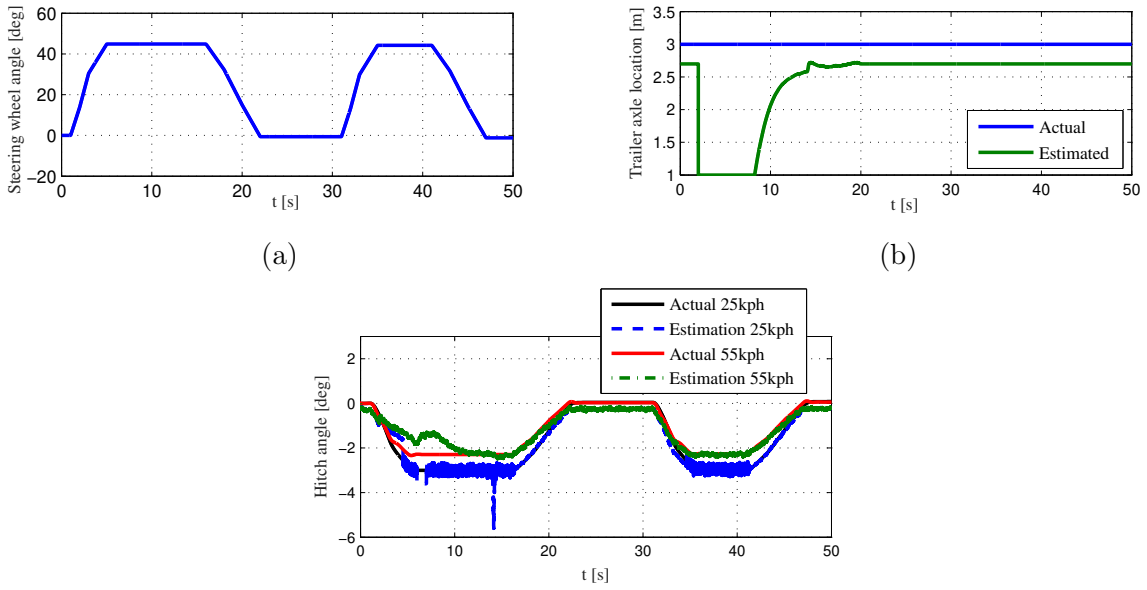

Figure 5.8: a) Steering wheel angle, b) Estimated trailer axle location, c) Estimated hitch angle - multiple step steer maneuvers.

5.5.2 Experimental Tests: Ultra-Sonic Sensors

In order to evaluate the proposed method and validate the concept with real sensory data, a test setup was created, as shown in Fig. 5.9. A board was used to represent the vehicle's rear bumper in full scale while two other boards, connected by a hinge joint, were used to represent the trailer's frontal face. The hinge joint allows setting different angles of the trailer frontal face. Four locations were created on the single board as the locations of the ultra-sonic sensors. These locations were almost the same as those on a vehicle's rear bumper. A potentiometer was also installed at the hitch location as a reference to directly measure the hitch angle. The ultra-sonic sensors were from Senix Company model TSPC-30S1-485, as shown in Fig. 5.9, with the optimum range of 3m, which can provide analog outputs.

The sensors provide 0-5 V analog output that is read and transferred to a Matlab/Simulink code. To validate the hitch angle estimation by the ultra-sonic sensors data, the V-nose shape trailer with the front face angle of $\alpha = 8\,\text{deg}$ is considered. Fig. 5.10a

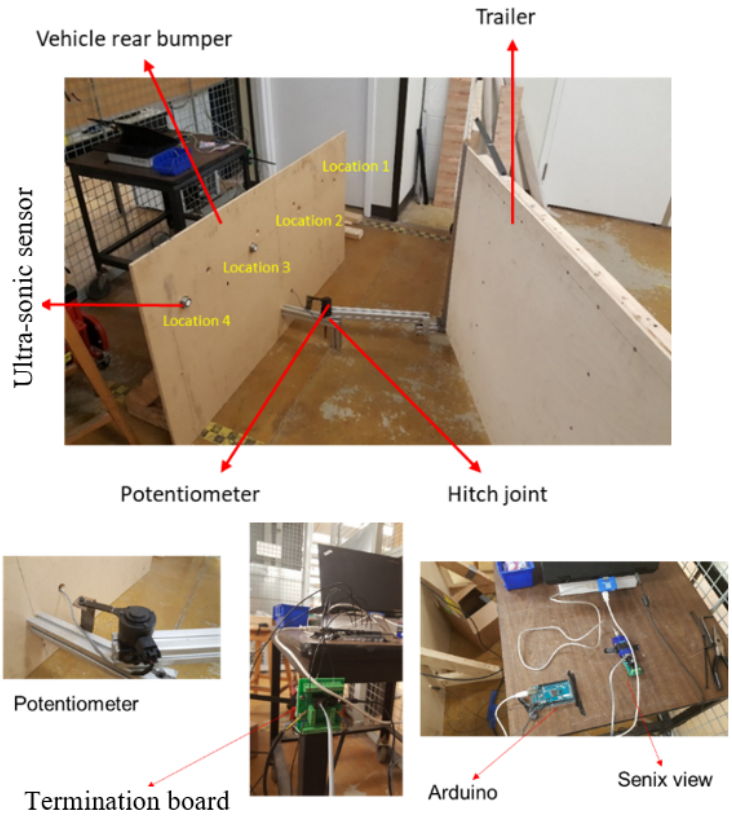

Figure 5.9: Ultra-sonic sensor test set-up.

and 5.10b show the results obtained from the estimation algorithm in terms of identified trailer front shape and estimated hitch angle, respectively. As can be seen in Fig. 5.10a, the algorithm detects the front shape correctly ($\alpha = 8\,\text{deg}$). However, in the first 2-2.5 seconds, the algorithm is not working until the two conditions become satisfied, as described before.

The results show a good match between the estimated and measured hitch angle.

5.5.3 Experimental Studies: Hitch Angle Estimation

Several experiments have been done on an electrified Chevrolet Equinox sport utility vehicle (SUV) with a single axle trailer (Fig. 4.6) to verify the proposed estimation scheme. The

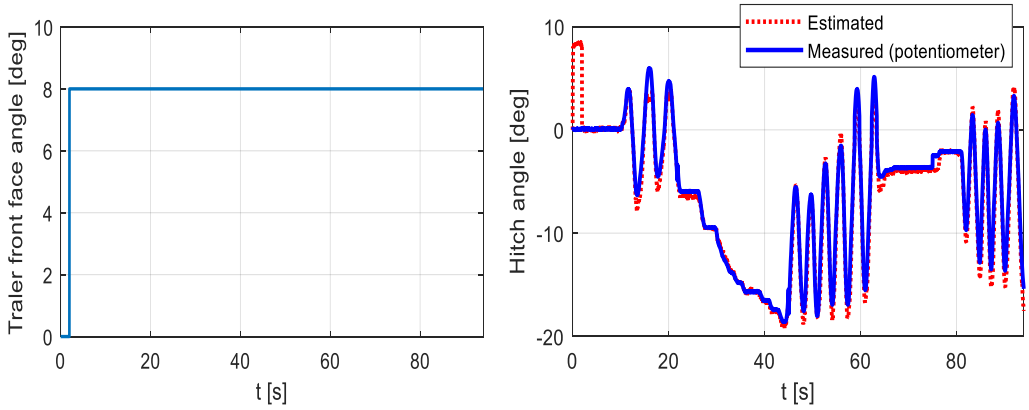

Figure 5.10: a) Identified trailer front shape, b) Comparison between the estimated hitch angle and ground truth.

Chevrolet Equinox has an all-wheel-independent-drive configuration (AWD). The specifications of the vehicle and trailer are listed in Table 4.1. To validate the hitch angle estimation with the actual value of the hitch angle, a potentiometer is connected to the ball joint at the hitch point. The longitudinal/lateral accelerations and yaw rate of the vehicle are measured with a 6-axis IMU (and GPS) system RT2000. Estimation of the test vehicle tire cornering stiffness and side slip angle was done in [181, 182, 155]. The hitch angle estimation algorithm also requires the wheel speed and wheel torques which can be measured using the regular ABS wheel speed sensors, and electric actuators, respectively.

Measured signals are communicated using a CAN-bus. Real-time acquisition and processing of sensory information and the developed algorithm is realized using the dSPACE MicroAutobox. The dSPACE compiles measurements for MATLAB/Simulink, and the hitch angle estimation algorithm run in MATLAB/Simulink by utilizing the provided measurements. The sampling frequency for the experiment is set to 200 [Hz]. It is worth mentioning that the ultrasound sensors had the lowest sampling frequency in our test set-up [40 Hz]. Therefore, ultra-sonic sensor data has been re-sampled in post processing.

The step steer maneuver shown in Fig. 5.11, is applied to the test platform to investigate the performance of the estimation algorithm. As can be seen in Fig. 5.11, the estimated hitch angle follows the actual hitch angle with good agreement. Based on the data fusion

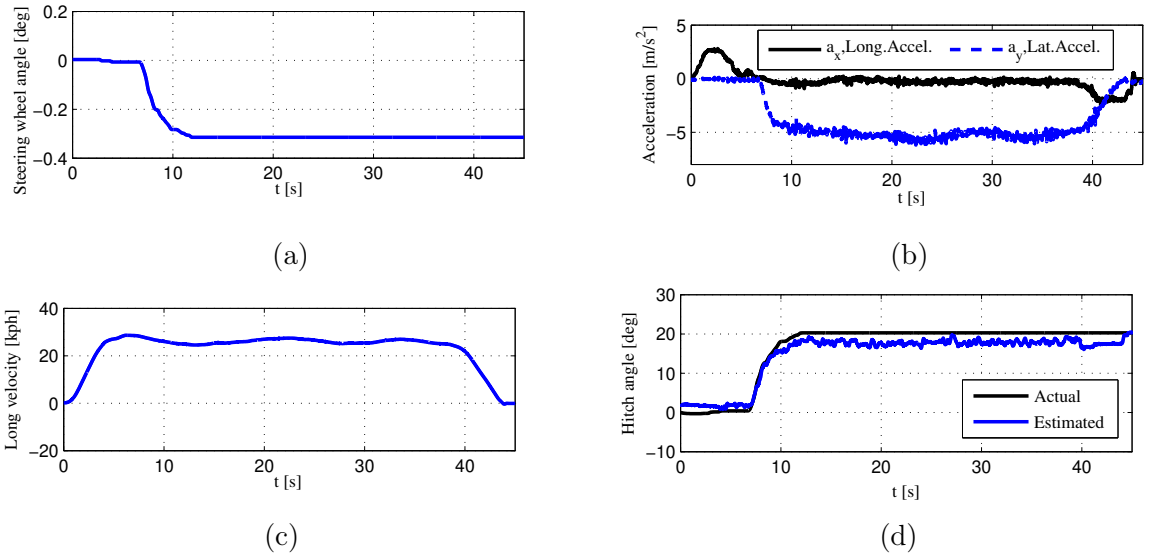

Figure 5.11: a) Steering wheel angle, b) Vehicle longitudinal/lateral accelerations, c) Vehicle longitudinal velocity, d) Estimated hitch angle - a step steer maneuver.

equation (5.38), the estimation algorithm for the hitch angle relies more on the kinematic method since the vehicle-trailer unit operates at low speed. It is worth mentioning that the small differences between the estimated and actual hitch angles right at the beginning of the test (Fig. 5.11) is due to the misalignment of the trailer with the towing vehicle.

In the second test, a series of double lane change maneuvers are applied to the vehicle-trailer system as shown in Fig. 5.12. As can be seen in the results shown in Fig. 5.12, there is a good agreement between the estimated hitch angle and the hitch angle ground truth.

5.5.4 Discussions

Given the simulation/experimental results, the estimated hitch angle by ultra-sonic sensors is accurate enough for normal environmental conditions. However, the humidity and sever weather conditions may affect the results. To address this issue, the sensor reliability signals were used in the voting block. Moreover, given that the axle location is a trailer geometry parameter, there is no need to estimate it for all the operation time.

As can be seen in the simulation/experiment results, the hitch angle estimation algo-

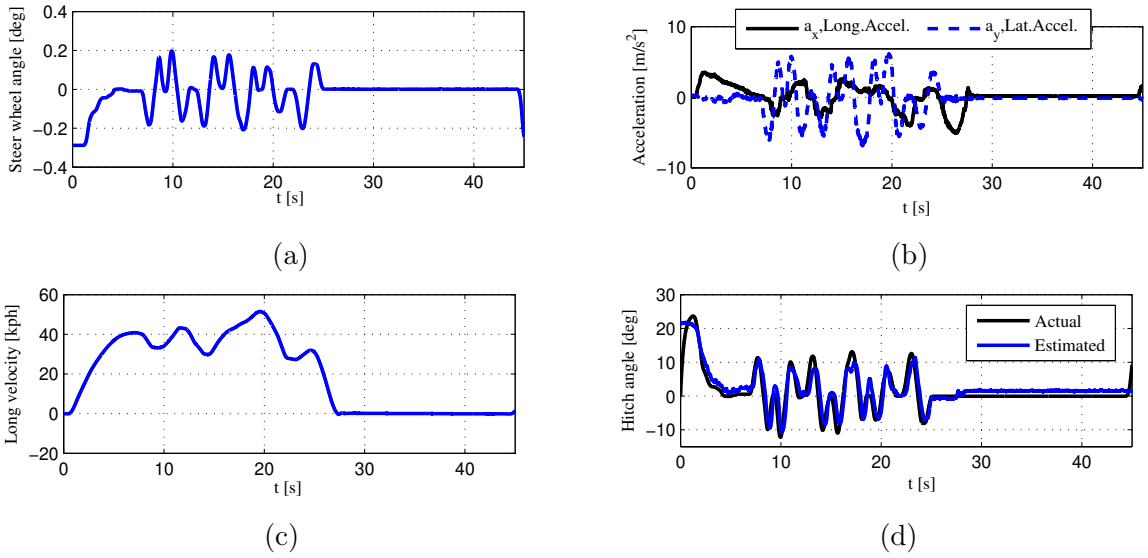

Figure 5.12: a) Steering wheel angle, b) Vehicle longitudinal/lateral accelerations, c) Vehicle longitudinal velocity, d) Estimated hitch angle - multiple double lane change maneuvers.

rithm accurately determines hitch angle. The maximum error that the algorithm provides is 16% for both high and low speed operations. Based on the experimental results, it can be concluded that fusing the kinematic and dynamic methods to the hitch angle estimated by the ultra-sonic sensors improves the hitch angle estimation since the sensors may fail to detect the trailer face correctly.

In normal driving, it has been shown that the accuracy of the proposed hitch angle estimation algorithm is not much affected by the trailer mass estimation error, however, this may not be true in more severe driving, and an improved trailer mass estimation would be required.

5.6 Conclusions

In this chapter, a complete solution for hitch angle estimation of a towing vehicle with a ball type box trailer with a flat or symmetric V-nose frontal face was developed, evaluated, and experimentally tested. For the proposed method, direct calculation of hitch angle based on ultra-sonic sensors was first presented. Kinematics and dynamics of the vehicle-trailer were

then used to develop algorithms for the hitch angle estimation. The trailer axle location, mass, and front face angle were estimated to make the hitch angle estimation algorithm independent of geometry.

It is shown that the hitch angle estimation can be used for ball type box trailers with a flat or symmetric V-nose frontal face by first estimating the trailer axle location, mass, and front face angle. The simulation and experimental studies showed promising results in estimating the hitch angle.

Chapter 6

Vehicle-Trailer Lateral Tire Forces and Hitch-Forces Estimation

6.1 Introduction

In this chapter, the lateral vehicle tire force and hitch-force are estimated for a vehicle-trailer combination. The contribution of this chapter is developing optimal real-time longitudinal/lateral coupling force and lateral tire force estimators robust to surface friction and independent to the power-train configuration and trailer geometry. The proposed hitch-force estimation method is modular and can be used for any ball type trailer without any priori information on the trailer parameters.

The difference between the proposed hitch-force estimation algorithm with other hitch-force estimation techniques presented in the literature is that, the proposed hitch-force estimation relies on the vehicle unit measurements (indirect measurements) that are available on the commercialized vehicles, while the reported hitch-force estimation techniques in the literature are based on the direct hitch-force measurements coming from an embedded sensor which may not be available on the conventional vehicles. Moreover, the existed vehicle lateral tire force estimators in the literature are for vehicle unit itself and when a trailer connects to a towing vehicle the vehicle lateral tire force estimators may not work as the dynamic of the system changes.

The remaining of this chapter is as follows: In Section 6.2, a vehicle-trailer system

model is presented in the state space form. In Section 6.3, algorithms to estimate the hitch-forces are developed and discussed, and the state constraints are presented. The estimator stability analysis and estimation error convergence rate are investigated in Section 6.4. Finally, simulation and experimental results are provided in Section 6.5 with discussions.

6.2 System Model for Hitch Force Estimation

A 3-DoF model is considered to drive dynamic equation of a vehicle-trailer system. Fig. 3.1 illustrates a schematic representation of a vehicle-trailer system. In Fig. 3.1, m_1, m_2, I_{z1} I_{z2}, r_1, and r_2 are the mass, yaw moments, and yaw rate of the vehicle and trailer, respectively. Longitudinal and lateral velocities at the vehicle Centers of Gravity (CG) are denoted by u_1 and v_1, respectively. $F_{xf,i}$, $F_{xr,i}$, $F_{xt,i}$, $F_{yf,i}$, $F_{yr,i}$, and, $F_{yt,i}$ with $i \in (R, L)$ in which R and L refer to the Right and Left side of the vehicle, are the longitudinal/lateral tire forces at front and rear axles of the vehicle, and trailer's axle, respectively. F_{xT} and F_{yT} represent the coupling forces, also known as hitch-forces, in longitudinal and lateral directions, respectively. The equations of motion for the vehicle-trailer system are as follows:

$$\begin{aligned} m_1 a_{x1} = \sum F_x = F_{xrL} + F_{xrR} + F_{xfL}\cos\delta \\ +F_{xfR}\cos\delta + F_{xT} - F_{yfL}\sin\delta - F_{yfR}\sin\delta + w_{fx}, \end{aligned} \tag{6.1}$$

$$\begin{aligned} m_1 a_{y1} = \sum F_y = F_{yfL}\cos\delta + F_{yfR}\cos\delta + F_{yrL} \\ +F_{yrR} + F_{yT} + (F_{xfL} + F_{xfR})\sin\delta + w_{fy}, \end{aligned} \tag{6.2}$$

$$\begin{aligned} I_{z1}\dot{r}_1 = \sum M_z = a_1(F_{yfL} + F_{yfR})\cos\delta - (F_{yrL} + F_{yrR})b_1 \\ +a_1(F_{xfL} + F_{xfR})\sin\delta - (b_1 + e)F_{yT} + w_r, \end{aligned} \tag{6.3}$$

where longitudinal and lateral accelerations at the vehicle and trailer CG are denoted by a_{x1}, a_{y1}, a_{x2} and a_{y2}, respectively.

Since the longitudinal/lateral load transfer, pitch and body-roll of the vehicle-trailer have less influence on the yaw stability, they are neglected [150]. w_{fx}, w_{fy}, and w_r represent the longitudinal/lateral uncertainties due to the acceleration measurement, aerodynamic

forces, inaccurate geometry and forces. Given that the uncertainties are mostly contributed to the sensor measurements, the uncertainties of the model are assumed to be Gaussian. In the planar kinematics equations (6.1) to (6.3), the steering angle, longitudinal/lateral accelerations, and yaw rate are measurable. The vehicle geometric parameters such as CG location and wheel base are assumed to be known, and the trailer geometric parameters are unknown due to unavailability of such geometrical and inertial parameters for various trailers in the market. The main goal is to estimate the lateral tire forces and hitch-point forces by taking advantage of optimal state observers. Accordingly, by considering the wheel dynamics, the longitudinal tire forces can be estimated [155]. The wheel dynamic equation is given in (4.5). In [155], longitudinal forces were estimated based on the idea of Proportional-Integral-Derivative, PID, observer. Therefore, the longitudinal tire forces, F_{xfL}, F_{xfR}, F_{xrL}, and F_{xrR}, are assumed to be known in the proposed estimation algorithm.

To estimate the lateral tire forces and hitch-forces, the vehicle-trailer equations of motion, shown in equations (6.1) to (6.3), are considered. The longitudinal and lateral kinematics of the vehicle yield the following relations

$$a_{x1} = \dot{u}_1 - r_1 v_1, \tag{6.4}$$

$$a_{y1} = \dot{v}_1 + r_1 u_1. \tag{6.5}$$

By taking the time derivative of equations (6.4) and (6.5), and replacing $\dot{u}_1$ and $\dot{v}_1$ with $\dot{u}_1 = a_{x1} + r_1 v_1$ and $\dot{v}_1 = a_{y1} - r_1 u_1$, (6.4) and (6.5) change to

$$\dot{a}_{x1} = \ddot{u}_1 - \left(\frac{\sum_i F_{y_i}}{m_1} - r_1 u_1 \right) r_1 - \left(\frac{\sum_i M_{z_i}}{I_{z1}} \right) v_1, \tag{6.6}$$

$$\dot{a}_{y1} = \ddot{v}_1 + \left(\frac{\sum_i F_{x_i}}{m_1} + r_1 v_1 \right) r_1 + \left(\frac{\sum_i M_{z_i}}{I_{z1}} \right) u_1, \tag{6.7}$$

where the vehicle-trailer equation of motion shown in equations (6.1) to (6.3) are used to obtain equations (6.6) and (6.7). To simplify the model, a single-track model is considered and the axle forces, F_{xi} and F_{yi} where $i \in [f, r]$, are replaced by the tire forces in both longitudinal and lateral directions ($F_{xi} = F_{xiL} + F_{xiR}$ and $F_{yi} = F_{yiL} + F_{yiR}$). The left hand

side of equations (6.6) and (6.7) can be obtained by taking time derivatives of equations (6.1) and (6.2) as follows:

$$\dot{a}_{x1} = \frac{1}{m_1}[\dot{F}_{xf}\cos\delta - F_{xf}\dot{\delta}\sin\delta + \dot{F}_{xr} + \dot{F}_{xT} - \dot{F}_{yf}\sin\delta - F_{yf}\dot{\delta}\cos\delta + \bar{w}_{fx}], \tag{6.8}$$

$$\dot{a}_{y1} = \frac{1}{m_1}[\dot{F}_{yf}\cos\delta - F_{yf}\dot{\delta}\sin\delta + \dot{F}_{yT} + \dot{F}_{yr} + \dot{F}_{xf}\sin\delta + F_{xf}\dot{\delta}\cos\delta + \bar{w}_{fy}]. \tag{6.9}$$

Considering equations (6.1) to (6.3), equations (6.6) to (6.9) yield to

$$\begin{aligned}\frac{1}{m_1}[\dot{F}_{xf}\cos\delta - F_{xf}\dot{\delta}\sin\delta + \dot{F}_{xT} - \dot{F}_{yf}\sin\delta + \dot{F}_{xr} - F_{yf}\dot{\delta}\cos\delta + \bar{w}_{fx}] = \\ \ddot{u}_1 - [\frac{F_{yf}\cos\delta}{m_1} + \frac{F_{yr}}{m_1} + \frac{F_{yT}}{m_1} + \frac{F_{xf}\sin\delta}{m_1} + \frac{w_{fy}}{m_1} - r_1 u_1]r_1 - [\frac{F_{xf}\sin\delta a_1}{I_{z1}} \\ + \frac{F_{yf}\cos\delta a_1}{I_{z1}} - \frac{F_{yr}b_1}{I_{z1}} - \frac{(b_1+e)F_{yT}}{I_{z1}} + \frac{w_r}{I_{z1}}]v_1,\end{aligned} \tag{6.10}$$

$$\begin{aligned}\frac{1}{m_1}[\dot{F}_{yf}\cos\delta - F_{yf}\dot{\delta}\sin\delta + \dot{F}_{yT} + \dot{F}_{xf}\sin\delta + \dot{F}_{yr} + F_{xf}\dot{\delta}\cos\delta + \bar{w}_{fy}] = \\ \ddot{v}_1 + [\frac{F_{xf}\cos\delta}{m_1} + \frac{F_{xr}}{m_1} + \frac{F_{xT}}{m_1} - \frac{F_{yf}\sin\delta}{m_1} + \frac{w_{fx}}{m_1} + r_1 v_1]r_1 + [\frac{F_{xf}\sin\delta a_1}{I_{z1}} \\ + \frac{F_{yf}\cos\delta a_1}{I_{z1}} - \frac{F_{yr}b_1}{I_{z1}} - \frac{(b_1+e)F_{yT}}{I_{z1}} + \frac{w_r}{I_{z1}}]u_1.\end{aligned} \tag{6.11}$$

Moreover, the time derivative of (6.3) results in

$$I_{z1}\ddot{r}_1 = [(\dot{F}_{xf} - F_{yf}\dot{\delta})\sin\delta + (\dot{F}_{yf} + F_{xf}\dot{\delta})\cos\delta]a_1 - \dot{F}_{yr}b_1 - (b_1+e)\dot{F}_{yT} + \bar{w}_r, \tag{6.12}$$

where $\bar{w}_{fx}$, $\bar{w}_{fy}$,and $\bar{w}_r$ are due to time derivatives of noise/uncertainties in the longitudinal, lateral and yaw directions, respectively. The lateral/longitudinal accelerations and yaw rate of the vehicle, measured by an Inertia-Measurement-Unit (IMU), and the longitudinal/lateral velocities, measured by a Global-Positioning-System (GPS), are considered as the measurement signals. As the considered system is non-autonomous, defining the state vector as $\mathbf{x} = \left[\ F_{yf}, F_{yr}, F_{yT}, F_{xT}, \dot{F}_{yf}, \dot{F}_{yr}, \dot{F}_{yT}\ \right]^T$ and the output (measurement) vector

as $y = \left[\ a_{x1}, a_{y1}, r_1\ \right]^T$ the system dynamics in equations (6.10) to (6.12) represent in state space form for small steering angle δ as follows:

$$\begin{aligned}\dot{\mathbf{x}} &= \mathbf{A}(\delta)\mathbf{x} + \mathbf{B} + \mathbf{w}_x,\\ \mathbf{y} &= \mathbf{H}(\delta)\mathbf{x} + \mathbf{D} + \mathbf{v}_y,\end{aligned} \tag{6.13}$$

where $\mathbf{w}_x$ and $\mathbf{v}_y$ correspond to the process and measurement uncertainties, respectively, as the model first and second derivatives are contributed with noises. The linearized system model matrices around its main equilibrium point are obtained as follows:

$$\mathbf{A}(\delta) = \begin{bmatrix} \delta & 0 & 0 & 0 & 0 & a_{16} & a_{17} \\ a_{21} & a_{22} & a_{23} & l_1 & -1 & 0 & -1 \\ a_{31} & 0 & 0 & 0 & a_{35} & a_{36} & 0 \\ a_{41} & a_{42} & a_{43} & 0 & \delta & 0 & 0 \\ & & & \mathbf{0}_{3\times 7} & & & \end{bmatrix}, \tag{6.14a}$$

$$\mathbf{B} = \begin{bmatrix} \frac{I_{z1}\ddot{r}_1 - a_1\dot{F}_{xf}\delta - a_1 F_{xf}\dot{\delta}}{a_1} \\ b_{21} \\ \frac{-I_{z1}\ddot{r}_1 + a_1\dot{F}_{xf}\delta + a_1 F_{xf}\dot{\delta}}{(b_1+e)} \\ b_{41} \\ \mathbf{0}_{3\times 1} \end{bmatrix}, \tag{6.14b}$$

$$\mathbf{H}(\delta) = \begin{bmatrix} -\frac{\delta}{m_1} & 0 & 0 & \frac{1}{m_1} & \\ \frac{1}{m_1} & \frac{1}{m_1} & \frac{1}{m_1} & 0 & \mathbf{0}_{3\times 3} \\ \frac{a_1}{I_{z1}} & -\frac{b_1}{I_{z1}} & -\frac{e+b_1}{I_{z1}} & 0 & \end{bmatrix}, \tag{6.14c}$$

$$\mathbf{D} = \begin{bmatrix} \frac{F_{xf}+F_{xr}}{m_1} & \frac{F_{xf}\delta}{m_1} & \frac{F_{xf}\delta a_1}{I_{z1}} \end{bmatrix}^T. \tag{6.14d}$$

$\mathbf{A}(\delta)$ and $\mathbf{B}$ matrix elements are presented in Appendix A. As can be seen in (6.14a), the last three rows of the matrices $\mathbf{A}(\delta)$ and $\mathbf{B}$ are zeros, meaning that the second derivative of forces are assumed to be zero; however, as the first derivative of the forces are involved in the system model, they are required to be presented in the state space vector.

It is assumed that the vehicle-trailer longitudinal velocity is constant during the maneuver. Therefore, given that the steering angle is bounded, matrices $\mathbf{A}(\delta)$ and $\mathbf{H}(\delta)$ are time-varying and physically bounded.

Remark 6.1: The system shown in (6.13) is observable and the time-varying observability matrix of the system is given by [183, 184]

$$\mathbf{O}_n = \begin{bmatrix} \tau_1^T & \tau_2^T & \cdots & \tau_n \end{bmatrix}^T, \tau_1 = H(\delta), \tau_{i+1} = \tau_i A(\delta) + \dot{\tau}_i. \tag{6.15}$$

The system shown in (6.13) is observable and its observability is satisfied by holding the full rank condition, $\mathbf{O}_7 = 7$, for the operating regions of the steering angle and its time derivatives. The system shown in (6.13) is not observable for the case where $\delta = 0$ and $K\pi$ for integer values of K, however, in this case ($\delta = 0$), there is no lateral force on the tires. Moreover, situations where $\delta = K\pi$ never happen due to the steering system's geometrical constraints. The discretized form of the system equations describes as follows:

$$\begin{aligned} \mathbf{x}_{k+1} &= \mathbf{A}_d \mathbf{x}_k + \mathbf{B}_d + \mathbf{w}_k, \\ \mathbf{y}_k &= \mathbf{H}\mathbf{x}_k + \mathbf{D} + \mathbf{v}_k, \end{aligned} \tag{6.16}$$

where, $\mathbf{A}_d = e^{\mathbf{A}(\delta)T_s}$ and $\mathbf{B}_d = \int e^{\mathbf{A}(\delta)\tau}\mathbf{B}d\tau$ are the discretized form of the system matrices $\mathbf{A}(\delta)$ and $\mathbf{B}(\delta)$. The process and the measurement noise becomes Gaussian with zero means and the covariance of $\mathbf{Q}_k \in \mathbf{R}^{7\times7}$ and $\mathbf{R}_k \in \mathbf{R}^3$, respectively. The covariance $\mathbf{Q}_k$ and $\mathbf{R}_k$ matrices are considered as a tuning parameters for reducing the hitch-force estimation error. $\mathbf{w}_k$ and $\mathbf{v}_k$ are white and uncorrelated noises ($E(w_k, w_j^T) = Q_k\delta_{k-j}$, $E(v_k, v_j^T) = R_k\delta_{k-j}$, and $E(v_k, w_j^T) = 0$), where δ_{k-j} is the Kronecker delta function of $k - j$. Moreover, the measured accelerations usually come with noises and bias. A bias-removal method in low or high frequencies and observer based approaches for removing the noises are used [185].

6.3 Force Estimation

A constrained observer for the lateral tire forces and hitch-forces is designed in this section. Taking into account that the systems dynamic (6.14c) is time-varying with respect to the steering angle, the suggested estimation method must be designed for the corresponding uncertain Linear-Parameter-Varying (LPV) system. The lateral tire forces and hitch-forces are estimated using the presented vehicle body dynamic, acceleration, and yaw rate measurements.

6.3.1 Constraints

Consider the system presented in (6.16). As mentioned, there is no lateral tire forces and lateral hitch-forces when $\delta = 0$. Moreover, by investigating the linear tire model, e.g. $F_{yf} = C_f \alpha_f$ where C_f is the tire cornering stiffness and $\alpha_f = \delta - (v_1 + a_1 r_1)/u_1$ is the tire slip angle, it can conclude that the lateral tire forces magnitude are related to the vehicle longitudinal velocity and as the longitudinal speed increases, the lateral tire forces become larger. Therefore, based on the physical and dynamical considerations, the states satisfy the following constraint:

$$|\mathbf{x}_k| < \boldsymbol{\beta}|\delta|u_1, \tag{6.17}$$

where $\boldsymbol{\beta} = [n_1, n_2, n_3/(|\delta|u_1), n_4/(|\delta|u_1), n_5, n_6, n_7]^T$ in which $n_i, i \in [1, 2, ..., 7]$ is the state threshold designed parameter that is designed to keep the estimated state bounded for harsh maneuvers which makes the vehicle-trailer unstable (e.g. trailer snaking and jack-knifing). n_i are the designed positive parameters that for the simulated and experimental test vehicle are designed based on several tests in Section 6.5.

Moreover, the maximum longitudinal hitch-force occurs when the vehicle-trailer system is in acceleration or deceleration conditions. The coupling forces, specially the longitudinal hitch-force, are mainly contributed to the vehicle traction forces shown in (4.5). The maximum value of the longitudinal hitch-force at time step k, i.e., $x_{4,k}$, occurs when the vehicle-trailer accelerate/decelerate with no steering angle. Therefore, a constraint on longitudinal hitch-force is defined as follows:

$$x_{4,k} < \mathbf{R}_t(\mathbf{T}_t - \mathbf{I}\dot{\boldsymbol{\omega}}_t), \tag{6.18a}$$

$$\mathbf{R}_t = \begin{bmatrix} R_{eff,fL}^{-1} & R_{eff,fR}^{-1} & R_{eff,rL}^{-1} & R_{eff,rR}^{-1} \end{bmatrix}, \tag{6.18b}$$

$$\mathbf{T}_t = \begin{bmatrix} T_{fL} & T_{fR} & T_{rL} & T_{rR} \end{bmatrix}^T, \tag{6.18c}$$

$$\boldsymbol{\omega}_t = \begin{bmatrix} \dot{\omega}_{fL} & \dot{\omega}_{fR} & \dot{\omega}_{rL} & \dot{\omega}_{rR} \end{bmatrix}^T, \tag{6.18d}$$

$$\mathbf{I} = \begin{bmatrix} I_{\omega,fL} & 0 & 0 & 0 \\ 0 & I_{\omega,fR} & 0 & 0 \\ 0 & 0 & I_{\omega,rL} & 0 \\ 0 & 0 & 0 & I_{\omega,rR} \end{bmatrix}, \tag{6.18e}$$

where $\mathbf{T}_t$ represents the total effective torques at each corner, $\dot{\boldsymbol{\omega}}_t$ represents the wheel rotational acceleration at each corner, $\mathbf{R}_t$ and $\mathbf{I}$ are the effective radius and wheel momentum of inertia of the tires, respectively. The defined constraints are considered in a designed cost function to estimate the lateral tire forces and hitch-forces which is discussed in the next subsection.

6.3.2 Lateral Tire Forces and Hitch-Force Estimations

For vehicle motion dynamics state/parameter identification and estimation, Unscented Kalman Filter (UKF) and Extended Kalman Filter (EKF) techniques are typically utilized [166, 168, 167]. The literature indicates that EKF has succeeded in precise estimation for nonlinear model of the vehicle [170, 186]. The UKF addresses the state uncertainty distribution approximation issues of the EKF method. The UKF is used in [172, 187] to include non Gaussian noises as well. The UKF is an extension of the Unscented Transformation (UT) which is a method for calculating the statics of the random variable [172].

The UT is used for predicting the system states which requires the state distribution. The state distribution is resembled based on a Gaussian random variable, which is spread through the system model (6.16). A minimal set of carefully chosen sample-points are considered to predict the system states at the next time step. Sample-points which are a set of deterministic vectors whose ensemble mean and covariance of the states are defined as [173]

$$\boldsymbol{\Sigma}_{k-1}^{(i)} = \hat{\mathbf{x}}_{k-1} + \tilde{\mathbf{x}}^{(i)},\ i = 1, \ldots,\ 2n, \tag{6.19a}$$

$$\tilde{\mathbf{x}}^{(i)} = \left(\sqrt{n\mathbf{P}_{k-1}^{+}}\right)_i^T,\ i = 1, \ldots, n, \tag{6.19b}$$

$$\tilde{\mathbf{x}}^{(n+i)} = -\left(\sqrt{n\mathbf{P}_{k-1}^{+}}\right)_i^T,\ i = 1, \ldots, n, \tag{6.19c}$$

where n is the number of states. $\mathbf{P}_{k-1}^{+}$ is a posterior state estimation error covariance which is defined later. The sample-points, provide the posterior mean and covariance up to a second-order approximation [188]. The true mean and covariance of the measurement and model random variable can be captured by propagating the sample-points to the system model (6.16) as follows:

$$\boldsymbol{\Sigma}_k^{(i)} = \mathbf{A}_d \boldsymbol{\Sigma}_{k-1}^{(i)} + \mathbf{B}_d. \tag{6.20}$$

To obtain a prior state estimation, the sample-points are combined as follows:

$$\hat{\zeta}_k = \frac{1}{2n} \sum_{i=1}^{2n} \hat{\mathbf{\Sigma}}_k^{(i)}. \tag{6.21}$$

A prior state estimation error covariance is obtained as follows:

$$\mathbf{P}_k^- = \frac{1}{2n} \sum_{i=1}^{2n} \left(\hat{\mathbf{\Sigma}}_k^{(i)} - \hat{\boldsymbol{\zeta}}_k \right) \left(\hat{\mathbf{\Sigma}}_k^{(i)} - \hat{\boldsymbol{\zeta}}_k \right)^T + \mathbf{Q}_{k-1}. \tag{6.22}$$

To be able to calculate the state covariance $\mathbf{P}_k^+$, the predicted measurement requires. The predicted measurement obtains by propagating sample-points to vehicle-trailer system model (6.16), and they merged to calculate the predicted measurement vector by the following relations:

$$\begin{aligned} \hat{\mathbf{y}}_k^{(i)} &= \mathbf{H} \hat{\mathbf{\Sigma}}_k^{(i)} + \mathbf{D}, \\ \hat{\mathbf{y}}_k &= \frac{1}{2n} \sum_{i=1}^{2n} \hat{\mathbf{y}}_k^{(i)}. \end{aligned} \tag{6.23}$$

The covariance of the predicted measurement and state estimation error are described as follow:

$$\begin{aligned} \mathbf{P}_y &= \frac{1}{2n} \sum_{i=1}^{2n} \left(\hat{\mathbf{y}}_k^{(i)} - \hat{\mathbf{y}}_k \right) \left(\hat{\mathbf{y}}_k^{(i)} - \hat{\mathbf{y}}_k \right)^T + \mathbf{R}_k, \\ \mathbf{P}_{xy} &= \frac{1}{2n} \sum_{i=1}^{2n} \left(\hat{\mathbf{\Sigma}}_k^{(i)} - \hat{\boldsymbol{\zeta}}_k \right) \left(\hat{\mathbf{y}}_k^{(i)} - \hat{\mathbf{y}}_k \right)^T. \end{aligned} \tag{6.24}$$

Eventually, a posterior state estimation error covariance, $\mathbf{P}_k^+$, is obtained as follow:

$$\mathbf{P}_k^+ = \mathbf{P}_k^- - \mathbf{P}_{xy} (\mathbf{P}_{xy} \mathbf{P}_y^{-1})^T. \tag{6.25}$$

To be able to address the state constraints, an optimization argument is considered. The optimization argument minimize the lateral tire forces and hitch-force estimations errors with respect to the current measurement, predicted state values, and the state

constraints. The following cost function is designed to estimate the lateral tire forces and hitch-forces[189, 190, 191]

$$\hat{\mathbf{x}}_k = \min_{\hat{x}_k} J(\hat{\mathbf{x}}_k) = \min_{\hat{x}_k} (\|\mathbf{y}_k - \hat{\mathbf{y}}_k)\|^2_{\mathbf{Z}} + \|\hat{\mathbf{x}}_k - \hat{\boldsymbol{\zeta}}_k\|^2_{\mathbf{N}}),$$

s.t.

$$\begin{aligned} \hat{\mathbf{x}}_k = \mathbf{A}_d \hat{\mathbf{x}}_{k-1} + \mathbf{B}_d + \mathbf{L}\left(\mathbf{y}_{k-1} - \mathbf{H}\hat{\mathbf{x}}_{k-1} - \mathbf{D}\right), \\ |\hat{\mathbf{x}}_k| < \boldsymbol{\beta}|\delta|u_1, \\ \hat{\boldsymbol{x}}_{4,k} < \mathbf{R}_t(\mathbf{T}_t - \mathbf{I}\dot{\boldsymbol{\omega}}_t), \end{aligned} \tag{6.26}$$

where $\mathbf{Z} \in \mathbf{R}^{3\times3}$ and $\mathbf{N} \in \mathbf{R}^{7\times7}$ are positive definite weight matrices, $\mathbf{L} \in \mathbf{R}^{7\times3}$ is the observer gain vector which is discussed in the next section. In the cost function (6.26), the first term penalizes the difference between the predicted measurement and sensor measurements, and the second term penalizes the difference between the state estimation and prediction.

Remark 6.2: The estimated lateral tire forces and hitch-forces are obtained by solving the presented cost function with respect to the physical and dynamical constraints described in (6.17), system model, and predicted states' value.

To initiate the estimation algorithm, the states estimate and covariance terms are initialized as $\hat{\mathbf{x}}_0 = E[\mathbf{x}_0]$, $\mathbf{P}_0^+ = E\left[(\mathbf{x}_0 - \hat{\mathbf{x}}_0)(\mathbf{x}_0 - \hat{\mathbf{x}}_0)^T\right]$, respectively. The overall algorithm for lateral tire forces and hitch-force estimations is shown in Fig. 6.1.

The road friction coefficient affects the tire forces and since the tire forces are estimated in real-time based on the wheel dynamics as describes in (4.5), the presented hitch-force estimation algorithm is independent from the road friction coefficient. Moreover, the vehicle acceleration measurements address the vehicle state changes with respect to varying road friction coefficients. Given that the observability is a sufficient condition for implementation of optimal filters (e.g. Kalman filter) or estimation algorithms, the estimation error of the UT-based state observer is investigated in [175]. Due to the fact that the systems dynamic (6.16) is time-varying with respect to the steering angle (LPV), evaluating the eigenvalues does not lead to asymptotic stability. Therefore, the estimation stability analysis should be done for the LPV systems. The estimation error convergence is investigated in the following section.

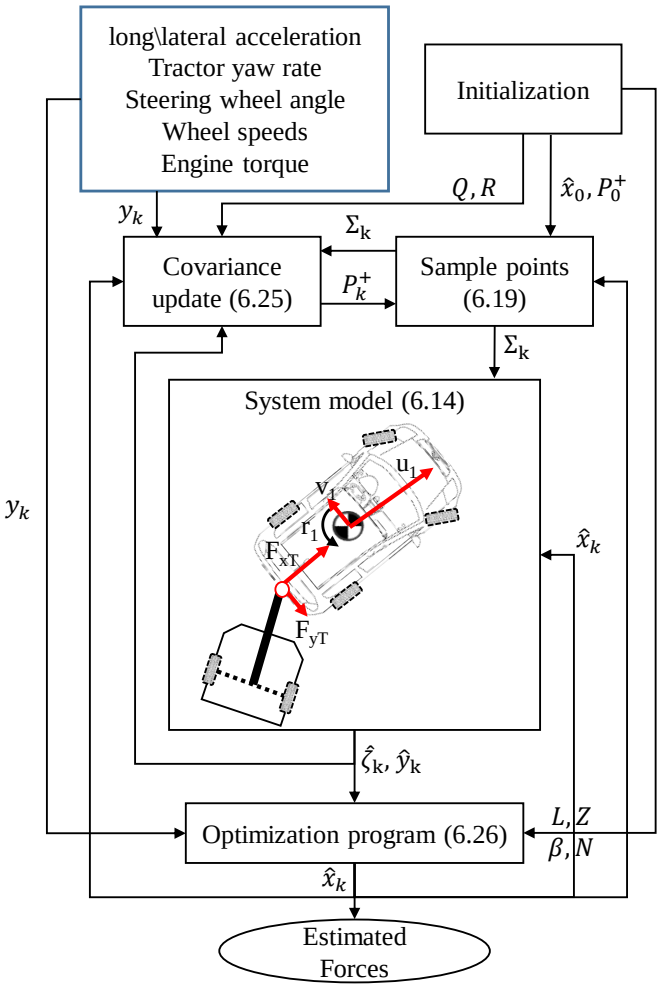

Figure 6.1: Overall force estimations scheme

6.4 Stability Analysis

The error dynamic is considered in this section to guarantee the stability of the estimator. As mentioned, the measurements are the longitudinal/lateral accelerations and yaw rate which are provided by IMU sensor. Sample-points propagation through the system model, decreases the effect of noise caused by the measurement or model uncertainties/disturbances considering the error between the actual and estimated measurement values. As shown in the hitch-force estimation algorithm, the designed observer has the

following prediction process to correct the state estimation by using a sequence of measurement

$$\dot{\hat{\mathbf{x}}} = \mathbf{A}(\delta)\hat{\mathbf{x}} + \mathbf{B} + \mathbf{L}\left(\mathbf{y} - \mathbf{H}\hat{\mathbf{x}} - \mathbf{D}\right). \tag{6.27}$$

The system dynamic shown in (6.27) is a linear parameter varying system. As mentioned, the bounded time-varying parameter is the steering angle $\delta \in [\delta_l, \delta_u]$, where δ_l and δ_u are the lower and upper bounds of the steering angle, respectively. The state estimation error dynamic $\dot{\mathbf{e}_f} = \dot{\mathbf{x}} - \dot{\hat{\mathbf{x}}}$ yields to

$$\dot{\mathbf{e}_f} = \underbrace{\left(\mathbf{A}(\delta) - \mathbf{L}\mathbf{H}(\delta)\right)}_{\mathbf{A_e}(\delta)}\mathbf{e}_f + \begin{bmatrix} 1 & -\mathbf{L} \end{bmatrix}\mathbf{\Omega}, \tag{6.28}$$

where $\mathbf{\Omega} = \begin{bmatrix} \mathbf{v} & \mathbf{w} \end{bmatrix}^T$.

Remark 6.3: The error dynamics (6.28) of the proposed estimator is affinely quadratically stable over all possible values of the steering angle if $\mathbf{A}_e(\delta_m)$ is stable (δ_m is the average value of δ over the parameter spam).

Proof.(Based on definition) The state matrix $\mathbf{A}_e(\delta)$ is said to be affinely dependent on the parameter δ when known and fixed matrices $\mathbf{A}_0$ and $\mathbf{A}_1$ exist such that $\mathbf{A}_e(\delta) = \mathbf{A}_0 + \delta\mathbf{A}_1$, where $\mathbf{A}_0$ and $\mathbf{A}_0$ are obtained as follows:

$$\mathbf{A}_0(\delta) = \begin{bmatrix} & 0 & \frac{b_1}{a_1} & \frac{e+b_1}{a_1} \\ \mathbf{G}_{7\times4} & -1 & 0 & -1 \\ & \frac{-a_1}{e+b_1} & \frac{-b_1}{e+b_1} & 0 \\ & \multicolumn{3}{c}{\mathbf{0}_{4\times3}} \end{bmatrix}, \tag{6.29}$$

$$\mathbf{A}_1(\delta) = \begin{bmatrix} 1-\frac{L_{11}}{m_1} & & 0 & \\ -l_1-\frac{L_{21}}{m_1} & & 0 & \\ -\frac{a_1}{e+b_1}-\frac{L_{31}}{m_1} & & 0 & \\ -\frac{L_{41}}{m_1} & \mathbf{0}_{7\times3} & 1 & \mathbf{0}_{7\times2} \\ -\frac{L_{51}}{m_1} & & 0 & \\ -\frac{L_{61}}{m_1} & & 0 & \\ -\frac{L_{71}}{m_1} & & 0 & \end{bmatrix}, \tag{6.30}$$

where $\mathbf{G}$ is presented in Appendix A. As mentioned, the steering angle and its rate are the bounded time-varying parameter in the sets $\delta_p \in [\delta_l, \delta_u]$ and $\dot{\delta}_p \in [\dot{\delta}_l, \dot{\delta}_u]$. The Lyapunov

stability theory is considered to investigate the stability of the designed observer. The Lyapunov candidate function $V(e_f, \delta)$ is defined as follows:

$$V(e_f, \delta) = e_f^T P(\delta) e_f, \tag{6.31}$$

where $P(\delta) = P_0 + \delta P_1$. A linear system shown in (6.28) is affinely quadratically stable over all possible values of the steering angle if $\mathbf{A}_e(\delta_m)$ is stable and there exists an affine positive definite Lyapunov function $V(e_f, \delta)$ such that $dV(e_f, \delta, \dot{\delta})/dt < 0$ for all initial conditions x_0 and the additional multi-convexity constraint $A_1^T P_1 + P_1 A_1 \geq 0$ [192]. The condition $\dot{V} < 0$ yields to

$$A_e^T(\delta_p) P(\delta_p) + P(\delta_p) A_e(\delta_p) + P(\dot{\delta}_p) - P_0 < 0, \tag{6.32}$$

for all $(\delta, \dot{\delta})$ in the specified range. Given the test vehicle parameters listed in Table. 6.1 and observer gains L

$$L = 10 \begin{bmatrix} 0.6 & 0.74 & 16 & 0.6 & 9.2 & 41 & 0.6 \\ 0.74 & 0.6 & 21 & 9.2 & 0.6 & 3.1 & 0.55 \\ 16 & 21 & 0.6 & 41 & 3.1 & 0.6 & 0.6 \end{bmatrix}^T, \tag{6.33}$$

which is obtained by several simulation tests to satisfy the stable $\mathbf{A}_e(\delta)$ in (6.28), the symmetric matrix $P(\delta_p)$ is obtained by solving (6.32). ■

As the error dynamics is affinely quadratically stable for the selected observer gains L, there exist at least one possible solution for $P(\delta_p)$ that satisfies the condition in (6.32). The observer gain value for the simulated and experimental test vehicle are used in Section 6.5.

6.5 Simulation and Experimental Test

In this section the presented lateral tire forces and hitch-force estimations algorithm is validated by both simulation and experimental studies.

6.5.1 Simulation Results

To evaluate the proposed estimation algorithm, a vehicle-trailer model in CarSim with the parameters listed in Table. 6.1 is used. The simulation runs with the sampling rate of

200 Hz for different maneuvers on the road with different friction coefficients with various velocities to evaluate the proposed hitch-forces and lateral tire force estimations algorithm in different conditions. The process and measurement noise covariance matrices set to $\mathbf{Q} = 29.8^2 \times \text{diag}[0.01, 0.02, 0.05, 1, 1, 1, 1]$ and $\mathbf{R} = 1.98^2 \times \text{diag}[0, 0, 1, 1, 1]$, for all the tests.

The vehicle longitudinal/lateral accelerations and yaw rate are available through the CarSim model and used in the designed estimator. The estimated vehicle lateral tire forces and hitch-forces are compared with the actual values provided by CarSim for different maneuvers.

Four test scenarios are considered to test the performance of the proposed algorithm. The first scenario is multiple DLC maneuvers with driver gas/brake pedal inputs. The vehicle-trailer model with the parameters listed in Table. 6.1 is used to evaluate the proposed estimation algorithm.

Table 6.1: Vehicle-trailer parameters for force estimation

Description, (symbol)	Units	Value
Vehicle's mass, (m_1)	kg	1860
Vehicle's moment yaw of inertia, (I_{z1})	$kg.m^2$	3397
Vehicle's CG to front axle, (a_1)	m	1.21
Vehicle's CG to rear axle, (b_1)	m	1.74
Vehicle's rear axle to hitch-point, (e)	m	1.27
Effective tire radius, (R_{eff})	m	0.39
Trailer's mass, (m_2)	kg	465
Trailer's moment of inertia, (I_{z2})	$kg.m^2$	1764
Trailer's CG to hitch-point, (a_2)	m	2
Trailer's CG to axle, (b_2)	m	1

The second scenario is designed to test the proposed estimator accuracy with respect to the different vehicle-trailer longitudinal velocity. To do so, the vehicle-trailer unit as

described in Table. 6.1 is simulated in a DLC maneuver with different constant speeds of 25, 35, 45, and 55 km/h.

As mentioned, the hitch-force estimation algorithm is independent from the trailer mass and geometry. Therefore, the third simulation scenario is considered to test the performance of the hitch-force estimation algorithm with respect to different trailer configurations. In this scenario, three trailers with different geometries and payload are considered as listed in Table. 6.2.

Table 6.2: Trailer parameters

	Axle location $[m]$	Trailer length $[m]$	Payload $[kg]$
Trailer 1	2	4	No load
Trailer 2	3	4	100
Trailer 3	2	3	200

For the fourth test scenario, a step-steer maneuver is considered. The vehicle-trailer is simulated in a road surface with varying road friction coefficients to show the effect of road friction coefficient into the force estimation results. The road friction coefficients set to 0.5 and 0.85 for the right and left half of the simulated field, respectively.

DLC maneuver with driver gas/brake pedal inputs

For the first simulation scenario, a DLC maneuver, with high slip and lateral excitation is conducted with the All Wheel Drive (AWD) simulated vehicle to show the accuracy of the estimation algorithm. A series of double lane change maneuvers with the driver gas/brake pedal inputs' profile are shown in Fig. 6.2.

To account for noises and disturbances in actual measurement signals, a Gaussian noise with zero mean and 0.01 covariance have been added to the CarSim longitudinal/lateral acceleration measurement outputs as seen in Fig. 6.3 zoomed area. Fig. 6.3 illustrates the noisy longitudinal and lateral accelerations of the DLC maneuver.

Estimated vehicle lateral tire forces and hitch-forces are illustrated in Fig. 6.4 by minimizing the presented cost function. The estimation results have delay for almost 60 mil-

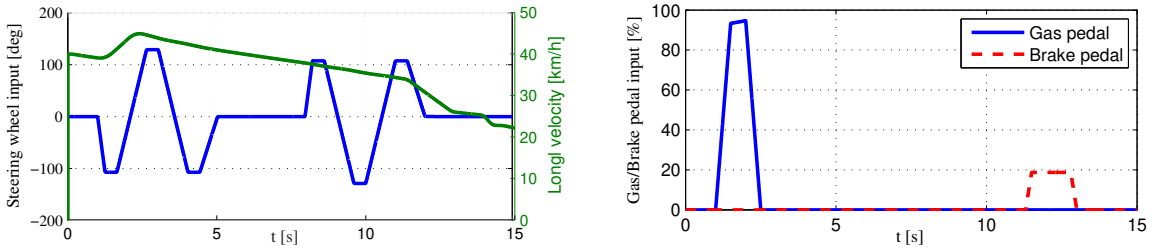

(a) (b)

Figure 6.2: a) Steering wheel angle and vehicle longitudinal velocity, b) Gas/Brake pedal inputs - DLC maneuver.

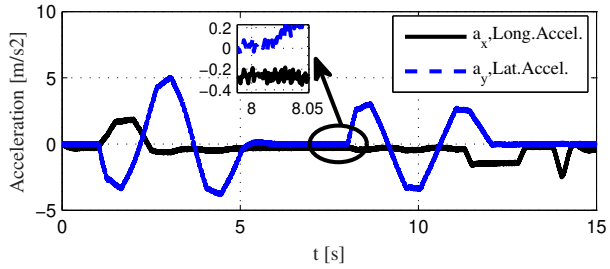

Figure 6.3: Noisy measured longitudinal and lateral accelerations - DLC maneuver test.

liseconds since in the proposed estimation algorithm, the true mean and covariance of the measurement and model random variable are captured by propagating the sample-points to the system model and it increases the computational burden.

DLC maneuver with different constant velocities

The performance of the designed estimator with respect to different constant longitudinal velocities are shown in Fig. 6.5. The aim of these simulations is to illustrate the effect of longitudinal velocity on the lateral tire forces and hitch-force estimation results. To do so, the steering wheel angle shown in Fig. 6.2.a is applied to the vehicle-trailer and the vehicle-trailer drives with the constant longitudinal speeds of 25, 35, 45, and 55 km/h. The estimated vehicle lateral tire forces and hitch-forces for the constant speed of 25 and 55 km/h are illustrated in Fig. 6.5.

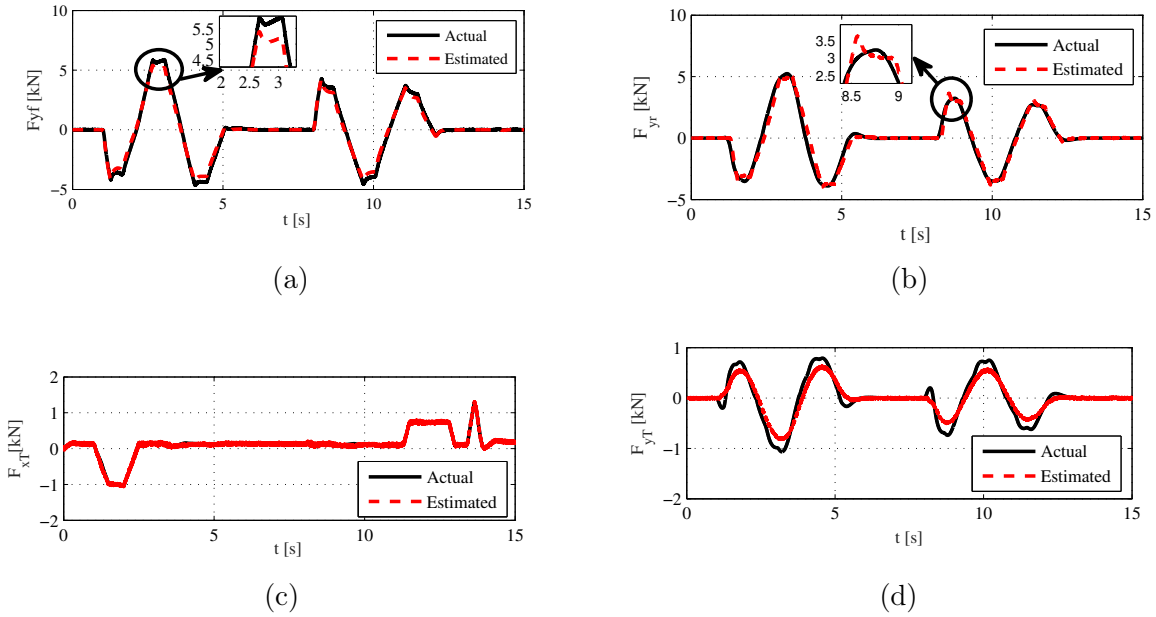

Figure 6.4: a) Lateral front tire force estimation b) Lateral rear tire force estimation c) Longitudinal hitch-force estimation d) Lateral hitch-force estimation - DLC maneuver test.

As Fig. 6.5 illustrates, although the lateral tire forces and hitch-force estimations error in the DLC maneuver (This maneuver uses only the steering angle shown in Fig. 6.2.a, not the torque/brake inputs in Fig. 6.2.b) increase by increasing the longitudinal speed, the Normalized Root Mean Square (NRMS) of the error defined by $\bar{\zeta} = (\sqrt{\Sigma_{i=1}^{N_p}(\hat{p}_i - p_i)^2/N_p})/p_m$ where the measured and estimated signals are denoted by p and $\hat{p}$, respectively, N_p is the number of colected signal samples during a driving scenario, and $p_m = \max_{i=1\ldots N_p} |p_i|$ illustrate the maximum value of the measured signals. The NRMS of the estimator with respect to different longitudinal velocities is less than 24 percent as shown in Table. 6.3.

The hitch-force estimation error is mainly because of the delay in the estimator. The delay in the estimator makes the difference between the actual and estimated value large since the estimated forces' value are almost 60 milliseconds before the current actual forces' value. Moreover, the force estimation errors may have several resources and the most possible one is the lack of accurate system model, for instance, the roll dynamic and the aerodynamic forces, which have not been modeled in the presented vehicle-trailer model could cause the error.

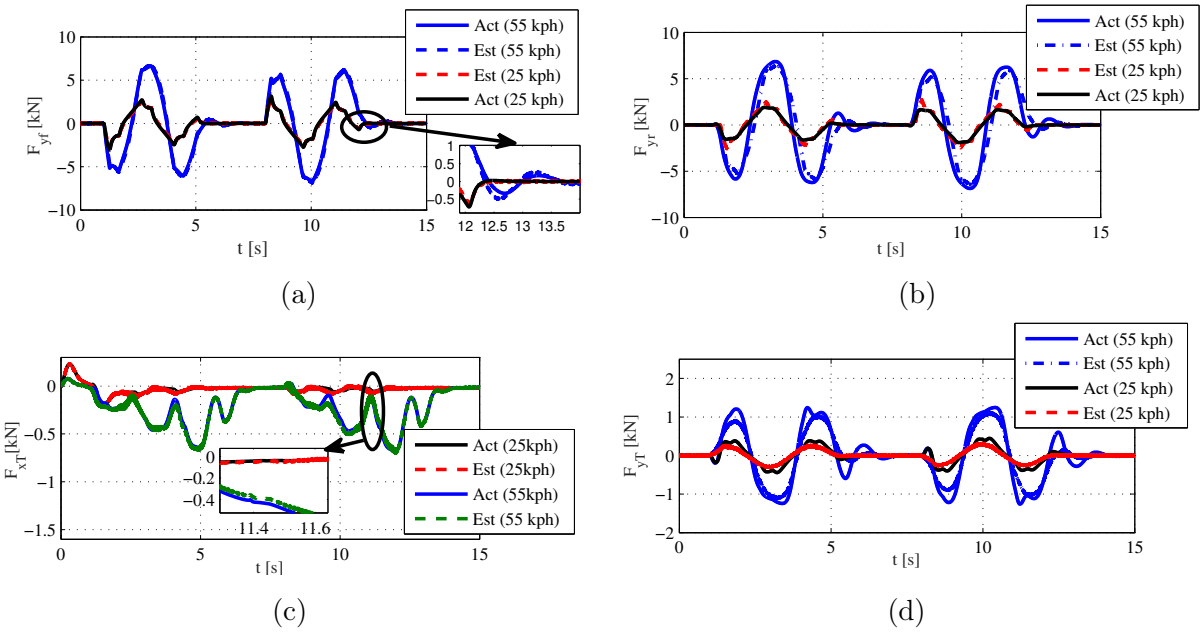

Figure 6.5: a) Lateral front tire force estimation b) Lateral rear tire force estimation c) Longitudinal hitch-force estimation d) Lateral hitch-force estimation - different velocities test.

DLC maneuver with different trailer payloads/geometries

To test the proposed algorithm with respect to different trailer types as described in Table. 6.2, the steering wheel angle shown in Fig. 6.2.a, and the gas/brake pedal, shown in Fig. 6.2.b, were applied to the vehicle-trailer. Fig. 6.6 shows the estimated hitch-forces and lateral tire forces with respect to the different trailer geometries/payloads.

The estimated hitch-forces and lateral tire forces are presented in Fig. 6.6. As can be seen in Fig. 6.6, the maximum hitch-force estimation error with respect to the three different trailers, describes in Table. 6.2, is almost 14 present. By changing the trailer geometry/mass, the hitch-force estimation error remains in an acceptable region which is less than 15 percent. The error acceptable region is defined based on the vehicle-trailer stability control purposes. If the force estimation errors are less that 15 percent, the stability controller unit is able to make the trailer unit stable [60]. The proposed algorithm can estimate the lateral tire forces and hitch-forces for ball type box trailers with different masses

Table 6.3: NRMS of the errors for the longitudinal/lateral hitch-forces and lateral tire force estimations at dry and wet road.

Estimated force	@ u_1=25 km/h [%]	@ u_1=35 km/h [%]	@ u_1=45 km/h [%]	@ u_1=55 km/h [%]
		Dry road		
F_{yf}	3.51	3.34	3.49	4.11
F_{yr}	5.91	6.55	8.88	9.09
F_{xT}	4.62	4.67	4.5	5.9
F_{yT}	19.1	20.2	22.5	23.9
		Wet road		
F_{yf}	3.51	3.3	3.5	4.21
F_{yr}	6.01	6.68	9.21	9.5
F_{xT}	4.62	4.6	4.6	6.2
F_{yT}	19.26	20.19	22.7	24.5

and geometries since the designed estimator relies on the vehicle's measurements. As the observability of the system is satisfied, the changes in the trailer parameters can cause changes in the vehicle acceleration and yaw rate trend that are utilized in the proposed estimation algorithm.

Step-steer maneuver with varying road friction coefficient

The proposed hitch-force estimation algorithm is evaluated in a field with different friction coefficients. A Step-Steer (SS) maneuver with the driver gas/brake pedal inputs shown in Fig. 6.7 is considered.

The longitudinal and lateral accelerations of the SS maneuver correspond with noises (Gaussian noise with zero mean and 0.01 covariance) are shown in Fig. 6.7. The noises have been added to the actual acceleration results provided by CarSim to account for noises

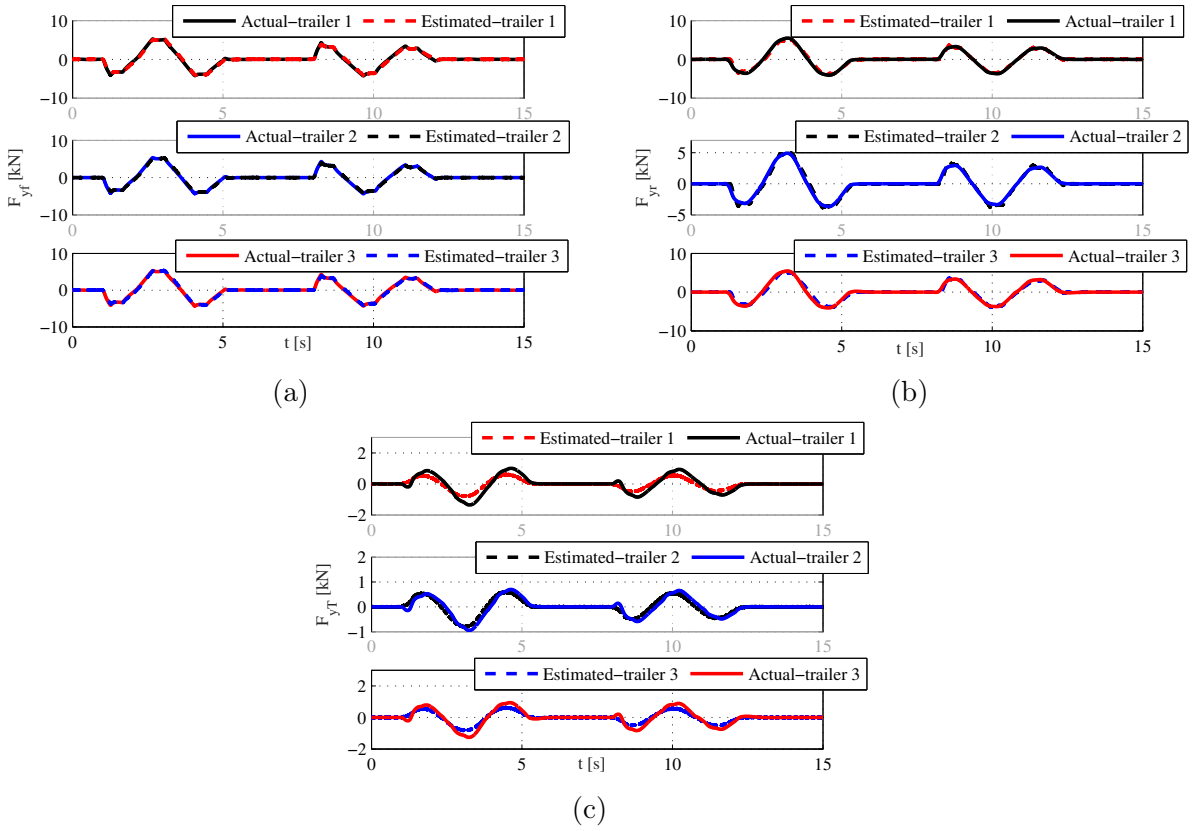

Figure 6.6: a) Lateral front tire force estimation b) Lateral rear tire force estimation c) Lateral hitch-force estimation - different trailer geometries/masses tests.

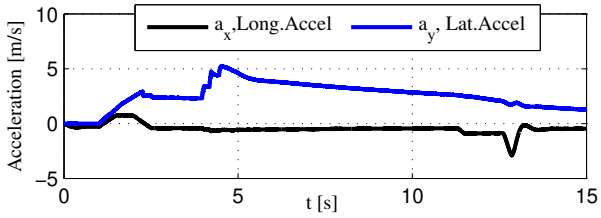

Figure 6.7: Noisy measured longitudinal and lateral acceleration - SS maneuver.

and disturbances in actual measurement signals by sensors. The simulation runs for 15 seconds and the initial speed is 40 km/h, Fig. 6.8a, on a road surface with varying friction coefficient as illustrates in Fig. 6.9.

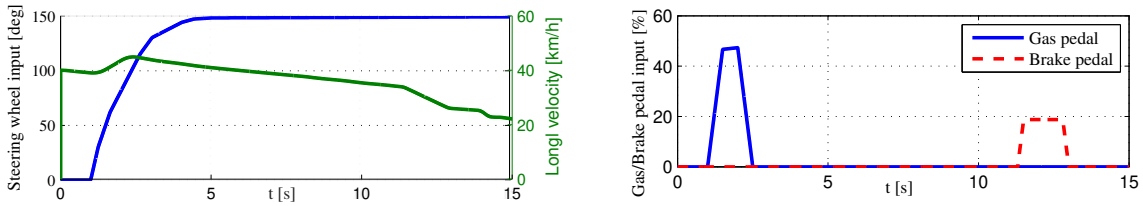

(a) (b)

Figure 6.8: a) Steering wheel angle and vehicle longitudinal velocity, b) Gas/Brake pedal input - SS maneuver.

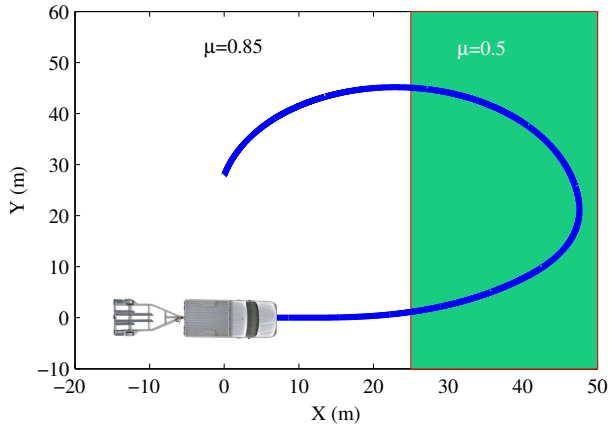

Figure 6.9: Vehicle-trailer path on the simulated test field with a dual-friction coefficient surface.

The performance of the lateral tire force and hitch-force estimations algorithm on a varying friction test field is shown in Fig. 6.10. As Fig. 6.10 illustrates, by changing the road friction coefficient from 0.85 to 0.5, oscillations occur on the actual lateral tire forces and hitch-forces in the transient mode. The oscillations (Fig. 6.10.b zoomed area) occur since by changing the road friction coefficient, the slip ratio changes in both longitudinal and lateral directions which affect the tire forces. The proposed hitch-force estimator can be used to compensate for oscillations due to slippery surfaces (Fig. 6.10) since the road friction coefficient affects the tire forces which are estimated based on the wheel dynamics shown in (4.5).

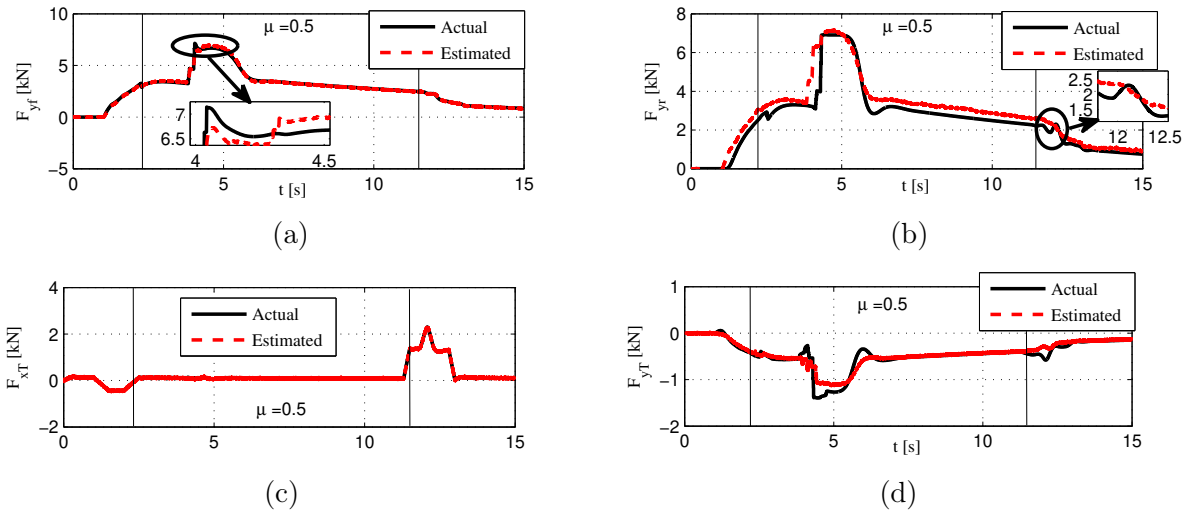

Figure 6.10: a) Lateral front tire force estimation b) Lateral rear tire force estimation c) Longitudinal hitch-force estimation d) Lateral hitch-force estimation - varying friction road test.

6.5.2 Experimental Studies: Force Estimations

Electrified vehicles have a significant impact on the chassis system, energy, climate issue, and active actuation controls [193]. The test vehicle is an electrified Chevrolet Equinox sport utility vehicle (SUV) with a single axle trailer as shown in Fig. 4.6. As the vehicle is electrified, the driving and braking torque on each wheel are measurable. Each motor has up to $\pm 1600 Nm$ and an ABS module is available on this vehicle. The longitudinal/lateral accelerations and yaw rate of the vehicle are measured with a 6-axis IMU (and GPS) system RT2000. The main parameters of the vehicle are listed in Table. 4.1.

Steering wheel angle sensor, located in the steering column, is to provide steering angle and rate of turn. A Global-Positioning-System (GPS) is installed on the vehicle to measure the longitudinal and lateral speed of the vehicle accurately. A 6-axis IMU is mounted inside of the vehicle, close to the CG location. Measured signals are communicated using a CAN-bus. Real-time acquisition and processing of sensory information and the developed hitch-force estimation algorithm is realized using the dSPACE MicroAutoBox II. As mentioned before, the dSPACE compiles measurements for MATLAB/Simulink, and the lateral tire fores and hitch-force estimations algorithm runs in MATLAB/Simulink by utilizing the

provided measurements. The sampling frequency for the experiment is fixed to 200 [Hz]. The trailer is designed to be adjustable in payload and CG location to test the performance of the hitch-force estimation algorithm with respect to different trailer types.

Ground truth is a critical part of state estimation to validate the estimation algorithm. To find the lateral tire forces' ground truth, the force sensors mounted on each wheel are used. Measuring the hitch-force ground truths are not easy since the forces are internal. The hitch-forces can be measured directly using force transducers; however, it is costly and calibrating the sensor for this purpose is going to be time consuming. As the direct measurement of the hitch-forces are not available, the indirect measurement is used for the hitch-force ground truths. To do so, the vehicle runs for two exactly the same maneuvers, one time with the trailer attached to the vehicle and one time without the trailer. As the vehicle tire forces are measured by sensors, the hitch-forces are obtainable by following the vehicle equations of motion. The longitudinal hitch-force ground truth is obtainable by making the difference between the total longitudinal tire forces on the two exactly the same tests. The calculated hitch-forces are compared with the estimated value to check the performance of the proposed estimator. To make sure that the two maneuvers are exactly the same, road cones are used to guide the driver to make the two exactly the same tests with and without the trailer (e.g. when vehicle-trailer reaches to a specific cone, stop accelerating). The performance of the proposed lateral tire forces and longitudinal/lateral hitch-force estimator in the experimental test are shown in Fig. 6.12.

The first experimental test is designed to test the performance of the longitudinal hitch-force estimation. To do so, the vehicle (Equinox) starts from a stationery point, $u_1 = 0$, and keep accelerating till the speed reaches to 26 km/h, then it runs forward with constant speed. The described experimental test is conducted for two conditions: the vehicle with trailer and the vehicle without the trailer. Fig. 6.11c illustrates the longitudinal velocity of the two tests (with and without the trailer attached to the vehicle). As can be seen in Fig. 6.11c, the two tests are close to each other. Therefore, the longitudinal hitch-force ground truth is obtainable by comparing the longitudinal tire forces, Fig. 6.11b, of these two tests. The estimated longitudinal hitch-force compared with the longitudinal hitch-force ground truth is shown in Fig. 6.11d. The longitudinal hitch-force ground truth is not accurate at the beginning of the test, from t=0 to t=1.8, as the two test accelerating time were not the same at the beginning. As can be seen the hitch-forces is estimated by the vehicle sensor measurement without any priori information required from the trailer.

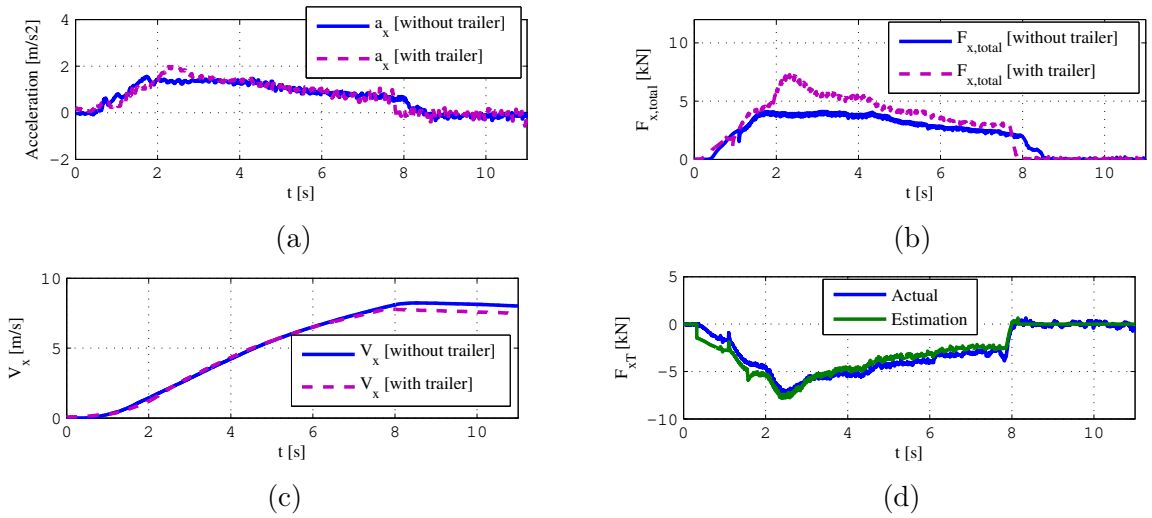

Figure 6.11: a) Measured longitudinal acceleration b) Total longitudinal vehicle tire forces c) Longitudinal velocity d) Longitudinal hitch-force estimation - experimental test on dry road.

To test the performance of the lateral tire forces and hitch-force estimations algorithm, the second experimental test is considered. In this test, the vehicle with trailer starts from a stationery point and keep accelerating to reach the speed of 25 km/h. Then the vehicle-trailer runs with the constant speed and while the speed is constant, a double lane change maneuver applies as shown in Fig. 6.12a. The estimated front and rear lateral tire forces compared with the ground truth are shown in Fig. 6.12b and Fig. 6.12c, respectively.

As can be seen, the lateral tire forces are estimated for the vehicle-trailer configuration, and the estimated longitudinal and lateral hitch-forces are shown in Fig. 6.12d and Fig. 6.12e, respectively. Although the hitch-forces ground truth are not available for the second experiment test, the estimated hitch-forces values make sense with respect to the vehicle-trailer equations of motion (the absolute magnitude of the hitch-forces and longitudinal/lateral tire forces satisfy the vehicle-trailer equations of motion in both longitudinal and lateral directions).

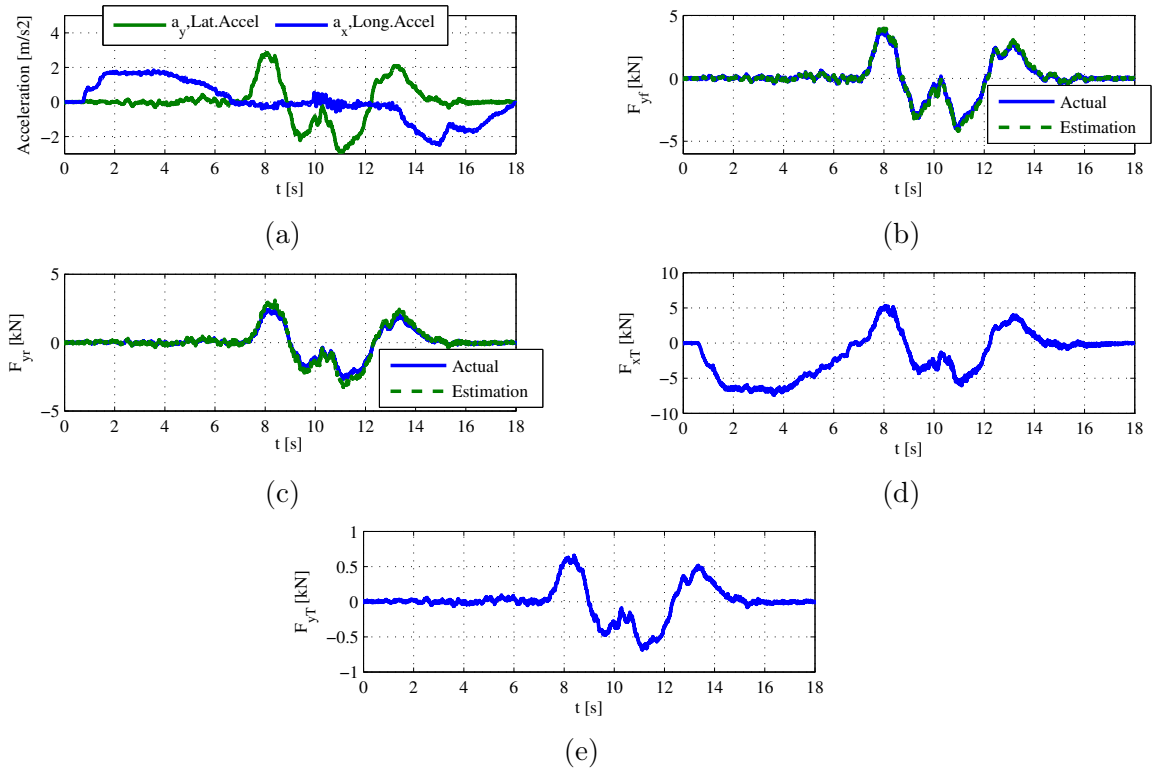

Figure 6.12: a) Measured longitudinal and lateral acceleration b) Lateral front tire force estimation c) Lateral rear tire force estimation d) Longitudinal hitch-force estimation e) Lateral hitch-force estimation - experimental test on dry road.

6.5.3 Discussions

The unscented transformation was used to predict the states at the current time step based on the estimated states value at the previous time step. On the other hand, an stable observer was also used to estimate the states value simultaneously. Then, the optimization problem found the optimum agreement between these two state estimations based on the state constraints. The proposed state estimators with the state constraints, (6.26) can handle dry and slippery roads with error NRMS ε_n <9.5% for the longitudinal hitch-force and lateral tire forces. In spite of low excitation, which is challenging for current lateral force estimators in production vehicles, especially for vehicle-trailer combination, and the observed oscillations in the measured lateral acceleration due to several passing through

dry and wet surfaces, the proposed algorithm exhibits accurate estimates in the transient mode which is promising.

The developed estimation algorithm provided the estimated lateral hitch-force value with NRMS ε_n <24% error, however, the large percentage of error was mainly because of the 60 millisecond delay in the estimator. With respect to the results, it was concluded that estimating the lateral hitch-force with the vehicle measurement unit is challenging and the proposed estimator is not able to address the large lateral slip for the trailer caused by large trailer payload for heavy trailers. Therefore, the estimation algorithm for the **lateral** hitch-force estimation needs to improve. To improve the lateral hitch-force estimation, the states of the trailer should be measured/provided or estimated (e.g. hitch angle measurement or trailer parameter estimation). Then, the hitch-force estimation algorithm can improve/modify by utilizing estimated trailer parameters which is one of the suggested future research directions in this area to continue this work.

6.6 Conclusions

In this chapter, the proposed vehicle-trailer dynamic model was used to estimate the longitudinal/lateral hitch-forces and lateral tire forces. To make the estimation algorithm generic, the presented model was derived in a way that it can address the hitch-forces and lateral tire forces without any priori information from the trailer. It was shown that the presented hitch-forces algorithm was independent of trailer mass and geometry, and can estimate the hitch-forces for any ball type trailers. Uncertainty of the model was studied and the proposed observer was utilized to estimate the states of the system. The stability of the proposed model-based estimator was investigated. The estimation error is converged, as the system was observable and the system matrices were bounded. Moreover, it has been shown that the proposed algorithm is capable of estimating the hitch-forces and lateral tire forces on dry, wet, and icy roads as the selected measurement signals are able to address the effect of road surfaces on the model. The proposed approach was implemented in both high-fidelity CarSim simulator software and experimental set-up for valuation. The proposed estimator provided hitch-force estimated value with the maximum error of about 9 percent.

Chapter 7

Vehicle-Trailer Lateral Velocity Estimation

7.1 Introduction

Vehicle velocity in both lateral and longitudinal directions plays an important role in stability control systems. To measure the longitudinal/lateral velocities, Global-Positioning-Systems (GPSs) can be used; however, they suffer from poor accuracy, signal availability, and refreshing frequency in the most commonly used GPSs in vehicles. Variety approaches has been proposed for lateral velocity estimation in the literature. Based on the literature, the current lateral velocity estimators are all for single vehicle units that cannot be used for vehicle-trailer combinations. When a trailer connects to the towing vehicle the vehicle lateral velocity estimators exist on the literature may not work as the dynamic of the system changes. Thus, the lateral velocity estimation needs to be investigated individually for vehicle-trailer configuration. Therefore, the contribution of this chapter is developing an optimal real-time vehicle-trailer lateral velocity estimator robust to the road condition. The proposed vehicle-trailer lateral velocity estimation is designed based on the developed vehicle-trailer lateral dynamics. In this model, the LuGre tire model is used, and the non-linearity of the model for large slip angles described in Chapter 3 is investigated.

This chapter is organized as follows: In Section 7.2, the vehicle-trailer system model is presented in the state space form. An observer is designed for the lateral velocity estimation

in Section 7.2 with stability analysis. Finally, the proposed lateral velocity estimator is validated by simulation and experimental tests with discussion in Section 7.3.

7.2 Vehicle-Trailer Lateral Velocity Estimation

In this section, the proposed lateral velocity estimator design for the vehicle-trailer system based on the lateral dynamics presented in the previous chapter, is proposed. As described in Chapter 3, the lateral dynamics (3.29) addresses the non-linear behaviour of the system. Therefore, to estimate the lateral velocity, the lateral dynamics model (3.29) is considered where the state vector is $\mathbf{x} = [v_1, r_1, \dot{\theta}, \theta]^T$. As the conventional vehicles have Inertia-Measurement-Unit, IMU, the lateral acceleration a_{y1} and yaw rate of the vehicle r_1 are measurable by the vehicle's IMU. Moreover, the hitch angle θ is also measurable by the ultra-sound sensors that are mounted on the rear bumper of the vehicle [39, 41]. Thus, the measurement vector is defined as $\mathbf{y} = [a_{y1}, r_1, \theta]^T$ which can be written as follows:

$$\begin{aligned} \dot{\mathbf{x}} &= \bar{\mathbf{A}}\mathbf{x} + \bar{\mathbf{B}}\delta, \\ \mathbf{y} &= \mathbf{C}_y\mathbf{x} + \mathbf{D}_y\delta, \end{aligned} \tag{7.1a}$$

$$\mathbf{C}_y = \begin{bmatrix} \beta_f + \beta_r + \beta_t & C_{y,12} & -\beta_t\, l_2 & -\beta_t u \\ 0 & 1 & 0 & 0 \\ 0 & 0 & 0 & 1 \end{bmatrix}, \tag{7.1b}$$

$$\mathbf{D}_y = \begin{bmatrix} \beta_f & 0 & 0 \end{bmatrix}^T, \tag{7.1c}$$

$$C_{y,12} = a_1\beta_f - b_1\beta_r - (l_2 + c)\beta_t + m_2 u, \tag{7.1d}$$

$$\beta_f = \Lambda_f \frac{m_1 g b_1 - \frac{m_2 g a_2 e}{l_2}}{l_1}, \beta_t = \Lambda_t \frac{m_2 g a_2}{l_2}, \tag{7.1e}$$

$$\beta_r = \Lambda_r \left(m_1 g a_1 + \frac{m_2 g a_2 (l_1 + e)}{l_2} \right), \tag{7.1f}$$

where, $\Lambda_i, i \in [f, r, t]$ are defined in (3.22). The time-varying observeability matrix of the system (7.1a) is given by [184]

$$\mathbf{O}_n = \begin{bmatrix} \tau_1^T & \tau_2^T & \cdots & \tau_n \end{bmatrix}^T, \tag{7.2a}$$

$$\tau_1 = \mathbf{C}_y, \tau_{i+1} = \tau_i \bar{\mathbf{A}} + \dot{\tau}_i. \tag{7.2b}$$

The system (7.1a) is observable, and its observeability is satisfied by holding the full rank condition ($\mathbf{O}_4 = 4$). The system (7.1a) is not observable for the case where the wheel speed is zero; however, in this case, there is no lateral velocity for the vehicle-trailer unit. Given the nonlinear behavior of the system, the system is linearized around the equilibrium point using zero order hold technique and then the discretized form of the system is obtained. The discretized form of the system model (7.1a) is expressed as

$$\mathbf{x}_{k+1} = \mathbf{A}_d \mathbf{x}_k + \mathbf{B}_d \delta_k + \mathbf{w}_k, \tag{7.3a}$$

$$\mathbf{y}_k = \mathbf{C}_y \mathbf{x}_k + \mathbf{D}_y \delta_k + \mathbf{v}_k, \tag{7.3b}$$

where the subscript k for $k = 0, 1, 2, \ldots$ denotes the value of a variable at discretized time instant $t = kT_s$ with sampling time T_s, $\mathbf{A}_d = e^{\bar{\mathbf{A}} T_s}$ and $\mathbf{B}_d = \int_0^{T_s} e^{\bar{\mathbf{A}}\tau} \bar{\mathbf{B}} d\tau$. Given that the measurements and system contain noises and uncertainties, $\mathbf{w}_k$ and $\mathbf{v}_k$ are used to denote the process and measurement noise, respectively.

$\mathbf{w}_k$ and $\mathbf{v}_k$ are assumed to be uncorrelated Gaussian processes with zero mean and the covariances of $\mathbf{Q} \in \mathbf{R}^{4\times4}$ and $\mathbf{R} \in \mathbf{R}^{3\times3}$, respectively, satisfying $E(w_k, w_j^T) = Q\delta_{k-j}$, $E(v_k, v_j^T) = R\delta_{k-j}$, and $E(v_k, w_j^T) = 0$, where δ_{k-j} is the Kronecker delta function of $k - j$. Here, a bias-removal method is used for removing the measurement biases so that the above zero-mean Gaussian noise assumption holds [185].

The state $\mathbf{x}$ is proposed to be estimated, based on the discretized model (7.3) with the above assumptions. The Unscented Transformation (UT) is a method for calculating the statics of the random variable [171]. The UT is used for predicting the system states which requires the state distribution [166]. The state distribution is resembled based on a Gaussian random variable, which is spread through the system model (7.3). A minimal set of carefully chosen sample-points are considered to predict the system states at the next

time step. Sample-points which are a set of deterministic vectors whose ensemble mean and covariance of the states are defined as [173]

$$\mathbf{\Sigma}_{k-1}^{(i)} = \hat{\mathbf{x}}_{k-1} + \tilde{\mathbf{x}}_{k-1}^{(i)},\ i = 1, \ldots,\ 2n, \tag{7.4a}$$

$$\tilde{\mathbf{x}}_{k-1}^{(i)} = \left(\sqrt{n\mathbf{P}_{k-1}^{+}}\right)_{i}^{T},\ i = 1, \ldots, n, \tag{7.4b}$$

$$\tilde{\mathbf{x}}_{k-1}^{(n+i)} = -\left(\sqrt{n\mathbf{P}_{k-1}^{+}}\right)_{i}^{T},\ i = 1, \ldots, n, \tag{7.4c}$$

where $n = 4$ is the dimension of the state x_k in (7.3), $\tilde{\mathbf{x}}_{k-1}^{(i)}$ denotes the sample-points that are obtained by the unscented transformation, and $\mathbf{P}_{k-1}^{+}$ is a posteriori state estimation error covariance matrix which is defined later. The sample-points, provide the posterior mean and covariance up to second-order approximation [188]. The true mean and covariance of the measurement and model random variable can be captured by propagating the sample-points to the system model (7.3) as follows:

$$\mathbf{\Sigma}_{k}^{(i)} = \mathbf{A}_d \mathbf{\Sigma}_{k-1}^{(i)} + \mathbf{B}_d \delta_{k-1}. \tag{7.5}$$

To obtain a priori state estimation, the sample-points are combined as

$$\hat{\zeta}_k = \frac{1}{2n} \sum_{i=1}^{2n} \hat{\mathbf{\Sigma}}_{k}^{(i)}. \tag{7.6}$$

A priori state estimation error covariance matrix is shown in (6.22). To calculate the state covariance $\mathbf{P}_k^{+}$, the predicted measurement is required. The predicted measurements are obtained by propagating sample-points through the vehicle-trailer system model (7.3), and they are merged to calculate the predicted measurement vector as follows:

$$\hat{\mathbf{y}}_{k}^{(i)} = \mathbf{C}_y \hat{\mathbf{\Sigma}}_{k}^{(i)} + \mathbf{D}_y \delta_k, \tag{7.7a}$$

$$\hat{\mathbf{y}}_k = \frac{1}{2n} \sum_{i=1}^{2n} \hat{\mathbf{y}}_{k}^{(i)}. \tag{7.7b}$$

The covariance of the predicted measurement and state estimation error are described as

$$\mathbf{P}_{y,k} = \frac{1}{2n}\sum_{i=1}^{2n}\left(\hat{\mathbf{y}}_k^{(i)} - \hat{\mathbf{y}}_k\right)\left(\hat{\mathbf{y}}_k^{(i)} - \hat{\mathbf{y}}_k\right)^T + \mathbf{R}, \tag{7.8}$$

$$\mathbf{P}_{xy,k} = \frac{1}{2n}\sum_{i=1}^{2n}\left(\hat{\mathbf{\Sigma}}_k^{(i)} - \hat{\boldsymbol{\zeta}}_k\right)\left(\hat{\mathbf{y}}_k^{(i)} - \hat{\mathbf{y}}_k\right)^T. \tag{7.9}$$

Eventually, a posterior state estimation error covariance matrix, $\mathbf{P}_k^+$, is obtained in the following form:

$$\mathbf{P}_k^+ = \mathbf{P}_k^- - \mathbf{P}_{xy,k}(\mathbf{P}_{xy,k}\mathbf{P}_{y,k}^{-1})^T. \tag{7.10}$$

As shown in (7.5), the unscented transformation is used to predict the states at the current time step based on the estimated states value at the previous time step. To be able to address the state constraints, an optimization argument is considered. The optimization argument minimizing the lateral velocity estimation errors with respect to the current measurement, predicted state values, and state constraints. The following cost function is designed to estimate the lateral vehicle velocity:

$$J(\hat{\mathbf{x}}_k) = \|\mathbf{y}_k - \hat{\mathbf{y}}_k)\|_{\mathbf{N}}^2 + \|\hat{\mathbf{x}}_k - \hat{\boldsymbol{\zeta}}_k\|_{\mathbf{S}}^2, \tag{7.11}$$

where $\|.\|_{\mathbf{N}}$ and $\|.\|_{\mathbf{S}}$ are the Euclidean norms weighted by $\mathbf{N} \in \mathbf{R}^{3\times3}$ and $\mathbf{S} \in \mathbf{R}^{4\times4}$, respectively. In the cost function (7.11), the first term penalizes the difference between the predicted measurement and sensor measurements, and the second term shows the difference between the state estimation and prediction. The lateral velocity estimation are obtained by minimizing the objective function (7.11) subject to the vehicle-trailer model as follows [189, 190, 191]:

$$\min_{\hat{x}_k} J(\hat{\mathbf{x}}_k),$$

s.t.

$$\begin{aligned}
\hat{\mathbf{x}}_k &= \mathbf{A}_d\hat{\mathbf{x}}_{k-1} + \mathbf{B}_d\delta_{k-1} + \mathbf{L}\left(\mathbf{y}_{k-1} - \mathbf{C}_y\hat{\mathbf{x}}_{k-1} - \mathbf{D}_y\right),\\
|\hat{\mathbf{x}}_{3,k} - \hat{\mathbf{x}}_{2,k}| &\leq \beta_1|r_2|,\\
|\hat{\mathbf{x}}_k - \hat{\mathbf{x}}_{k-1}| &< \boldsymbol{\beta}_2,\\
|\hat{\mathbf{x}}_{1,k}| &< \beta_3|\delta_k|u,
\end{aligned} \tag{7.12}$$

where r_2 represents the trailer yaw rate. $\mathbf{L} \in \mathbf{R}^{4\times3}$ is the observer gain vector which is discussed in the next subsection.

Based on the linear hitch coupling shown in (3.6) the solution of the cost function should satisfy $|\hat{\mathbf{x}}_{3,k} - \hat{\mathbf{x}}_{2,k}| \leq \beta_1 |r_2|$ where β_1 is the design constraint weight. Moreover, by following the dynamical constraints, the second state constraint is considered to avoid sudden changes in the state estimation results. The $\boldsymbol{\beta}_2$ weight is the state difference threshold that is designed based on the several simulation tests. Given that there is no lateral velocity when $\delta = 0$, and the lateral velocity becomes larger by increasing the longitudinal velocity in the lateral movements, the state threshold design parameter, β_3, is considered as shown in (7.12) to limit the estimator with a physical constraint.

The lateral velocity estimation is obtained by solving the presented cost function with respect to the physical and dynamical constraints, system model, and predicted states' values.

To initiate the estimation algorithm, the states estimate and covariance terms are initialized as $\hat{\mathbf{x}}_0 = E[\mathbf{x}_0]$, $\mathbf{P}_0^+ = E\left[(\mathbf{x}_0 - \hat{\mathbf{x}}_0)(\mathbf{x}_0 - \hat{\mathbf{x}}_0)^T\right]$, respectively. The overall algorithm for lateral velocity estimation is shown in Fig. 7.1.

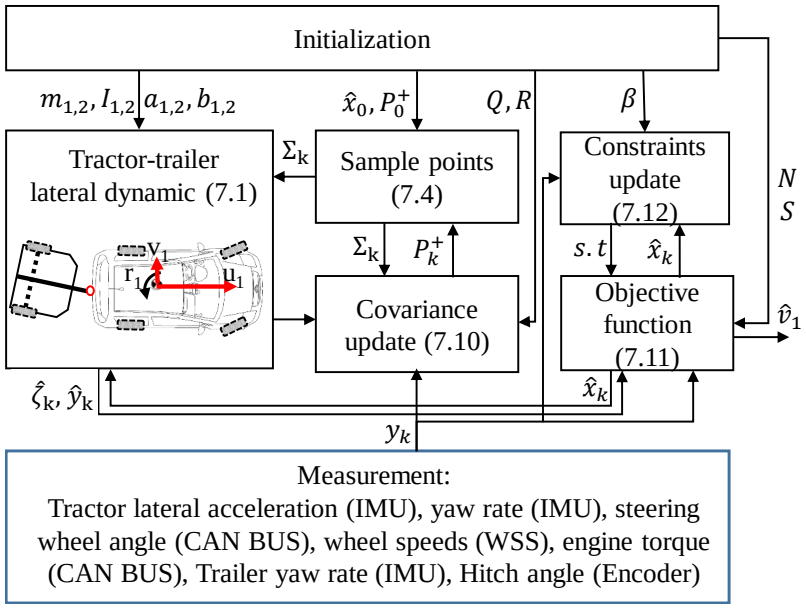

Figure 7.1: Overall lateral velocity estimation procedure.

Given that the observeability is a sufficient condition for implementation of optimal filters (e.g. Kalman filter) or estimation algorithms, the estimation error of the UT-based observer was investigated in [175].

7.3 Simulation and Experimental Studies

In this section, the presented vehicle-trailer lateral dynamics is analysed, and the proposed lateral velocity estimation scheme is validated by both simulation and experimental studies.

7.3.1 Simulation Results

In this subsection, the effect of non-linear term $\mathbf{H}(t)$, shown in (3.25), is first analysed to investigate its magnitude with respect to the slip angles. This analysis can be used for state-observer purposes to cancel the effect of this non-linear term by tuning the observer gains as it is a function of vehicle-trailer slip angles. To analyse the effect of slip angle on non-linear term $\mathbf{H}(t)$ for pure-slip model, a vehicle-trailer model in CarSim with the parameters listed in Table. 7.1 is used.

Fig. 7.2, illustrates the magnitude of the non-linear term $\mathbf{H}(t)$ with respect to the vehicle front, rear, and trailer slip angles.

The magnitude of the norm $\mathbf{H}(t)$ with respect to the slip angle pairs of (α_f, α_r), (α_f, α_t), (α_r, α_t), and $(\alpha_f, \alpha_r, \alpha_t)$ is shown in Fig. 7.2. As can be seen in Fig. 7.2, the norm $\mathbf{H}(t)$ is an ellipsoid shape function in 3-D space and bounded with respect to the slip angles. It has been shown in [156], the norm $\mathbf{H}(t)$ is bounded in the absence of trailer, and now as can be seen in Fig. 7.2, the term $\mathbf{H}(t)$ is also bounded for vehicle-trailer system. As $\mathbf{H}(t)$ is bounded, the state-observer or controller weights/gains can be tuned based on this analysis.

To evaluate the proposed lateral velocity estimation algorithm, several tests have been performed. The vehicle lateral acceleration, yaw rate, steering angle, longitudinal velocity, and trailer yaw rate are available through the CarSim model and used in the designed estimator. The estimated vehicle lateral velocity is compared with the actual values provided by CarSim for different maneuvers. There are two tests considered in the simulation section. First, a multi-double lane change maneuver, with high slip and lateral excitation

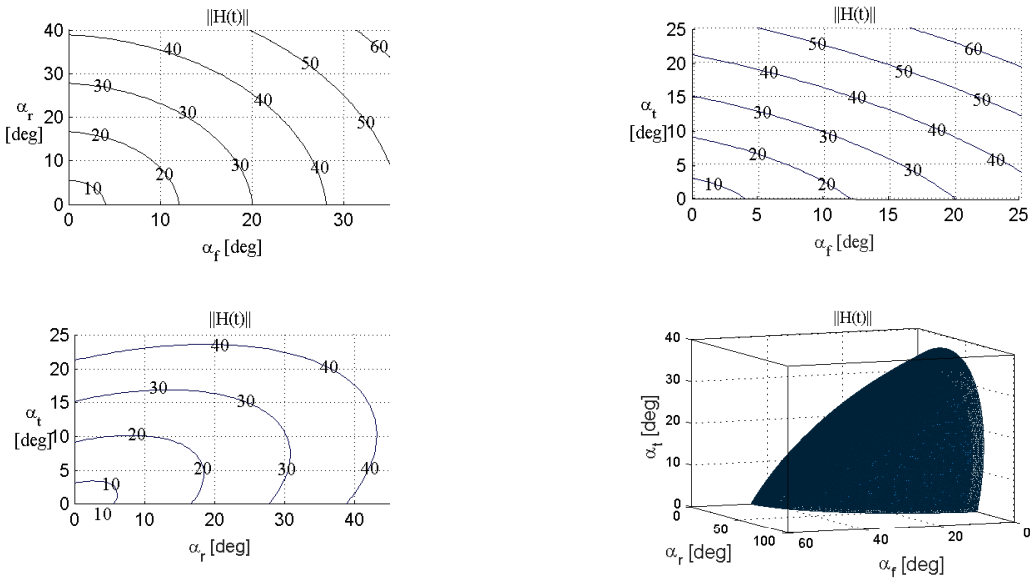

Figure 7.2: Effect of vehicle-trailer slip angles on $||\mathbf{H}(t)||$ on dry road, u = 55[km/h].

Table 7.1: Vehicle-trailer parameters

Description (symbol)	Units	Value
Vehicle's mass (m_1)	kg	1860
Vehicle's yaw moment of inertia (I_{z1})	$kg.m^2$	3397
Vehicle's CG to front axle (a_1)	m	1.21
Vehicle's CG to rear axle (b_1)	m	1.74
Vehicle's rear axle to hitch-point (e)	m	1.27
Effective tire radius (R_{eff})	m	0.39
Trailer's mass (m_2)	kg	2175
Trailer's yaw moment of inertia (I_{z2})	$kg.m^2$	4920
Trailer's CG to hitch-point (a_2)	m	2.8
Trailer's CG to axle (b_2)	m	0.8

is conducted with an All Wheel Drive (AWD) simulated vehicle with trailer with the parameters listed in Table. 7.1 to evaluate the lateral velocity estimation algorithm. A series of double lane change maneuvers with the driver gas/brake pedal inputs' profile are shown in Fig. 7.3.

To account for noises and disturbances in actual measurement signals, a Gaussian noise with zero mean and 0.01 covariance have been added to the CarSim measurement outputs as seen in Fig. 7.4a zoomed area. Fig. 7.4 illustrates the noisy longitudinal/lateral accelerations and the vehicle/trailer yaw rate of the DLC maneuver.

Estimated vehicle lateral velocity is illustrated in Fig. 7.5 by minimizing the presented cost function with respect to the state constraints and the measurement prediction. By propagating the sample-points to the vehicle-trailer system model, the lateral velocity is estimated by the proposed estimation algorithm. As can be seen in the results, the suggested lateral velocity scheme provides appropriate correspondence with actual lateral velocity provided by CarSim.

The performance of the designed estimator with respect to different constant longitu-

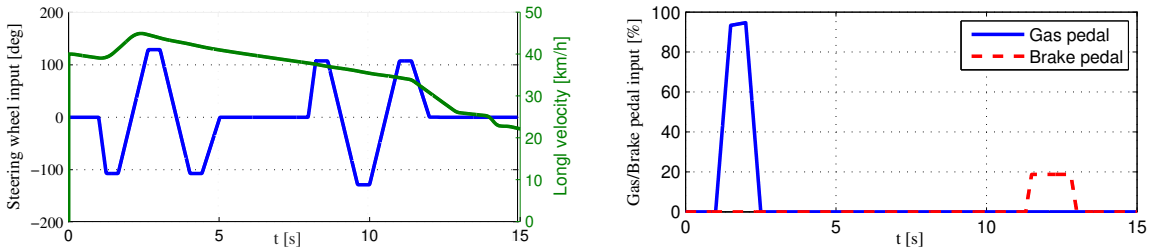

(a) (b)

Figure 7.3: a) Steering wheel angle and vehicle longitudinal velocity, b) Gas/Brake pedal inputs - DLC maneuver.

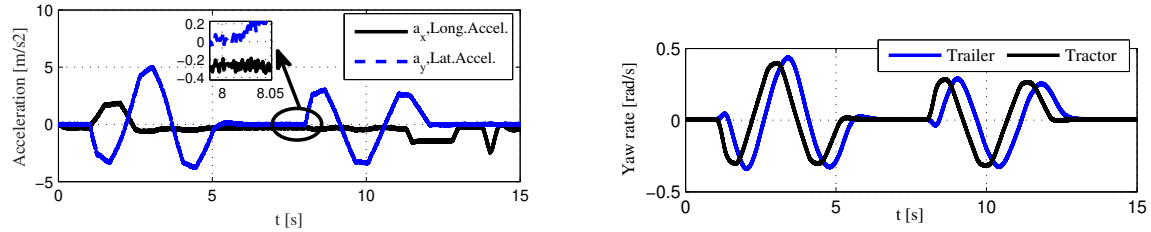

(a) (b)

Figure 7.4: a) Noisy measured longitudinal/lateral accelerations b) Vehicle and trailer yaw rate - DLC maneuver test.

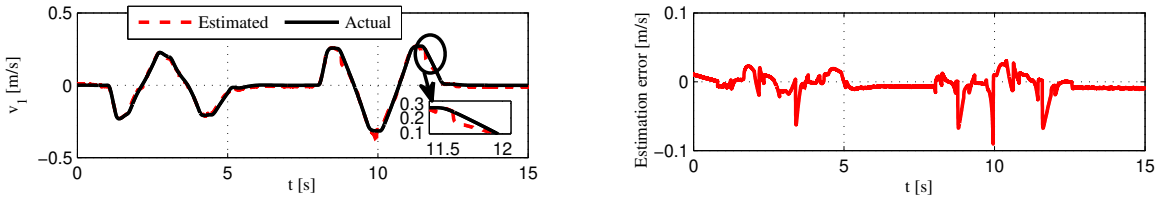

(a) (b)

Figure 7.5: a) Lateral velocity estimation b) Lateral velocity estimation error - DLC maneuver test.

dinal velocities on dry and wet roads is also tested. The aim of these simulations is to illustrate the effect of longitudinal velocity on the lateral velocity estimation results as the longitudinal velocity, u, exists in the system matrices and can change the system charac-

teristic equation. To do so, the steering wheel angle shown in Fig. 7.3a is applied to the vehicle-trailer and the vehicle-trailer drives with the constant longitudinal velocities of 25, 35, 45, and 55 km/h. The simulation runs for both dry and wet roads and the NRMS of the error for lateral velocity estimation is shown in Table. 7.2. The critical velocity obtained by analyzing the location of the eigenvalues of the system model shown in (7.1a) is 15.9 m/s while the critical velocity obtained by analyzing the understeer coefficient shown in (3.13b) is 14.6 m/s. Therefore, the simulation tests run for the longitudinal speeds listed in Table. 7.2. Moreover, the process and measurement noise covariance matrices set to $\mathbf{Q} = 23diag[0.1, 0.22, 0.01, 0.57]$ and $\mathbf{R} = 1.98diag[1, 0.1, 0.1]$, for all the tests.

Table 7.2: NRMS of the errors for the lateral velocity estimator at dry and wet roads.

Road condition	@ u=25 km/h [%]	@ u=35 km/h [%]	@ u=45 km/h [%]	@ u=55 km/h [%]
Dry	6.52	6.33	6.47	7.09
Wet	6.54	6.64	7.51	9.19

As Table. 7.2 illustrates, the maximum error percentage with respect to different longitudinal velocities is less than 9.21%. The lateral velocity estimation errors reported in Table. 7.2, may have several resources and the most possible one is the lack of accurate system model, for instance, the roll dynamics and the aerodynamic forces, which have not been modeled in the presented vehicle-trailer model could cause the error. Moreover, as mentioned in Chapter 3, the LuGre tire model requires tire parameters that are obtained by tire experiment tests. As there are six tire parameters in the model, if the measurement has some error, the error will propagate and accumulate thought the system model.

For the second test, an Step Steer (SS) maneuver on a varying friction surface with the driver gas/brake pedal input shown in Fig. 7.6 is considered.

The vehicle-trailer is simulated in a road surface with varying road friction coefficient to show the effect of road friction coefficient changing in the vehicle lateral velocity estimation results. The proposed lateral velocity estimation algorithm is evaluated in a simulated test field with different friction coefficients. The road friction coefficients set to 0.5 and 0.85 for the right and left half of the field, respectively as illustrated in Fig. 7.6c.

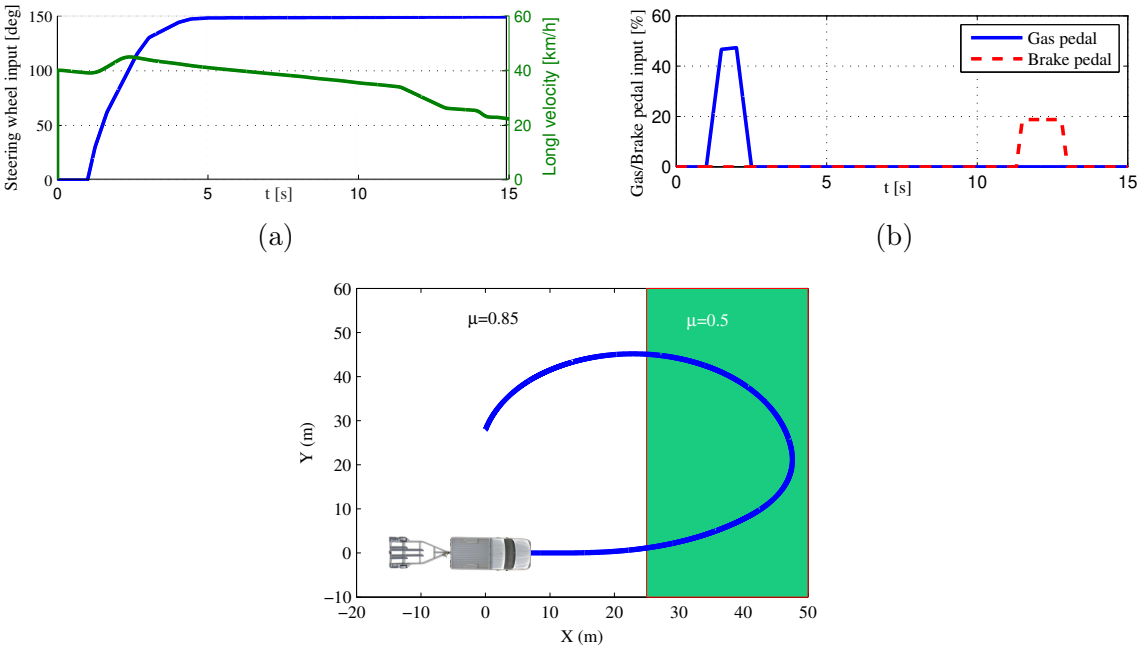

Figure 7.6: a) Steering wheel angle and vehicle longitudinal velocity, b) Gas/Brake pedal inputs c) Vehicle-trailer path on the simulated test field with a dual-friction coefficient surface input - SS maneuver.

The lateral acceleration of the SS maneuver correspond with noises (Gaussian noise with zero mean and 0.01 covariance) and vehicle and trailer yaw rates are shown in Fig. 7.7. The simulation runs for 15 seconds with the initial speed of 40 km/h on a road surface with varying friction coefficient as illustrated in Fig. 7.6c.

The performance of the lateral velocity estimation algorithm on a varying friction test field is shown in Fig. 7.8. As Fig. 7.8 illustrates, by changing the road friction coefficient from 0.85 to 0.5, oscillations occur on the actual lateral velocity due to the vehicle and trailer lateral slippage in the transient mode. The oscillations occur since by changing the road friction coefficient, the slip ratio changes in both longitudinal and lateral directions which affect the slip angle.

As the slip angle is modeled in the vehicle-trailer lateral dynamics, the proposed lateral velocity estimator can be used to compensate for oscillations due to slippery surfaces since

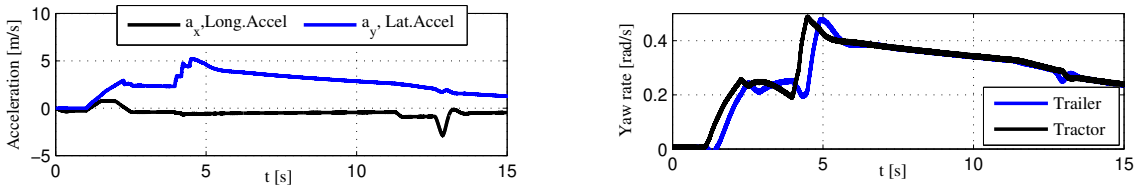

(a) (b)

Figure 7.7: a) Measured longitudinal/lateral accelerations b) Vehicle and trailer yaw rate - SS maneuver.

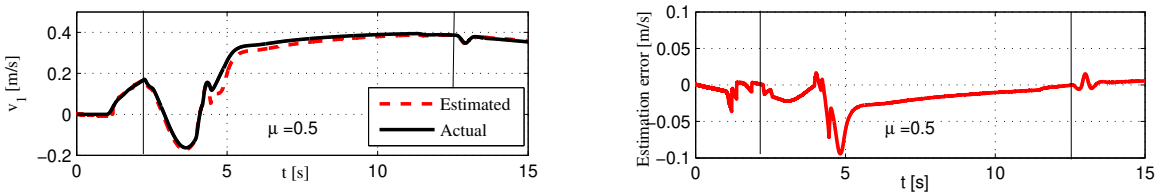

(a) (b)

Figure 7.8: a) Lateral velocity estimation b) Lateral velocity estimation error - SS maneuver.

the tire model updates as the road friction coefficient changes as described in (3.14a). Therefore, the proposed estimation algorithm is capable of estimating the lateral velocity on dry, wet, and icy roads; however, the road friction coefficient is assumed to be given which may not be available all the time.

7.3.2 Experimental Studies

The test vehicle is an electrified Chevrolet Equinox sport utility vehicle (SUV) with a single axle trailer as shown in Fig. 4.6. As mentioned, the torque on each wheel is measurable directly from the each motor drive. Each motor can provide up to $\pm 1600 Nm$, and the longitudinal/lateral accelerations and yaw rate of the vehicle are measured with a 6-axis IMU (and GPS) system RT2000. The longitudinal/lateral accelerations and yaw rate of the trailer are also measurable by a 3-axis convectional IMU mounted on the trailer. The main parameters of the vehicle and trailer are listed in Table. 4.1. Identification/Estimation of the LuGre tire parameters was done by analysing the test vehicle standard tire experimental

curves in [155].

A sensor located in the steering column is used to measure the steering angle. A Global-Positioning-System (GPS) is installed on the vehicle to measure the longitudinal and lateral velocities of the vehicle accurately. A 6-axis IMU is mounted inside of the vehicle, close to the CG location. Measured signals are communicated using a CAN-bus. Real-time acquisition and processing of sensory information and the developed lateral velocity estimation algorithm is realized using a dSPACE. The sampling frequency for the experiment is fixed to 200 [Hz], and the lateral velocity reference, ground truth, is provided by the GPS sensor.

Two step steer maneuvers are considered in the experimental studies to validate the proposed lateral velocity estimation. The vehicle-trailer is tested in a test track with the two step steer maneuvers, with lateral excitation in both positive and negative directions, to validate the proposed vehicle lateral velocity estimation scheme. The path of the vehicle-trailer in the testing is shown in Fig. 7.9a, and the steering wheel angle, longitudinal/lateral accelerations, and vehicle yaw rate are shown in Fig. 7.9.

The test duration is 20 seconds and the vehicle (Equinox) with trailer starts from a stationery point, $u = 0$, and accelerates till the speed reaches 34 km/h, then two step steers are applied while it runs forward with the constant speed. The performance of the lateral velocity estimation algorithm is shown in Fig. 7.9e.

The estimated lateral velocity compared with the ground truth is shown in Fig. 7.9e. The results show that the developed lateral velocity estimator provides reliable and accurate estimation for a vehicle-trailer system. The experimental results of the measured accelerations and vehicle yaw rate are depicted in Fig. 7.9 for this maneuver. Fluctuations of the measured lateral acceleration and sudden changes of the vehicle yaw rate in Fig. 7.9 substantiate the arduous characteristics of the driving scenario. As can be seen in the results, the proposed algorithm estimates the vehicle lateral velocity with error NRMS ε_n <5.3%. The actual, ground truth, lateral velocity measured by GPS signal has settling time error for the first step steer maneuver which happens because of the device's internal estimator drift. The maximum estimation error percentage occurs at $t = 5$ sec; however, the ground truth signal has the settling time error at that time. As confirmed via the above experimental results, the suggested lateral velocity estimator provides appropriate correspondence with GPS measurements.

The proposed lateral velocity estimator with the state constraints, (7.12) can handle

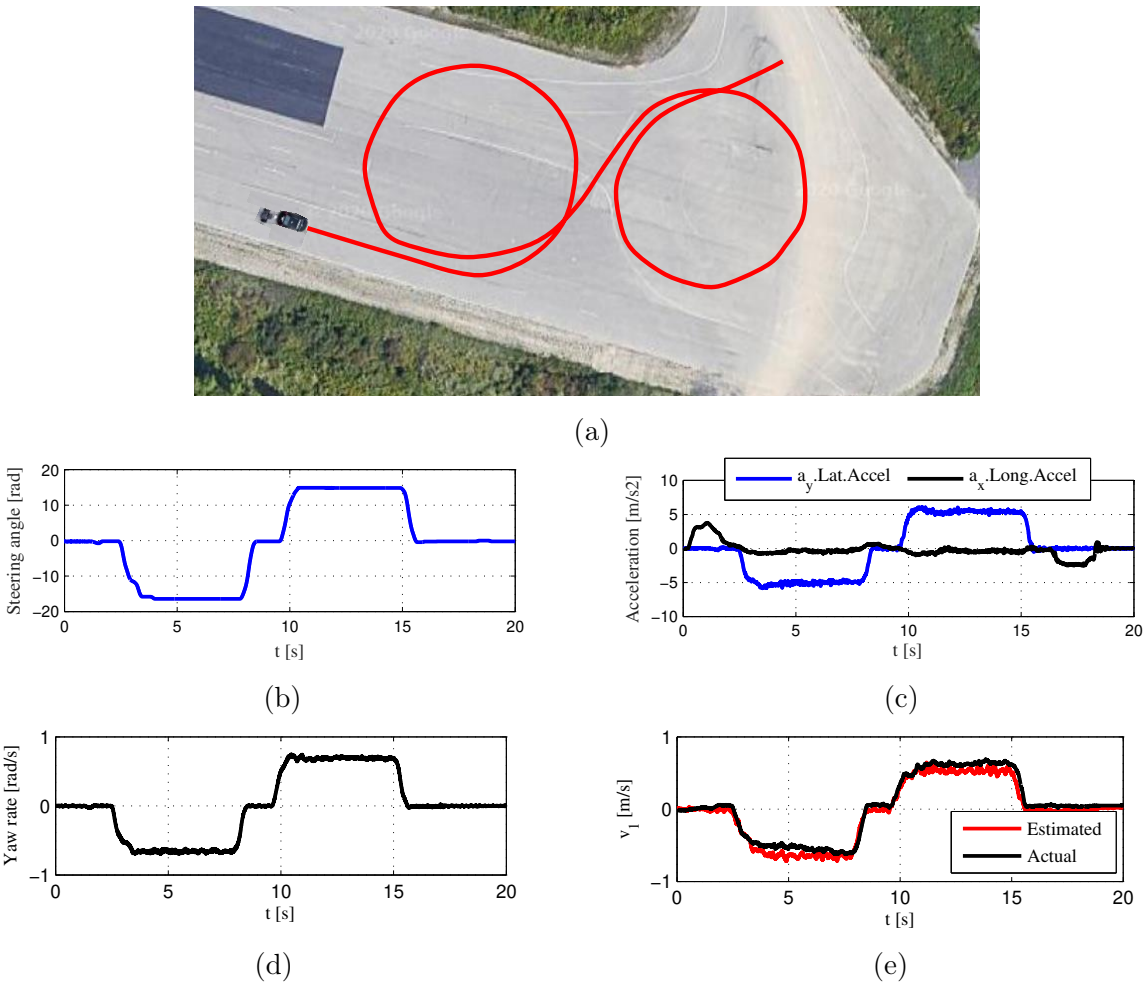

Figure 7.9: a) Vehicle-trailer path on the test field b) Steering wheel angle c) Measured longitudinal/lateral accelerations d) Vehicle yaw rate e) Lateral velocity estimation.

dry and slippery roads with error NRMS ε_n <9.5% for the vehicle lateral velocity as shown in Table. 4.1. In spite of low excitation, which is challenging for current lateral velocity estimators in production vehicles, especially for vehicle-trailer combination, and the transient mode for passing through dry/wet to wet/dry surfaces, the new algorithm exhibits accurate estimates that is promising and can estimate the vehicle lateral velocity in the transient mode too. However, it is worth mentioning that the road friction coefficient is assumed to be given which may not be available all the time.

Although the developed estimation algorithm estimates the lateral velocity of the vehicle, the trailer lateral velocity can be found directly from (3.5).

7.4 Conclusions

In this chapter, the steady-state LuGre model was utilized to model the vehicle-trailer lateral dynamics. It was shown that the non-linear term $\mathbf{H}(t)$ in (3.25) contains yaw rate, hitch angle rate, and lateral velocity. Therefore, the vehicle-trailer lateral dynamics with the pure-slip LuGre tire model was expressed in an LPV system, which is practical for the control/estimation applications for mitigating the effect of non-linear terms.

The proposed vehicle-trailer model was then used to estimate the lateral velocity of the vehicle. To make the estimation algorithm generic, the presented model was derived in a way that it can address both small and large slip angles. Uncertainty of the model was studied and the stability of the lateral velocity estimation error dynamic model was investigated using an affine quadratic stability approach. The proposed system is observable and as the stability of the lateral velocity estimation error dynamics is guaranteed, the estimation error is converged. It was also shown that the proposed method is capable of estimating the lateral velocity on dry and wet roads. The proposed estimation algorithm was implemented in both high-fidelity CarSim software and also experimental set-up for valuation. The results showed a strong agreement between the estimated and measured lateral velocities in several maneuvers.

Chapter 8

Road Angle Estimation for Vehicle-Trailer Systems

8.1 Introduction

As the road bank and grade angles significantly affect the vehicle longitudinal/lateral dynamics, recent developments in vehicular active safety systems have emphasized on the need for real-time estimation of the road angles [82, 95]. Although road angle estimation has been investigated for vehicles, scholarly work on road angle estimation for vehicle-trailer is very scarce.

In [194], a vehicle roll dynamic model was considered to estimate road bank angles, while the steady-state approximation of the bank angle was used as a reference to obtain the estimation error and tune the observer gains. An unknown input sliding mode observer was used in [195] to estimate the road bank angle by considering a linear single track vehicle model. In this observer, it was assumed that the tire cornering stiffness and road friction were known, which may not be the case in certain situations. A similar method was proposed to estimate the vehicle velocity with road angle adaptation in [196].

The road and vehicle roll/pitch angles both appear in the vehicle roll/pitch dynamics [197]. Therefore, in [198, 199], the road angles were separated from the vehicle roll/pitch angles by considering the vehicle roll/pitch dynamic model and applying a nonlinear observer. Similarly, an unknown input observer was used in [200] to estimate the road angles,

however, the road angles were assumed to be constant.

Alternatively, the global positioning system (GPS) data were used in some road angle measurement studies, however, these studies suffer from poor accuracy, signal losses, frequency variations, and lack of signal reception in some geographical areas in the most commonly used GPSs in vehicles. A two antenna GPS receiver was used in [201] to estimate the parameters that impact the vehicle roll stability, including the road bank angle and roll dynamics parameters. By combining vehicle roll and pitch dynamic models and taking the advantage of switching observer scheme, the road angles were estimated in [202], however, the vehicle roll angle, which was assumed to be available, may not be measurable/accessible for commercial vehicles.

The remainder of this chapter is organized as follows: In Section 8.2, the vehicle-trailer pitch/roll dynamics are analyzed, and the proposed model-based road angle estimation approach is described. In Section 8.3, the overall structure of the proposed non-model-based approach is presented and a machine learning based road angle estimator is designed using Recurrent Neural Network (RNN) with Long-Short-Term-Memory (LSTM) gates. A sensitivity analysis with respect to all available measurements from the vehicle-trailer system, which are used as the inputs to the network, is also presented in Section 8.3, along with a discussion of selection of the inputs of the network on this sensitivity analysis. In Section 8.4, training and testing the designed LSTM-RNN estimator with a set of real-time vehicle-trailer system data is explained. The road angle estimation results with the model-based and machine learning approaches are presented and compared in Section 8.5 with discussion.

8.2 Model-Based Estimator

In this section, the vehicle-trailer roll/pitch dynamic models linked with the road angles are analyzed to develop a reliable estimator for the road bank/grade angles for a vehicle-trailer systems. To do so, first, the vehicle and trailer body angles are estimated by utilizing the corner displacements measured by the suspension height sensors. Then, the vehicle-trailer roll and pitch dynamics are employed to relate the vehicle's frame, body, and road angles.

It is assumed that using an IMU attached to the vehicle body, the body roll, pitch, and yaw rates are measurable. The vehicle body roll and pitch rates are related to the

road angle rates over the roll and pitch dynamics. Thus, an Unknown Input Observer (UIO) approach is considered to estimate the road bank and grade angles based on the vehicle-trailer responses. More details are presented in the following subsections.

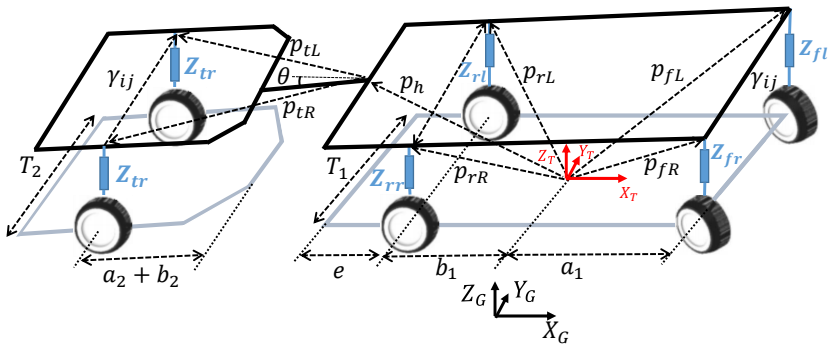

Figure 8.1: Height sensors and sprung mass kinematics of a vehicle-trailer system.

8.2.1 Vehicle-Trailer Roll and Pitch Angle Kinematics

As the vehicle-trailer roll and pitch dynamics are incorporated with road angles, the vehicle-trailer roll/pitch dynamics are considered to estimate the road angles. To do so, the vehicle roll and pitch angles should estimate first. The vehicle roll and pitch rates are measured by an IMU attached to the vehicle unit. As the measured vehicle roll and pitch angle rates have noises, the vehicle roll and pitch angles cannot be estimated by integrating the measured values. Therefore, the vehicle-trailer roll/pitch sprung mass kinematics are used to find the vehicle-trailer roll and pitch angles based on the vehicle-trailer corner displacements. The vehicle-trailer sprung mass model is illustrated in Fig. 8.1. In Fig. 8.1, the vehicle and trailer corner normal displacements $Z_{ij}, ij \in [fL, fR, rL, rR]$ are measured by suspension height sensors.

The auxiliary coordinates (x_a, y_a, z_a) are obtained by rotating the global coordinates about the z_G axis by the vehicle, not trailer, yaw angle ψ, whereas the vehicle frame coordinate (x_f, y_f, z_f) is a right-handed orthogonal axis system located at the vehicle center of gravity [203], and it is parallel to the road surface. The suspension height sensor position vectors for both vehicle and trailer are described in the frame coordinate system

$(x_f,\, y_f,\, z_f)$ as follows:

$$p_{rL} = \begin{bmatrix} -b_1 & \frac{T_1}{2} & Z_{rL} \end{bmatrix}^T, \tag{8.1}$$

$$p_{rR} = \begin{bmatrix} -b_1 & -\frac{T_1}{2} & Z_{rR} \end{bmatrix}^T, \tag{8.2}$$

$$p_{fL} = \begin{bmatrix} a_1 & \frac{T_1}{2} & Z_{fL} \end{bmatrix}^T, \tag{8.3}$$

$$p_{fR} = \begin{bmatrix} a_1 & -\frac{T_1}{2} & Z_{fR} \end{bmatrix}^T, \tag{8.4}$$

$$p_h = \begin{bmatrix} -(e+b_1) & 0 & Z_h \end{bmatrix}^T, \tag{8.5}$$

$$Z_h = \frac{(Z_{rL}+Z_{rR})}{2}\left(1 - e\left(\frac{\frac{(Z_{fL}+Z_{fR})}{2} - \frac{(Z_{rL}+Z_{rR})}{2}}{(a_1+b_1)\frac{(Z_{rL}+Z_{rR})}{2}}\right)\right), \tag{8.6}$$

where a_1, b_1, and e are the front axle to CG, rear axle to CG and hitch point distances, respectively. The vehicle and trailer track width are illustrated by T_1 and T_2, respectively. By having the hitch point to vehicle CG, the trailer corner displacement vector in vehicle coordinates is found as:

$$p_{tL} = \begin{bmatrix} p_{hx} - l_t\cos\psi + \frac{T_2}{2}\sin\psi \\ p_{hy} + l_t\sin\psi + \frac{T_2}{2}\cos\psi \\ p_{hz} + Z_{tL} \end{bmatrix}, \tag{8.7}$$

$$p_{tR} = \begin{bmatrix} p_{hx} - l_t\cos\psi - \frac{T_2}{2}\sin\psi \\ p_{hy} + l_t\sin\psi - \frac{T_2}{2}\cos\psi \\ p_{hz} + Z_{tR} \end{bmatrix}, \tag{8.8}$$

where a_2 and b_2 are the trailer CG to hitch point and trailer axle distances, respectively. Relative position vector $\gamma_{ij}, ij, mn \in [fL, fR, rL, rR, tL, tR]$ between the two corners for both vehicle and trailer can be calculated from:

$$\gamma_{ij,mn} = p_{mn} - p_{ij}. \tag{8.9}$$

The normal vectors for the vehicle and trailer sprung mass at each corner are then obtained as the cross product of two relevant position vectors at each corner.

$$\mathcal{N}_{ij} = \gamma_{ij,mn} \times \gamma_{ij,pq}$$
$$ij, mn, pq \in [fL, fR, rL, rR, tL, tR], \tag{8.10}$$

where $\mathcal{N}_{ij} = [\mathcal{N}_{ij}^x, \mathcal{N}_{ij}^y, \mathcal{N}_{ij}^z]^T$ is the sprung mass normal vector at each corner that can be used to estimate the vehicle and trailer roll/pitch angles. The vehicle and trailer roll/pitch angles, $\psi_{v_{ij}}$, $\psi_{t_{ij}}$, $\theta_{v_{ij}}$, and $\theta_{t_{ij}}$ can be obtained using the corresponding normal vector N_{ij} as follows:

$$\bar{\psi}_{v_{ij}} = \arccos \frac{\mathcal{N}_{ij}^x}{||\mathcal{N}||}, ij \in [fL, fR, rL, rR], \tag{8.11}$$

$$\bar{\psi}_{t_{ij}} = \arccos \frac{\mathcal{N}_{ij}^x}{||\mathcal{N}||}, ij \in [tL, tR,], \tag{8.12}$$

$$\bar{\theta}_{v_{ij}} = \arccos \frac{\mathcal{N}_{ij}^y}{||\mathcal{N}||}, ij \in [fL, fR, rL, rR], \tag{8.13}$$

$$\bar{\theta}_{t_{ij}} = \arccos \frac{\mathcal{N}_{ij}^y}{||\mathcal{N}||}, ij \in [tL, tR,]. \tag{8.14}$$

As can be seen in (8.14), by using different combinations of the suspension sensors, four vehicle roll/pitch angle estimates and two trailer roll/pitch angle estimates can be obtained. Then a data fusion technique can be used to increase the accuracy as $\bar{\psi}_{v_{ij}}$ are all equal to $\bar{\psi}_v$. Therefore, a weighted average will be used to have reliable estimates in case of existing outlier data due to uneven surfaces at each corner as follows:

$$\bar{\psi}_v = \Sigma_{ij} \beta_{ij} \bar{\psi}_{v_{ij}}, \bar{\theta}_v = \Sigma_{ij} \Gamma_{ij} \bar{\theta}_{v_{ij}}, \tag{8.15}$$

where $\sum \Gamma_{ij} = 1$ and $\sum \beta_{ij} = 1$ are the weight for the obtained roll and pitch angles based on the ij corner measurements. To check the possibility of being an outlier on sensor measurements because of road disturbances, such as bumps and uneven surfaces at each corner, the vehicle body angle rate measurements provided by an IMU attached to the

vehicle body is considered as explained in [204]. For instance, if only one of the tires faces with uneven surfaces or road bumpers, the Γ or β weights corresponding to that corner becomes zero. The estimated vehicle and trailer roll/pitch angles estimation, $\bar{\psi}_v$, $\bar{\theta}_v$ are used to estimate the road grade and bank angles by applying an unknown input observer which is explained in the next subsection.

8.2.2 Unknown Input Observer

As the vehicle-trailer roll and pitch dynamics are incorporated with road angles, the vehicle-trailer roll/pitch dynamics are considered to estimate the road angles. The estimated vehicle roll/pitch angles provided from vehicle-trailer roll and pitch angle kinematic equations (8.16) to (8.19) are utilized in the vehicle-trailer roll and pitch dynamic models to estimate the road angles.

The road bank and grade angles are estimated using unknown input observers (UIO) in this subsection. A general form of the UIO is used to estimate the unknown inputs which are representing the road angles with implementation of the vehicle body angles and their rates as outputs. Vehicle-trailer roll and pitch dynamic models are used for the proposed UIO as shown in Fig. 8.2.

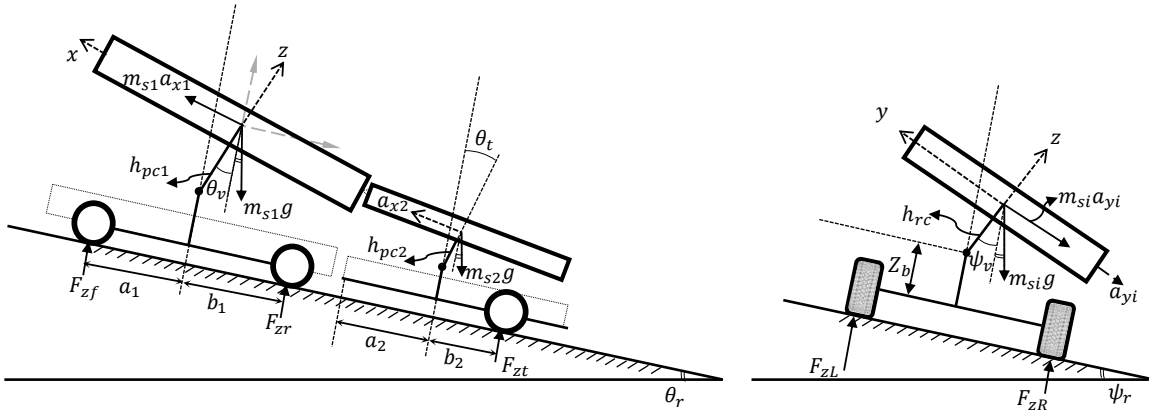

Figure 8.2: Roll and pitch models of a vehicle-trailer system with the road angles.

As can be seen in Fig. 8.2, the road bank and grade angles are denoted by ψ_r and θ_r, respectively. By considering the vehicle-trailer roll and pitch motions, the vehicle and

trailer roll/pitch dynamics can be expressed as:

$$(I_{x_1} + m_{s_1} h_{rc_1}^2)\ddot{\psi}_v = C_{\psi_1}\dot{\psi}_v + k_{\psi_1}\psi_v + (m_{s_1} h_{rc_1})\left(-a_{y_1} + g\sin(\psi_v + \psi_r)\right), \tag{8.16}$$

$$(I_{x_2} + m_{s_2} h_{rc_2}^2)\ddot{\psi}_t = C_{\psi_2}\dot{\psi}_t + k_{\psi_2}\psi_t + (m_{s_2} h_{rc_2})\left(-a_{y_2} + g\sin(\psi_t + \psi_r)\right), \tag{8.17}$$

$$(I_{y_1} + m_{s_1} h_{pc_1}^2)\ddot{\theta}_v = C_{\theta_1}\dot{\theta}_v + k_{\theta_1}\theta_v + (m_{s_1} h_{pc_1})\left(a_{x_1} + g\sin(\theta_v + \theta_r)\right), \tag{8.18}$$

$$(I_{y_2} + m_{s_2} h_{pc_2}^2)\ddot{\theta}_t = C_{\theta_2}\dot{\theta}_t + k_{\theta_2}\theta_t + (m_{s_2} h_{pc_2})\left(a_{x_2} + g\sin(\theta_t + \theta_r)\right), \tag{8.19}$$

where the vehicle and trailer roll/pitch angles of the sprung mass are denoted by ψ_v, ψ_t, θ_v, and θ_t, respectively. The distances between the roll/pitch axes and the center of gravity are denoted by h_{rc} and h_{pc}, respectively. The moments of inertia about the roll and pitch axes parallel to the frame coordinate system are shown by I_x, I_y. Roll/pitch stiffness K_ψ, K_θ and damping C_ψ, C_θ are used for derivation of the roll and pitch dynamics. The system roll and pitch models presented in (8.16) to (8.19), can now be formed in the conventional state space form where the states are $x_\psi = \begin{bmatrix} \psi_v & \dot{\psi}_v & \psi_t & \dot{\psi}_t \end{bmatrix}^T$ and $x_\theta = \begin{bmatrix} \theta_v & \dot{\theta}_v & \theta_t & \dot{\theta}_t \end{bmatrix}^T$. Thus, the state space form of the model can be represented by $\dot{x}_q = A_q x_q + B_q u_q$ and $y_q = C_q x_q + D_q u_q$ where $q \in [\psi, \theta]$ as:

$$A_q = \begin{bmatrix} M_q & 0_{2\times 2} \\ 0_{2\times 2} & N_q \end{bmatrix}, B_q = \begin{bmatrix} 0 & 0 \\ \frac{H_{q_1}}{S_{q_1}} & 0 \\ 0 & 0 \\ 0 & \frac{H_{q_2}}{S_{q_2}} \end{bmatrix}, \tag{8.20}$$

$$M_q = \begin{bmatrix} 0 & 1 \\ \frac{-k_{q_1}}{S_{q_1}} & \frac{-C_{q_1}}{S_{q_1}} \end{bmatrix}, N_q = \begin{bmatrix} 0 & 1 \\ \frac{-k_{q_2}}{S_{q_2}} & \frac{-C_{q_2}}{S_{q_2}} \end{bmatrix}, \tag{8.21}$$

where $S_{\psi_i} = I_{x_i} + m_{s_i} h_{rc_i}^2$, $S_{\theta_i} = I_{y_i} + m_{s_i} h_{pc_i}^2$, $H_{\psi_i} = m_{s_i} h_{rc_i}$, $H_{\theta_i} = m_{s_i} h_{pc_i}$, $i \in [1, 2]$. The system matrices A_q, D_q are with appropriate dimensions where $[B_q, D_q]$ is full-column rank. Unknown input vector $u_q, q \in [\psi, \theta]$ is the vehicle-trailer roll and pitch dynamic

unknown inputs, which are defined as follows:

$$u_\psi = \begin{bmatrix} \dot{V}_y + rV_x + g\sin(\psi_v + \psi_r) \\ \dot{V}_y - a_2(\ddot{\theta} - \dot{r}_1) - \dot{V}_x\theta - c\dot{r}_1 + rV_x + g\sin(\psi_t + \psi_r) \end{bmatrix},$$
$$u_\theta = \begin{bmatrix} -\dot{V}_x + rV_y + g\sin(\theta_v + \theta_r) \\ rV_y - \dot{V}_x - (a_2 + c)r - a_2r\dot{\theta} - V_xr\theta + g\sin(\theta_t + \theta_r) \end{bmatrix}, \tag{8.22}$$

where θ_r and ψ_r represent the road grade and bank angles. To estimate the road angles via unknown input observer technique, the discretize form of the system model is required. To do so, the step-invariance method [205] is considered to discretize the system equations of motion as follows:

$$x_\psi[k+1] = \bar{A}_\psi x_\psi[k] + \bar{B}_\psi u_\psi[k],$$
$$x_\theta[k+1] = \bar{A}_\theta x_\theta[k] + B_\theta u_\theta[k], \tag{8.23}$$

where $\bar{A}_\psi = e^{\bar{\mathbf{A}}_\psi T_s}$ and $\bar{\mathbf{B}}_d = \int_0^{T_s} e^{\bar{\mathbf{A}}\tau}\bar{\mathbf{B}}d\tau$ are the discretized form of the system matrices $\bar{\mathbf{A}}$ and $\bar{\mathbf{B}}$, respectively. By having the discretized system equations of motion, an unknown input observer [206, 207, 208, 209] is designed to estimate the road bank θ_r and grade ψ_r angles (unknown inputs u_q) using vehicle body's roll/pitch angles θ_v, ψ_v and their rates θ_v, ψ_v as measurements where the derivation of the vehicle roll/pitch rates are discussed in [204] by considering the vehicle road-body kinematics.

To design a feasible observer and to uniquely recover the unknown input $u_q[k]$ from the initial state $x[0]$, the output signals up to time step $k+L$ are considered, which means the observer has an L-delay inverse. The upper bound of the inherent delay L is defined as $L = n - null(D_q) + 1$ [204]. Thus, the output equation is calculated as follows:

$$y_q[0:L] = \mathcal{O}_q x[0] + \mathcal{J}_q u_q[0:L], \tag{8.24}$$

where

$$\begin{bmatrix} y_q[0] \\ y_q[1] \\ \vdots \\ y_q[L] \end{bmatrix} = \begin{bmatrix} \bar{C}_q \\ \bar{C}_q\bar{A}_q \\ \vdots \\ \bar{C}_q\bar{A}_q^L \end{bmatrix} x[0] + \begin{bmatrix} \bar{D}_q & 0 & \cdots & 0 \\ \bar{C}_q\bar{B}_q & \bar{D}_q & \cdots & 0 \\ \bar{C}_q\bar{A}_q\bar{B}_q & \bar{C}_q\bar{B}_q & \cdots & 0 \\ \vdots & \vdots & \ddots & \vdots \\ \bar{C}_q\bar{A}_q^{L-1}\bar{B}_q & \bar{C}_q\bar{A}_q^{L-2}\bar{B}_q & \cdots & \bar{D}_q \end{bmatrix} \begin{bmatrix} u_q[0] \\ u_q[1] \\ \vdots \\ u_q[L] \end{bmatrix}, \tag{8.25}$$

where $\mathcal{J}_q$ and $\mathcal{O}_q$ are the invertibility and observability matrices for pair A_q and C_q, respectively. The unknown input observer for a positive arbitrary L results in the following estimator, which provides the states $\hat{x}_\theta[k]$, $\hat{x}_\psi[k]$ as well as unknown inputs $\bar{u}_\theta[k]$, $\bar{u}_\psi[k]$:

$$\begin{aligned} \hat{x}_\psi[k+1] &= E_q \hat{x}_\psi[k] + F_q y_q[k:k+1], \\ \hat{u}_q[k] &= \begin{bmatrix} \bar{B}_q \\ \bar{D}_q \end{bmatrix}^{-1} \begin{bmatrix} \hat{x}_q[k+1] - \bar{A}_q \hat{x}_q[k] \\ y_q[k] - \bar{C}_q \hat{x}_q[k] \end{bmatrix}, \end{aligned} \tag{8.26}$$

where E_q and F_q are observer gain matrices that obtain by pole placement. For the test vehicle-trailers with parameters listed in Table. 4.1, the observer gain matrices E_q and F_q are obtained as follows [204, 210]:

$$\begin{aligned} E_\psi &= \begin{bmatrix} 4.25e-4 & 2.31e-5 & 4.05e-4 & 2.01e-5 \\ -1.53e-6 & 2.9e-4 & 2.53e-6 & 2.8e-4 \\ 3.15e-4 & 2.31e-5 & 3.95e-5 & 2.01e-5 \\ -1.03e-5 & 2.9e-5 & 2.93e-6 & 1.8e-4 \end{bmatrix}, \\ E_\theta &= \begin{bmatrix} 3.895e-4 & 2.05e-5 & 4.05e-4 & 2.01e-5 \\ 0.94e-6 & 2.34e-4 & 2.53e-6 & 1.9e-4 \\ 3.59e-4 & 1.95e-5 & 2.35e-5 & 1.91e-5 \\ 0.94e-6 & 2.74e-4 & 2.03e-6 & 1.5e-4 \end{bmatrix}. \end{aligned} \tag{8.27}$$

The road bank angle $\hat{\theta}_r$ is then obtained by employing the estimated unknown input $\hat{u}_\theta$ from (8.26) and the vehicle's roll/pitch angle from (8.15) as follows:

$$\begin{aligned} \hat{\theta}_r[k] &= \arcsin \frac{\hat{u}_\theta[k] - \dot{V}_y[k] - r[k]V_x[k]}{g} - \bar{\theta}_v[k], \\ \hat{\psi}_r[k] &= \arcsin \frac{\hat{u}_\psi[k] + \dot{V}_x[k] - r[k]V_y[k]}{g} - \bar{\psi}_v[k]. \end{aligned} \tag{8.28}$$

As can be seen in (8.28), the estimated vehicle roll/pitch angles and their rates are used for the road grade and bank angle estimations. To estimate the vehicle roll/pitch angles, the suspension height sensor measurements are used. However, as the suspension height sensor measurements are incorporated with noises, taking the time derivative of the estimated vehicle roll/pitch angles (8.15) to calculate the roll/pitch angle rates is not a proper choice. Therefore, the vehicle roll and pitch angle rates provided by vehicle's IMU

are used by considering the transformation between the vehicle's frame and body coordinate as illustrated in [204]. As mentioned, there are two alternatives for estimating the road angles including model-based and non-model-based approaches. The overall algorithm that contains both model-based and non-model-based approaches for road angle estimation is shown in Fig. 8.3.

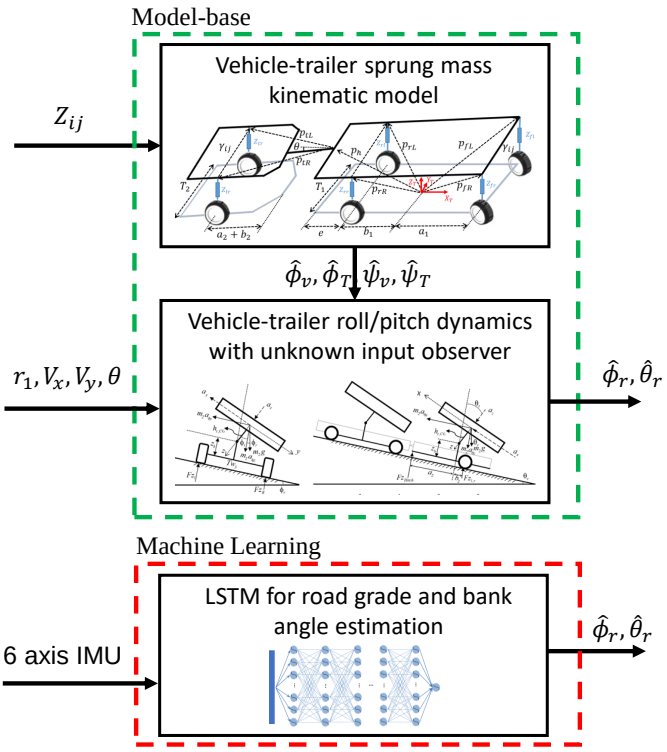

Figure 8.3: Overall road angle estimation procedure.

The following section investigates the non-model-based method for estimating the road bank and grade angles.

8.3 Machine Learning Based Approach

An observer is designed to estimate road angles and the stability of the designed observer was formally established in Section 8.2. As an alternative approach, a neural network is

also designed, trained, and tested for road angle estimations in this section. To be able to design a network that can differentiate between the road and body angles, the vehicle roll and pitch angles are considered in the network output signals. In this section, the vehicle-trailer roll and pitch dynamics are used to define appropriate inputs for the network.

8.3.1 Input Feature Selection - Sensitivity Analysis

A sensitivity analysis over all of the measurable inputs is provided to check the importance of the measurable vehicle states and parameters with respect to the road angles. The Gradient Boosting Regression Tree (GBRT) is used to evaluate the input importance. GBRT begins by training a decision tree in which each observation is assigned an equal weight. By evaluating the first tree, the weights of those observations that are difficult to classify, are increased. By evaluating the weights for neurons, the importance of the inputs with respect to the outputs which are vehicle roll/pitch and road bank/grade angles is generated. The importance of the inputs with respect to the road and vehicle angles are shown in Fig. 8.4.

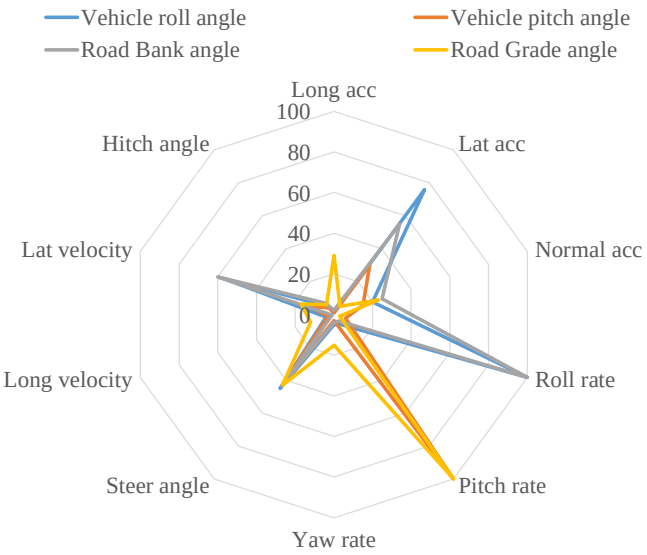

Figure 8.4: The input feature importance of the all available measurements for road angle estimation.

As can be seen in Fig. 8.4, the hitch angle, longitudinal acceleration, and yaw rate of the vehicle are less important and have less effect on the network for estimating the vehicle roll/pitch angles and road angles than the other available inputs. Therefore, there is no need to consider all of the available inputs for the network since their effectiveness are not the same.

Moreover, the vehicle-trailer pitch and roll dynamic models shown in (8.16) to (8.19) indicate that the road grade/bank angles have direct relation with vehicle roll and pitch angles. Thus, by considering both the vehicle-trailer roll/pitch dynamics and sensitivity analysis results, the input vector to train/test the network is considered as follows:

$$\mathbf{A_t} = \begin{bmatrix} \dot{\psi}_v & \dot{\theta}_v & r & a_x & a_y & V_x & V_y & \delta \end{bmatrix}^T. \tag{8.29}$$

In order to propose a generic method to estimate the vehicle roll/pitch angles as well as the road angles, the vehicle parameters should be incorporated in the model. Hence, the input vector is normalized by the vehicle parameters which are mostly related to the outputs. As can be seen in (8.16) to (8.19), the vehicle CG height, mass, and wheel-base are the vehicle parameters that present in the vehicle-trailer roll/pitch dynamic models. Therefore, the input vector $\mathbf{A_t}$ shown in (8.29) is normalized over these parameters and rewritten as follows:

$$\mathbf{A_t} = \begin{bmatrix} \frac{\dot{\psi}_v}{h_{rc1}} & \frac{\dot{\theta}_v}{h_{rc1}} & \frac{r}{a_1+b_1} & \frac{a_x}{m_{s1}} & a_y & V_x & V_y & \delta \end{bmatrix}^T. \tag{8.30}$$

As the vehicle-trailer is a dynamic system, the history of the data should be considered for training/testing the network. As a result, a long short term memory neural network is considered as describe in the next subsection.

8.3.2 Long Short-Term Memory Structure

In conventional neural networks, there are only full connections between adjacent layers, but no connection among the nodes within the same layer. This type of network may fall into failure when dealing with the temporal–spatial problems. In Recurrent Neural Network (RNN), the feedback is from a hidden unit activation of last time step to current time step. The feedback connection gives RNN the ability to memorize the information of previous

inputs and to model the temporal contextual information as shown in Fig. 8.5. Although, RNNs can be trained in principle since it is provided with all the relevant information, it could be difficult due to the resulting long-term dependencies [211, 212] vanishing problem, and exploding gradients issues that occur when calculating back-propagation across long time steps. Therefore, to make an accurate state estimation, a long-term sequence is demanded.

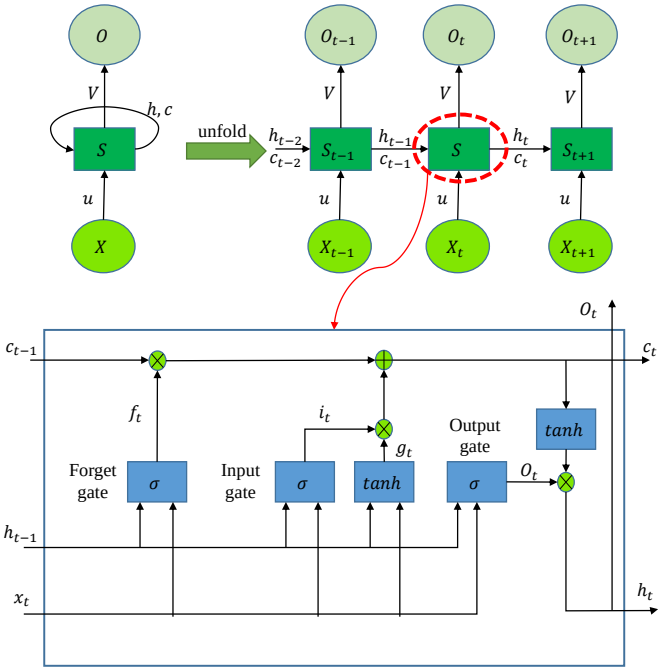

Figure 8.5: The LSTM structure with input/output gates.

Long Short-Term Memory (LSTM) network is a special kind of RNN with a unit of computation called memory cell, which replaces traditional nodes in the hidden layer of an RNN [213, 214]. By treating the hidden layer as a memory unit, LSTM network can cope with the correlation within time series in both short and long terms. The structure of the memory unit is shown in Fig. 8.5. As Fig. 8.5 illustrates, the memory cell in LSTM model is a composite unit that contains input gate layer, forget gate layer, update gate layer, and output gate layer. Each gate yields a state variable at time t as follows [215]:

$$
\begin{aligned}
i_t &= \sigma(w_{xi}x_t + w_{hi}h_{t-1} + b_i),\\
f_t &= \sigma(w_{xf}x_t + w_{hf}h_{t-1} + b_f),\\
o_t &= \sigma(w_{xo}x_t + w_{ho}h_{t-1} + b_o),\\
g_t &= tanh(w_{xc}x_t + w_{hc}h_{t-1} + b_c),\\
c_t &= f_t \odot c_{t-1} + i_t \odot g_t,\\
h_t &= O_t \odot tanh(c_t),
\end{aligned} \tag{8.31}
$$

where $\sigma(x) = \frac{1}{1+e^{-x}}$ is the sigmoid function; i_t, f_t, o_t, and g_t are input gate vector, forget gate vector, output gate vector, and state update vector, respectively; w_{xi}, w_{xf}, w_{xo}, w_{xc}, w_{hi}, w_{hf}, w_{ho}, w_{hc} are the weight vectors for linear combination; b_i, b_f, b_o, and b_c are the relative bias; $\odot$ is element-wise multiplication.

8.3.3 Data Set

To train and test the network both experimental and simulation test results are considered. A high-fidelity CarSim model is used to collect the data for almost 165 maneuvers for three different vehicles with different trailers attached to them as shown in Table. 8.1. For instance, 27 Single Lane Change (SLC) maneuvers are considered in CarSim including 7 tests on flat road and 7 tests on banked/graded roads with E-class-SUV, 7 tests on flat road and 6 tests on banked/graded roads with Pick-up truck.

Moreover, at each test, the trailer parameters including weight and geometrical parameters have been changed to collect sufficient data. The simulated vehicle-trailers are driven on the road with both grade and bank angles. As the vehicle with trailer drives over the simulated path, all the available information including vehicle/trailer responses and surrounding environment data such as the local road grade and bank angles are collected to be used as a ground truth for evaluating the estimation results.

For the experimental collected data, an electric Chevrolet Equinox AWD with a trailer shown in Fig. 4.6, has been used as the test vehicle-trailer systems. The specifications of the vehicle and the trailer are listed in Table. 4.1. The Equinox-trailer system is capable of collecting the required data for training/testing the designed LSTM and model-based estimator by having the required sensors including: 6-axis IMU, GPS, wheel speed sensor, torque measurement sensor, and potentiometer sensor. The longitudinal and lateral velocities/accelerations and roll/pitch/yaw rates of the vehicle and trailer are measured with a

Table 8.1: Test scenarios for road angle estimation

Simulation [CarSim]		Equinox test	
Maneuvers	Amount	Maneuvers	Amount
DLC	29	DLC	9
SLC	27	SLC	7
Sine	29	Sine	8
SS	14	SS	7
Random	13	Random	5
Full-turn	12	Full-turn	4

6-axis IMU (and GPS) system RT2000. The wheel speed and wheel torques which can be measured using the regular ABS wheel speed sensors, and electric actuators, respectively.

As the electric Equinox with trailer is driven on the test field which has both grade and bank angles, all the available sensory measurement data are collected to train the designed network. To compare the estimation results, the vehicle roll and pitch angles ground truth are obtained by the 6-axis IMU attached to the vehicle. For the ground truth road angle values, the GPS data right at each corners of the test field are collected and the test field bank and grade angles are calculated.

8.4 Simulation and Experiment Tests

In this section, the presented road angle estimation algorithms are validated by both simulation and experimental tests. Moreover, the performance of the designed observer and machine learning based algorithms in these tests are compared.

8.4.1 Model-Based Estimation Results

The model-based road angle estimator performance is examined by utilizing a CarSim model with the parameters listed in Table. 4.1. The simulations were conducted on road

settings with different slopes to evaluate the road angle estimation. The road angle estimation algorithm requires steering wheel angle, suspension deflection at each corner, hitch angle, and longitudinal/lateral velocities, which can be measured using the CAN bus, suspension height sensor, ultra-sonic sensors, and GPS units, respectively. The required variables can be estimated using various techniques in the literature, e.g. [110]. In the simulation presented next, the vehicle-trailer starts moving straight on a road with 20 degree grade angle with a constant speed of 40 km/h (CarSim longitudinal controller) for 15 seconds. The steering angle and longitudinal/lateral accelerations of the vehicle are shown in Fig. 8.6 for this test.

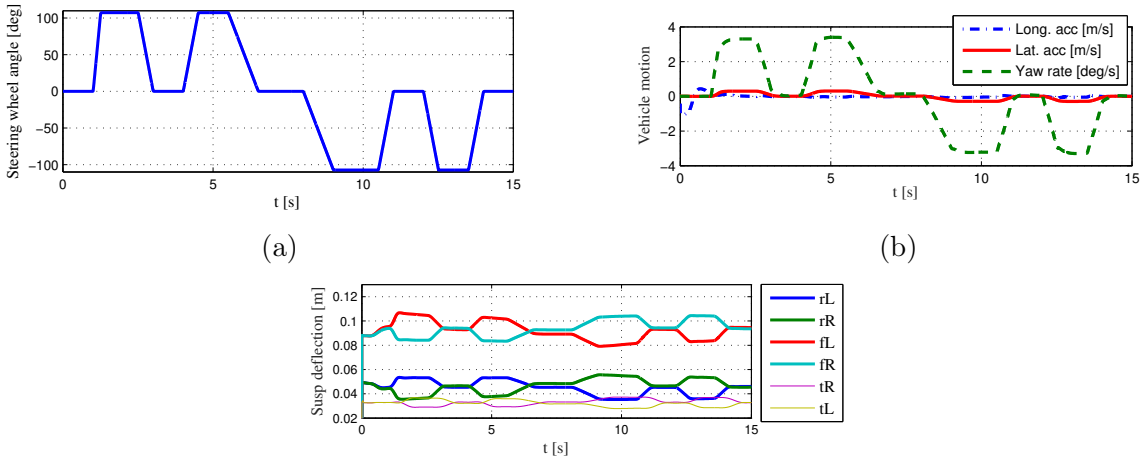

Figure 8.6: a) Steering wheel angle, b) Vehicle longitudinal/lateral accelerations, c) Vehicle-trailer suspension deflection, for multi-double-lane-change maneuvers on a road with 15% slope.

The algorithm runs in real-time and uses the measured/estimated data while the vehicle-trailer is running with constant velocity and the steering angle profile shown in Fig. 8.6. The simulation results for road angle estimation is shown in Fig. 8.7.

As can be seen in Fig. 8.6c, the suspension height sensors measure the vehicle and trailer suspension deflection at each corner and these data are used to estimate the vehicle roll and pitch angles as illustrated in Fig. 8.7b. By utilizing the corner suspensions deflections data and the estimated vehicle roll and pitch angle, the road slope is estimated. As Fig. 8.7c and Fig. 8.7d illustrate, the estimated road grade and bank angles have almost 9% errors out of

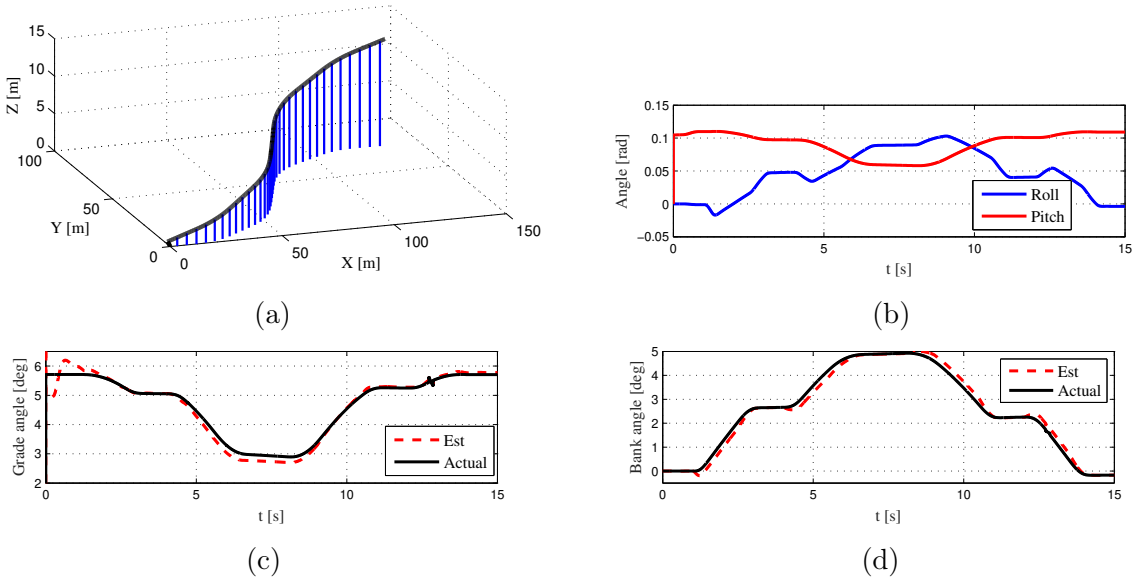

Figure 8.7: a) Vehicle-trailer simulated path, b) Vehicle-trailer roll and pitch angle, c) Road bank angle estimation results, d) Road grade angle estimation results for multi-double-lane-change maneuvers on a road with 7% slope.

the actual road grade/bank angles. Moreover, as the stability of the method is guaranteed mathematically, the results justify the convergence of the road angle estimation error as well for both grade and bank angles.

The algorithm is also tested on a road with varying slopes. In this test the vehicle-trailer follows the same speed and maneuver as used in the first simulation. The vehicle-trailer path, acceleration, and suspension height measurements are shown in Fig. 8.8.

As can be seen in Fig. 8.8, the road slope is estimated on a road with varying slopes by utilizing the corner suspension deflections data and the estimated vehicle roll and pitch angles. As Fig. 8.8d and Fig. 8.8e illustrate, the estimated road grade and bank angles have almost 10% errors with respect to the actual road angles. The algorithm performance is also tested for step-steer, double lane change, and random-steer maneuvers on a road with higher/lower grade and bank angles and the estimation NRMS are reported in Table. 8.2. It is worth mentioning that the same accuracy for small road angles that are reported in [204] is expected since the proposed model-based estimator is an extension of the road angle estimator presented in [204] for vehicle unit only.

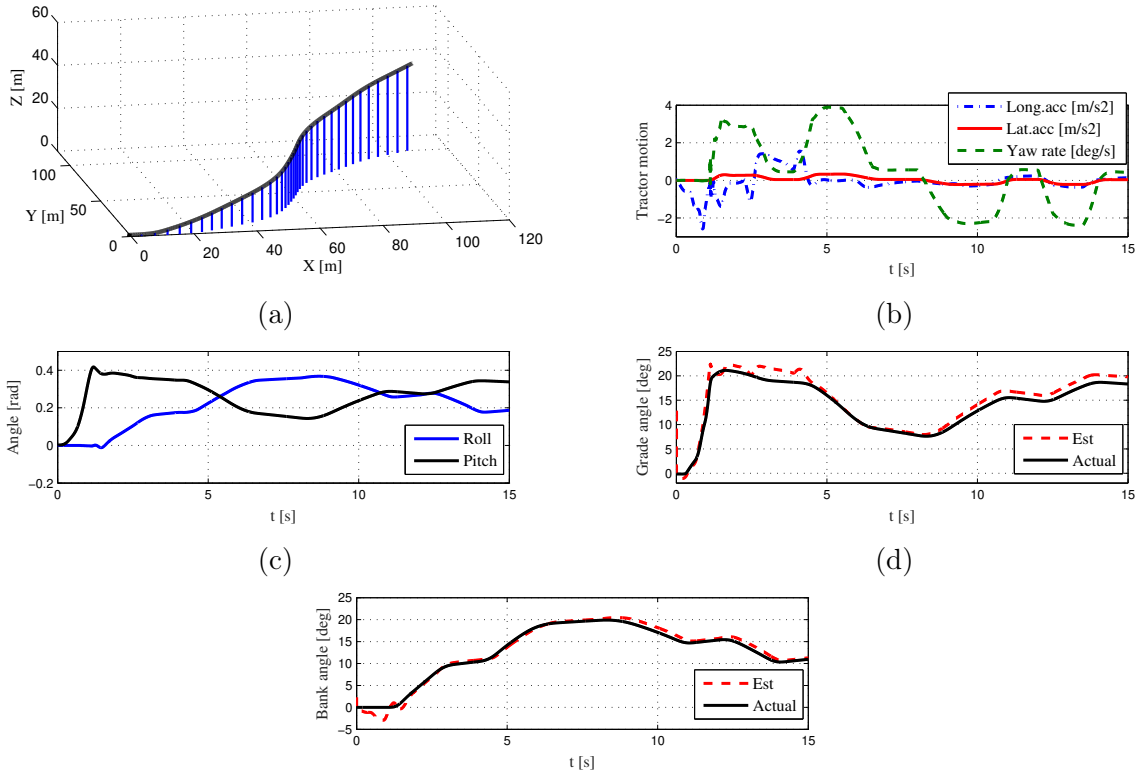

Figure 8.8: a) Vehicle-trailer simulated path, b) Vehicle-trailer roll and pitch angle, c) Road bank angle estimation results, d) Road grade angle estimation results for multi-double-lane-change maneuvers on a road with 20% slope.

8.4.2 ML-Based Estimation Results

As mentioned in Section 8.3, a recurrent neural network with long-short-term-memory cell is used to estimate the road grade/bank angles as well as the vehicle roll and pitch angles. An adaptive learning rate optimization algorithm called Adam optimizer is considered for training the network. By training the network with the data-set that contains both simulation and experimental test data, the road and vehicle angles are estimated by feeding the test data (unseen data) to the network described in Section 8.3. In average, the RNN takes three hours to train with an Intel Core i7 machine, a Nvidia GeForce 670 GPU, and 32 GB of RAM. However, it has a very fast running time and can be implemented for

real-time testing.

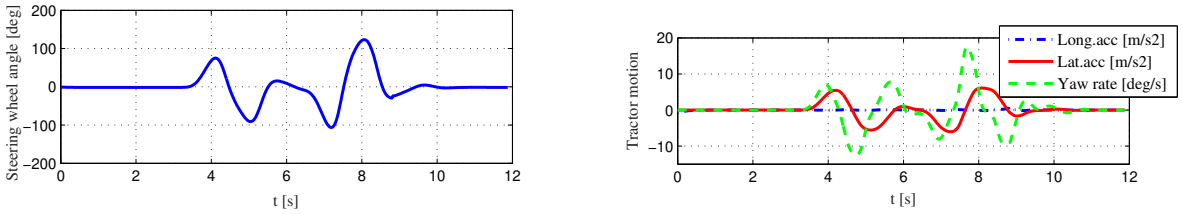

(a) (b)

Figure 8.9: a) Steering wheel angle b) Vehicle longitudinal/lateral accelerations, for a double-lane-change maneuvers on a road with 15% slope.

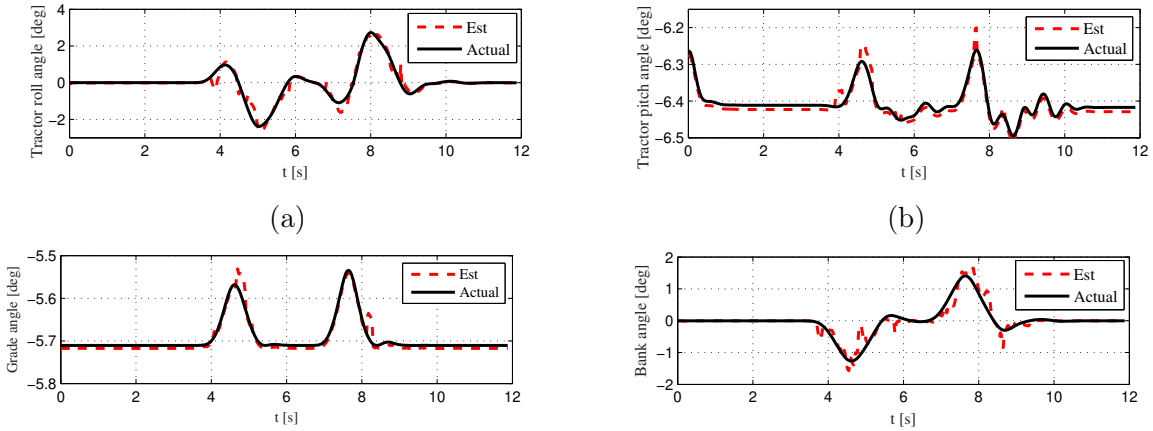

(a) (b)

(c) (d)

Figure 8.10: a) Vehicle-trailer simulated path, b) Vehicle-trailer roll and pitch angle, c) Road bank angle estimation results, d) Road grade angle estimation results for a double-lane-change maneuvers on a road with 15% slope.

To investigate the performance of the designed RNN based road angle estimator, a double lane change maneuver is considered as illustrated in Fig. 8.9. The vehicle roll/pitch angles as well as the road grade and bank angle estimations are shown in Fig. 8.10. As can be seen in Fig. 8.10, the NRMS of the road angle estimation error is 8%, which is almost the same with the model-based estimation NRMS. Moreover, the NRMS of the pitch/roll angle estimations error is 6.4 percent errors, which means the ML based algorithm can

estimate the roll and pitch angles with the same accuracy that model-based estimator has. This happens because the input measurement signals contain signals related to the vehicle body and can address the vehicle motion more precisely whereas the road angles have less impact on the vehicle dynamic.

The comparison between the designed model-based and RNN estimators for the road angles is investigated in the discussion section. The algorithms have been tested for a step-steer, double lane change, and random steer maneuvers and the results are reported in Table. 8.2.

8.5 Discussions

The estimated road angle results illustrate that both model-based and RNN approaches are capable of estimating road angles; however, their performances differ. Due to the fact that the RNN inputs are designed based on the vehicle-trailer roll and pitch dynamic models, the designed network is a pre-existed function estimator between the measured inputs to the outputs.

To compare the performance of the model-based and RNN road angle estimators, a maneuver involving a random steering, has been considered. The test runs for 25 seconds. The estimation errors for both RNN and model-based approaches are reported in Table. 8.2.

As can be seen in Table. 8.2, the NRMS error of RNN is less than the model-based estimator. This is because the error convergence rate in RNN method is much higher than that for the model-based approach. In fact, there is no settling time for the RNN method since its output is calculated by multiplying the predefined weights by the inputs.

The model-based estimator error increases for harsh maneuvers since the linearity assumptions are violated. However, if the training data-set is rich enough and contains adequate data for hash maneuvers, the estimation error for the RNN based estimator will not increase as the network is trained for harsh maneuvers as well. The road angle estimation results show that the RNN algorithm is generic and, if the vehicle specifications change, the algorithm can still estimate the road angle since the vehicle parameters, including the vehicle mass, wheel-base, and CG height, are considered in the input vector. Therefore, the algorithm can estimate the road angle properly.

Table 8.2: NRMS of the errors for the road angle estimators at dry and wet roads.

Estimated force	@ u_1=25 km/h [%]	@ u_1=35 km/h [%]	@ u_1=45 km/h [%]	@ u_1=55 km/h [%]
Dry road				
UIO	3.51	3.34	3.49	4.11
RNN-LSTM	5.91	6.55	8.88	9.09
Wet road				
UIO	3.51	3.3	3.5	4.21
RNN-LSTM	6.01	6.68	9.21	9.5

The simulation was run for both dry and wet roads, and the NRMS of the error for road angle estimation is shown in Table. 8.2. As Table. 8.2 illustrates, the maximum error percentage with respect to different longitudinal velocities is less than 9.5%. The road angle estimation errors may have several resources, and the most possible one is the lack of an accurate system model. For instance, the vehicle-trailer roll and pitch dynamic models have more degrees of freedom than considered in the presented vehicle-trailer model. Moreover, as mentioned in Section 8.3, the spring and damper coefficients in both roll and pitch dynamic models have been obtained by simulation/experiment tests, which may cause the errors and decrease the accuracy.

The error of RNN method could further decrease if the network were trained with a more-comprehensive data-set with more vehicle-trailer configuration information. In this research, three different types of vehicle have been considered in the data-set used to train and test the network. There is no doubt that increasing the accuracy of the method requires more data with different types of vehicles and trailers.

8.6 Conclusions

In this chapter, two approaches have been introduced to estimate road angle: model-based and machine learning approaches. For model-based approach, we have proposed

a road angle estimation methodology that includes an unknown input observer for the roll and pitch dynamics of the vehicle with trailer. Observer gain matrices were designed to guarantee a fast convergence rate by system pole placement. Road disturbances and outliers were isolated in the proposed method through the use of a dynamic threshold based on the longitudinal and lateral excitations of the vehicle. Fast convergence and robustness against harsh excitations, road disturbances, and outliers are among the advantages of the proposed methodology. The test results for the model-based road angle estimator reported almost 11% errors.

Moreover, it has been shown that the ML-based approach has high potential for the road angle estimation and is applicable for vehicle-trailers with different configurations since its inputs were designed based on the vehicle-trailer roll/pitch dynamic models and normalized by the vehicle wheel-base, mass, and CG height. Thus, re-training of the network is not needed for different towing vehicles. Moreover, since the vehicle roll/pitch angles are coupled with the road angles, to be able to differentiate between these angles, the vehicle roll and pitch angles are also considered as the outputs of the network. Thus, with supervised training, the RNN is trained to differentiate between them. The maximum error percentage for the ML-based road angle estimator was 8%.

A comparison of the performances of the developed unknown input observer and the machine learning based estimator supports the following conclusions:

- Both the proposed model and non-model-based algorithms can estimate road angles in various driving conditions.
- Neither the model-based nor the non-model-based approach requires any information about the road friction, tire forces, and tire parameters, a promising finding that confirms that the algorithms can perform reliably for different road conditions.

The simulation results demonstrate that the road angle estimation error is not affected as road friction changes. Improving the ML-based estimator will need more experimental data for training and testing.

Chapter 9

Conclusion and Future Works

9.1 Conclusions

The main objective of this research was to design real-time state and parameter estimation algorithms for vehicle-trailer systems. To make the estimation algorithm practical and implementable on most of the vehicle-trailer systems, a design for estimating trailer parameters and states was proposed using common sensors available in vehicle-trailer systems.

In the design of the estimators, it was shown that adding a non-linear tire model to improve the fidelity of the model could improve the estimation accuracy. By considering the LuGre tire model in the vehicle-trailer model, the system model became non-linear, which was shown how to separate the linear and nonlinear parts. Based on the proposed model, solutions for estimating the states and parameters of an unknown trailer were developed.

One of the main challenges for estimating vehicle-trailer parameters/states was changing the trailer parameters such as mass due to the payload during the operation. To tackle this challenge, two approaches were introduced to estimate trailer mass: dynamic system model-based and machine learning approaches. In the design of the estimators, it was shown that the stability of the dynamic system model-based estimation algorithm was guaranteed mathematically, and the test results indicated the convergence of the trailer mass estimation error with the accuracy of almost 12% . Moreover, it has been shown that the ML-based approach has high potential for trailer mass estimation and is applicable

for vehicle-trailers with different configurations since its inputs were designed based on the vehicle-trailer dynamic models. It has been shown that how selecting and normalizing the input feature is important. As the inputs of the DNN contain the vehicle parameters, including the vehicle mass, tire sizes, and geometry, it has been shown that the designed DNN can be used for any towing vehicle with different specifications. The maximum error percentage for the DNN based trailer mass estimator was 10%.

Given that the hitch angle has an important role in vehicle-trailer states/parameters estimation as it relates the vehicle's states that most of them are measurable with the trailer states, a complete and comprehensive solution for hitch angle estimation of a towing vehicle with a ball type trailer with a flat or symmetric V-nose frontal face was developed, evaluated, and experimentally tested in this thesis. In the design of hitch angle estimator, first the direct calculation of hitch angle based on ultra-sonic sensors was considered. Due to the ultra-sonic sensors failure in severe weather conditions, kinematics and dynamics of the vehicle-trailer were then used to develop algorithms for the hitch angle estimation. Given that the kinematics and dynamics of the vehicle-trailer were dependent of trailer axle location, mass, and front face angle, their estimated values were used in the proposed hitch angle estimation algorithm to make the algorithm independent of trailer's geometry.

The proposed vehicle-trailer dynamic model in Chapter 3 was utilized to estimate the longitudinal/lateral hitch-forces and lateral tire forces. To make the estimation algorithm generic, the presented model was derived in a way that it can address the hitch-forces and lateral tire forces without any priori information require from the trailer. Although trailer mass estimation is available, it was shown that the presented hitch-forces algorithm was independent of trailer mass and geometry, and can estimate the hitch-forces for any ball type trailers. Uncertainties of the model were studied and the proposed observer was utilized to estimate the states of the system, and the stability of the proposed model-based estimator was investigated. In the design, it has been shown that the estimation error was converged, as the system was observable and the system matrices were bounded. Moreover, it has been shown that the presented algorithm was capable of estimating the hitch-forces and lateral tire forces on dry, wet, and icy roads as the selected measurement signals were able to address the effect of road surfaces on the model.

Given the vehicle-trailer dynamic models introduced in the third chapter, the vehicle-trailer lateral dynamics with the pure-slip LuGre tire model was expressed in an LPV system, which is practical for the control/estimation applications for mitigating the effect of

non-linear terms. In the design, it has been shown that how much important the nonlinear part is. Then, the proposed vehicle-trailer model was used to estimate the lateral velocity of the vehicle. To make the estimation algorithm generic, the presented model was derived in a way that it can address both small and large slip angles. Moreover, the stability of the lateral velocity estimation error dynamic model was investigated using an affine quadratic stability approach.

Additionally, an unknown input observer and ML-based approaches were designed to estimate the road grade and bank angles based on the roll and pitch dynamics of the vehicle-trailer system. In the design, observer gain matrices were designed to guarantee a fast convergence rate by system pole placement. Road disturbances and outliers were isolated in the provided method through the use of a dynamic threshold based on the longitudinal and lateral excitations of the vehicle. It has been shown that the ML-based approach has high potential for road angle estimation and is applicable for vehicle-trailers with different configurations since its inputs were designed based on vehicle-trailer roll/pitch dynamic models and normalized by the vehicle wheel-base, mass, and CG height. Thus, re-training of the network is not needed for different towing vehicles. The maximum error percentage for the ML-based road angle estimator was 8%, which was almost the same with the model-based estimator error.

To conclude, seven estimation algorithms have been developed in this thesis to estimate the trailer parameters including, trailer mass, axle location, frontal face angle, hitch angles, hitch forces, tire forces, lateral velocity, and road angles. To estimate the mentioned parameters and states both model-based and non-model-based approaches have been considered.

9.2 Future Works

Suggestions are made in this section are for potential future works to enhance the accuracy of the developed vehicle-trailer state and parameter estimators.

More accurate models for vehicle-trailers: The accuracy of the proposed lateral velocity, trailer mass, hitch forces, hitch angle, and road angles estimation approaches can be enhanced by employing a general chassis model and more precise vehicle dynamic model with higher degrees of freedom. The main purpose of such model is to estimate vehicle/trailer parameters and states more accurately with implementation of an integrated

parameter/state observers to overcome estimation errors due to uncertainties in the model and road conditions. The mentioned methodology provides a better modeling of the vehicle/trailer behaviours by considering a vehicle/trailer model close to the actual behaviour. However, this will increase the computational cost of the state estimators.

Moreover, in order to design a reliable tire force estimator to address demanding cases with combined longitudinal and lateral excitations, a precise vehicle model is needed. Specifically, the imprecision of the vehicle dynamics can be rooted in an inaccurate tire forces due to not considering the camber angle at each corner. The current corner-based lateral velocity estimation does not include the camber angle effect, but the tire forces and consequently the vehicle's planar and roll dynamics are indeed affected by the camber angle at each corner. Therefore, incorporation of the tires' camber angles into the vehicle planar kinetics can result in better performance of the current lateral velocity and force estimators.

Improve the model of the unknown input observer for combined bank and grade cases: Road-body kinematics has been investigated in this thesis to increase the accuracy of the measurement in the road angle estimator by defining the correlation between the road angle rates and the pitch/roll rates of the vehicle-trailer system. However, there are some errors for the combined bank and grade cases which stems from separated vehicle roll and pitch dynamics in the observer model. Therefore, considering the coupled roll and pitch dynamics in the unknown input observer structure can improve the accuracy of the estimator.

Moreover, tire forces and the vehicle-trailer lateral/longitudinal dynamics have not been integrated into the roll/pitch dynamics for the bank/grade angle estimations because of unavailability of road friction information. Employing road classification data in the tire forces and the expected vehicle-trailer responses facilitates estimation of the road angles. This is because of distinguishing between the measured accelerations due to road angles and the ones due to the vehicle kinematics in various maneuvers. Consequently, by including tire forces, which are obtained from road friction information, the road angles can be estimated more accurately.

The closed-form lateral dynamics with combined-slip model for the stability controllers: The suggested general forms of the vehicle-trailer lateral models in Section 3.2 provide a framework to achieve analytical solutions for vehicle-trailer's optimal stability control problems. This has a significant advantage over the cascaded methods that need

slip ratio/angles to overcome with the forces and then to calculate vehicle-trailer states by solving lateral dynamics and tire forces. This is more pronounced for designing stability controllers in vehicle-trailer configuration to handle harsh maneuvers, over-steering characteristics of the vehicle-trailer, and several high-slip cases.

Using hybrid estimators for vehicle-trailer states/parameters: Vehicle/Trailer parameters such as mass, moment of inertia, and CG location are not fixed and can change in any vehicle-trailer system. Therefore, the designed estimator needs to actively estimate these parameters. To estimate the vehicle/trailer states and parameters both model-based and non-model-based techniques can be considered. Such hybrid methods are gaining tractions in the academia and industry. Hybrid methods are built upon understandings of the nature of the system, and the network needs to be constructed in a way that captures the physical principles without significantly increase the network complexity and thus causes much slower training. For instant, a model-based technique has been used to estimate the hitch angle (Chapter 5). The proposed algorithm was required the trailer mass. In this thesis, ML-based algorithms have been used to estimate the trailer mass and road angles (Chapters 4 and 8). Now, a hybrid method can be designed to combine these two algorithms together.

References

[1] Ashley Wettlaufer, Roxana O Florica, Mark Asbridge, Douglas Beirness, Jeffrey Brubacher, Russell Callaghan, Benedikt Fischer, Gerrit Gmel, Sameer Imtiaz, Robert E Mann, and A McKiernan. Estimating the harms and costs of cannabis-attributable collisions in the canadian provinces. *Drug and Alcohol Dependence*, 173:185–190, 2017.

[2] M Bouteldja, A Koita, V Dolcemascolo, and JC Cadiou. Prediction and detection of jackknifing problems for tractor semi-trailer. *IEEE Vehicle Power and Propulsion Conference*, pages 1–6, 2006.

[3] Xuejun Ding, Steve Mikaric, and Yuping He. Design of an active trailer-steering system for multi-trailer articulated heavy vehicles using real-time simulations. *Proceedings of the Institution of Mechanical Engineers, Part D: Journal of Automobile Engineering*, 227(5):643–655, 2013.

[4] Hocine Imine, Leonid M Fridman, and Tarek Madani. Steering control for rollover avoidance of heavy vehicles. *IEEE Transactions on Vehicular Technology*, 61(8):3499–3509, 2012.

[5] Mohammad Manjurul Islam, Leo Laine, and Bengt Jacobson. Inverse model control including actuator dynamics for active dolly steering in high capacity transport vehicle. *IEEE Intelligent Vehicles Symposium (IV)*, pages 1024–1031, 2015.

[6] Reza Hajiloo, Mehdi Abroshan, Amir Khajepour, Alireza Kasaiezadeh, and Shih-Ken Chen. Integrated steering and differential braking for emergency collision avoidance in autonomous vehicles. *IEEE Transactions on Intelligent Transportation Systems*, 2020.

[7] Karel Kural, Pavlos Hatzidimitris, Nathan van de Wouw, Igo Besselink, and Henk Nijmeijer. Active trailer steering control for high-capacity vehicle combinations. *IEEE Transactions on Intelligent Vehicles*, 2(4):251–265, 2017.

[8] Sina Milani, Y Samim Ünlüsoy, Hormoz Marzbani, and Reza N Jazar. Semitrailer steering control for improved articulated vehicle manoeuvrability and stability. *Nonlinear Engineering*, 8(1):568–581, 2019.

[9] Kaiqiang Pan, Hongyu Zheng, and Jianjun Wu. Research on the control strategy of trailer tracking tractor for articulated heavy vehicles. *SAE Technical Paper*, 2019.

[10] Mattia Zanchetta, Davide Tavernini, Aldo Sorniotti, Patrick Gruber, Basilio Lenzo, Antonella Ferrara, Koen Sannen, Jasper De Smet, and Wouter De Nijs. Trailer control through vehicle yaw moment control: Theoretical analysis and experimental assessment. *Mechatronics*, 64:102282, 2019.

[11] Haiping Du and Nong Zhang. Designing h_∞/gh_2 static-output feedback controller for vehicle suspensions using linear matrix inequalities and genetic algorithms. *Vehicle System Dynamics*, 46(5):385–412, 2008.

[12] Zongyu Liu, Hongyu Zheng, and Wenkai Xu. A model-based mass estimation and optimal braking force distribution algorithm of tractor and semi-trailer combination. *SAE Technical Paper*, 2013.

[13] Selim Solmaz, Mehmet Akar, and Robert Shorten. Online center of gravity estimation in automotive vehicles using multiple models and switching. *9th International Conference on Control, Automation, Robotics and Vision*, pages 1–7, 2006.

[14] King Tin Leung, James F Whidborne, David Purdy, and Phil Barber. Road vehicle state estimation using low-cost gps/ins. *Mechanical Systems and Signal Processing*, 25(6):1988–2004, 2011.

[15] John Limroth. Real-time vehicle parameter estimation and adaptive stability control. 2009.

[16] Hassan Shraim, Mustapha Ouladsine, Leonid Fridman, and Monica Romero. Vehicle parameter estimation and stability enhancement using sliding modes techniques. *International Journal of Vehicle Design*, 48(3-4):230–254, 2008.

[17] LK Chen and YA Shieh. Jackknife prevention for articulated vehicles using model reference adaptive control. *Proceedings of the Institution of Mechanical Engineers, Part D: Journal of Automobile Engineering*, 225(1):28–42, 2011.

[18] SJ Raftery, JAL Grigo, and Jeremy Edward Woolley. *Heavy vehicle road safety: Research scan*. Number CASR100. Centre for Automotive Safety Research, University of Adelaide, 2011.

[19] Junmin Wang and Ming-Feng Hsieh. Vehicle yaw-inertia-and mass-independent adaptive steering control. *Proceedings of the Institution of Mechanical Engineers, Part D: Journal of Automobile Engineering*, 223(9):1101–1108, 2009.

[20] Liang Chu, Yong Fang, Mingli Shang, Jianhua Guo, and Feikun Zhou. Estimation of articulation angle for tractor semi-trailer based on state observer. *International Conference on Measuring Technology and Mechatronics Automation*, 2:158–163, 2010.

[21] H Yuan and H Zhu. Anti-jackknife reverse tracking control of articulated vehicles in the presence of actuator saturation. *Vehicle System Dynamics*, 54(10):1428–1447, 2016.

[22] Thaker Nayl, George Nikolakopoulos, and Thomas Gustafsson. A full error dynamics switching modeling and control scheme for an articulated vehicle. *International Journal of Control, Automation and Systems*, 13(5):1221–1232, 2015.

[23] Thaker Nayl, George Nikolakopoulos, and Thomas Gustfsson. Switching model predictive control for an articulated vehicle under varying slip angle. *20th Mediterranean Conference on Control & Automation (MED)*, pages 890–895, 2012.

[24] Youngshik Kim. Investigation of parameter estimation of a car-trailer system using condition numbers. *International Journal of Software Engineering and Its Applications*, 8(5):231–242, 2014.

[25] Christian Lundquist, Wolfgang Reinelt, and Olof Enqvist. Back driving assistant for passenger cars with trailer. *SAE Technical Paper*, 2006.

[26] Moritz Werling, Philipp Reinisch, Michael Heidingsfeld, and Klaus Gresser. Reversing the general one-trailer system: Asymptotic curvature stabilization and path

tracking. *IEEE Transactions on Intelligent Transportation Systems*, 15(2):627–636, 2013.

[27] Li Xu, Eric Tseng, Thomas Pilutti, and Steven Schondorf. Yaw rate based trailer hitch angle estimation for trailer backup assist. *SAE Technical Paper*, 2017.

[28] Ashok Dahal, Jakir Hossen, Chennupati Sumanth, Ganesh Sistu, Kazumi Malhan, Muhammad Amasha, and Senthil Yogamani. Deeptrailerassist: Deep learning based trailer detection, tracking and articulation angle estimation on automotive rear-view camera. *Proceedings of the IEEE International Conference on Computer Vision Workshops*, pages 1–8, 2019.

[29] Christopher de Saxe and David Cebon. Measurement of articulation angle by image template matching. *Proceedings of the Institution of Mechanical Engineers, Part D: Journal of Automobile Engineering*, 233(14):3801–3815, 2019.

[30] Connor Fry Sykora. Trailer sway control using an active hitch. Master's thesis, University of Waterloo, 2017.

[31] Zheng Hu and Erick Michael Lavoie. Multi-stage solution for trailer hitch angle initialization, November 28 2017. US Patent 9,827,818.

[32] Seungki Kim, J Yang, and Kun Soo Huh. Articulation angle estimation and control for reversing articulated vehicles. *13th International Symposium on Advanced Vehicle Control*, pages 533–540, 2017.

[33] Kunle Olutomilayo and Daniel R Fuhrmann. Estimation of trailer-vehicle articulation angle using 2d point-cloud data. *IEEE Radar Conference*, pages 1–6, 2019.

[34] Zygimantas Ziaukas, Mark Wielitzka, Tobias Ortmaier, and Jan-Philipp Kobler. Simultaneous estimation of steering and articulation angle in a truck-semitrailer combination solely based on trailer signals. *American Control Conference (ACC)*, pages 2509–2514, 2019.

[35] Christopher de Saxe and David Cebon. A visual template-matching method for articulation angle measurement. *IEEE 18th International Conference on Intelligent Transportation Systems*, pages 626–631, 2015.

[36] C Fuchs, F Neuhaus, and D Paulus. 3d pose estimation for articulated vehicles using kalman-filter based tracking. *Pattern Recognition and Image Analysis*, 26(1):109–113, 2016.

[37] Christian Fuchs, Benjamin Knopp, Dieter Zöbel, and Dietrich Paulus. Model-based evaluation of practical sensor noise impacts in articulated vehicle driving scenarios. *IEEE Intelligent Vehicles Symposium (IV)*, pages 577–582, 2017.

[38] Zhe Leng and Mark A Minor. Curvature-based ground vehicle control of trailer path following considering sideslip and limited steering actuation. *IEEE Transactions on Intelligent Transportation Systems*, 18(2):332–348, 2016.

[39] Vejlupek Josef. Trailer backing-up assistant using ultrasound sensors based control units to safely back-up the car with trailer. *17th International Conference on Mechatronics-Mechatronika (ME)*, pages 1–6, 2016.

[40] Sepehr Pourrezaei Khaligh, Akram M Abdel-Rahman, Anston Emmanuel, and Grant L Meade. System and method for determining a hitch angle based on an input from a sensor and a kinematic model of a vehicle and a trailer, and for controlling the vehicle based on the hitch angle, January 8 2019. US Patent 10,173,722.

[41] Amin Habibnejad Korayem, Alireza Pazooki, Laleh Durali, Amir Khajepour, Baris Fidan, Anushya Viraliur Ponnuswami, and Sepehr Pourrezaei Khaligh. Hitch angle estimation of a towing vehicle with arbitrary configuration. *IEEE Transactions on intelligent transportation systems*, 2021.

[42] Ulf Larsson, Caj Zell, Kalevi Hyyppa, and Ake Wernersson. Navigating an articulated vehicle and reversing with a trailer. *IEEE International Conference on Robotics and Automation*, pages 2398–2404, 1994.

[43] Jong-Hwa Yoon and Huei Peng. Robust vehicle sideslip angle estimation through a disturbance rejection filter that integrates a magnetometer with gps. *IEEE Transactions on Intelligent Transportation Systems*, 15(1):191–204, 2013.

[44] Giseo Park, Seibum B Choi, Dongyoon Hyun, and Jounghee Lee. Integrated observer approach using in-vehicle sensors and gps for vehicle state estimation. *Mechatronics*, 50:134–147, 2018.

[45] Mark Wielitzka, Alexander Busch, Matthias Dagen, Tobias Ortmaier, and G Serra. Unscented kalman filter for state and parameter estimation in vehicle dynamics. pages 56–75. InTech, 2018.

[46] Lars Imsland, Tor A Johansen, Thor I Fossen, HåVard FjæR Grip, Jens C Kalkkuhl, and Avshalom Suissa. Vehicle velocity estimation using nonlinear observers. *Automatica*, 42(12):2091–2103, 2006.

[47] Jiwon J Oh and Seibum B Choi. Vehicle velocity observer design using 6-d imu and multiple-observer approach. *IEEE Transactions on Intelligent Transportation Systems*, 13(4):1865–1879, 2012.

[48] Chinar Ghike and Taehyun Shim. 14 degree-of-freedom vehicle model for roll dynamics study. *SAE Technical Paper*, 2006.

[49] Yubiao Zhang, Amir Khajepour, and Mansour Ataei. A universal and reconfigurable stability control methodology for articulated vehicles with any configurations. *IEEE Transactions on Vehicular Technology*, 2020.

[50] Naser Esmaeili, Reza Kazemi, and Hamed Tabatabaei. Design of a new integrated controller (braking and steering) to maintain the stability of a long articulated vehicle. *Proceedings of the Institution of Mechanical Engineers, Part C: Journal of Mechanical Engineering Science*, 234(5):981–1013, 2020.

[51] Alexander A Brown and Sean N Brennan. Lateral vehicle state and environment estimation using temporally previewed mapped lane features. *IEEE Transactions on Intelligent Transportation Systems*, 16(3):1601–1608, 2014.

[52] Ehsan Mohammadbagher, Neel P Bhatt, Ehsan Hashemi, Baris Fidan, and Amir Khajepour. Real-time pedestrian localization and state estimation using moving horizon estimation. In *2020 IEEE 23rd International Conference on Intelligent Transportation Systems (ITSC)*, pages 1–7. IEEE, 2020.

[53] Amin Habibnejad Korayem, Shahab Kazemi, and Saeed Rafee Nekoo. Sub-optimal sliding mode control on a cooperative manipulator using stereo vision machine feedback. In *2017 5th RSI International Conference on Robotics and Mechatronics (ICRoM)*, pages 15–20. IEEE, 2017.

[54] Lghani Menhour, Brigitte d'Andréa Novel, Michel Fliess, Dominique Gruyer, and Hugues Mounier. An efficient model-free setting for longitudinal and lateral vehicle control: Validation through the interconnected pro-sivic/rtmaps prototyping platform. *IEEE Transactions on Intelligent Transportation Systems*, 19(2):461–475, 2017.

[55] R Hajiloo, M Shahrokhi, and H Salarieh. Adaptive delayed feedback chaos control of a class of uncertain chaotic systems subject to external disturbance. *Iranian Journal of Science and Technology, Transactions of Mechanical Engineering*, 43(1):517–525, 2019.

[56] H Kaveh, H Salarieh, and R Hajiloo. On the control of unknown continuous time chaotic systems by applying takens embedding theory. *Chaos, Solitons & Fractals*, 109:53–57, 2018.

[57] R Hajiloo, H Salarieh, and A Alasty. Chaos control in delayed phase space constructed by the takens embedding theory. *Communications in Nonlinear Science and Numerical Simulation*, 54:453–465, 2018.

[58] Mir Saman Rahimi Mousavi and Benoit Boulet. Estimation of the state variables and unknown input of a two-speed electric vehicle driveline using fading-memory kalman filter. *IEEE Transactions on Transportation Electrification*, 2(2):210–220, 2016.

[59] Hui Zhang, Guoguang Zhang, and Junmin Wang. Sideslip angle estimation of an electric ground vehicle via finite-frequency $\mathcal{H}_\infty$ approach. *IEEE Transactions on Transportation Electrification*, 2(2):200–209, 2015.

[60] Yubiao Zhang, Amir Khajepour, Ehsan Hashemi, Yechen Qin, and Yanjun Huang. Reconfigurable model predictive control for articulated vehicle stability with experimental validation. *IEEE Transactions on Transportation Electrification*, 2020.

[61] Caizhen Cheng and David Cebon. Parameter and state estimation for articulated heavy vehicles. *Vehicle System Dynamics*, 49(1-2):399–418, 2011.

[62] Laura Ryan Ray. Nonlinear state and tire force estimation for advanced vehicle control. *IEEE Transactions on Control Systems Technology*, 3(1):117–124, 1995.

[63] Omar Khemoudj, Hocine Imine, and Mohamed Djemai. Robust observation of tractor-trailer vertical forces using inverse model and exact differentiator. *SAE International Journal of Materials and Manufacturing*, 3(1):278–289, 2010.

[64] Omar khemoudj, Hocine Imine, and Mohamed Djemai. Heavy duty vehicle tyre forces estimation using variable gain sliding mode observer. *International Journal of Vehicle Design*, 62(2-4):274–288, 2013.

[65] Amin Habibnejad Korayem, Amir Khajepour, and Baris Fidan. Estimation of tractor-trailer hitch-forces and lateral tire forces independent of trailer type and geometry. *Submitted*.

[66] CB Winkler, RD Ervin, and MR Hagan. On-board estimation of the rollover threshold of tractor semitrailers. *Vehicle System Dynamics*, 33(sup1):540–551, 1999.

[67] Evan Gartley and David M Bevly. Online estimation of implement dynamics for adaptive steering control of farm tractors. *IEEE/ASME Transactions on Mechatronics*, 13(4):429–440, 2008.

[68] Aleksander Hac, Daniel Fulk, and Hsien Chen. Stability and control considerations of vehicle-trailer combination. *SAE International Journal of Passenger Cars-Mechanical Systems*, 1(2008-01-1228):925–937, 2008.

[69] Ehsan Hashemi, Alireza Kasaiezadeh, Amir Khajepour, Nikolai Moshchuk, and Shih-Ken Chen. Robust estimation and experimental evaluation of longitudinal friction forces in ground vehicles. *ASME International Mechanical Engineering Congress and Exposition*, 2014.

[70] Shouyang Wei, Yuan Zou, Xudong Zhang, Tao Zhang, and Xiaoliang Li. An integrated longitudinal and lateral vehicle following control system with radar and vehicle-to-vehicle communication. *IEEE Transactions on Vehicular Technology*, 68(2):1116–1127, 2019.

[71] HB Pacejka and IJM Besselink. Magic formula tyre model with transient properties. *Vehicle System Dynamics*, 27(S1):234–249, 1997.

[72] Carlos Canudas-de Wit, Panagiotis Tsiotras, Efstathios Velenis, Michel Basset, and Gerard Gissinger. Dynamic friction models for road/tire longitudinal interaction. *Vehicle System Dynamics*, 39(3):189–226, 2003.

[73] Efstathios Velenis, Panagiotis Tsiotras, Carlos Canudas-De-Wit, and Michel Sorine. Dynamic tyre friction models for combined longitudinal and lateral vehicle motion. *Vehicle System Dynamics*, 43(1):3–29, 2005.

[74] M Bouteldja, A El Hadri, JC Cadiou, and V Dolcemascolo. Application of a non-linear sliding mode observer for truck tyre forces estimation. *International Journal of Vehicle Systems Modelling and Testing*, 2(1):16–37, 2007.

[75] Hocine Imine and Vittorio Dolcemascolo. Sliding mode observers to heavy vehicle vertical forces estimation. *International Journal of Heavy Vehicle Systems*, 15(1):53–64, 2008.

[76] N M'Sirdi, A Boubezoul, A Rabhi, and L Fridman. Sliding modes observers for estimation of performance of heavy vehicles. 2007.

[77] Paul M Siegrist. A methodology for monitoring tyre-forces on off-highway mining trucks. 2004.

[78] Marco Viehweger, Cyrano Vaseur, Sebastiaan van Aalst, Manuel Acosta, Enrico Regolin, Angel Alatorre, Wim Desmet, Frank Naets, Valentin Ivanov, Antonella Ferrara, et al. Vehicle state and tyre force estimation: demonstrations and guidelines. *Vehicle System Dynamics*, pages 1–28, 2020.

[79] Yizhai Zhang, Jingang Yi, and Tao Liu. Embedded flexible force sensor for in-situ tire–road interaction measurements. *IEEE Sensors Journal*, 13(5):1756–1765, 2013.

[80] Lloyd E Davis and Jonathan M Bunker. *Suspension testing of 3 heavy vehicles–methodology and preliminary frequency analysis*. State of Queensland (Department of Main Roads) & Queensland University, 2008.

[81] David M Bevly, Jihan Ryu, and J Christian Gerdes. Integrating ins sensors with gps measurements for continuous estimation of vehicle sideslip, roll, and tire cornering stiffness. *IEEE Transactions on Intelligent Transportation Systems*, 7(4):483–493, 2006.

[82] Zeyu Ma, Yunqing Zhang, and James Yang. Velocity and normal tyre force estimation for heavy trucks based on vehicle dynamic simulation considering the road slope angle. *Vehicle System Dynamics*, 54(2):137–167, 2016.

[83] Hamze Ahmadi Jeyed and Ali Ghaffari. Nonlinear estimator design based on extended kalman filter approach for state estimation of articulated heavy vehicle. *Proceedings of the Institution of Mechanical Engineers, Part K: Journal of Multi-body Dynamics*, 233(2):254–265, 2019.

[84] Omar Khemoudj, Hocine Imine, Mohamed Djemai, and L Fridman. Variable gain sliding mode observer for heavy duty vehicle tyre forces estimation. *11th International Workshop on Variable Structure Systems (VSS)*, pages 522–527, 2010.

[85] Yiming Li, Qin Shi, and Duoyang Qiu. Parameter identification of tractor-semitrailer model under steering and braking. *Mathematical Problems in Engineering*, 2019.

[86] M Bouteldja, AE Hadri, JC Cadiou, JA Davila, and L Fridman. Observation and estimation of dynamics performance of heavy vehicle via second order sliding modes. *International Workshop on Variable Structure Systems*, pages 280–285, 2006.

[87] Nacer K M'Sirdi, A Boubezoul, Abdelhamid Rabhi, and Leonid M Fridman. Estimation of performance of heavy vehicles by sliding modes observers. *Third International Conference on Informatics in Control, Automation and Robotics*, pages 360–365, 2006.

[88] Yuichiro Hirose, Mitsuru Enomoto, Takashi Sasaki, Eiichi Yasuda, and Masatoshi Hada. Ride comfort evaluation of horizontal vibration in tractor-trailer considering human body motion of driver. *SAE Technical Paper*, 2013.

[89] Zhu Tianjun and Zong Changfu. An advanced methodology for rollover warning of heavy duty truck based on kalman filter state estimation. *International Conference on Intelligent Computation Technology and Automation*, 1:466–469, 2010.

[90] Zheshuo Zhang, Manicka Dhanasekar, David P Thambiratnam, and Liang Ling. Ride comfort for the articulated truck drivers crossing raised rail-road crossings. *Proceedings of the 25th International Symposium on Dynamics of Vehicles on Roads and Tracks*, page 75, 2017.

[91] BP Jeppesen and D Cebon. Analytical redundancy techniques for fault detection in an active heavy vehicle suspension. *Vehicle System Dynamics*, 42(1-2):75–88, 2004.

[92] Caizhen Cheng and David Cebon. Improving roll stability of articulated heavy vehicles using active semi-trailer steering. *Vehicle System Dynamics*, 46(S1):373–388, 2008.

[93] Graeme Morrison and David Cebon. Sideslip estimation for articulated heavy vehicles in low friction conditions. *IEEE Intelligent Vehicles Symposium (IV)*, pages 65–70, 2015.

[94] Aleksander Hac and Melinda D Simpson. Estimation of vehicle side slip angle and yaw rate. *SAE Transactions*, pages 1032–1038, 2000.

[95] Graeme Morrison. Sideslip estimation for articulated heavy vehicles at the limits of adhesion. *Vehicle System Dynamics*, 54(11):1601–1628, 2016.

[96] Mehdi Abroshan, Reza Hajiloo, Ehsan Hashemi, and Amir Khajepour. Model predictive-based tractor-trailer stabilisation using differential braking with experimental verification. *Vehicle System Dynamics*, pages 1–24, 2020.

[97] Jocelyn Darling, Derek Tilley, and B Gao. An experimental investigation of car—trailer high-speed stability. *Proceedings of the Institution of Mechanical Engineers, Part D: Journal of Automobile Engineering*, 223(4):471–484, 2009.

[98] MA Alonso Fernandez and RS Sharp. Caravan active braking system-effective stabilisation of snaking of combination vehicles. *SAE Technical Paper*, 2001.

[99] Eungkil Lee. *Design optimization of active trailer differential braking systems for car-trailer combinations.* PhD thesis, 2016.

[100] Rafay Shamim, Md Manjurul Islam, and Yuping He. A comparative study of active control strategies for improving lateral stability of car-trailer systems. *SAE Technical Paper*, 2011.

[101] Smitha Vempaty and Yuping He. A review of car-trailer lateral stability control approaches. *SAE Technical Paper*, 2017.

[102] MFJ Luijten. Lateral dynamic behaviour of articulated commercial vehicles. 2010.

[103] JWLH Maas. Jackknife stability of a tractor semi-trailer combination. 2007.

[104] Tao Sun, Eungkil Lee, and Yuping He. Non-linear bifurcation stability analysis for articulated vehicles with active trailer differential braking systems. *SAE International Journal of Materials and Manufacturing*, 9(3):688–698, 2016.

[105] Sarah Hernandez and Kyung Hyun. Fusion of weigh-in-motion and global positioning system data to estimate truck weight distributions at traffic count sites. *Journal of Intelligent Transportation Systems*, 24(2):201–215, 2020.

[106] Janusz Gajda, Ryszard Sroka, Marek Stencel, Tadeusz Zeglen, Piotr Piwowar, Piotr Burnos, and Zbigniew Marszalek. Design and accuracy assessment of the multi-sensor weigh-in-motion system. *IEEE International Instrumentation and Measurement Technology Conference (I2MTC) Proceedings*, pages 1036–1041, 2015.

[107] Shengyao Jia, Qing Li, and Xiong Li. Signal acquisition and processing of the moving vehicle weighting system. *WSEAS Transaction on Signal Processing*, 3(6):113–122, 2010.

[108] Muhammad Nasiruddin Mahyuddin, Jing Na, Guido Herrmann, Xuemei Ren, and Phil Barber. Adaptive observer-based parameter estimation with application to road gradient and vehicle mass estimation. *IEEE Transactions on Industrial Electronics*, 61(6):2851–2863, 2013.

[109] Werner Kober and Wolfgang Hirschberg. On-board payload identification for commercial vehicles. *IEEE International Conference on Mechatronics*, pages 144–149, 2006.

[110] A. Habibnejad Korayem, A. Khajepour, and B. Fidan. Trailer mass estimation using system model-based and machine learning approaches. *IEEE Transactions on Vehicular Technology*, 69(11):12536–12546, 2020.

[111] I Kim, H Kim, J Bang, and K Huh. Development of estimation algorithms for vehicle's mass and road grade. *International Journal of Automotive Technology*, 14(6):889–895, 2013.

[112] Ling-Yuan Hsu and Tsung-Lin Chen. Vehicle full-state estimation and prediction system using state observers. *IEEE Transactions on Vehicular Technology*, 58(6):2651–2662, 2008.

[113] Naser Esmaeili, Reza Kazemi, and S Hamed Tabatabaei Oreh. An adaptive sliding mode controller for the lateral control of articulated long vehicles. *Proceedings of the Institution of Mechanical Engineers, Part K: Journal of Multi-body Dynamics*, 233(3):487–515, 2019.

[114] Roman Kamnik, Friedrich Boettiger, and Ken Hunt. Roll dynamics and lateral load transfer estimation in articulated heavy freight vehicles. *Proceedings of the Institution of Mechanical Engineers, Part D: Journal of Automobile Engineering*, 217(11):985–997, 2003.

[115] Xu Hongguo, Peng Tao, Liu Hongfei, Xu Yan, and Ren Xia. Improved algorithm of dynamic lateral load transfer for tractor-semitrailer. *Third International Conference on Measuring Technology and Mechatronics Automation*, 2:374–377, 2011.

[116] Dongyoon Hyun and Reza Langari. Modeling to predict rollover threat of tractor-semitrailers. *Vehicle System Dynamics*, 39(6):401–414, 2003.

[117] Abubaker Abdulwahab and Rakesh Mishra. Estimation of ltr rollover index for a high-sided tractor semitrailer vehicle under extreme crosswind conditions through dynamic simulation. *23rd International Conference on Automation and Computing (ICAC)*, pages 1–6, 2017.

[118] Sughosh J Rao. *Development of a hardware in the loop simulation system for heavy truck ESC evaluation and trailer parameter and state estimation*. PhD thesis, The Ohio State University, 2013.

[119] Raj Bridgelall. Connected vehicle approach for pavement roughness evaluation. *Journal of Infrastructure Systems*, 20(1):04013001, 2014.

[120] Zhenzhong Chu, Daqi Zhu, and Simon X Yang. Observer-based adaptive neural network trajectory tracking control for remotely operated vehicle. *IEEE Transactions on Neural Networks and Learning Systems*, 28(7):1633–1645, 2016.

[121] Xiaotong Dong, Yi Jiang, Zhou Zhong, Wei Zeng, and Wei Liu. An improved rollover index based on bp neural network for hydropneumatic suspension vehicles. *Mathematical Problems in Engineering*, 2018.

[122] Jun Guo, Sunwoo Kim, Henk Wymeersch, Walid Saad, and Wei Chen. Guest editorial: Introduction to the special section on machine learning-based internet of vehicles: Theory, methodology, and applications. *IEEE Transactions on Vehicular Technology*, 68(5), 2019.

[123] Tommaso Novi, Renzo Capitani, and Claudio Annicchiarico. An integrated artificial neural network–unscented kalman filter vehicle sideslip angle estimation based on inertial measurement unit measurements. *Proceedings of the Institution of Mechanical Engineers, Part D: Journal of Automobile Engineering*, 233(7):1864–1878, 2019.

[124] Alexander Schoen, Andy Byerly, Brent Hendrix, Rishikesh Mahesh Bagwe, Euzeli Cipriano dos Santos, and Zina Ben Miled. A machine learning model for average fuel consumption in heavy vehicles. *IEEE Transactions on Vehicular Technology*, 68(7):6343–6351, 2019.

[125] Hamid Taghavifar. Neural network autoregressive with exogenous input assisted multi-constraint nonlinear predictive control of autonomous vehicles. *IEEE Transactions on Vehicular Technology*, 68(7):6293–6304, 2019.

[126] David R Woerner, Raman Ranganathan, and Alley C Butler. Developing an artificial neural network for modeling heavy vehicle rollover. *SAE Transactions*, pages 551–561, 2000.

[127] Yechen Qin, Reza Langari, Zhenfeng Wang, Changle Xiang, and Mingming Dong. Road excitation classification for semi-active suspension system with deep neural networks. *Journal of Intelligent & Fuzzy Systems*, 33(3):1907–1918, 2017.

[128] Chen Lv, Yang Xing, Chao Lu, Yahui Liu, Hongyan Guo, Hongbo Gao, and Dongpu Cao. Hybrid-learning-based classification and quantitative inference of driver braking intensity of an electrified vehicle. *IEEE Transactions on Vehicular Technology*, 67(7):5718–5729, 2018.

[129] Sebastian Blume, Philipp Maximilian Sieberg, Niko Maas, and Dieter Schramm. Neural roll angle estimation in a model predictive control system. *IEEE Intelligent Transportation Systems Conference (ITSC)*, pages 1625–1630, 2019.

[130] Javier García Guzmán, Lisardo Prieto González, Jonatan Pajares Redondo, Mat Max Montalvo Martinez, L Boada, and María Jesús. Real-time vehicle roll angle estimation based on neural networks in iot low-cost devices. *Sensors*, 18(7):2188, 2018.

[131] Torben Gräber, Stefan Lupberger, Michael Unterreiner, and Dieter Schramm. A hybrid approach to side-slip angle estimation with recurrent neural networks and kinematic vehicle models. *IEEE Transactions on Intelligent Vehicles*, 4(1):39–47, 2018.

[132] Wang Wei, Bei Shaoyi, Zhang Lanchun, Zhu Kai, Wang Yongzhi, and Hang Weixing. Vehicle sideslip angle estimation based on general regression neural network. *Mathematical Problems in Engineering*, 2016.

[133] A Rakotomamonjy, Rodolphe Le Riche, David Gualandris, and Zaid Harchaoui. A comparison of statistical learning approaches for engine torque estimation. *Control Engineering Practice*, 16(1):43–55, 2008.

[134] Xianjian Jin, Guodong Yin, and Nan Chen. Advanced estimation techniques for vehicle system dynamic state: A survey. *Sensors*, 19(19):4289, 2019.

[135] AH Korayem, Mohsen Irani Rahaghi, H Babaee, and Moharam Habibnejad Korayem. Maximum load of flexible joint manipulators using nonlinear controllers. *Robotica*, 35(1):119–142, 2017.

[136] Morgan Mangeas, Shbastien Glaser, and V Dolcemascolo. Neural networks estimation of truck static weights by fusing weight-in-motion data. *Proceedings of the Fifth International Conference on Information Fusion*, 1:456–462, 2002.

[137] Daniel Arnström. State estimation for truck and trailer systems using deep learning, 2018.

[138] Erkan Kayacan, Erdal Kayacan, Herman Ramon, and Wouter Saeys. Modeling and identification of the yaw dynamics of an autonomous tractor. *9th Asian Control Conference (ASCC)*, pages 1–6, 2013.

[139] Tom Kraus, Hans Joachim Ferreau, Erdal Kayacan, H Ramon, J De Baerdemaeker, M Diehl, and W Saeys. Moving horizon estimation and nonlinear model predictive

control for autonomous agricultural vehicles. *Computers and Electronics in Agriculture*, 98:25–33, 2013.

[140] Erkan Kayacan, Erdal Kayacan, Herman Ramon, and Wouter Saeys. Distributed nonlinear model predictive control of an autonomous tractor–trailer system. *Mechatronics*, 24(8):926–933, 2014.

[141] Felipe Núnez, Sergio Navarro, Alberto Aguado, and Aldo Cipriano. State estimation based model predictive control for lhd vehicles. *IFAC Proceedings Volumes*, 41(2):1448–1453, 2008.

[142] Lukas Caup, Jan Salmen, Ibro Muharemovic, and Sebastian Houben. Video-based trailer detection and articulation estimation. *IEEE Intelligent Vehicles Symposium (IV)*, pages 1179–1184, 2013.

[143] Christian Fuchs, Frank Neuhaus, and Dietrich Paulus. Advanced 3-d trailer pose estimation for articulated vehicles. *IEEE Intelligent Vehicles Symposium (IV)*, pages 211–216, 2015.

[144] Hocine Imine, Abdelaziz Benallegue, Tarek Madani, and Salim Srairi. Rollover risk prediction of heavy vehicle using high-order sliding-mode observer: Experimental results. *IEEE Transactions on Vehicular Technology*, 63(6):2533–2543, 2013.

[145] Zhiguo Zhao, Yeqin Wang, Xiaoming Hu, Yukai Tao, and Jinsheng Wang. Research on identification method of heavy vehicle rollover based on hidden markov model. *Open Physics*, 15(1):479–485, 2017.

[146] Tong Wu and John Y Hung. State estimation for a tractor-trailer system using adaptive unscented kalman filter. *Southeast Conference*, pages 1–5, 2017.

[147] Hiroki Tomiyama, Michihisa Iida, and Toho Oh. Estimation of the sideslip angle of an articulated vehicle by an observer. *Engineering in Agriculture, Environment and Food*, 4(3):66–70, 2011.

[148] Ulf Andersson, Gianantonio Bortolin, Staffan Backén, and Thomas Gustafsson. Estimation of sideslip angles of a volvo a25e articulated all-wheel drive hauler based on gps/ins measurements. *SAE Technical Paper*, 2011.

[149] Amin Habibnejad Korayem, Amir Khajepour, and Baris Fidan. A review on vehicle-trailer state and parameter estimation. *IEEE Transactions on intelligent transportation systems*, 2021.

[150] Yuping He and Jing Ren. A comparative study of car-trailer dynamics models. *SAE International Journal of Passenger Cars-Mechanical Systems*, 6(2013-01-0695):177–186, 2013.

[151] Amir Khajepour, M Saber Fallah, and Avesta Goodarzi. *Electric and hybrid vehicles: technologies, modeling and control-a mechatronic approach*. John Wiley & Sons, 2014.

[152] Joško Deur, Jahan Asgari, and Davor Hrovat. A 3d brush-type dynamic tire friction model. *Vehicle System Dynamics*, 42(3):133–173, 2004.

[153] Wei Liang, Jure Medanic, and Roland Ruhl. Analytical dynamic tire model. *Vehicle System Dynamics*, 46(3):197–227, 2008.

[154] Panagiotis Tsiotras, Efstathios Velenis, and Michel Sorine. A lugre tire friction model with exact aggregate dynamics. *Vehicle System Dynamics*, 42(3):195–210, 2004.

[155] Ehsan Hashemi, Mohammad Pirani, Amir Khajepour, Baris Fidan, Alireza Kasaiezadeh, Shih-Ken Chen, and Bakhtiar Litkouhi. Integrated estimation structure for the tire friction forces in ground vehicles. *IEEE International Conference on Advanced Intelligent Mechatronics (AIM)*, pages 1657–1662, 2016.

[156] Ehsan Hashemi, Mohammad Pirani, Amir Khajepour, and Alireza Kasaiezadeh. A comprehensive study on the stability analysis of vehicle dynamics with pure/combined-slip tyre models. *Vehicle System Dynamics*, 54(12):1736–1761, 2016.

[157] Rajesh Rajamani, Gridsada Phanomchoeng, Damrongrit Piyabongkarn, and Jae Y Lew. Algorithms for real-time estimation of individual wheel tire-road friction coefficients. *IEEE/ASME Transactions on Mechatronics*, 17(6):1183–1195, 2011.

[158] Wanki Cho, Jangyeol Yoon, Seongjin Yim, Bongyeong Koo, and Kyongsu Yi. Estimation of tire forces for application to vehicle stability control. *IEEE Transactions on Vehicular Technology*, 59(2):638–649, 2009.

[159] Moustapha Doumiati, A Victorino, Daniel Lechner, G Baffet, and A Charara. Observers for vehicle tyre/road forces estimation: experimental validation. *Vehicle System Dynamics*, 48(11):1345–1378, 2010.

[160] Amit K Sanyal, Taeyoung Lee, Melvin Leok, and N Harris McClamroch. Global optimal attitude estimation using uncertainty ellipsoids. *Systems & Control Letters*, 57(3):236–245, 2008.

[161] Madhulika Das and Chitralekha Mahanta. Disturbance observer based optimal second order sliding mode controller for nonlinear systems with mismatched uncertainty. In *2016 IEEE First International Conference on Control, Measurement and Instrumentation (CMI)*, pages 361–365. IEEE, 2016.

[162] AH Korayem, SR Nekoo, and MH Korayem. Sliding mode control design based on the state-dependent riccati equation: theoretical and experimental implementation. *International Journal of Control*, 92(9):2136–2149, 2019.

[163] Shant Abraham and Johan Nilsson. Trailer parking assist. Master's thesis, Chalmers University of Technology, 2013.

[164] P Bolzern, RM DeSantis, and Arturo Locatelli. An input-output linearization approach to the control of an n-body articulated vehicle. *Journal of Dynamic Systems, Measurement, and Control*, 123(3):309–316, 2001.

[165] Ehsan Hashemi, Mohammad Pirani, Amir Khajepour, Alireza Kasaiezadeh, Shih-Ken Chen, and Bakhtiar Litkouhi. Corner-based estimation of tire forces and vehicle velocities robust to road conditions. *Control Engineering Practice*, 61:28–40, 2017.

[166] S Antonov, A Fehn, and A Kugi. Unscented kalman filter for vehicle state estimation. *Vehicle System Dynamics*, 49(9):1497–1520, 2011.

[167] Rudolph Emil Kalman. A new approach to linear filtering and prediction problems. 1960.

[168] Simon Haykin. *Kalman filtering and neural networks*, volume 47. John Wiley & Sons, 2004.

[169] B-C Chen and F-C Hsieh. Sideslip angle estimation using extended kalman filter. *Vehicle System Dynamics*, 46(S1):353–364, 2008.

[170] Inkeun Kim, Jaesung Bang, and Kunsoo Huh. Estimation of the climbing angle in the presence of yawing motion. *Proceedings of the Institution of Mechanical Engineers, Part D: Journal of Automobile Engineering*, 229(9):1263–1275, 2015.

[171] Daphne Koller and Nir Friedman. *Probabilistic graphical models: principles and techniques*. MIT press, 2009.

[172] Simon J Julier and Jeffrey K Uhlmann. New extension of the kalman filter to nonlinear systems. *Signal Processing, Sensor Fusion, and Target Recognition VI*, 3068:182–193, 1997.

[173] Dan Simon. *Optimal state estimation: Kalman, H infinity, and nonlinear approaches*. John Wiley & Sons, 2006.

[174] M Pengov, B D'Andréa-Novel, E Fenaux, S Grazi, and F Zarka. A comparison study of two kinds of observers for a vehicle. *European Control Conference (ECC)*, pages 1068–1073, 2001.

[175] Eric A Wan and Rudolph Van Der Merwe. The unscented kalman filter for nonlinear estimation. *Proceedings of the IEEE Adaptive Systems for Signal Processing, Communications, and Control Symposium*, pages 153–158, 2000.

[176] Harry Berghuis and Henk Nijmeijer. A passivity approach to controller-observer design for robots. *IEEE Transactions on Robotics and Automation*, 9(6):740–754, 1993.

[177] Ai-Guo Wu, Guang-Ren Duan, and Yan-Ming Fu. Generalized pid observer design for descriptor linear systems. *IEEE Transactions on Systems, Man, and Cybernetics, Part B (Cybernetics)*, 37(5):1390–1395, 2007.

[178] Ying Zhang, Yingjie Zhang, Zhaoyang Ai, Yun Feng, Jing Zhang, and Yi Lu Murphey. Estimation of electric mining haul trucks' mass and road slope using dual level reinforcement estimator. *IEEE Transactions on Vehicular Technology*, 68(11):10627–10638, 2019.

[179] Anurag Bhardwaj, Wei Di, and Jianing Wei. *Deep Learning Essentials: Your hands-on guide to the fundamentals of deep learning and neural network modeling*. Packt Publishing Ltd, 2018.

[180] DT Reindl, WA Beckman, and JA Duffie. Evaluation of hourly tilted surface radiation models. *Solar energy*, 45(1):9–17, 1990.

[181] Milad Jalali, Ehsan Hashemi, Amir Khajepour, Shih-ken Chen, and Bakhtiar Litkouhi. A combined-slip predictive control of vehicle stability with experimental verification. *Vehicle system dynamics*, 56(2):319–340, 2018.

[182] Amin Habibnejad Korayem, Amir Khajepour, and Baris Fidan. Vehicle-trailer lateral velocity estimation using constrained unscented transformation. *Vehicle System Dynamics*, pages 1–28, 2020.

[183] Leonard M Silverman and HE Meadows. Controllability and observability in time-variable linear systems. *SIAM Journal on Control*, 5(1):64–73, 1967.

[184] Roland Tóth. *Modeling and identification of linear parameter-varying systems*, volume 403. Springer, 2010.

[185] Jihan Ryu and J Christian Gerdes. Integrating inertial sensors with global positioning system (gps) for vehicle dynamics control. *Journal of Dynamic Systems, Measurement, and Control*, 126(2):243–254, 2004.

[186] Bin Wang, Qi Cheng, Alessandro Correa Victorino, and Ali Charara. Nonlinear observers of tire forces and sideslip angle estimation applied to road safety: Simulation and experimental validation. *15th International IEEE Conference on Intelligent Transportation Systems*, pages 1333–1338, 2012.

[187] Rudolph Van Der Merwe and Eric A Wan. Efficient derivative-free kalman filters for online learning. *European Symposium on Artificial Neural Networks*, pages 205–210, 2001.

[188] Fredrik Gustafsson and Gustaf Hendeby. Some relations between extended and unscented kalman filters. *IEEE Transactions on Signal Processing*, 60(2):545–555, 2011.

[189] Chongyang Hu, Yan Liang, Linfeng Xu, and Xiaohui Hao. Unscented recursive filtering for inequality constrained systems. *IEEE Access*, 7:19077–19088, 2019.

[190] Zahra Razavinasab, Malihe M Farsangi, and Mojtaba Barkhordari. Robust output feedback distributed model predictive control of networked systems with communication delays in the presence of disturbance. *ISA transactions*, 80:12–21, 2018.

[191] Dan Sui, Tor Arne Johansen, and Le Feng. Linear moving horizon estimation with pre-estimating observer. *IEEE Transactions on automatic control*, 55(10):2363–2368, 2010.

[192] Pascal Gahinet, Pierre Apkarian, and Mahmoud Chilali. Affine parameter-dependent lyapunov functions and real parametric uncertainty. *IEEE Transactions on Automatic control*, 41(3):436–442, 1996.

[193] Wei Wang, Xinbo Chen, and Junmin Wang. Motor/generator applications in electrified vehicle chassis—a survey. *IEEE Transactions on Transportation Electrification*, 5(3):584–601, 2019.

[194] Hongtei Eric Tseng. Dynamic estimation of road bank angle. *Vehicle system dynamics*, 36(4-5):307–328, 2001.

[195] Lghani Menhour, Daniel Lechner, and Ali Charara. Design and experimental validation of linear and nonlinear vehicle steering control strategies. *Vehicle system dynamics*, 50(6):903–938, 2012.

[196] Lin-Hui Zhao, Zhi-Yuan Liu, and Hong Chen. Sliding mode observer for vehicle velocity estimation with road grade and bank angles adaptation. In *2009 IEEE Intelligent Vehicles Symposium*, pages 701–706. IEEE, 2009.

[197] Jihwan Kim, Hyeongcheol Lee, and Seibum Choi. A robust road bank angle estimation based on a proportional–integral h- filter. *Proceedings of the Institution of Mechanical Engineers, Part D: Journal of automobile engineering*, 226(6):779–794, 2012.

[198] Christopher R Carlson and J Christian Gerdes. Optimal rollover prevention with steer by wire and differential braking. In *ASME International Mechanical Engineering Congress and Exposition*, volume 37130, pages 345–354, 2003.

[199] Lars Imsland, Håvard Fjær Grip, Tor A Johansen, Thor I Fossen, Jens C Kalkkuhl, and Avshalom Suissa. Nonlinear observer for vehicle velocity with friction and road bank angle adaptation-validation and comparison with an extended kalman filter. Technical report, SAE Technical Paper, 2007.

[200] Lars Imsland, Tor Arne Johansen, Håvard Fjær Grip, and Thor I Fossen. On non-linear unknown input observers–applied to lateral vehicle velocity estimation on banked roads. *International Journal of Control*, 80(11):1741–1750, 2007.

[201] Jihan Ryu, Eric J Rossetter, and J Christian Gerdes. Vehicle sideslip and roll parameter estimation using gps. In *Proceedings of the AVEC International Symposium on Advanced Vehicle Control*, pages 373–380, 2002.

[202] Ling-Yuan Hsu and Tsung-Lin Chen. Estimating road angles with the knowledge of the vehicle yaw angle. *Journal of dynamic systems, measurement, and control*, 132(3), 2010.

[203] ISO 8855. Road vehicles—vehicle dynamics and road—holding ability—vocabulary. 2011.

[204] Ehsan Hashemi, Reza Zarringhalam, Amir Khajepour, William Melek, Alireza Kasaiezadeh, and Shih-Ken Chen. Real-time estimation of the road bank and grade angles with unknown input observers. *Vehicle system dynamics*, 55(5):648–667, 2017.

[205] Gene F Franklin, J David Powell, Michael L Workman, et al. *Digital control of dynamic systems*, volume 3. Addison-wesley Reading, MA, 1998.

[206] Andrea Cristofaro and Tor Arne Johansen. Fault tolerant control allocation using unknown input observers. *Automatica*, 50(7):1891–1897, 2014.

[207] CL Robinson and PR Kumar. Sending the most recent observation is not optimal in networked control: Linear temporal coding and towards the design of a control specific transport protocol. In *2007 46th IEEE Conference on Decision and Control*, pages 334–339. IEEE, 2007.

[208] Shreyas Sundaram and Christoforos N Hadjicostis. Delayed observers for linear systems with unknown inputs. *IEEE Transactions on Automatic Control*, 52(2):334–339, 2007.

[209] Shreyas Sundaram and Christoforos N Hadjicostis. Partial state observers for linear systems with unknown inputs. *Automatica*, 44(12):3126–3132, 2008.

[210] Amin Habibnejad Korayem, Amir Khajepour, and Baris Fidan. Road angle estimations for a vehicle-trailer with machine learning and system model-based approaches. *Submitted*.

[211] Yoshua Bengio, Patrice Simard, and Paolo Frasconi. Learning long-term dependencies with gradient descent is difficult. *IEEE transactions on neural networks*, 5(2):157–166, 1994.

[212] Sepp Hochreiter, Yoshua Bengio, Paolo Frasconi, Jürgen Schmidhuber, et al. Gradient flow in recurrent nets: the difficulty of learning long-term dependencies, 2001.

[213] Felix A Gers and Jürgen Schmidhuber. Recurrent nets that time and count. In *Proceedings of the IEEE-INNS-ENNS International Joint Conference on Neural Networks. IJCNN 2000. Neural Computing: New Challenges and Perspectives for the New Millennium*, volume 3, pages 189–194. IEEE, 2000.

[214] Sepp Hochreiter and Jürgen Schmidhuber. Long short-term memory. *Neural computation*, 9(8):1735–1780, 1997.

[215] Long Xin, Pin Wang, Ching-Yao Chan, Jianyu Chen, Shengbo Eben Li, and Bo Cheng. Intention-aware long horizon trajectory prediction of surrounding vehicles using dual lstm networks. In *2018 21st International Conference on Intelligent Transportation Systems (ITSC)*, pages 1441–1446. IEEE, 2018.

[216] Li Li, Fei-Yue Wang, and Qunzhi Zhou. Integrated longitudinal and lateral tire/road friction modeling and monitoring for vehicle motion control. *IEEE Transactions on Intelligent Transportation Systems*, 7(1):1–19, 2006.

[217] Dan Sui and Tor Arne Johansen. Linear constrained moving horizon estimator with pre-estimating observer. *Systems & Control Letters*, 67:40–45, 2014.

[218] Harry Magadhlela Ngwangwa, Philippus Stephanus Heyns, FJJ Labuschagne, and Grant K Kululanga. Reconstruction of road defects and road roughness classification using vehicle responses with artificial neural networks simulation. *Journal of Terramechanics*, 47(2):97–111, 2010.

[219] Philippe Nitsche, Rainer Stütz, Michael Kammer, and Peter Maurer. Comparison of machine learning methods for evaluating pavement roughness based on vehicle response. *Journal of Computing in Civil Engineering*, 28(4):04014015, 2014.

[220] JI Park, JY Yoon, DS Kim, and KS Yi. Roll state estimator for rollover mitigation control. *Proceedings of the Institution of Mechanical Engineers, Part D: Journal of Automobile Engineering*, 222(8):1289–1312, 2008.

[221] CL Kanali. Prediction of axle loads induced by sugarcane transport vehicles using statistical and neural-network models. *Journal of Agricultural Engineering Research*, 68(3):207–213, 1997.

[222] Zachary Brock, James Nelson, and Ross L Hatton. A comparison of lateral dynamic models for tractor-trailer systems. *IEEE Intelligent Vehicles Symposium (IV)*, pages 2052–2059, 2019.

[223] Weiwen Deng, Yong H Lee, and Ming Tian. An integrated chassis control for vehicle-trailer stability and handling performance. *SAE Transactions*, pages 1041–1046, 2004.

[224] Tina Mirfakhraie, Ramiro Liscano, Shenjin Zhu, and Yuping He. A wireless-communication-based active safety system for articulated heavy vehicles. *ASME International Mechanical Engineering Congress and Exposition*, 2015.

[225] Md Manjurul Islam, Yuping He, Shenjin Zhu, and Qiushi Wang. A comparative study of multi-trailer articulated heavy-vehicle models. *Proceedings of the Institution of Mechanical Engineers, Part D: Journal of Automobile Engineering*, 229(9):1200–1228, 2015.

[226] Xuanzuo Liu, Anil K Madhusudhanan, and David Cebon. Minimum swept-path control for autonomous reversing of a tractor semi-trailer. *IEEE Transactions on Vehicular Technology*, 68(5):4367–4376, 2019.

[227] Ashley L Dunn. *Jackknife stability of articulated tractor semitrailer vehicles with high-output brakes and jackknife detection on low coefficient surfaces*. PhD thesis, The Ohio State University, 2003.

[228] Caizhen Cheng, Richard Roebuck, Andrew Odhams, and David Cebon. High-speed optimal steering of a tractor–semitrailer. *Vehicle System Dynamics*, 49(4):561–593, 2011.

[229] David JM Sampson and David Cebon. Achievable roll stability of heavy road vehicles. *Proceedings of the Institution of Mechanical Engineers, Part D: Journal of Automobile Engineering*, 217(4):269–287, 2003.

[230] Caizhen Cheng. *Enhancing safety of actively-steered articulated vehicles*. PhD thesis, University of Cambridge, 2009.

[231] Iwona Adamiec-Wójcik, Jan Awrejcewicz, Witold Grzegożek, and Stanisław Wojciech. Dynamics of articulated vehicles by means of multibody methods. 2015.

[232] Zeyu Ma, Xuewu Ji, Yunqing Zhang, and James Yang. State estimation in roll dynamics for commercial vehicles. *Vehicle System Dynamics*, 55(3):313–337, 2017.

[233] I Adamiec-Wójcik and S Wojciech. Calibration of an articulated vehicle model. *Mathematical Modeling*, 2(2):65–68, 2018.

[234] Der-Ho Wu. A theoretical study of the yaw/roll motions of a multiple steering articulated vehicle. *Proceedings of the Institution of Mechanical Engineers, Part D: Journal of Automobile Engineering*, 215(12):1257–1265, 2001.

[235] Xiujian Yang, Juntao Song, and Jin Gao. Fuzzy logic based control of the lateral stability of tractor semitrailer vehicle. *Mathematical Problems in Engineering*, 2015.

[236] Yong Sun, Liang Li, Bingjie Yan, Chao Yang, and Gongyou Tang. A hybrid algorithm combining ekf and rls in synchronous estimation of road grade and vehicle mass for a hybrid electric bus. *Mechanical Systems and Signal Processing*, 68:416–430, 2016.

[237] Ardalan Vahidi, Anna Stefanopoulou, and Huei Peng. Recursive least squares with forgetting for online estimation of vehicle mass and road grade: theory and experiments. *Vehicle System Dynamics*, 43(1):31–55, 2005.

[238] Boyuan Li, Jiawei Zhang, Haiping Du, and Weihua Li. Two-layer structure based adaptive estimation for vehicle mass and road slope under longitudinal motion. *Measurement*, 95:439–455, 2017.

[239] Morteza Taiebat, Austin L Brown, Hannah R Safford, Shen Qu, and Ming Xu. A review on energy, environmental, and sustainability implications of connected and automated vehicles. *Environmental science & technology*, 52(20):11449–11465, 2018.

[240] Ehsan Hashemi, Alireza Kasaiezadeh, Saeid Khosravani, Amir Khajepour, Nikolai Moshchuk, and Shih-Ken Chen. Estimation of longitudinal speed robust to road conditions for ground vehicles. *Vehicle System Dynamics*, 54(8):1120–1146, 2016.

[241] Xiangwen Zhang, Yong Xu, Ming Pan, and Fenghua Ren. A vehicle abs adaptive sliding-mode control algorithm based on the vehicle velocity estimation and tyre/road friction coefficient estimations. *Vehicle System Dynamics*, 52(4):475–503, 2014.

[242] Thomas A Wenzel, KJ Burnham, MV Blundell, and RA Williams. Dual extended kalman filter for vehicle state and parameter estimation. *Vehicle system dynamics*, 44(2):153–171, 2006.

[243] Amin Habibnejad Korayem, Saeed Rafee Nekoo, and Moharam Habibnejad Korayem. Optimal sliding mode control design based on the state-dependent riccati equation for cooperative manipulators to increase dynamic load carrying capacity. *Robotica*, 37(2):321–337, 2019.

APPENDIX

Appendix A

$\boldsymbol{A(\delta)}$, $\boldsymbol{B(\delta)}$, and $\mathbf{G}$ matrix elements are obtained as follows:

$$a_{21} = -l_1\delta + \frac{a_1 u_1 m_1}{I_{z1}}, a_{42} = -a_{22} - l_1, a_{31} = -\frac{a_1\delta}{(e+b_1)}, a_{35} = -\frac{a_1}{(e+b_1)},$$
$$a_{41} = -l_1 - \frac{a_1 v_1 m_1}{I_{z1}}, a_{36} = \frac{-b_1}{e+b_1}, a_{22} = -\frac{-b_1 u_1 m_1}{I_{z1}}, a_{23} = -\frac{(e+b_1)u_1 m_1}{I_{z1}},$$
$$a_{43} = -a_{23} - l_1, a_{17} = \frac{e+b_1}{a_1}, a_{16} = \frac{b_1}{a_1}, \tag{A.1}$$

$$b_{21} = m_1\ddot{v}_1 + F_{xf}r_1 + F_{xr}r_1 + m_1 v_1 r_1^2 + \frac{m_1 u_1 F_{xf}\delta a_1}{I_{z1}} - \dot{F}_{xf}\delta - F_{xf}\dot{\delta},$$
$$b_{41} = m_1\ddot{u}_1 + F_{xf}\delta r_1 + m_1 v_1 r_1^2 - \dot{F}_{xf} - \frac{m_1 v_1 F_{xf}\delta a_1}{I_{z1}} - \dot{F}_{xr}\dot{\delta}, \tag{A.2}$$

$$\mathbf{G} = \begin{bmatrix} -\frac{L_{12}+a_1 L_{13}}{m_1} & -\frac{L_{12}}{m_1} + \frac{L_{13}b_1}{I_{z1}} & G_{13} & G_{14} \\ -\frac{L_{22}+a_1 L_{23}}{m_1} & G_{22} & G_{23} & G_{24} \\ -\frac{L_{32}+a_1 L_{33}}{m_1} & -\frac{L_{32}}{m_1} + \frac{L_{33}b_1}{I_{z1}} & G_{33} & G_{34} \\ a_{41} - \frac{L_{42}+a_1 L_{43}}{m_1} & G_{42} & G_{43} & G_{44} \\ -\frac{L_{52}+a_1 L_{53}}{m_1} & -\frac{L_{52}}{m_1} + \frac{L_{53}b_1}{I_{z1}} & G_{53} & G_{54} \\ -\frac{L_{62}+a_1 L_{63}}{m_1} & -\frac{L_{62}}{m_1} + \frac{L_{63}b_1}{I_{z1}} & G_{63} & G_{64} \\ -\frac{L_{72}+a_1 L_{73}}{m_1} & -\frac{L_{72}}{m_1} + \frac{L_{73}b_1}{I_{z1}} & G_{73} & G_{74} \end{bmatrix}, \tag{A.3}$$

$$G_{22} = -a_{23} - \frac{L_{22}}{m_1} + \frac{L_{23}b_1}{I_{z1}}, G_{42} = a_{42} - \frac{L_{42}}{m_1} + \frac{L_{43}b_1}{I_{z1}},$$
$$G_{13} = -\frac{L_{12}}{m_1} + \frac{L_{13}(e+b_1)}{I_{z1}}, G_{14} = -\frac{L_{11}}{m_1},$$
$$G_{23} = a_{23} - \frac{L_{22}}{m_1} + \frac{L_{23}(e+b_1)}{I_{z1}}, G_{24} = r_1 - \frac{L_{21}}{m_1},$$
$$G_{33} = -\frac{L_{32}}{m_1} + \frac{L_{33}(e+b_1)}{I_{z1}}, G_{34} = -\frac{L_{31}}{m_1},$$
$$G_{43} = a_{43} - \frac{L_{42}}{m_1} + \frac{L_{43}(e+b_1)}{I_{z1}}, G_{44} = -\frac{L_{41}}{m_1},$$
$$G_{53} = -\frac{L_{52}}{m_1} + \frac{L_{53}(e+b_1)}{I_{z1}}, G_{54} = -\frac{L_{51}}{m_1},$$
$$G_{63} = -\frac{L_{62}}{m_1} + \frac{L_{63}(e+b_1)}{I_{z1}}, G_{64} = -\frac{L_{61}}{m_1},$$
$$G_{73} = -\frac{L_{72}}{m_1} + \frac{L_{73}(e+b_1)}{I_{z1}}, G_{74} = -\frac{L_{71}}{m_1}. \tag{A.4}$$